PALAEOSECULAR VARIATION OBSERVED IN SPELEOTHEMS FROM WESTERN CHINA AND NORTHERN SPAIN.

Thesis submitted in accordance with the requirements of the University of Liverpool for the degree of Doctor in Philosophy.

by Steven J. Openshaw.

July 1996.

ORIGINAL COPY TIGHTLY BOUND

Abstract.

This study has produced records of the palaeosecular variation (PSV) of the earth's magnetic field using speleothems from W. China and N. Spain. The ultimate aim of this project was to produce contemporaneous records of PSV in order to confirm that the speleothems had accurately recorded geomagnetic field behaviour. From Sichuan Province, China, five speleothems were collected of which four were measured for their records of PSV. Eight Spanish speleothems from the Cantabrian coast were collected but their weak magnetisation allowed only one reliable record to be produced.

All speleothem sub-samples were weakly magnetised and had, on average, initial intensities of $<100 \times 10^{-8} Am^2kg^{-1}$. Nevertheless, the majority of sub-samples were stable during alternating-field and thermal demagnetisation and each displayed a single primary component of magnetisation after removal of any secondary overprints. Using acquisition and demagnetisation of isothermal remanent magnetisation, the remanence of each speleothem was inferred to be carried by a mixture of multi and single-domain (titano-) magnetite and also by haematite in significant quantities. A depositional remanence from flooding appears to be the primary mode of remanence acquisition. This was partially confirmed by the linear relationship between sub-sample intensity and weight % detritus.

Sub-samples from each speleothem were dated alpha-spectrometrically using uranium-thorium disequilibrium. In the majority of sub-samples the low concentrations of uranium, the high levels of detrital contamination and the initially low chemical yields raised the associated dating inaccuracies to above the quoted level for alpha spectrometry of 5-10% (Schwarcz, 1989). Two Spanish speleothems had high uranium concentrations and little, or no, detrital contamination. Percent age errors of these speleothems ranged from 1 to 6%. Comprehensive analyses of the efficiencies of two electrodeposition methods were conducted due to initially low chemical recoveries of isotopes. A significant improvement in plating efficiency was achieved with a modified version of the Hallstadius (1984) procedure. This method gave chemical yields of between 40 and 90% for uranium and thorium after its adoption as a routine procedure.

In order to correct more analytically for the detrital contamination, the leachate/leachate method of Schwarcz and Latham (1989) was tested. The maximum likelihood estimation data treatment technique (Ludwig and Titterington, 1994) was used to calculate dates from these analyses. Tests on Mexican speleothem SSJ2 (Lean, 1995) produced good results allowing a revised dating scheme to be adopted. Tests on some sub-samples from Chinese speleothems were generally unsuccessful due to analytical problems. A further dating method using the isotope ^{210}Pb was undertaken on the top surface of one speleothem. This confirmed that the speleothem had been active during the past 150 years. The growth rates calculated from uranium-thorium disequilibrium and ^{210}Pb dating of this speleothem were significantly different due to the inaccuracies of the former technique and its inability to resolve growth rate changes over short periods.

Despite the dating errors associated with the Chinese speleothems their PSV records compared well with each other and also with other contemporaneous records from China and Japan. The Spanish record was also comparable with a lake sediment record from the UK. In addition, there was also some agreement with PSV modelled from observatory records from both China and Spain. Thus, the global coverage of speleothem PSV records has been usefully expanded, further reinforcing the value of these deposits as a compliment to records from sediments and archaeological materials.

I declare that the content of this thesis is my own work and that it has not been submitted for examination at any other university.

Steven Justin Openshaw (July 1996)

Acknowledgements

It is a difficult task for me to thank all those who have assisted me in the pursuit of this project. There have been so many to whom I remain deeply indebted even if just for their continued interest in my work, which lets face it is probably the most important encouragement! I split my thanks amongst the academic and caving community.

Thanks must be expressed to my supervisors, Alf Latham and John Shaw, who got the project off the ground and continued to support my research needs throughout my studies. I must also thank Peter Appleby for his valuable assistance for the work on ^{210}Pb dating. Of course, one of the most important aspects of Ph.D. training are the development of interpersonal skills and the ability to swap ideas with others in the same field. For help in developing these skills I am grateful (in no particular order) to (especially) Jennifer, Jimmy, John Share, Gregg, Helen, Yang Shanlin, Liu Xuming, Candy, Dot, Graham, Silvia, Pete Roe (briefly!), John Eyre, Tim (Matey), Neil, Young Zhang, Old Zhang, Prof. Zhu Xuewen and Igor. For my fieldwork and conference attendance I give thanks to the NERC for Spain and the first visit to China plus Boulder 1995; the British Council for China visit number two and additionally to the IAGA Young Scientists Fund for financial assistance with Boulder 1995.

Thanks to the UK caving community are amongst the most difficult to express truly. If not for their help and endless enthusiasm I think the logistics behind this project would have been insurmountable. I take this opportunity to express my pleasure in having received help from so many. Off the top of my head, specific thanks go to the following clubs:- MUSS, Bolton PC and the Matienzo CPC. People are probably too numerous for me to remember them all but here goes: Andy Quin, Julie Bridgeman, Arthur, Phil and Hillary Papard, Joe and Liz Turner, Ron and Jill Obvious, Worm and Carol, Bar German, Ian and Beryl Hopley, Juan, Penny and Jenny Corrin, Pete Smith and family, Lank and Liz Mills, Ratprick, Ray McGarry, Phil Miles, Dave Salerman, Toby and Jane Chiltern, Andy Eavis, Kenny Taylor, Paul Seddon and the many other members of the China Caves Project team, Pete Eagan, the amazing Andy Pringle, John Palmer and Germ, Stevie Weevy and Suzie Woozy *et al.*

I must also thank my parents, Tony and Thailia, and my Nan, from whom I have received so much support during my studies. This support has included feats over and above the call of parental duty and I cannot thank them enough but to say "Look what you've made me do now!" Finally there is one other person, who through her love, affection and understanding has kept me on the right track throughout my time in Liverpool, particularly in the final year...Candy. Thanks.

This thesis is dedicated to

Mum and Dad

for their continual support throughout my studies

As the morning sun rises over the naked limestone mountains of Matienzo a new day of subterranean exploration dawns.....

What could possibly go wrong?

The oft quoted motto of the
Bolton Speleological Club

List of abbreviations

λ	Decay constant: the probability of decay per unit time
σ	One standard deviation
χ	Susceptibility (m^3 kg^{-1})
α_{95}	Radius of the cone of 95% confidence about the mean.
a.s.l.	above sea level
AF	Alternating field
cpm	Counts per minute
CRM	Chemical remanent magnetisation
DIF	Differential isotopic fractionation
DRM	Depositional remanent magnetisation
GADF	Geocentric axial dipole field
IGRF	International Geomagnetic Reference Field
IRM	Isothermal remanent magnetisation (Am^2 kg^{-1})
ka	thousand years
L/L	Leachate/leachate
M	Molar
Ma	Million years
MAD	Maximum angular deviation
MD	Multi-domain
MDF	Median destructive field (mT)
MLE	Maximum likelihood estimation
mm yr^{-1}	Reciprocal growth rate in millimetres per year
mT	Milli-tesla
NRM	Natural remanent magnetisation (Am^2 kg^{-1})
pH	Negative log of the hydrogen ion
ppm	Parts per million
PSV	Palaeosecular variation
SD	Single domain
SIRM	Saturation isothermal remanent magnetisation (Am^2 kg^{-1})
$t_{1/2}$	Half-life
T_b	Blocking temperature (°C)
T_c	Curie temperature (°C)
VGP	Virtual geomagnetic pole
VRM	Viscous remanent magnetisation

Contents.

4. URANIUM-SERIES DISEQUILIBRIUM DATING OF CALCITE SPELEOTHEMS USING THE $^{230}Th/^{234}U$ AND ^{210}Pb TECHNIQUES.

5. COLLECTION AND PREPARATION OF SPELEOTHEMS.

6. PALAEOSECULAR VARIATION RECORDS AND DATING OF SPELEOTHEMS FROM XINGWEN, CHINA.

7. PALAEOSECULAR VARIATION RECORDS AND DATING OF SPELEOTHEMS FROM MATIENZO, CANTABRIA, SPAIN.

8. ROCK MAGNETISM OF CHINESE AND SPANISH SPELEOTHEMS.

9. CONCLUSIONS AND THE POTENTIAL FOR FUTURE WORK.

1. Study objectives and thesis structure.

1.1. Introduction.

Changes in the direction and intensity of the Earth's magnetic field over periods between 100 and 10,000 years are termed secular variation (SV). There are many historical and observational records of global SV covering the past 400 years. In order to model SV beyond 400 years geomagnetists are reliant on ancient records of SV, termed palaeosecular variation (PSV). These PSV records can be obtained from a variety of materials including lacustrine and marine sediments, lavas, baked clays and, as in this study, speleothems. However, for a material to provide a useful record of PSV it must satisfy the following criteria. Firstly, and perhaps most importantly, the material must contain sufficient magnetic material to yield a measurable signal using available equipment. Secondly, it must remain undisturbed after deposition or have undergone movement whose magnitude can be accurately measured. Thirdly, it must be possible to constrain the age of the material either by dating it directly or by its association with materials of known age. Fourthly, the material must have accumulated at a sufficient rate so that the palaeosecular variation signal is of a resolution that illustrates the shortest periods of geomagnetic field change. Finally, one must also demonstrate that the magnetisation is primary and that it represents ambient field at the time of formation.

Lavas and baked clays are commonly used to provide information on PSV but can only provide discontinuous records of field change. Thus, lavas and baked clays are not ideal for the production of long period PSV records. Of sediment and speleothem PSV records the majority are derived from sediments which are widely available and often satisfy the criteria above. Frequently, sediments have high accumulation rates and therefore record high resolution PSV data. They can also hold records of a continuous nature covering many tens of thousands of years. This is a unique advantage that is only associated with sediments over these long timescales. However, sedimentary records are frequently affected by the depositional processes which can sometimes make them palaeomagnetically ambiguous. A partial review of these problems associated with

sedimentary records are presented by King and Channell (1991) and Verosub (1977). These problems are also are summarised here so that an immediate comparison can be drawn with PSV records from speleothems.

The processes of sedimentation are such that magnetic grains within a sedimentary sequence do not necessarily remain aligned with the ambient geomagnetic field at the time of deposition (Verosub, 1977). The magnetisation in many sedimentary records is therefore a post-depositional detrital remanent magnetisation (pdDRM; section 3.7.3). A magnetic grain aligned with the ambient field while in fluid suspension may, upon settling, be re-oriented by the geometry of the substrate. The degree of re-orientation depends somewhat on grain shape but usually causes sediments to record remanent inclinations that are shallower than the ambient field (Levi and Banerjee, 1990). In addition, there will be some unknown lag in time between deposition on the substrate and the point when grains cease to physically rotate, termed 'lock-in depth'. Lock-in occurs at a depth where the degree of compaction prevents further rotation of magnetic grains and is a function mainly of sedimentation rate. Thus, between settling and lock-in, grains are free to rotate into alignment with the ambient field (McIntosh, 1993; Tauxe and Kent, 1984; Verosub, 1977). It is also possible for sediments to be disturbed below the lock-in depth. The compaction process may cause pore waters to migrate initiating further movement and re-alignment of some magnetic grains. Occasionally, mathematical deconvolution functions have been employed in an attempt to account for post-depositional disturbances (Hyodo *et al*, 1993).

Benthic organisms in the upper layers of sediments can additionally re-work the sediment fabric; termed bioturbation. Furthermore, microcellular organisms (sulphate-reducing bacteria) that live in sediments have been shown to produce biogenic magnetite and siderite (Lovely *et al*, 1993; Moskowitz *et al*, 1989). The contribution to the total remanence in a sediment from these magnetic minerals is a relatively unexplored facet of palaeomagnetism but recent work has suggested that it can completely overprint the remanence from detrital grains (Maher and Taylor, 1988; Karlin *et al*, 1987).

The physical effects of sampling on the sediment fabric must also be considered. The entry of the core barrel and subsequent sub-sampling may introduce unknown disturbances into the records. However, multiple coeval sub-sampling can lessen these effects when working with larger diameter cores. In addition, the attitude of the core barrel at depth may be unknown and it is often not possible to orient cores with respect to the azimuth.

Constraining a sedimentary PSV record to a timescale is normally achieved using calibrated ^{14}C methods, effective up to around 30 ka. However, the accuracy of the ^{14}C dating method is affected by the presence of 'old' carbon which can be a problem when dating young sediments (Aitken, 1990). In older records comparison of the pollen assemblage to the marine oxygen isotope records is often used (for example Thouveny *et al*, 1990).

The ability for speleothems to record PSV reliably has been demonstrated in several studies (for example Lean *et al*, 1995; Perkins and Maher, 1993; Morinaga *et al*, 1989; Latham *et al*, 1987, 1989). These studies have unequivocally shown that speleothems have the potential to record PSV of a comparable resolution to sediments but without many of the problems outlined above. The main attractions of speleothems as recorders of PSV are that in contrast to sediments they do not suffer the remanence lock-in depth problem (Latham *et al*, 1986), can be accurately oriented prior to removal from the cave and do not appear to contain inclination errors (Lean *et al*, 1995; Perkins and Maher, 1993; Latham *et al*, 1989). They can also grow continuously (with some exceptions) but they are unlikely to contain such long PSV records as do sediments. Instead, longer records can be built up from multiple overlapping records collected from the same locality. Speleothems also appear to record the ambient field instantaneously during crystallisation which perhaps makes them one of the most important sources for obtaining absolute records of PSV (Latham and Ford, 1993; Latham *et al*, 1986).

Dating of speleothem PSV records is normally performed using the uranium-thorium disequilibrium method and alpha-spectrometry up to the dating limit of 350 ka (Ivanovich and Harmon, 1992). This dating method is relatively rapid, inexpensive and

methods have been developed to correct for contamination from detritally derived isotopic components (Kaufman, 1993; Schwarcz and Latham, 1989; Ku and Liang, 1984). Recent advances in the sensitivity of mass-spectrometers now allows very high resolution dating up to 500 ka with minimal errors ($\leq \pm 1\%$) and can help to reduce the effects of detrital contamination (Li *et al*, 1989).

1.2. Thesis objectives.

Currently, the main aims in speleothem palaeomagnetic research are to acquire and compare speleothem PSV records from similar locations in order to ensure repeatability, and to expand the global extent and time-span of such sets of records. Thus, the objectives of this thesis were to collect a number of contemporaneously growing speleothems of Holocene age from in China and Spain. From each of these speleothems it was hoped to produce a record of palaeosecular variation which could be dated absolutely using uranium-series disequilibrium. Rock magnetic studies would then constrain the types of magnetic carriers of remanence and give some clues as to the likely mode of remanence acquisition as this is still not a settled issue. With this achieved it would then be possible, for each site, to compare the individual PSV records on a known timescale thus assessing the fidelity of the recording process and to gain information on the local palaeofield. Comparisons could then be made on a wider scale with PSV records from differing sites and materials. Thus, inferences on the fidelity of speleothem records could be made.

1.3. Structure of the thesis.

This thesis is divided into nine chapters. Chapters 2 and 3 provide essential background information on the Earth's magnetic field, basic rock magnetic theories and demagnetisation methods. Chapter 4 presents a detailed account of the uranium-series disequilibrium dating and includes information on U-Th dating, alpha-spectrometry, methods to deal with detrital contamination when dating calcite samples and also details

the ^{210}Pb dating technique tested on one speleothem collected in this study. At the beginning of Chapter 5 a brief synopsis is included on the findings of previous speleothem workers. The remainder of Chapter 5 covers the methods of field sampling, sample preparation and sub-sampling of speleothems and also describes the palaeomagnetic methods used to obtain directions from individual sub-samples. Chapters 6 and 7 present the demagnetisation characteristics, uranium-series dating, and palaeomagnetic results from each speleothem from China and Spain respectively. The overall interpretations of the speleothem PSV records and comparisons with other contemporaneous PSV are made at the end of each results chapter. Chapter 8 presents the rock magnetic data from both the Chinese and Spanish speleothems and compares the carriers of remanence to those found in previous speleothem studies. Conclusions using the palaeomagnetic, dating and rock magnetic results from Chapters 4 and 6 to 8 are made in Chapter 9. Suggestions for future studies on speleothems based on this work are included at the end of Chapter 9. Appendices A to I contain data on the palaeomagnetic directions, susceptibilities and NRM intensities of sub-samples from each speleothem. Appendix J contains the uranium-series chemical procedures and a detailed description of the electroplating method adopted after experimentation during this study. Appendix K contains the raw data from the leachates analyses from several sub-samples from the Chinese speleothems.

2. Characteristics of the Earth's magnetic field.

This chapter briefly introduces the basic properties of the Earth's magnetic field of which an awareness is required in a palaeomagnetic study of this nature.

2.1. Introduction.

Some of the first recorded scientific investigations were studies on the behaviour of the Earth's magnetic field (Needham, 1962). More recently, studies of the Earth's field have been made on three broad fronts. The first covers the **geomagnetic field** itself and its long term changes, for example, secular variation, excursions and reversals. The second front is the study of plate motions and reconstructions using palaeomagnetic methods. Finally, there is the most complex branch; that of the mathematical modelling of the field's behavioural patterns based on historical and ancient data and of trying to explain its origin in the Earth's fluid core.

Our understanding of the long term behaviour of the Earth's magnetic field is limited by the fact that instrumental data exists only for the past four centuries. Other sources of data are needed to extend coverage beyond this point. Two sources of information are generally used; evidence from ancient civilisations (archaeomagnetism) and evidence left as a result of natural geological processes (palaeomagnetism). Rock magnetism is used to illustrate the types of magnetic minerals present and their ability to acquire and record the geomagnetic field under varying temperatures and ambient field directions. Rock magnetism is discussed in Chapter 3.

The Earth's magnetic field is generated within the liquid outer core from the flow of electric currents and this process is termed the geodynamo (section 2.6). Detailed description of these processes is beyond the scope of this thesis, but the reader can refer to Merrill and McElhinny (1983) or Tarling (1983) for a general theory. In order to describe the magnetic field mathematically the most frequently used tool is spherical

harmonic analysis. This technique is suitable when the quantities of interest lie on the surface of a sphere. The reader is referred to Chapman and Bartels (1940, 1962) and Merrill and McElhinny (1983) for further details.

2.2. The geomagnetic field.

The present-day magnetic field of the Earth can be represented, to a first approximation, by a geocentric axial dipole inclined at 11.5° to the geographic axis. The **geomagnetic poles** are defined as the points where a line extended through the dipole axis intersects the Earth's surface. Accounting for approximately 90% of the present internal field, the **dipole field** is the dominant field source, the remaining 10% is ascribed to the **non-dipole field**. The non-dipole field comprises of drifting and non-drifting components (Tarling, 1983; Yukutake, 1993). It is generally assumed that when the combined effects of the dipole and non-dipole fields are averaged over long periods of time, they approximate to a **geocentric axial dipole field (GADF)** i.e. the magnetic poles, to a first approximation, coincide with the Earth's spin axis. Both the dipole and non-dipole parts of the field change over time. Changes with periods less than a year are thought to be external in origin (due to magnetic storms in the ionosphere) whilst periods of 1 - 10^4 years are due to internal sources (Chapman and Bartels, 1951). These long term changes are termed **palaeosecular variation,** henceforth shortened to **PSV.**

In order to describe the magnetic field at a point on the Earth's surface the total intensity (F), declination (D) and inclination (I) are measured. These elements and their relationships are shown in Figure 2.1. Declination is considered to be positive eastwards and inclination positive (negative) in the northern (southern) hemisphere.

Secular changes in the components of the magnetic field are often illustrated using isomagnetic charts. These charts show equal values of a magnetic element at some instant in time connected by contours. For example, Figure 2.2 shows the changes in the vertical component of the non-dipole field between 1929 and 1980 (Merrill and McElhinny, 1983).

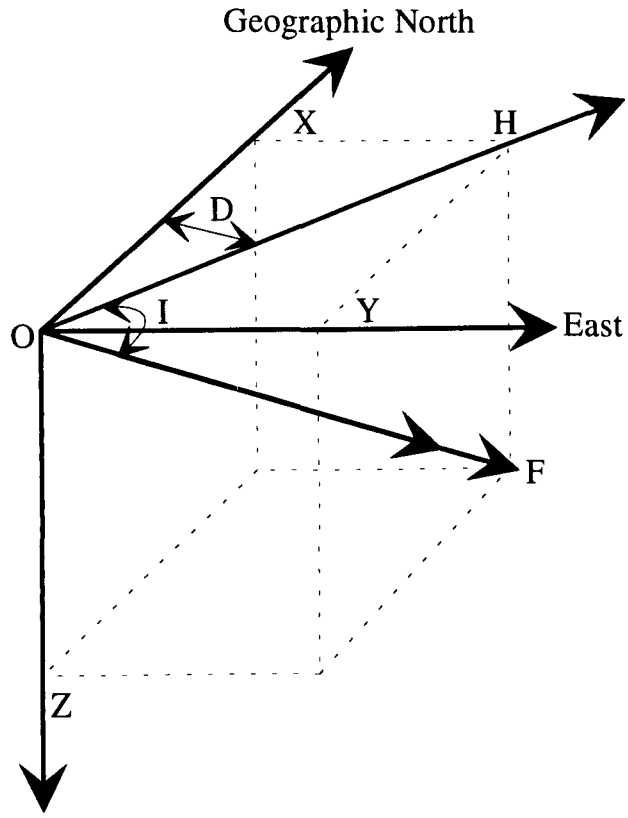

Figure 2.1. Main elements of the geomagnetic field. D = Declination, I = Inclination, F = Total Intensity. The horizontal component of the field is calculated by $H = FCos\ I$ and the vertical component by $Z = FSin\ I$. From Merrill and McElhinny (1983).

2.3. Secular variation recorded on the historical timescale.

PSV is a complex phenomenon and is derived from a number of interacting and transitory magnetic fields whose effects combine to produce locally and globally recognisable field patterns. It is generally assumed that dipole and non-dipole elements of the field are linked as both are produced from complex fluid motions in the outer core. Historical records from the past 400 years, although of poorer quality than modern observatory records, have been used extensively to gain information on PSV. This section highlights the main features that make up the PSV.

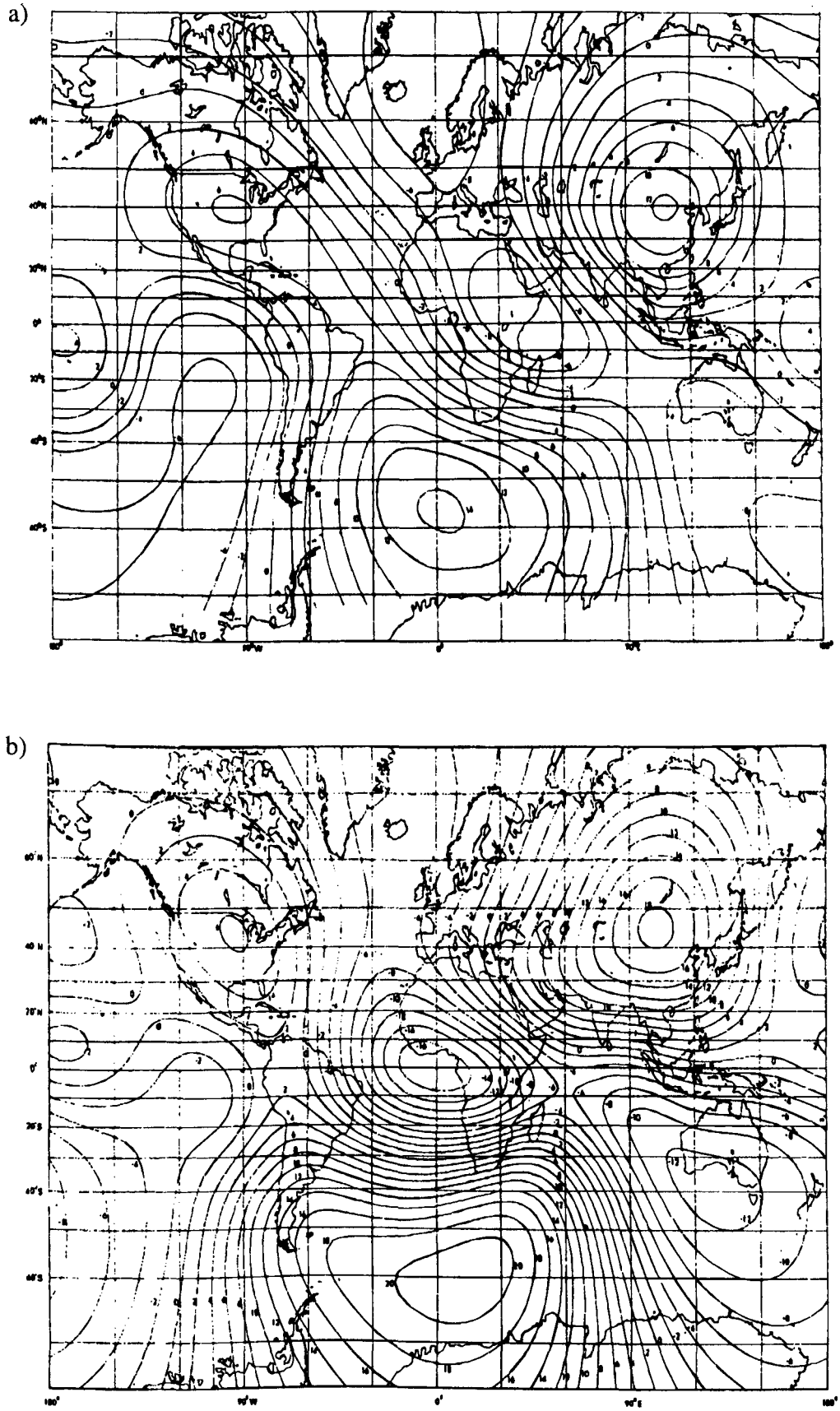

Figure 2.2. Vertical component of the non-dipole field for a) 1929 and b) 1980 with contours in units of 2000nT (from Merrill and McElhinny, 1983).

2.3.1. Decrease in the moment of the magnetic dipole.

Since Gauss' analysis in 1838 the moment of the dipole field as a whole has decreased at a rate of approximately 5% per century (Leaton and Malin, 1967). Should this trend continue the dipole field would decay to zero in a further 2 ka (Figure 2.3).

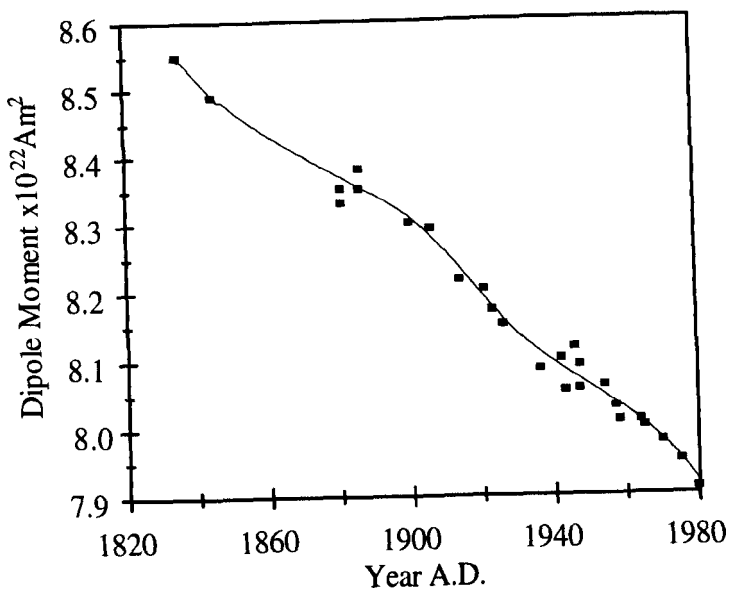

Figure 2.3. Variation of the dipole moment with time from successive spherical harmonic analyses since Gauss. From Merrill and McElhinny (1983).

2.3.2. Drift of the dipole field.

Over the past 150 years the total dipole field intensity, F, has increased (decreased) in the northern (southern) hemisphere. This has occurred in conjunction with the decrease of geomagnetic field moment. These tendencies have been interpreted as a northward shift of the geomagnetic dipole at a rate of 2 km/yr (Nagata, 1965).

2.3.3. Precessional rotation of the dipole.

Over the past 160 years time series data obtained from spherical harmonic analysis of the geomagnetic field components have shown evidence for westward drift of

the dipole. Calculated drift speeds of the order 0.05° of longitude per year show that although the azimuthal angle of the dipole axis has changed, its polar angle has remained constant. This is a major characteristic of PSV (Nagata, 1965).

2.3.4. The westward drift of the non-dipole field.

Early knowledge about westward drifting of the main features of the Earth's field were demonstrated by Halley (1692). He stated that a point of zero declination moved 23° from Cape d'Agulhas to the meridian of St. Helena in 90 years (a drift rate of 0.26°/yr). Bauer (1895) estimated drift rates of 0.08° to 0.26°/yr using the movement of the agonic lines (declination = 0). From these studies it is evident that westward drift has persisted during the last few centuries (Burlatskaya *et al*, 1965).

Based on the initial work by Vestine *et al* (1947), Bullard *et al* (1950) quantitatively confirmed the westward drift of the non-dipole field using the spherical harmonics from data for the epoch 1907 to 1945. They calculated that the average westward drift rate was 0.18°/yr. Thus, the non-dipole field would circuit the Earth in 2 ka a period which was originally thought to be sufficient to average out PSV. Many subsequent studies have also estimated mean westward drift rates of the order 0.2°/yr during the last century (Yukutake, 1993, 1962; Yang *et al*, 1993; Nagata, 1965; Adam *et al*, 1964). Yukutake (1962) also pointed out that the main features of historically recorded PSV in London, Paris and Tokyo all had drift rates of around 0.4°/yr.

2.3.5. Standing and drifting non-dipole components.

Approximately half of the drifting features exhibited by the non-dipole field cannot be explained by the westward drift alone. Drift rates of some features are found to be around 0.3°/yr; greater than the established rate of non-dipole drift (Yukutake, 1967, 1970; Yukutake and Tachinaka, 1969). It is also very clear from examination of non-dipole field anomalies over time that not all features are drifting. For example, measurements of the Mongolian Anomaly located over the Asian continent, show that its location has been constant for the past 200 years whilst its intensity and areal extent have

increased. Gubbins and Kelly (1993) used observatory data to model field behaviour and suggested that the Mongolian anomaly, and other anomalies, have been in existence in some form at similar locations over the last 2.5 Ma.

Yukutake and Tachinaka (1969) account for the rapid drift of non-dipole features by separating the non-dipole field into two components. The *drifting* part of the non-dipole field migrates westwards at a little over 0.3°/yr whilst the effect of the *standing* part lowers the mean rate of drift to 0.2°/yr. This would suggest that, during certain epochs, the standing field will be intensified by the superimposition of a drifting field and subsequently weakened by its continued westward drift. The global pattern of the non-dipole field from the seventeenth century to present could be attributed to this effect.

There is some argument that this arbitrary separation is not physically meaningful and indeed some features of non-dipole activity cannot be explained by the two component model. Dodson (1979) suggests that some of the drifting parts of the non-dipole field may be obscured by the present configuration of the standing and drifting foci. This may have the effect of masking contributions from these weaker anomalies and thus make interpretation tenuous. Indeed the addition of a small eastward drifting component can account for some of the recorded features of PSV (Yukutake, 1979).

Yukutake (1968) estimated the free decay time of the non-dipole field to be of the order of 7 ka. Therefore, potential exists for non-dipole field anomalies to have been influential during historical observations. It is therefore possible that individual anomalies may exist in excess of 2 ka; a period which is insufficient to average out the effects PSV. For example, Cox and Doell (1964), Yukutake (1993) and Peng and King (1992) suggest that, from studies on the palaeomagnetic behaviour of lavas in Hawaii, the present low rates of secular change in the Pacific have endured during the past few million years.

2.4. Palaeomagnetic records of secular variation.

Records of PSV from historical data show field behaviour for the past 400 years. The question of whether these records are representative of PSV through geologic time has to be answered using different techniques. Archaeomagnetic and palaeomagnetic records have the potential to provide the data which reveal ancient field behaviour beyond 400 years. Unfortunately, the geographic distribution of these records is not uniform, with a general bias to greater coverage in the northern hemisphere.

The quantity of PSV data from some areas have allowed the construction of palaeomagnetic master curves; data compiled from contemporaneous records covering specific geographic areas. Data from these master curves have been used to estimate secular changes in declination and inclination and/or intensity over wide areas and to highlight the differences between them. For example, archaeomagnetic master curves covering the past 10 000 to 15 000 years (^{14}C dating) are available for Bulgaria (Kovacheva, 1980), Paris (Thellier, 1981) and South-western USA (Eighmy, 1991).

The majority of records are from rapidly and continuously deposited lake sediments and these have been used to characterise the directional behaviour of the geomagnetic field from present to in excess of 50 ka. Records such as these have been obtained from European lakes such as Windermere (Thompson, 1975), Lac du Bouchet (Creer, 1989) and from North American lakes such as the Great Lakes (Creer and Tucholka, 1982) and Thunder Bay (Mothersill, 1979).

Using global palaeointensity data obtained from lavas and baked clays, the average geomagnetic dipole moment has been estimated back to 12 ka. (McElhinny and Senanayake, 1982). These data showed that the decrease in the dipole moment, seen in historical times, can be traced back to 2.5 ka when it began to decrease. (Figure 2.4).

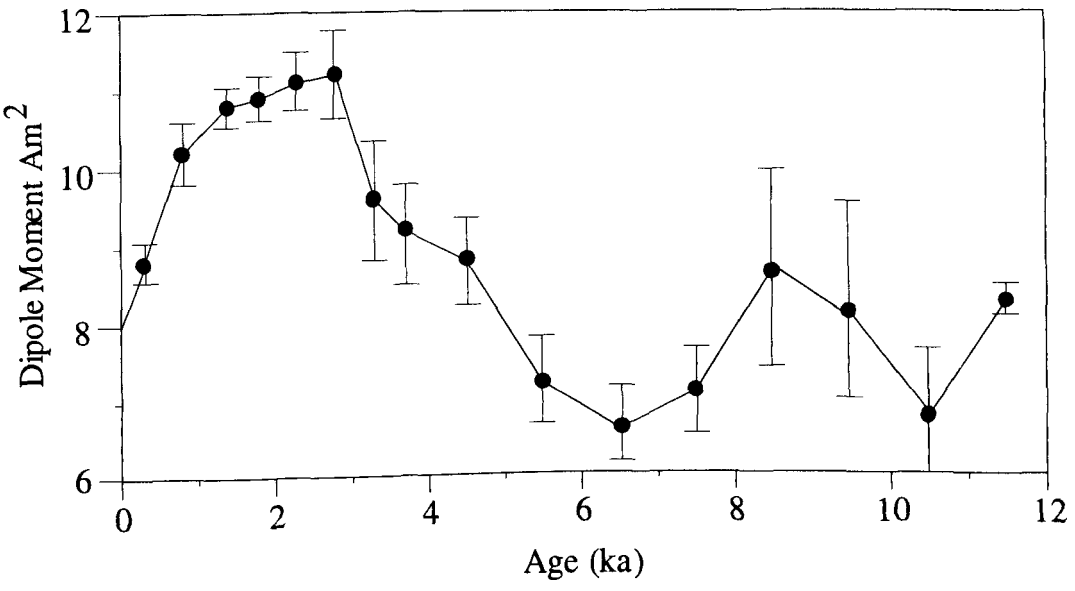

Figure 2.4. Global average dipole moment over the past 12 Ka (after McElhinny and Senanayake, 1982).

Despite problems associated with depositional and post-depositional effects which can affect the PSV recorded in sedimentary sequences, they generally offer the highest resolution and most continuous records (for example Levi and Karlin, 1989). Marine deep-sea sediments have been used for data over the 10^6 year time scale.

Westward drift of non-dipole anomalies, which are so apparent in historical records, can also be identified in palaeomagnetic records. This has been achieved by the estimation of the time-lags between dated PSV features at sites of the same latitude. A recent study using this technique was made by Yang *et al* (1993) who tracked the migration of a non-dipole anomaly from China to Greece using archaeointensity data. They estimate that the lag between palaeointensity maxima and minima in China and Greece is 800 years and infer a westward drift rate of 0.13° per year.

The sense of drift within a continuous palaeomagnetic record is frequently deduced from the construction of **Virtual Geomagnetic Poles** (**VGPs**). A VGP is a representation of the geomagnetic north pole on the surface of the Earth at particular

instant in time, derived from declination and inclination (Merrill and McElhinny, 1983). Since a VGP is a 'spot reading', successive calculations of VGP positions from, say, a lake sediment sequence, will show progression of the pole over time. According to Runcorn's rule (1959), a clockwise (anti-clockwise) precession of the VGP path indicates that westward (eastward) drift has occurred. However, re-analysis of Runcorn's rule by Skiles (1970) and Dodson (1979) have shown that under some conditions anti-clockwise rotation of the VGPs can occur even though the apparent drift is to the west.

Generally, over the past 10 ka, the westward drift appears to have predominated compared with eastward drift. There are however, notable exceptions including eastward drifting in the British master curve between 1.1 and 0.6 ka (Turner and Thompson, 1981) and in N. American lake records between 20 and 8 ka (Lund, 1983). Using computer synthesis of PSV, Creer (1983) suggested that eastward drift can be caused by the interference of two or more standing non-dipole sources which fluctuate in intensity.

2.5. Reversals and excursions of the geomagnetic field.

Although field excursions and reversals are not encountered in this study they are discussed so that the full range of geomagnetic field behaviours have been covered. Two of the most striking features of recorded field behaviour are the ability of the Earth's field to deviate beyond the bounds of 'normal' PSV (approximately ±40°), termed **excursions**, and to periodically invert its polarity state, **reversals**.

2.5.1. Excursions of the field.

Excursions of the geomagnetic field are said to have occurred when the geomagnetic field leaves its near axial position and migrates equatorially before returning. This migration is usually in excess of 40° in latitude (Barbetti and McElhinny, 1972). The duration of an excursion is usually of the order of 10^2 - 10^3 years, a relatively short time geologically, and it is suggested that they are 'failed' or 'aborted' reversals

(Hoffman, 1986). Their short duration and apparently localised nature means that they are rarely recorded in other contemporaneous records.

Several field excursions within the Brunhes chron (the past 720 ka) have been well documented. The best examples are the Mono Lake Event at 30-25 Ka (Denham and Cox, 1971) and the Blake Event at 120-110 ka which have also been identified over a wide geographic area (Petrova and Pospelova, 1990).

2.5.2. Reversals of the field.

Evidence for periodic inversions of the Earth's field polarity were discovered in rocks of identical age that had magnetisation directions opposed to the present magnetic field (Mercanton, 1926). Subsequently, the polarity timescale has been extended back to 170 Ma using lavas from the sea-floor spreading centres (Cox, 1982) and further using marine magnetic anomaly data

The geomagnetic record on a geologic timescale reveals periods of long-term constant polarity, called **chrons**, lasting 10^5-10^6 years and shorter periods of field reversal within each chron termed **sub-chrons**. Chrons and sub-chrons are of normal or reversed polarity; the current field configuration is regarded as normal. The frequency of field reversal has increased rapidly and symmetrically since the Cretaceous quiet period when the field was a constant normal polarity from 107-85 Ma (Jacobs, 1984).

It is generally accepted that a polarity reversal is preceded by the decay of the field intensity to 10-25% of its original value. Early models attempted to describe the reversal in terms of the decay of the dipole field to zero and its subsequent build up in the opposite sense (Creer and Ispir, 1970). If the field becomes dominated by non-dipole terms during a reversal, we might expect the transitional field at a number of widely separated sites to show a wide variety of behaviours; the result of the influence of different non-dipole elements. This hypothesis of transitional field behaviour is supported by data from lavas (Prévot and Camps, 1993), but records from sediments tell a contradictory tale. Tric *et al* (1991) and Laj *et al* (1991) demonstrate that widely

separated sedimentary records of the same reversal show similar transitory behaviour. When sequential field directions are represented by VGPs, the paths that they trace show confinement to two antipodal bands of longitude over the Americas and Eastern Asia. Clearly, if the westward drift of the non-dipole field were dominant during a reversal, then this could not occur. The effects of smoothing on sedimentary records and the discontinuous nature of lava records has lead to considerable argument as to which process provides the more reliable record. It is argued that the preferred bands of longitude shown by transitional VGPs from sedimentary sequences are artefacts of the pre- and post-reversal VGP positions due to post-depositional remagnetisation processes (Langereis *et al*, 1992).

The confinement of the transitional VGPs to longitudinal bands should not occur if they are influenced by the solid mantle (Gubbins, 1994). Studies such as that of Laj *et al* (1991) therefore demonstrate the effect of the mantle on the geomagnetic field during a reversal. Indeed, Gubbins (1987) suggests that the geomagnetic field is dominated by four 'hot' patches of positive flux, two situated near to each pole. Two negative flux patches exist beneath southern Africa and beneath South America which have been shown to have intensified and migrated southward. These flux patches may account for the recent decrease in the dipole moment and may be enough to periodically trigger the reversal of the field. Gubbins (1987) also suggested that the increase in the rate of reversals since the Cretaceous quiet period may be related to the growth of the African flux patch since 85 Ma.

2.6. The geodynamo.

The geodynamo is the driving force behind the Earth's magnetic field. The field itself is generated within the fluid outer core, found between 2900 and 5150 km below the Earth's surface. The outer core is mainly composed of iron with accessory nickel and other light elements (silicon, oxygen, sulphur and magnesium). It is thought that currents generated by the motion of the outer core induce the magnetic field. As these currents

are subject to free-decay there must be some mechanism of self perpetuation in order to maintain the field; this is the geodynamo (Merrill and McElhinny, 1983).

There are several suggestions available that would maintain the magnetic field at present levels. Gubbins *et al* (1979) suggest five power sources - radioactive heating by decay of ^{40}K, primordial heating and freezing of the inner core, gravitational energy release, release of energy by latent heat of crystallisation and finally precessional and tidal forcing. It is likely that a combination of these energy sources produces the geomagnetic field. However, in any model of the geodynamo the short and long term trends in the field behaviour must be accounted for. These trends may reflect changes in the core's energy balance.

The relationships between the behavioural trends of PSV and periodic reversal of the field are an important area for the development of geomagnetic field models. These models attempt to describe changes in the geomagnetic field using observational, historic and palaeomagnetic data. However, at the current time there are few models that can compare accurately with the observed behaviour of the field (Hagee and Olsen, 1991; Gubbins, 1991; Gubbins and Sarsen, 1994; Olsen, 1981). This is an area of ongoing research and its effectiveness is continually improved by the addition of more widespread palaeomagnetic data.

3. Basic Rock Magnetism.

3.1. Introduction.

Rock magnetism is concerned with the magnetic minerals in rocks and their ability to record field change over time. Particular importance is placed on the behaviour of magnetic minerals in the presence of a weak field, such as that of the earth, and the method of acquiring a remanence in such a field. This chapter is not intended to be an exhaustive account of rock magnetism but is written in order to outline the basic properties of the magnetic minerals. Where specific rock magnetic tests are performed on samples in this study the theory and the methodology behind them is covered in chapter 8. Useful texts covering rock magnetism theory and practice can be found in Stacey and Banerjee, (1974); O'Reilly (1984) and Thompson and Oldfield (1986).

3.2. Atomic mechanisms.

Two processes exist whereby electric charges can induce a magnetic field within an atom. Firstly, a spin of an electron about its axis gives rise to a **spin dipole moment**. Secondly the orbital motion of an electron about the nucleus gives rise to an **orbital electron moment** (Figure 3.1).

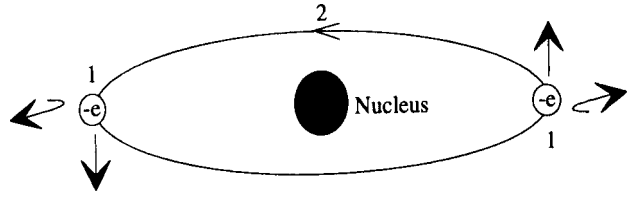

Figure 3.1. Spin dipole moments (1) and orbital electron moments (2).

The presence of an applied magnetic field imparts all substances with a magnetic moment by forcing electrons to precess about the applied field. However, the subsequent reaction to the applied field varies according to the atomic configuration in the material. The **magnetic susceptibility** (χ) of a substance can give some idea as to what type of configuration is present. It is defined as the magnetisation per unit of applied field thus;

$$J = c\chi \qquad \textbf{3.1}$$

where J is the intensity of acquired magnetisation and c is the magnetisation per unit of applied field.

If the outer electron shell is complete, the application of a magnetic field causes precession in the orbits of electrons, inducing a magnetic moment that is antiparallel to the applied field and gives a negative susceptibility. The moment is very weak and is immediately lost upon removal of the field. This property of **diamagnetism** is shown by all substances and results in a susceptibility of about 10^{-8} m^3kg^{-1}. For example, calcite shows a purely diamagnetic behaviour in an applied field.

An incomplete outer electron shell forces electron moments to align with an applied field, giving rise to **paramagnetic** behaviour. Since the moments are aligned parallel to the applied field, the net moment is much greater and produces susceptibilities of 10^{-3}-10^{-8} m^3kg^{-1}. Thermal energy at room temperature is sufficient to destroy paramagnetism when the applied field is removed.

Diamagnetism and paramagnetism are reliant upon the presence of an applied field but in some cases members of the iron group can retain a **permanent (spontaneous) magnetisation**, even after removal of the field. In these cases, spin moments of unpaired electrons in the 3d orbital shell may become coupled directly (**direct exchange**) or indirectly (**superexchange**) by an intermediate anion. Direct exchange produces moments that are either parallel or antiparallel, depending on the degree of overlap of electron orbits. Superexchange coupling affects the iron oxides,

with coupling usually achieved via an intermediate oxygen anion, producing moments that are antiparallel.

3.2.1. Ferromagnetism.

In ferromagnets, exchange couplings are parallel and no intermediate ion is required. The effect is to produce a high spontaneous magnetisation, even in the absence of an applied field. Iron is an example of a ferromagnet (Figure 3.2a).

3.2.2. Antiferromagnetism.

Antiferromagnetic minerals require an intermediate anion for successful coupling. The coupling is antiparallel and balances out, since both sub lattice moments are equal, resulting in no net spontaneous magnetisation (Figure 3.2b). Lattice defects can however, cause the antiparallel couplings to become asymmetric. In **canted antiferromagnetic** materials, the asymmetry allows a weak net magnetisation to exist. Haematite is an example of a material with this type of coupling (Figure 3.2c).

3.2.3. Ferrimagnetism.

Ferrimagnetism occurs when antiparallel coupling of the two sub lattices is unequal. This gives rise to a weak net magnetic moment (Figure 3.2d). Examples of ferrimagnetic materials are magnetite, maghemite, titanomagnetite and pyrrhotite.

These variations in magnetic behaviour are controlled by interatomic separation. The ambient temperature is sufficient to destroy diamagnetic and paramagnetic moments after removal of the applied field. In ferro- and ferrimagnetic materials a net, field off, spontaneous magnetisation can be destroyed by increasing temperature. Above a critical temperature excitation is such that the coupling breaks down, thus randomising magnetic moments. For the ferromagnets, this critical temperature is called the **Curie temperature** (T_c) whereas for ferrimagnets it is the **Néel temperature** (T_n). Above these temperatures all Fe-type materials behave paramagnetically.

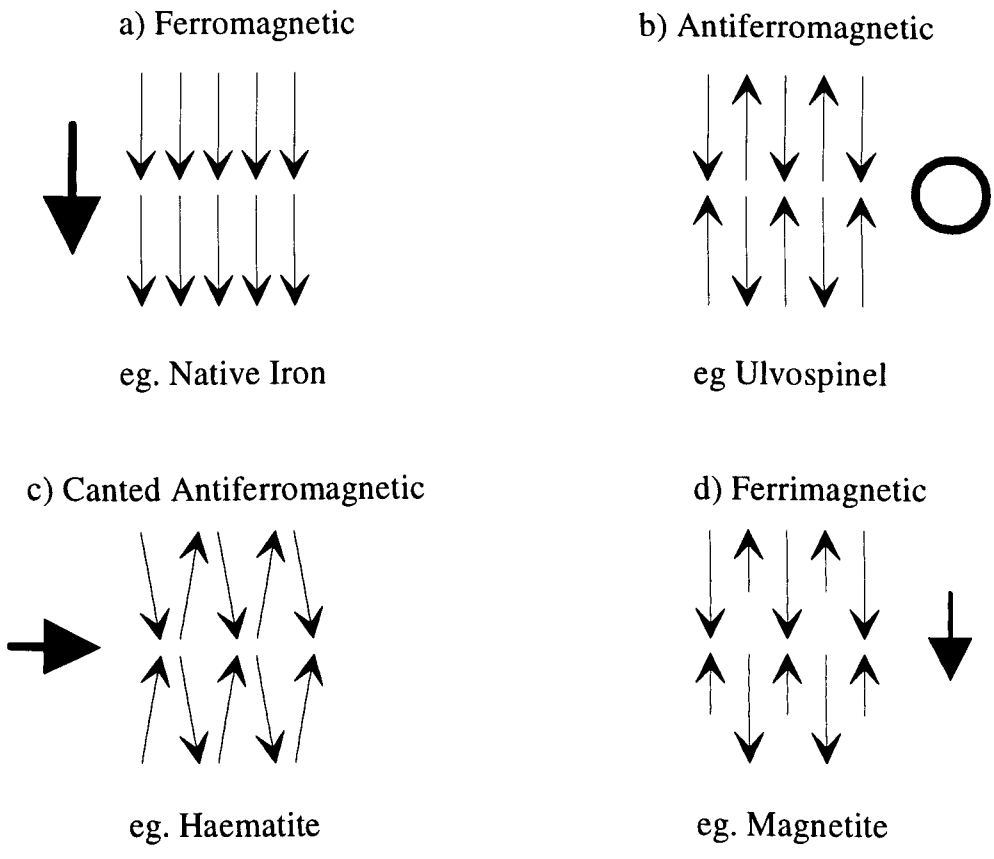

Figure 3.2. The variations in alignment of magnetic moments within a magnetic grain. The resultant moments produced by each sub-lattice configuration are shown by a large arrow.

3.3. Anisotropy.

Magnetic grains are generally easier to magnetise along one axis than another axis. This property is known as anisotropy and takes a number of forms. As energy is required to order magnetic moments, the remanence within a magnetic crystal takes a preferred orientation in the direction of minimum energy. As a result magnetisation along some crystal axes will be easier than along others, although the same degree of magnetisation can be achieved across all axes. This effect can lead to very high **coercive forces**; the field required to overcome internal forces and flip the magnetisation in to a direction with a component in the plane of the applied field. This is especially important for the magnetic minerals haematite and goethite. The resulting effect on magnetisation is called **magnetocrystalline anisotropy**.

Shape anisotropy results from the shape of a magnetic grain. Energy is minimised if magnetisation occurs along the long axis of an elongate grain. A spherical grain is equally hard to magnetise in any direction and therefore has zero shape anisotropy. Shape anisotropy is generally weak in low susceptibility minerals such as haematite but is particularly strong in magnetite.

Strain anisotropy may be produced from the effects of stress imposed on a grain. If a magnetic grain is subjected to mechanical stress, say, during compaction, the shape and structure of the grain may be permanently altered. This gives rise to **piezoremanent magnetisation**. If the grain is placed into a magnetic field then the energies maintaining the direction of magnetisation are increased, leading to the alteration of the shape of the grain; **magnetostriction**.

3.4. Magnetic domain theory.

At a certain critical grain size, the internal energy within a magnetic grain is minimised if internal magnetisations are divided into smaller volumes called **domains**. Within each domain the electron spins are coupled parallel and interactions between adjacent domains minimise magnetostatic forces so that no net magnetisation exists. Separating each domain are **Bloch walls** where spin moments from one domain rotate to that of another. The Bloch walls measure approximately 0.1 μm in thickness whilst domains themselves are of a similar size; 0.1-0.05 μm in magnetite (Stacey and Banerjee, 1974) but can be up to 1.5 μm in haematite (Banerjee, 1971). A grain which divides magnetically into more than one domain is called a **multidomain (MD)** grain.

Where grains have volumes less than the size of a domain wall, only one domain can exist, producing a **single domain (SD)** grain. Magnetisation is confined to the magnetic easy axis. **Superparamagnetic (SP)** grains are very small SD grains that have a room temperature thermal energy sufficient to destroy any permanent magnetisation. These superparamagnetic grains show a strong susceptibility when placed in a magnetic field. **Stable single domain (SSD)** grains are those in which thermal energy is

insufficient to destroy any permanent magnetisation. **Pseudo-single domain (PSD)** grains have sizes between single domain and multidomain grains and are, strictly speaking, multidomain but have single domain-like properties. SSD and PSD grains are of most interest to the palaeomagnetist as their remanences are preserved over the longest periods of time. Table 3.1 shows experimental data on domain-structure transition sizes for the most common magnetic minerals (Dunlop, 1981, 1990).

Mineral	SP - SD Transition Size (μm)	SD - MD Transition Size (μm)
Magnetite	0.025 - 0.03	0.11 - 0.28
Maghemite	-	0.06
Titanomagnetite:- x = 0.6	0.08	0.2 - 0.6
Titanohaematite:-		
x = 0.6, z = 0.4	0.05	0.75
x = 0.6, z = 0.7	0.09	2.4
Haematite	0.03	15
Pyrrhotite	-	1.6

Table 3.1. Critical SP - SD and SD - MD grainsize thresholds for the common magnetic minerals. After Dunlop (1981, 1990).

3.5. Effects of domain state on magnetisation properties.

3.5.1. Single domain grains.

In the absence of an external magnetic field, the magnetisation of a single domain grain will lie along the 'easy axis'. Application of an external field will cause the magnetisation vector of the grain to rotate in the direction of the field. If the field is sufficiently weak, the magnetisation vector will return to its original axis upon its removal. In a strong field the magnetisation will flip so as to lie along the easy axis that

has a component in the direction of the applied field. Removal of this applied field leaves the magnetisation in a new configuration. In a strong field, the change in direction may be immediate but in weaker fields may take longer since a large amount of energy is required to flip the magnetisation. In time the magnetisation reverts to the direction of the later field. This is called the **relaxation time** and is discussed further in section 3.7.4.

3.5.2. Multidomain grains.

If an external field is applied to a multidomain grain its domain walls will move in a direction that favours the growth of domains having magnetisations closest to that of the external field. The domain walls move past lattices defects, that act as energy barriers, as the field strength increases (**Barkhausen Jumps**). When the field is removed the internal energy may be insufficient to move the domain walls back past the imperfections and this results in a permanent magnetisation (Figure 3.3). An **isothermal remanent magnetisation (IRM)** has been imparted if, at a constant temperature, domains aligned with the external field remain aligned after its removal. If, at a particular strength of field, all possible domain movement has occurred, **saturation (Ms)** is achieved. Upon removal of the field; the remaining magnetisation decays to the **saturation isothermal remanent magnetisation (Mrs)** due to thermal agitation.

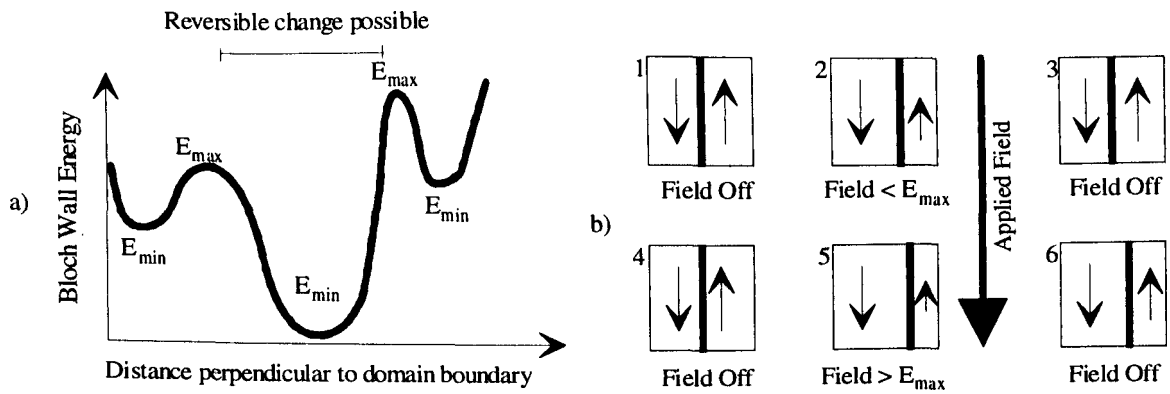

Figure 3.3. a) Effects of applied field on Bloch wall movement in MD grains. E_{min} represents the minimum energy positions of the wall, whilst E_{max} represents the energy required to prevent the return of domain walls to their original positions after removal of the field. After Thompson and Oldfield (1986). b) Diagrams representing domain volumes when, 1-3, field does not exceed E_{max}, and, 4-5, when E_{max} is exceeded.

3.5.3. Hysteresis properties of single and multidomain grains.

The application of external fields to both SD and MD grains defines some important rock magnetic properties. By applying a field first in one direction, then the other and back again, a hysteresis loop is produced. Figure 3.4 shows a typical hysteresis loop and the commonly measured rock magnetic parameters.

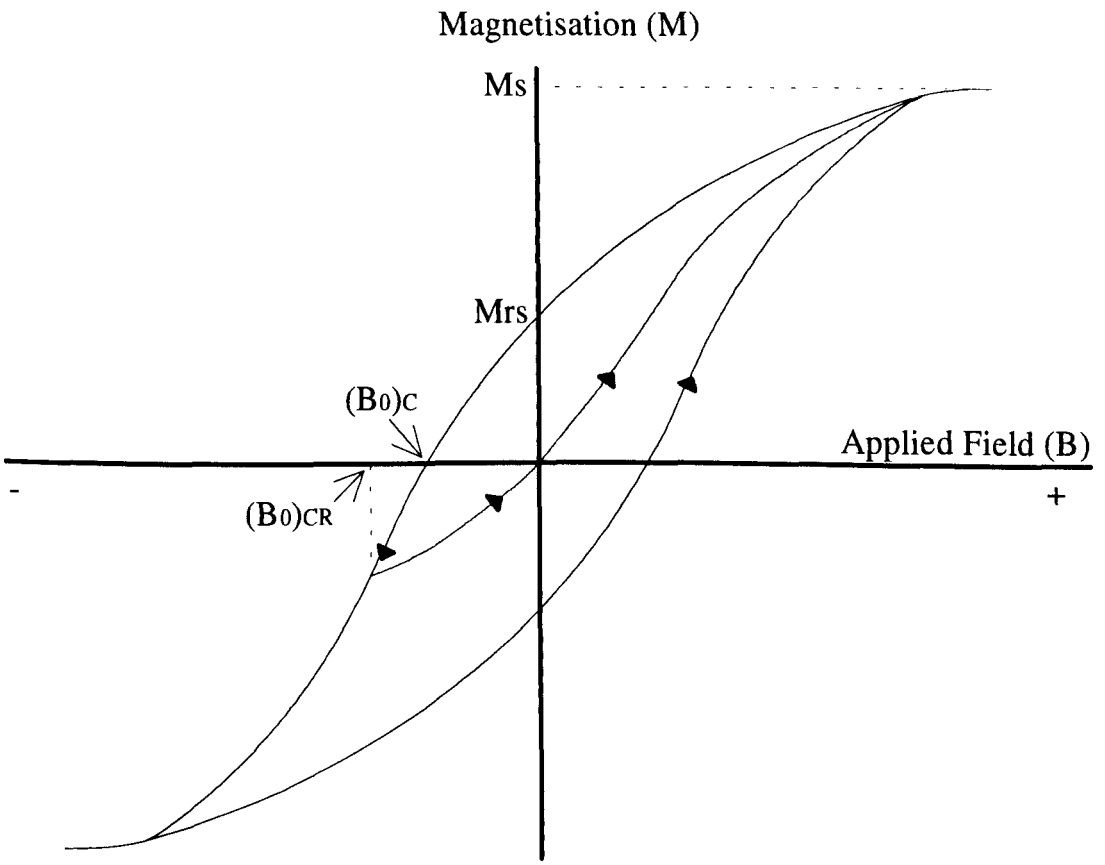

Figure 3.4. A typical hysteresis loop and some of the rock magnetic parameters that can be defined from it. Ms is the saturation magnetisation, the magnetisation induced in a large (>1 Tesla) field. Mrs is the magnetisation remaining after removal of a saturating field. (Bo)c is the 'backfield' required to reduce magnetisation zero in its presence. (Bo)cr is the field required to completely remove remanent magnetisation in field off conditions.

The relevance of Ms and Mrs, defined in section 3.5.2, are depicted clearly in a hysteresis loop (Figure 3.4). Two other useful parameters are also shown. **(Bo)**$_C$ is the value of the reverse field required to reduce the magnetisation to zero in its presence. This point is referred to as the **coercivity**. The field required to remove the magnetisation and leave no remanence in zero applied field is termed the **coercivity of remanence (Bo)**$_{CR}$.

Application of a field parallel to the easy axis of a SSD grain will produce a square hysteresis loop since there will be no effect until the internal energy is overcome and a sudden jump to saturation occurs. A field applied perpendicularly to a SSD grain produces a magnetisation that is lost on removal of the field and produces a linear hysteresis loop i.e. zero hysteresis. More commonly, a collection of randomly oriented SSD grains produces a loop of intermediate shape. A hysteresis loop produced by a randomly oriented collection of MD grains will be similar to that produced for SSD grains. However, a MD hysteresis loop will be narrower than a SD loop because the induced magnetisation is from movement of domain walls rather than from rotation of a single moment and requires less energy.

The ratio of Mrs and Ms in a sample can help to identify which domain states are present. Assuming an equidimensional, random orientation of SSD grains Mrs/Ms = 0.5, MD grains Mrs/Ms = 0.02 and SP grains Mrs/Ms = 0 (no hysteresis). Mixtures of SD and MD will produce intermediate Mrs/Ms ratios and, in extreme cases of mixing, can produce constricted hysteresis loops (Thompson and Oldfield, 1986).

3.6. Properties of the common magnetic minerals.

The largest sources of magnetic minerals are from the erosion and weathering of volcanic and plutonic rocks of the earth's crust. Compositions of the most common magnetic minerals, the iron oxides, are derived from varying proportions of FeO, TiO_2 and Fe_2O_3. The varying compositions of the iron oxide minerals are easily depicted on a ternary diagram as in Figure 3.5.

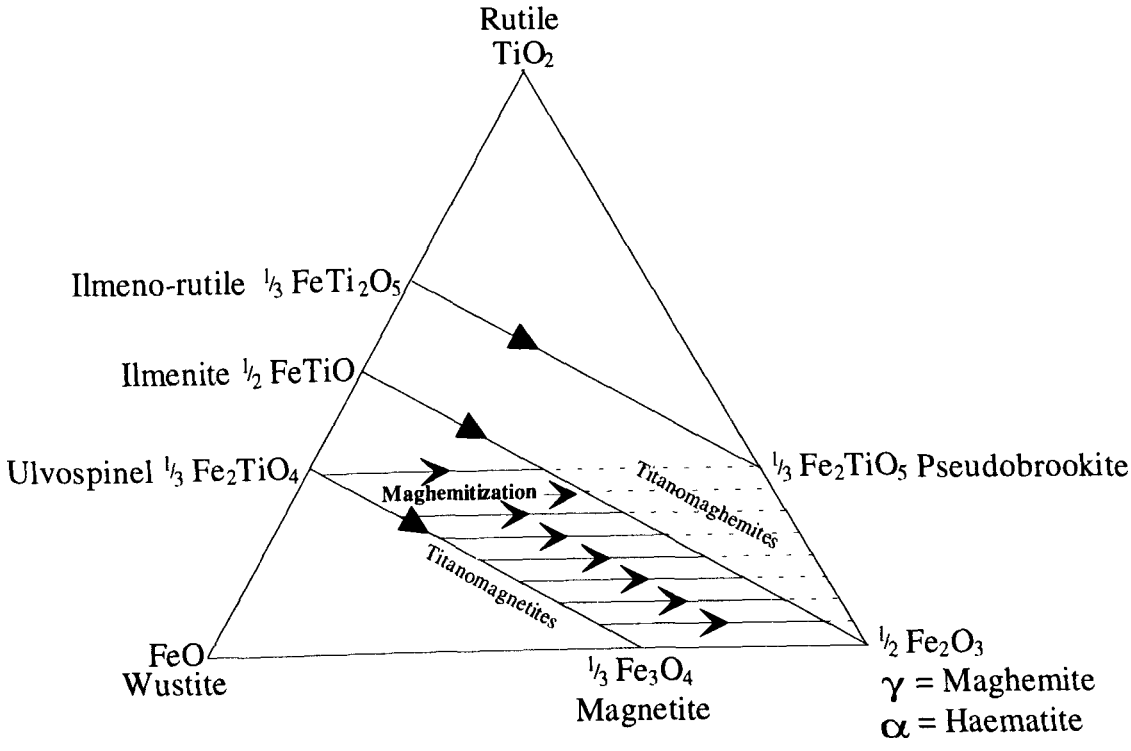

Figure 3.5. The FeO - TiO_2 - Fe_2O_3 ternary diagram showing compositional possibilities for the iron oxide magnetic minerals.

Upon crystallisation from a magma, magnetic minerals lie on the ulvospinel - magnetite solid solution series. Oxidation during geological time changes the compositional trend to the right of the diagram and downwards. The most stable end-product of oxidation is haematite, αFe_2O_3, and is, ultimately, likely to be a common magnetic mineral in many sedimentary rocks.

3.5.1. Magnetite and the Titanomagnetites.

The **titanomagnetite** group has two end members, the essentially non-magnetic **ulvospinel** ($\frac{1}{3}Fe_2TiO_4$) and **magnetite** ($\frac{1}{3}Fe_3O_4$). The titanomagnetite series forms a solid-solution series at temperatures in excess of 800°C. Intermediate compositions can result from quench cooling in an oxygen-poor environment. Generally this results in compositions in the range $0.75 > x > 0.45$ (where x is the Ti content). With greater Ti

content the Curie temperatures and saturation magnetisations decrease due to the increase in unit cell size and weakening of exchange interactions.

Magnetite is the product of cooling conditions, where deuteric oxidation occurs. It contains no titanium and is the most common magnetic mineral, occurring in primary or secondary form in igneous, sedimentary and metamorphic rocks. In appearance it is cubic (face centred), with the inverse spinel structure. A unit cell contains thirty two O^{2-} sites, eight tetrahedral sites Fe^{2+}, and sixteen octahedral sites shared uniformly between Fe^{2+} and Fe^{3+} cations (O'Reilly, 1984).

Magnetite is ferrimagnetic at temperatures below its Curie temperature of 575°C and has a spontaneous magnetisation of 92 $Am^2 kg^{-1}$. For single domain magnetite of ~ 0.7 μm, maximum coercivity is around $2x10^{-1}T$. Most theoretical parameters assume euhedral magnetite crystals, though, many magnetite crystals were constrained by the space available during growth. This results in the effects of shape anisotropy being much greater than magnetocrystalline anisotropy, making coercive forces greater than those for euhedral crystals. At temperatures, below -155°C, the crystal structure changes to orthorhombic, destroying magnetisation within MD grains but leaving SSD and PSD grains unaffected (Merrill, 1970; Ozima and Ozima, 1964). This produces a characteristic change in magnetisation, the Verwey transition (Verwey and Haayman, 1941).

3.5.2. Maghaemite and the Titanomaghaemites.

The **titanomaghaemites** form the partially oxidised spinel group (Figure 3.5) whilst its common member, maghemite, represents the extreme of low temperature oxidation. It has the same chemical composition as haematite with the spinel structure of magnetite of which it is a daughter. Its chemical formula is given by γFe_2O_3 to differentiate it from haematite (αFe_2O_3). Maghaemite oxidises by diffusion of cations to the surface of the crystal leaving $\frac{1}{9}$th of the cation sites vacant. Within the titanomaghaemite group, Curie temperatures increase with increased oxidation, maghaemite itself having a T_c of 640°C. Spontaneous magnetisation also increases with

oxidation from 70 $Am^2 kg^{-1}$ to ~ 85 $Am^2 kg^{-1}$. When heated in air, maghaemite inverts to haematite at temperatures of 250 - 350°C (O'Reilly, 1984) although temperatures as high as 600°C have been reported (Sidhu, 1988). This inversion is accompanied by a 99% decrease in spontaneous magnetisation.

3.5.3. Haematite and the Titanohaematites.

The **titanohaematites** have compositions with end-members **ilmenite**, **$FeTiO_3$**, and **haematite**, **αFe_2O_3** (Figure 3.5). Solid solutions are formed over 900°C but intermediate compositions are rare since quench-cooling is required. Titanohaematites have a corundum structure with a hexagonal close-packed lattice of oxygen ions with Fe and Ti ions held within the interstices.

Haematite is the most common of the titanomaghemites and is equally common in igneous, sedimentary and metamorphic rocks. Deuteric oxidation of titanomagnetite, reheating of titanomaghemite, and prolonged oxidation of magnetite at ambient temperatures can all lead to its production in significant quantities. Secondary formation can also occur by the dehydration of oxyhydroxide minerals (eg goethite, $\alpha FeOOH$) and by the precipitation from iron-saturated solutions in pore spaces (eg 'redbed' colouration). Haematite has a canted antiferromagnetic atomic configuration (Figure 3.2), producing a weak spontaneous magnetisation of 0.4 $Am^2 kg^{-1}$ and a Néel temperature of 675°C for pure bulk haematite (O'Reilly, 1984). Low temperature properties are characterised by a change in magnetic ordering at -10°C, where the mineral becomes totally antiferromagnetic and has virtually no spontaneous magnetisation. The properties of haematite are particularly grain-size dependent, exemplified by its coercivity. SD haematite grains of 1 - 3 μm have coercivities of up to 7 T whilst grains less than 0.2 μm are virtually non-magnetic (O'Reilly, 1984). Haematite in small volumes is difficult to detect, but since its coercive force and equivalent Curie temperatures are far greater than magnetite, it is a highly stable mineral.

3.5.4. Iron sulphides.

Pyrrhotite (Fe_7S_8) is the most magnetic member of the iron sulphide group which are the second most important group of magnetic minerals. It is a cation deficient clone of the mineral **troilite** (**FeS**), and is strongly ferrimagnetic up to its Curie temperature of 325°C. It is usually associated with igneous rock from sulphur-rich magmas and is a secondary mineral in marine sediments. For it to present a dominant palaeomagnetic signature is, however, rare. **Pyrite** (FeS_2) is paramagnetic at room temperature and **greigite** (Fe_3S_4) is uncommon but can be found in freshwater carbonate rocks as a product of authigenesis.

3.5.5. Iron Hydroxides and oxyhydroxides.

Commonly the result of prolonged weathering, **Goethite** (**αFeOOH**) is a weakly magnetic, canted antiferromagnetic mineral, with a Néel temperature of 70-170°C (O'Reilly, 1984). When cooled through its Néel temperature it can acquire a weak **thermoremanent magnetisation** (section 3.7.1) but, upon heating above 300°C, it dehydrates to haematite, producing a chemical remanent magnetisation (section 3.7.2). **Lepidocrocite** (**γFeOOH**) and **akaganeite** (**βFeOOH**) are other examples from this group which both exhibit paramagnetic behaviour at room temperatures. These minerals occur very infrequently and so are palaeomagnetically of little interest but are thought to convert to maghemite on heating to moderate temperatures.

3.5.6. Iron.

Iron is rarely found in terrestrial rocks but is common in extraterrestrial rocks such as lunar samples and meteorites. It has a high saturation magnetisation and a T_c of 780°C and can carry a high remanent magnetisation.

3.7. Acquisition of natural remanence within rocks.

The magnetisation of a rock is composed from an array of magnetic grains aligned with components of their magnetisation in the direction of the ambient field at the time of formation [The term 'formation' refers to recording of the field direction during cooling, deposition or growth]. However, for grains to retain the original field direction over geological time, they must be magnetically stable. Grains with longer **relaxation times,** τ (the time taken for thermal energy to break down the magnetisation to a new alignment based on a later ambient field) are stable and ideal for palaeomagnetic work. The relaxation time is almost entirely dependent upon the grain volume and the temperature; the greater the volume and lower the temperature, the longer the relaxation time will be. Since multidomain grains require less thermal energy to adapt to external field changes than single domain grains they are generally considered to be magnetically unstable. Therefore, single domain grains provide a more effective record of geomagnetic field changes in rocks since their relaxation time can be many millions of years.

The magnetisation of a rock sample acquired in a weak field, such as the earth's field, is termed the natural remanent magnetisation (NRM) or remanence. The NRM represents the summation of the following types of magnetisation.

3.7.1. Thermoremanent magnetisation.

Magnetic minerals cooling from above their Curie temperatures in the presence of a magnetic field will acquire a **thermoremanent magnetisation (TRM)**. Above the Curie temperature all minerals behave paramagnetically but as temperature is reduced below the Curie point a remanence is induced at the **blocking temperature** (T_b). At this point larger SD grains will have relaxation times of a few minutes whilst smaller SD grains will have even shorter relaxation times. As the rock continues to cool a greater number of grains will fall below their blocking temperatures, and will acquire a remanence in the direction of the ambient field. In a rock with a range of magnetic mineral grain sizes, a **blocking temperature spectrum** is produced. This range of

blocking temperatures can reflect the mineralogy and size of the magnetic grains within the rock.

A partial thermoremanent magnetisation (pTRM) can result if a rock is reheated at sometime during its later history. In the process of reheating not all grains will have their blocking temperatures exceeded. The overall effect is to allow realignment, to the current ambient field, of only those grains with blocking temperatures below the maximum temperature. This technique can be used in the laboratory to measure values of palaeointensity for igneous rocks and pottery (Thellier and Thellier, 1959).

3.7.2. Chemical remanent magnetisation.

A **chemical remanent magnetisation (CRM)** occurs when a magnetic mineral grows or is precipitated in the presence of a magnetic field below its T_c. It can also result from the alteration of minerals through weathering processes. During the growth of a mineral, a stable remanence in the direction of the ambient field may be acquired if the volume of the grain exceeds a critical volume; the **blocking volume (V_b)**. Below this volume the mineral behaves paramagnetically. At the blocking volume the relaxation time begins to increase rapidly. Although CRMs are generally of lower intensity than TRMs their stability's through time are comparable. Intergranular cements in sedimentary rocks may have NRMs primarily composed of a CRM. This is well demonstrated by the haematite cements of ancient red-beds (Dekkers and Linssen, 1989).

3.7.3. Depositional remanent magnetisation.

A **depositional remanent magnetisation (DRM)** is produced by the accumulation of magnetic minerals in a sedimentary rock. As a magnetic grain, with a previously acquired remanence, falls through a liquid, it is free to rotate to alignment with the ambient field. Thus, its incorporation into the sediment preserves this alignment, allowing a record of field change to build up over time, as further sedimentation occurs. If a grain is free to rotate in water-filled pore spaces, after it has been deposited, then a **post-depositional remanent magnetisation (pDRM)** may be acquired. Depending

upon the type of sediment, the time taken for compaction and subsequent 'lock-in' of the grain can range from days to tens of years. Thus the recorded PSV will be smoothed and detail can be lost.

Many soft sediment PSV records have an **inclination error**, where the recorded inclinations are shallower than the expected inclinations for that period of time (King, 1955). The mechanism behind this shallowing can be explained by assuming that oblate grains will rotate to lie horizontally at the water/sediment interface. This process may increase shape anisotropy along the long axis, giving rise to a reduced net inclination. An alternative explanation is to assume that spherical grains will rotate into hollows upon deposition and this will, statistically, produce a shallowing of the recorded inclination (Griffiths *et al*, 1960). The faithfulness of a PSV record dominated by DRM compared with the actual field can be further reduced by bioturbation, slumping and bedding effects.

3.7.4. Viscous remanent magnetisation.

The **primary remanence** is the remanence acquired at the time of formation. Since the direction of the primary remanence reflects the geomagnetic field at that time it is of greatest interest to the palaeomagnetist. The **secondary remanence** is that acquired after the formation of the rock. This secondary direction is likely to be that of the present or near-present field and is often termed **viscous remanent magnetisation (VRM)**. The VRM represents the magnetisation directions of grains with short relaxation times that have 'relaxed' to new geomagnetic field directions. Figure 3.6 shows the effect of secondary magnetisations on the primary magnetisation direction. To recover the primary remanence from a rock sample its VRM requires removal using magnetic cleaning techniques.

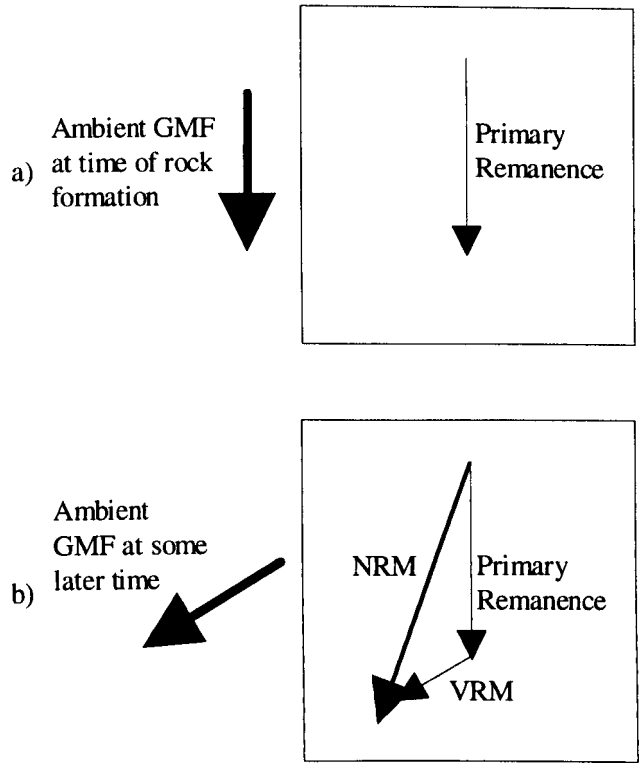

Figure 3.6. a) Primary (initial) remanence acquired at time of rock formation represents the direction of the geomagnetic field at that time. **b)** Magnetisation directions of grains with short relaxation times move to alignment with later geomagnetic field directions producing a secondary, viscous remanent magnetisation (VRM). The vectorial sum of the primary and secondary magnetisations is the NRM. Arrows in boxes show magnetisation directions of magnetic grains.

3.8. Demagnetisation techniques.

The primary magnetisation of a rock (that which is acquired at the time of the rocks formation) is of greatest palaeomagnetic interest. Secondary magnetisations acquired at a later stage require removal. Two cleaning methods are commonly used.

3.8.1. Alternating Field (AF) demagnetisation.

Alternating Field (AF) demagnetisation relies upon the spectrum of coercivities of grains within a sample. These coercivity ranges result from the presence of an assemblage of grain sizes and magnetic minerals within a particular sample. In an AF that is reduced slowly from some peak value, the magnetisations of any grains whose

coercivities are less than the peak field will flip backwards and forwards. If performed in zero field, then as the AF is reduced the magnetisation directions of these grains are randomised, along their easy axes. If successively larger peak AFs are applied, then grains of higher coercivity will be randomised and the sample will be further cleaned of secondary magnetisations.

A sample is normally rotated about 3 axes to enable the easy axes of SD grains to be presented parallel to the AF, whilst it is being reduced from peak value (Hutchings, 1967). This allows the maximum amount of randomisation per AF cycle. In order to randomise the alignment, AF demagnetisation is usually performed in zero applied field. This prevents the production of **anhysteretic remanent magnetisations (ARM)** which would produce a directional bias after the AF was reduced to zero in those grains whose coercivities were lower than the biasing field.

A coercivity spectrum can be built up by the application of stronger peak AFs. This can give information on the hard (high coercivity) and soft magnetisation components and on their contribution to the primary and secondary magnetisation directions. Normally, a VRM is contained by the softer components of magnetisation and is removed (cleaned) with the application of low strength AFs.

An advantage of AF demagnetisation is that it does not usually inflict physical changes upon samples since no heat is applied. It is also a very quick procedure allowing large numbers of samples to be demagnetised in a short space of time. It is more orthodox to use AF demagnetisation on samples with relatively low coercivities, such as magnetites. Haematite can posses ranges of coercivities beyond the range of AF's on most equipment. However, this is not to say that haematite cannot be AF demagnetised. Careful comparison with thermally demagnetised samples of the same material can be made to ensure that the true primary magnetisation is revealed and that the effects of thermal alteration do not affect the remaining NRM.

3.8.2. Thermal demagnetisation.

If a sample is heated in zero field, grains with blocking temperatures less than the maximum temperature will behave paramagnetically. Thus, when cooled from above their blocking temperatures, magnetisations are thermally randomised and their contribution to the NRM is effectively removed. As a sample will have a range of blocking temperatures (Section 3.7.1) successive heating and cooling cycles, each increasing in temperature, will produce a blocking temperature spectrum. Data from stepwise thermal demagnetisation can be used to identify low and high blocking temperature components of the NRM. Identification of magnetic minerals is also possible by heating to temperatures corresponding to known Curie points. At or above a temperature of 700°C the sample will effectively be completely demagnetised as haematite has a T_c of 675°C.

Thermal demagnetisation can have some undesirable effects including the oxidation and conversion of magnetic minerals. Changes in the magnetic mineralogy during stepwise thermal demagnetisation can be monitored using magnetic susceptibility. These changes may also be seen in the blocking temperature spectrum. Stepwise thermal demagnetisation by its nature, causes expansion and contraction of samples. Less homogeneous samples such as calcites and wet-sediments are likely to suffer from repeated heating and directions may become unreliable after a few steps.

4. Uranium-series disequilibrium dating of calcite speleothems using the $^{230}Th/^{234}U$ and ^{210}Pb techniques.

4.1. Introduction.

This chapter introduces the theory and methods behind the uranium series dating of calcite speleothems. Uranium-series disequilibrium is a useful method for the dating of relatively young materials and, in this study, the isotopes ^{230}Th - ^{234}U are utilised, allowing alpha-spectrometric dating up to 350 ka. Criteria and problems associated with the dating of speleothem are addressed, as are attempts at a relatively new technique of dating impure calcites, the leachate/leachate method. The second intention of this chapter is to introduce the reader to the ^{210}Pb dating method. This dating method is commonly applied to corals (Druffel *et al*, 1990), lacustrine deposits (Atkinson and Haworth, 1990), marine sediments (Oldfield *et al*, 1989) and peat deposits (Appleby *et al*, 1988). ^{210}Pb dating is applicable over the range 0 - ~150 years and its potential for dating young speleothems (stalagmites) has been investigated in this study.

The best reference text for all aspects of uranium-series disequilibria is Ivanovich and Harmon, 1992. It contains detailed information on the $^{230}Th/^{234}U$ and ^{210}Pb techniques and the laws of radioactive decay.

4.2. Uranium-series dating theory.

The U-Th dating method relies on the fact that the daughter isotopes of the actinides ^{238}U, ^{235}U, and ^{232}Th (the parent isotopes of three separate decay chains, Figure 4.1) will, from any initial disequilibrium, steadily grow in to **secular equilibrium** with their parents at a rate determined by their half-lives ($t_{1/2}$; the time taken for half of the initial activity of an isotope to decay). Secular equilibrium is the state in which the

daughters activities, in disintegrations per unit time, are equal to that of the parent isotope.

The highest concentrations of naturally occurring uranium and thorium are found in granites and pegmatites. Within the source rock, if closed-system conditions exist, a state of secular equilibrium is reached within 10^6 years. However, weathering of these crustal rocks affects U and Th isotopes differently due to their contrasting geochemical properties. Both U and Th are almost chemically immobile in their 4^+ states. However, U is easily oxidised to its 6^+ state, forming soluble uranyl complexes (UO_2^{2+}):

$$U^{4+} + 2H_2O \rightarrow UO_2^{2+} + 4H^+ + 2e^- \quad \textbf{4.1}$$

While thorium isotopes remain within the parent rock, uranium is transported by surface waters. In natural materials the two actinides, ^{238}U and ^{235}U are transported equally well, their ratio rarely departing from 137.5 ±0.5 (Rogers and Adams, 1969). Precipitation of uranyl complexes allows daughter isotopes to regrow towards secular equilibrium. In simple terms, the activities of parent and daughter isotopes, then allow an estimate of the age of a deposit.

There are many uranium-series dating methods that utilise different isotopes of ^{238}U, ^{235}U and ^{232}Th (Ivanovich and Harmon, 1992). These methods are divided in to two groups; the **daughter deficient** and the **daughter excess** methods. The daughter deficient methods are based on measuring the extent to which an initially absent daughter isotope has grown back to secular equilibrium with its parent. The daughter-excess methods use the decay of an initial excess of an unsupported intermediate daughter isotope, since the formation of the sample.

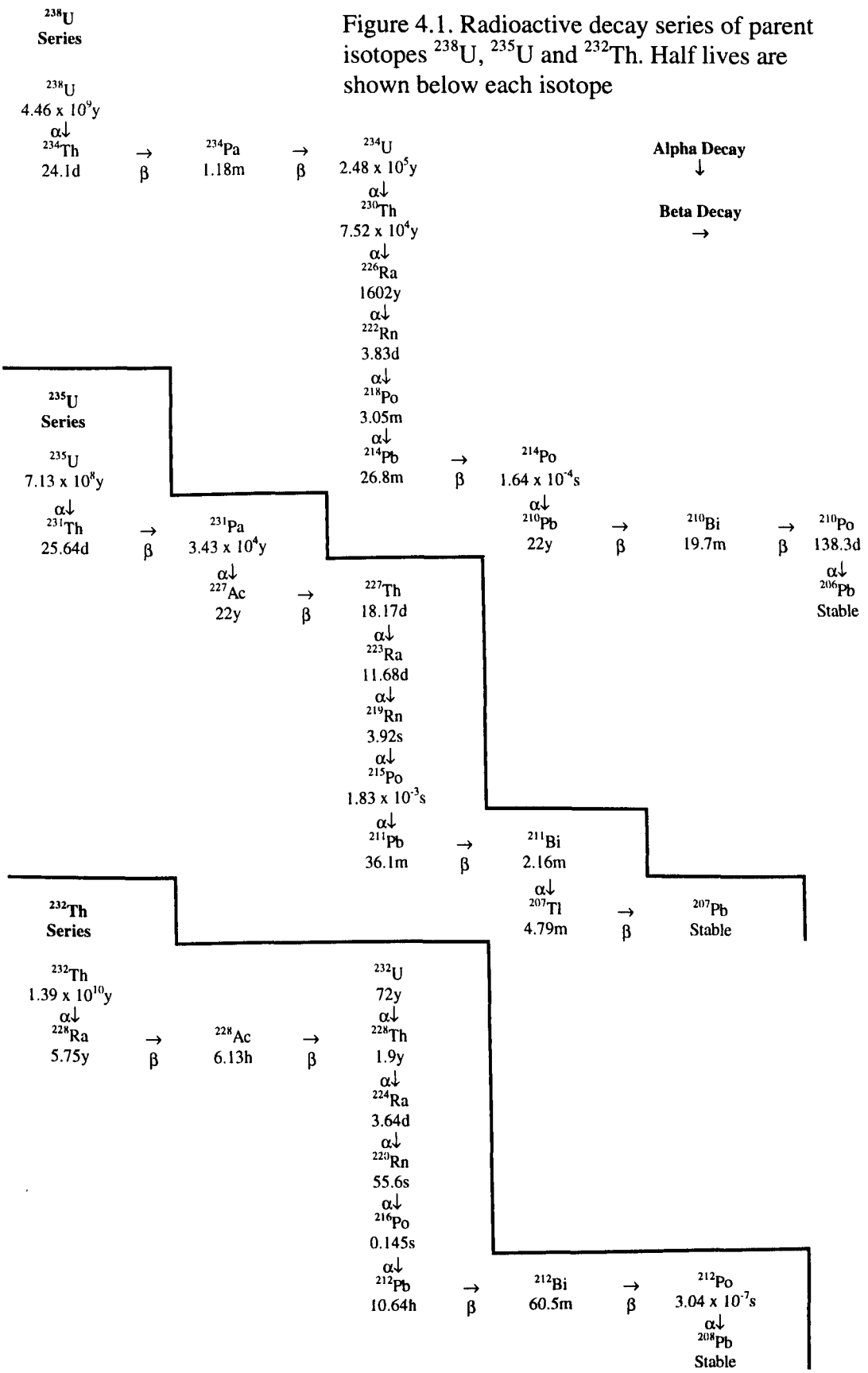

Figure 4.1. Radioactive decay series of parent isotopes ^{238}U, ^{235}U and ^{232}Th. Half lives are shown below each isotope

4.3. Dating calcite speleothems using the $^{230}Th/^{234}U$ method.

By far the most commonly used of the uranium-series techniques is the $^{230}Th/^{234}U$ (daughter-deficient) method. It relies on measurement of ^{238}U and its daughters ^{234}U and ^{230}Th. Using the $^{230}Th/^{234}U$ method, dating can be performed reliably up to 350 ka, using alpha-spectrometry and 500 ka using mass-spectrometry. As with all disequilibrium methods the $^{230}Th/^{234}U$ technique can only be applied to materials in which there has been no migration of isotopes after formation i.e. they are closed-systems.

Figure 4.1 shows the ^{238}U decay chain and the relationships and half lives (t½) of the isotopes used in this dating method. At the time of formation (t_0), a speleothem contains no ^{230}Th, and therefore at some later time (t) the ratio of $^{230}Th/^{234}U$ reflects how far the equilibrium has been approached and hence the time since deposition, as follows:

$$^{230}Th/^{234}U = \frac{1-e^{-\lambda 230 t}}{^{234}U/^{238}U} + \left[1 - \frac{1}{^{234}U/^{238}U}\right]\left[\frac{\lambda_{230}}{\lambda_{230}-\lambda_{234}}\right]\left[1-e^{-(\lambda 230-\lambda 234)t}\right] \qquad \textbf{4.2}$$

where λ_{230} and λ_{234} are the decay constants of ^{230}Th and ^{234}U and t is the time after formation (Ivanovich and Harmon, 1992).

Figure 4.2 shows a graphical representation of the relationship in equation 4.2 in a closed system with varying initial $^{234}U/^{238}U$ ratios. The vertical lines are termed isochrons (lines of equal age). The isochrons become closer together as the age increases; the limit of the dating method is approached as ^{230}Th moves into equilibrium with its parents. It is worth noting that for ages <30 ka the $^{230}Th/^{234}U$ activity ratio is almost independent of the $^{234}U/^{238}U$ activity ratio. In this age range equation 4.2 reduces to the more simple form:

$$^{230}Th/^{234}U = \left(1-e^{-\lambda 230 t}\right) \qquad \textbf{4.3}$$

Speleothems are formed by the precipitation of calcite from seepage waters entering a cave system through fissures in the overlying limestone. These seepage waters

are saturated with respect to $CaCO_3$ and precipitation, as calcite, is initiated by out-gassing of CO_2, or by evaporation of water. Precipitation may also be caused by the dissociation of Ca complexes (Ford and Williams, 1989).

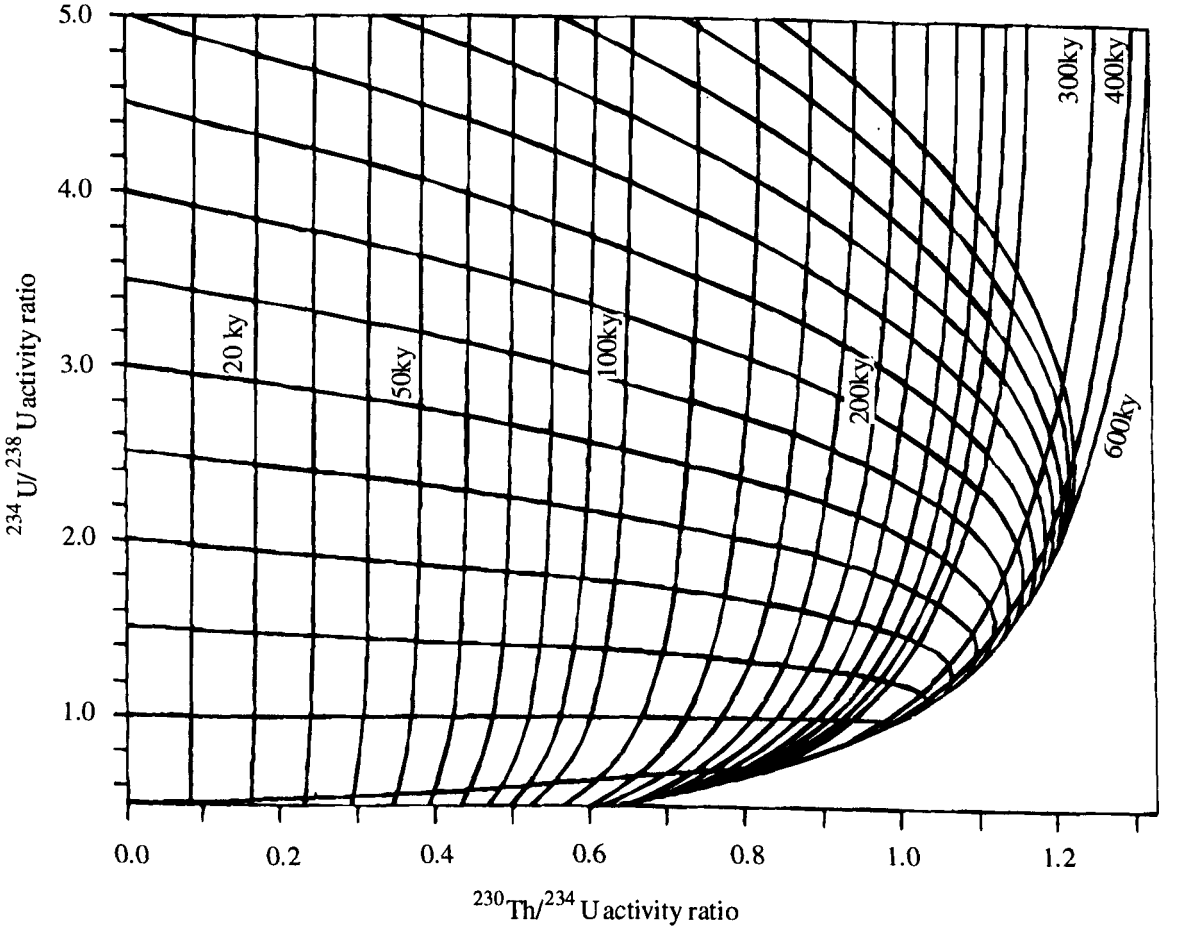

Figure 4.2. The variation of $^{238}U/^{234}U$ and $^{230}Th/^{234}U$ activity ratios in a closed system. Sub-vertical lines depict constant ages with differing $^{238}U/^{234}U$ activity ratios.

Uranium, carried in the drip waters in its 6^+ state, is incorporated into the precipitating calcite. Eh conditions subsequently fall, reducing uranium to its 4^+ state, uraninite. Since thorium is not generally carried in solution, the initial $^{230}Th/^{234}U$ ratio is zero and subsequently under normal circumstances thorium will be produced only from the decay of ^{234}U. However, contamination of the speleothem by detrital ^{230}Th will make the initial $^{230}Th/^{234}U$ ratio >0, necessitating a correction procedure in the dating equations. The procedures for making a correction for detrital thorium contamination are discussed in section 4.4.1.

Generally there are few opportunities for isotope migration to occur once a speleothem has been deposited and they can be treated as closed systems. Successive layers of calcite are precipitated on the speleothem by drip waters. On rare occasions these waters may become chemically 'aggressive'. In such situations whole calcite layers are dissolved leading to uranium migration producing an excess of ^{230}Th (section 4.4.4).

Because of these potential problems, suitability criteria for the uranium-series dating of speleothem are used and are valid, with adaptations, for most materials dated with this technique and are as follows;

1) The system must have remained closed to the migration of nuclides since deposition. The only changes in isotopic ratios are those caused by radioactive decay. For example, uranium migration was noted in many speleothems from Russia by Cherdyntsev (1971). He concluded that the ^{234}U/^{238}U ratios between samples of the same cave and those of different caves, in the same area, varied more than could be explained by age variations.

2) The speleothem must have grown during the period 0.1 - 350 ka. Beyond 350 ka the ^{230}Th/^{234}U ratios are too close to equilibrium to be distinguished against experimental errors using alpha-spectrometry. Mass-spectrometry is more precise and can resolve activities more effectively, to give ages up to ~500 ka (Chen *et al*, 1992)

3) A speleothem must contain at least 0.05 parts per million (ppm) uranium for alpha spectrometry (Ivanovich and Harmon, 1992). This is the minimum concentration required for alpha-spectrometry in order to resolve isotope peaks above alpha-counter background.

4) Detrital thorium contamination must be at a minimum so that the initial (t_0) ^{230}Th/^{234}U ratio = 0. The effects of detrital contamination are discussed in section 4.4

4.4. Factors affecting the U-Th dating of speleothems.

4.4.1. Detrital contamination.

All daughter deficient dating methods assume that the initial isotopic ratios are determinable. In clean speleothems, where detritus is absent, the initial $^{230}Th/^{234}U$ ratio is zero. If, however, a speleothem contains thorium-bearing detritus, a percentage of the total ^{230}Th in the sample will originate from the detritus and the remaining ^{230}Th will be from the decay of ^{234}U precipitated with the speleothem so that;

$$^{230}Th_{total} = {}^{230}Th_{authigenic} + {}^{230}Th_{detrital} \qquad 4.4$$

The incorporation of detritus into a speleothem is reflected by a ^{232}Th peak in the alpha spectrum; ^{232}Th has a half-life of 1.30×10^{10} years and its decay over the 350 ka period of the U-Th method is negligible. In view of ^{232}Th having an equivalent chemical behaviour to ^{230}Th in naturally occurring conditions, its presence indicates that detrital ^{230}Th is also likely to be present. If no correction is made for the presence of this detrital ^{230}Th, then age calculations based on isotope activities will yield increased sample ages.

In this study a correction was deemed necessary when the $^{230}Th/^{232}Th$ ratio fell below 25. Above a value of 25 the effects of detrital contamination are deemed to be negligible. However, a recent study by Bischoff and Fitzpatrick (1991) suggested that detrital contamination becomes significant when the $^{230}Th/^{232}Th$ ratio falls below 20. The effect of detrital thorium is most pronounced in young (<10 ka) speleothems where quantities of radiogenic thorium are low.

4.4.2. Simple correction procedures for detrital thorium contamination only.

A simple correction method to account for detrital thorium is often made using the $^{230}Th/^{232}Th$ ratios calculated from modern materials. The correction assumes that

these ratios reflect the initial $^{230}Th/^{232}Th$ ratio of the detritus in a speleothem thus allowing a correction to be made. Kaufman and Broecker (1965) found that an initial (t_0) $^{230}Th/^{232}Th$ ratio of 1.7 was apparent in lacustrine sediments. Later work by Blackwell and Schwarcz (1986) used a ratio of 1.25 when correcting initial isotopic ratios in travertines. Largely by convention, a value of 1.5 has been frequently adopted to correct speleothem dates, after work by Gascoyne *et al* (1981). This correction is largely superseded by the more precise methods outlined in section 4.4.3 but remains a useful method when material to date is in short supply and dates corrected with it are often satisfactory (for example Latham *et al*, 1986).

A similar, but more direct, approach is possible with speleothems that are active when collected. As the amount of radiogenic ^{230}Th in the calcite is effectively zero in the youngest sample then its measured $^{230}Th/^{232}Th$ ratio can represent the initial $(^{230}Th/^{232}Th)_0$ ratio of the detritus at t=0. This study has utilised such a procedure to correct for detrital input of ^{230}Th. In order to apply the correction to older samples further down the speleothem it is assumed that the initial $^{230}Th/^{232}Th$ ratio remains constant throughout each sub-sample and throughout the speleothem. However, this is not necessarily the case and more advanced methods can be used. Despite this, the dates calculated using this procedure are frequently acceptable.

4.4.3. Correcting for detrital uranium and thorium.

The methods above are often the only method available for correction when using alpha-spectrometry. The large quantities of material required to perform multiple analyses to recover the carbonate isotope ratios are often not available.

The $^{230}Th/^{234}U$ and $^{234}U/^{238}U$ ratios of the detritus are assumed to be at equilibrium using methods outlined in section 4.4.2 ($^{230}Th_{(D)}=^{234}U_{(D)}=^{238}U_{(D)}$) and the effects of detrital uranium components are ignored. However, detrital uranium can affect the initial isotopic ratios, especially in younger samples, and alternative methods exist to correct for its presence (Ivanovich and Harmon, 1992).

As ^{232}Th is an indication of not only detrital ^{230}Th but detrital ^{238}U and ^{234}U in addition, the correction made in the previous methods is only simplistic. More analytical correction methods employ partial leaching of single or multiple samples using weak acids and the use of isochron plots. A pair of isochron plots, constructed from ^{238}U, ^{234}U and ^{230}Th are normalised to ^{232}Th (Rosholt, 1976) in order to recover the carbonate components of $^{234}U/^{238}U$ and $^{230}Th/^{234}U$ which can be inserted in to equation 4.2. There are three common methods used to obtain the carbonate isotopic ratios; the leachate/residue (L/R) method, the leachate/leachate (L/L) method and the total sample dissolution (TSD) method. These methods are now discussed but are also more fully summarised in papers by Kaufman (1993) and also Ivanovich and Harmon (1992).

4.4.3.1. The Leachate-Residue (L/R) method.

Ku and Liang (1984) used the isotope activities of a leachate and its residue remaining after acid treatment to recover the carbonate isotope components. They found that the age calculated from the carbonate isotope ratios was correct providing that there was no **differential isotopic fractionation (DIF)** within the sample. DIF is defined as the preferential leaching of one or more isotopes from the detritus to the leachate compared to other isotopes. If DIF does not occur, an age calculation is possible from analysis of a single leachate-residue (L/R) pair. However, analyses of two or more coeval samples are usually performed to check for variable DIF. The isochron gradient of separate L/R pairs varies significantly when DIF occurs. Hillaire-Marcel and Causse (1989) found that by using this technique on calcareous concretions from glacial varves, a confirmation of the date for the first Wisconsinian ice advance in southern Quebec could be made. They found that variable uniformity of detritus in the concretions caused slope reproducibility problems when using leachates alone (**4.4.3.2.**)

4.4.3.2. The Leachate-Leachate (L/L) method.

The leachate-leachate (L/L) method was proposed by Schwarcz and Latham (1989) and Przybylowicz *et al* (1991). With this technique even if DIF occurs the slope

of the isochron is unaffected. They demonstrated that in the absence of DIF the L/L and L/R methods produce equivalent ages. The only requirements for the L/L method are that the detritus is uniform and that DIF is constant from one coeval sample to another.

The practice behind the method involves the leaching and analysis of a number of coeval samples ($n \geq 3$). Either, coeval samples with differing detrital contents can be leached in a single strength of the same acid, or a coeval sample can be divided into assays and be leached using different strengths of the same acid. The exact method used depends on the amount of material available, the latter method is often more practical with little material. By plotting leachate activities ($^{234}U/^{232}Th$) vs. ($^{230}Th/^{232}Th$) and ($^{238}U/^{232}Th$) vs. ($^{234}U/^{232}Th$) isochrons are constructed whose gradient yields the carbonate isotope ratios for $^{230}Th/^{234}U$ and $^{234}U/^{238}U$. Figure 4.3 shows a pair of L/L method isochron plots from samples from Hungary (Schwarcz and Latham, 1989).

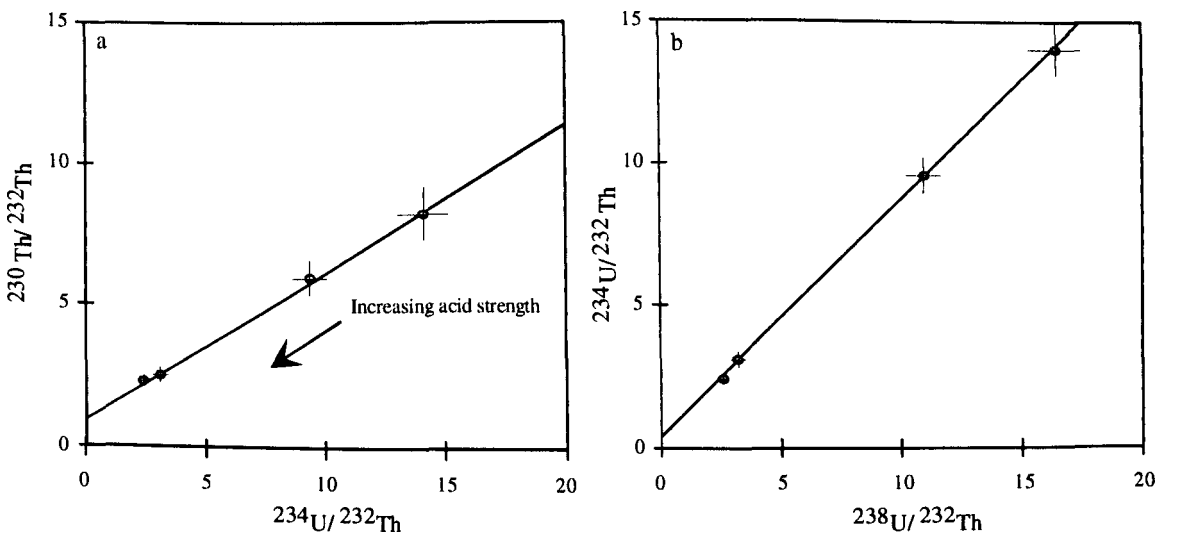

Figure 4.3. Results of theoretical leachate-leachate analysis, on coeval samples, using four acid strengths a) Isochron plot showing $^{234}U/^{232}Th$ vs. $^{230}Th/^{232}Th$ b) Isochron plot showing $^{238}U/^{232}Th$ vs. $^{234}U/^{232}Th$. Slope of lines reveal, respectively, $^{230}Th/^{234}U$ and $^{234}U/^{238}U$ of the true carbonate component. Note the increasing errors with weak acid analysis due to low leaching levels of ^{232}Th from detritus to leachate (Schwarcz and Latham, 1989).

When using the L/L method the 1 sigma errors of data points, based on counting statistics, increase with greater distance from the origin. Weak acid leachates have less ^{232}Th leached from the detritus, thus increasing the measurement errors. This has equal effect on both axes and therefore individual sample errors are ignored when calculating a best-fit isochron (Schwarcz and Latham, 1989). Careful design of the leaching techniques are required since a wide spread of data is required to define an accurate isochron. The greatest advantage of the method is that the effects of DIF are avoided. Additionally, laboratory procedures do not require the use of hydrofluoric (HF) and perchloric ($HCLO_3$) acids for sample dissolution and subsequently the time required for preparation and analysis are not increased significantly.

4.4.3.3. The Total Sample Dissolution (TSD) method.

The TSD method makes use of $HF/HCLO_3$ mixtures and requires the necessary safety equipment to deal with these acids. The method is also more time consuming since silicates may require several days for complete dissolution. Because of these additional problems the L/L method is most frequently used despite the fact that the TSD method is superior. The method involves the total dissolution of coeval samples ($n \geq 3$) in $HF/HCLO_3$ mixtures (Bischoff and Fitzpatrick, 1991; Ku *et al* 1979). Due to the fact that the detritus is dissolved with the carbonate member, the only requirement is that the detritus has a common $^{230}Th/^{232}Th$ ratio. The solution thus contains allogenic ^{230}Th, ^{234}U and ^{238}U plus detrital ^{230}Th, ^{232}Th, ^{234}U and ^{238}U and since the entire sample is dissolved the effects of variable DIF are averted i.e. chemical fractions of ^{230}Th, ^{232}Th, ^{234}U and ^{238}U are equal. The ^{232}Th represents the quantity of detrital contamination, allowing a series of equations in which the intercept at ^{232}Th = zero yields the carbonate ^{230}Th, ^{234}U and ^{238}U activities thus;

$$^{230}Th_S = \left[\left(^{230}Th_D - ^{230}Th_C\right)/^{232}Th_D\right]^{232}Th_S + ^{230}Th_C \qquad \textbf{4.5}$$

$$^{238}U_S = \left[\left(^{238}U_D - ^{238}U_C\right)/^{232}Th_D\right]^{232}Th_S + ^{238}U_C \qquad \textbf{4.6}$$

$$^{234}U_S = \left[\left(^{234}U_D - ^{234}U_C\right)/^{232}Th_D\right]^{232}Th_S + ^{234}U_C \qquad \textbf{4.7}$$

where $_S$ is the total sample, $_D$ is the detrital component and $_C$ is the carbonate component. The carbonate isotope components can be entered into equation 4.2 to give the true age of the sample.

Whichever leaching method is used (L/R, L/L or TSD) the additional aim is to ensure as wide a spread of datapoints as possible in order to fit the isochron with little ambiguity. This is usually achieved by the analysis of as many coeval samples as practical, usually ≥ 3.

4.4.4. Effects of organic contamination.

Organic material carried in the detritus may chelate U and Th into a number of compounds, usually humic or fulvic compounds (Lauritzen *et al*, 1986), causing U and Th losses, poor chemical yields and ill-defined alpha-spectra. The presence of organics becomes evident during the initial dissolution of the speleothem sub-sample, as large amounts of froth and/or by yellow colouration of the solution. Fulvic compounds, being acid soluble, give up their chelated U and Th at this stage but the humic compounds may not. Humic substances require further, more aggressive, treatment before they release chelated U and Th. In this study, humics were broken down using 1-3 mls of perchloric acid ($HCLO_3$) in small volumes of leachate which was subsequently refluxed for 30-45 minutes.

4.4.5. Effects of leaching due to weathering.

In speleothems the effects of weathering are rare and when dating, the affected areas may be avoided by alternative sampling. Areas of calcite re-solution are normally found in the calcite layer immediately beneath a hiatus. Re-solution may occur when formation waters become sufficiently acidic to dissolve speleothem growth layers.

Weathering is normally indicated by leaching of uranium isotopes, which may result in apparently older ages since the thorium remains whilst uranium is depleted. This may be shown by low uranium concentrations, excesses of thorium or anomalous $^{234}U/^{238}U$ ratios (Latham and Schwarcz, 1992).

4.5. Chemical procedures.

The laboratory chemical procedures used for speleothem $^{230}Th/^{234}U$ dating in this study are outlined briefly below. A detailed account of all procedures used during the study are presented in Appendix J.

4.5.1. Separation of Uranium and Thorium.

U and Th require chemical separation because they emit alpha particles of such similar energies they would otherwise overlap in an alpha spectrum. More specifically the overlaps occur with ^{238}U / ^{232}Th and ^{234}U / ^{230}Th. After washing in distilled water to remove any surface contaminant the sample was dissolved in acid; either 9M HCl or 7M HNO_3, both being equally effective. Care was taken during dissolution to prevent froth, caused by organics, spilling over the sides of the beaker. This called for the addition of acid a little at time. Upon complete dissolution, a radioactive monitor (spike) of known concentration was added to the solution. The spike contained the artificial isotopes of ^{232}U and ^{228}Th which were in secular equilibrium with an activity ratio of 1.027[1] allowing calculation of chemical yield and of concentrations of the uranium and thorium isotopes.

The uranium and thorium, now in solution, were co-precipitated as iron hydroxide, using $FeCl_3$. The iron was subsequently extracted using Iso-Propyl Ether (IPE) leaving uranium and thorium ions concentrated in acid solution. In a series of anion and cation exchange resins, the uranium and thorium isotopes were separated ready for

[1] The $^{232}U/^{228}Th$ spike activity ratio was determined by Mel Gascoyne.

electro-deposition onto 25 mm diameter steel planchets. After electrodeposition planchets were loaded into the alpha-spectrometer for counting. The counting period was varied according to the uranium concentration and chemical yield. In most cases counting was carried out for 7200 minutes (5 days) as most samples had low uranium concentrations (≤ 1 ppm) and yields were initially very low (<15%).

4.5.2. Electrodeposition of Uranium and Thorium.

Low chemical yields of uranium and thorium were of great concern when dating many sub-samples during the study. Typically yields were <15 % for uranium and <10 % for thorium. These low yields resulted in increased counting errors and increased standard deviations about an individual date. As all speleothems were young the low yields compounded the problems of counting the inherently low concentration of allogenic ^{230}Th.

A high resolution alpha-spectra is only obtained with a uniformly distributed, flat alpha source; a mono-atomic layer is deemed ideal (Lally, 1992). Foreign matter above the source or a non-uniform deposit will cause attenuation of emitted alpha particles resulting in a poorly resolved spectra. Electroplating is thus the favoured method for alpha source preparation as it generally satisfies these conditions. Many techniques exist for electroplating uranium and thorium but there is no one universally accepted method. Most of the methods involve cathodic deposition from either an alkaline or an acidic medium. For example, Campbell and Moss (1965) used an alkaline hypochlorate solution whilst Talvitie (1972) developed the use of an ammonium sulphate solution. Both methods obtain near quantitative deposition of the actinides, with yields in the region of 90-100 % for both uranium and thorium.

Chemical separation methods for uranium and thorium at Liverpool were virtually identical to those used at McMaster University (Latham, 1981). Electrodeposition appeared to be the most likely area of yield losses as this was the

major difference between the two methods, the McMaster laboratory using the TTA (thenoyltrifluoroacetone) extraction technique (Latham, 1981; Lally, 1992).

4.5.3. Electrodeposition apparatus.

The electrodeposition apparatus consisted of a 250 ml plastic bottle with the base removed. A hole in the centre of the bottle lid allowed the cathode, a brass bolt, brazed to a steel disk, to be connected to a constant current source. The planchet was placed into the lid, a rubber ring fitting inside the lid providing the seal when the lid was screwed onto the bottle (Figure 4.4a). A set of purpose built electro-deposition cells were used in later plating of uranium and thorium consisting of a Teflon tube, 20 mm internal diameter, bolted down onto a copper base. The steel planchet and rubber seal were trapped between the base and tube, thus forming a liquid-tight seal (Figure 4.4b). These later cells contained a maximum of 60 mls of electrolyte.

A platinum anode suspended in a glass tube was lowered into the solution. A constant current source (built by Dr. John Share, Liverpool University Geomagnetism Laboratory) provided connections for up to four electrodeposition cells with maximum currents of 0.6 A. The electrolyte used in initial plating of uranium and thorium was made up from H_2O, H_2SO_4 (5:1) with NaOH to pH 2.4-2.6 and is referred to as electrolyte 'A' in the following section.

A solution of standard uraninite was used for yield improvement tests. This solution originated from the McMaster laboratory and was known to have an activity of 0.75 Bq/ml. The uraninite had the advantage that, for approximate yield measurements its spectra could be assessed for uranium and thorium yields without the need for isotopic separation. Since the isotopes ^{238}U, ^{234}U and ^{230}Th are in secular equilibrium the number of counts in the ^{238}U peak represented the contribution of ^{234}U in the combined $^{234}U/^{230}Th$ peak. Thorium yields could be calculated by subtracting the ^{238}U counts from the combined $^{234}U/^{230}Th$ peak. A direct plate-out of the uraninite should, theoretically,

lead to a 100% yield. A series of simple electro-deposition experiments[2] were conducted to test the current method and to see if it could be improved, without dramatic procedural changes.

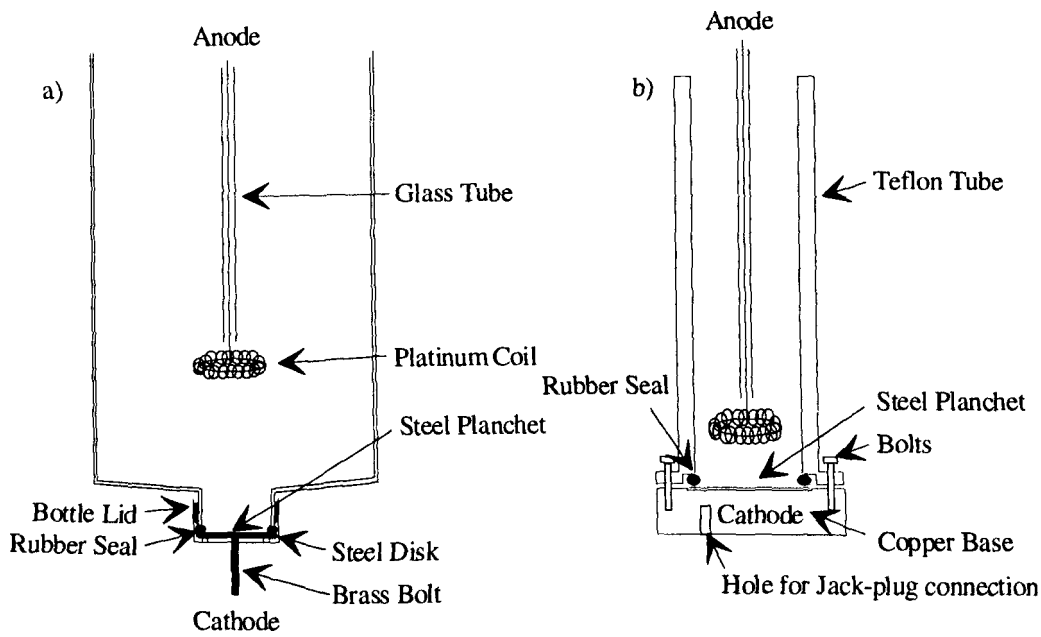

Figure 4.4 a) 250 ml capacity electrodeposition cell. b) 60 ml capacity electro-deposition cell.

4.5.3.1. Experiments and results.

1.) A volume of 0.5 mls of uraninite solution were plated-out directly, without chemical separation using electrolyte A. The electrolyte volume was 100 mls and electro-deposition was carried out for 4 hours at 0.5 A. These were the conditions under which all previous samples had been electro-plated. The yields were 27% U and 10% Th.

2.) Uranium and thorium in 0.5 mls of uraninite were separated using anion and cation

---

[2] Experiments 3,4 and 5 were performed with the assistance of C. Lean

exchange as normal. Electrolyte A was used and all other conditions were maintained as in experiment 1. This time 0.5 mls of spike were added to the uraninite to check the validity of yield calculation using uraninite alone. The two samples gave yields of 25% U, 7% Th and 22% U, 7% Th respectively. Yields were comparable with experiment 1.

3.) A reduction in the volume of electrolyte A to 50 mls with 0.5 mls of uraninite plated-out directly, gave yields of 25% U and 7% Th. All other conditions were maintained.

4.) Direct plate-out of 0.5 ml uraninite in 50 mls of electrolyte solution (electrolyte B) made from HNO_3 and H_2SO_4 (5:1) with H_2O and NH_3 to pH 2.1 (Latham, 1981). Plating was conducted for 4 hours giving yields of 15% U and 5% Th.

5.) 150 mls of electrolyte B with 0.5 ml uraninite, plated out directly for 4 hours at 0.5 A with very poor yields of 1% U and 3% Th.

6.) 0.5 ml uraninite with 50 mls of electrolyte C ($NaHSO_4$ + H_2O + NaOH + pH 2 buffer to pH 1.5-2.0). Electro-deposition was carried out for 3 hours at 0.5 A resulting in chemical yields of 22% U and 15% Th. The smaller, 60 ml capacity electro-deposition cell was used in this experiment. A small improvement in the Th yields was noted.

7.) The same conditions as in experiment 6 were maintained but 150 mls of electrolyte C was used in the larger electro-deposition cell giving yields of 5% U and 4% Th.

The preceding experiments showed that no significant improvements were made to the chemical yields, even when using a variety of electrolyte solutions. For experiments that gave reasonable results, yields were roughly comparable to those obtained normally. However, the exercise was useful in itself since it suggested that most of the yield problems emanated from the electrodeposition stage.

The TTA in benzene method of plating uranium and thorium isotopes has been used in many laboratories and was known to work effectively, although with less well defined spectra since deposition is often non-uniform (Latham, 1981). Two attempts

were made to plate uranium and thorium using this method, using a stalagmite from Kentucky as the medium. The uranium and thorium were chemically separated using ion exchange, as in routine analyses. For TTA deposition, however, thorium was extracted with 0.75M oxalic acid, using the technique of Latham (1981). As benzene is now a recognised carcinogen the TTA was dissolved in toluene. Both attempts failed due to overheating of the steel planchet which caused superheating and total loss of both uranium and thorium. No further experiments were conducted using the TTA method.

4.5.4. The Hallstadius electrodeposition method.

An electro-deposition technique, first proposed by Hallstadius (1984), was tested, initially using 0.5 mls of uraninite. The method is based on the modification of the proven Talvitie (1972) method and claimed to produce greater yields for the actinides of Am, Pu, U and Th. It is a simple technique to use and was adapted at Liverpool so that no changes to the preceding chemical procedures were necessary (Appendix J).

Uranium and thorium were eluted, as normal, from their ion exchange columns in 0.1M HCl and 6M H_2SO_4 respectively. The samples, in 50mls of acid, were heated gently in 100 ml beakers, to reduce their volumes to a few mls. In the case of thorium, the heating must be exceedingly gentle since H_2SO_4 boils and superheats violently. During the later stages of evaporation, the fume cupboard visor was raised so that a stream of air passed over the top of the beaker, encouraging a venturi effect which increased the rapidity of evaporation. Uranium reduced sufficiently in ~45 minutes whilst thorium took up to 120 minutes.

With the volume reduced, the beaker was removed from the heat source and 1 ml of 0.3M Na_2SO_4 was added when cool. The sample was then evaporated to total dryness, leaving a white residue in the bottom of the beaker. The Na_2SO_4 acts as a carrier during this stage, preventing adsorption of the actinides onto the walls of the beaker (Hallstadius, 1984). After cooling the beaker, 0.3 mls of H_2SO_4 were added. Gentle heating was then required to dissolve the residue ensuring that no loss of H_2SO_4

occurred by evaporation. Hallstadius reported corrosion of the planchet with H_2SO_4 volumes < 0.3 mls. 4 mls of double distilled H_2O and two drops of thymol blue indicator were then added and the pH was adjusted to 2.1 with NH_3, as indicated by a red to red-orange colour. The solution was then transferred to the electro-deposition cell. Since liquid volumes never exceeded 20 mls using this method, the 60 ml Teflon cells were used. After rinsing the beaker with 5 mls of 1% H_2SO_4 the pH was re-adjusted with NH_3 and checked with a pH meter. The sample was electrolysed for 90 to 120 minutes at 0.6A.

After the requisite period of electro-deposition, a few drops of NH_3 were added one minute before the current was turned off. This prevented back-stripping of uranium and thorium when the current ceased. The electrolyte was tipped out into the original beaker and distilled water was squirted into the cell before it was dismantled. During this stage it was important to rinse away any remaining electrolyte as quickly as possible so as to reduce the chance of yield loss. The planchet was washed in water and acetone before drying on a hotplate ready for labelling and counting. The experiments using this technique are described below.

4.5.4.1. Experiments and results.

1.) 0.5 mls of uraninite with 0.5 mls of spike were subjected to the normal chemical separation techniques using ion exchange. During reduction in the volume of the thorium eluant, excessive heating caused violent boiling and total loss. The uranium gave a yield of 53%.

2.) 0.5 mls of uraninite were mixed with 50 mls of 6M H_2SO_4. The volume was reduced successfully and a plating time of 90 minutes gave yields of 47% U and 45% Th.

3.) Ion exchange separation of uranium and thorium in 0.5 mls uraninite and 0.5 mls spike followed by electro-deposition for 120 minutes gave yields of 55% U and 50% Th.

4.) A repeat of experiment 3 gave yields of 60% U and 55% Th.

5.) Using stalagmite sample 15B from SC02, plus 0.5 ml spike, with uranium and thorium separated by ion exchange, a plating time of 120 minutes gave chemical yields of 54% U and 42% Th.

Due to these results the Hallstadius method was adopted for routine dating. It was felt that subsequent improvement to the technique could be achieved during the dating of speleothem samples.

Figure 4.5 shows bar graphs of U and Th yields and shows the increases in chemical yields. Initially the Hallstadius method was preferential to increased yields of uranium. For thorium there may have been incomplete drying of the Na_2SO_4 carrier before addition of H_2SO_4. Although the Hallstadius technique was a great improvement on the previous electro-deposition technique the yields were, and continue to be, variable although thorium yields have greater consistency. This is difficult to understand as the same procedures were followed sample after sample.

Subsequent changes in the procedures used in the modified Hallstadius method included a) longer drying periods for the residue and b) a cathode-anode spacing decreased to 5 mm. The yields were maintained at a satisfactory level for dating and the maximum uranium and thorium yields obtained to date are 90% and 87% respectively.

4.6. Standard Alpha-spectrometry.

The activities of relevant uranium and thorium isotopes were measured on an alpha spectrometer. The system used in this study comprises of six Canberra 7401 alpha counters with PIPS detectors (high resolution, low background). Isotope activities from each counter are interfaced with a Canberra multi-channel analyser and analogue to digital converter. A PC running Canberra's Windows software controls the acquisition and displays the counting spectra recorded from each alpha counter.

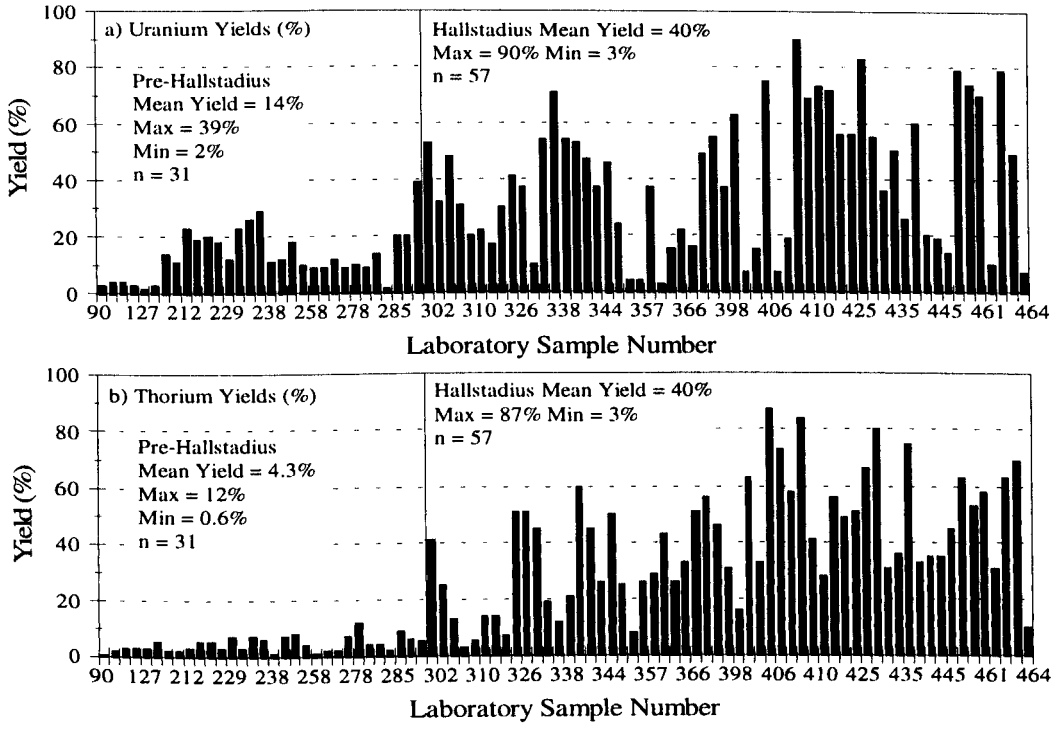

Figure 4.5. a) uranium and b) thorium chemical yields for both pre- and post- adoption of the Hallstadius method.

In order to calculate the alpha-counter efficiencies a calibration was carried out in late 1993 (Lean, 1995) using an alpha source of known activity (^{240}Pb, activity = 41.44 Bq). A counting efficiency of 30% was calculated with a source-detector spacing of 5 mm. The spike used during analysis had an activity of 17.1/ml. The equivalent activity of 1 ml of the spike was then calculated, based on the 30% counting efficiency, to provide a calibration factor of 5.1. This calibration factor was checked using a laboratory prepared standard, stalagmite 76001. This stalagmite sample was used in the Uranium-series Intercomparison Project (USIP). The USIP results are presented in Ivanovich and Warchal (1981) and results from the newly calibrated alpha counters were within the error limits of the USIP results (Lean, 1995).

4.7.1. Correction for counter background.

Two sources of background contamination are encountered during alpha-spectrometry. **Fixed background** is noise from the detector electronics and from incident cosmic rays on the detector. Fixed background is negligible when compared to **variable background** caused by alpha-recoil from the decay products of ^{232}U (Ivanovich and Murray, 1992). The products include ^{228}Th and ^{224}Ra which slowly build up on the detector surfaces. This is a disadvantage of the $^{232}U/^{228}Th$ spike but it is easily accounted for by regular monitoring.

Build up of ^{228}Th and ^{224}Ra from alpha-recoil was measured by monitoring the backgrounds of individual counters every 3 months. Each 'blank run' was made for 5 days with a clean planchet in place. Background counts were also obtained for ^{238}U, ^{234}U, ^{232}Th and ^{230}Th to subtract their small background contribution. Counts were made over the same region of interest that would contain counts from an actual sample. Table 4.2 shows the quarterly background counts, in counts per minute (cpm) for counter A to April 1995. Background counts are relatively steady until April 1994 when the Hallstadius electroplating method increased yields and consequently increased alpha recoil of ^{232}U daughters. The major increases were in the correction for ^{228}Th (and ^{232}U as it partially overlaps the ^{228}Th region). Until March 1994 the steady levels of background allowed mean correction values to be used. Post March 1994 the rising levels of background dictated that quarterly background counts were used.

4.8. Propagation of errors during uranium-series dating.

In order that quoted uranium-series dates are correctly interpreted we need to 1) determine their precision, the reproducibility of the result, and 2) their accuracy, the closeness of the result to the 'actual' value. Precision and accuracy are affected by counting errors, analytical errors and sample defects. Only counting errors are easily quantified since they are governed by laws of radioactivity (Ivanovich and Murray, 1992).

Period	^{238}U (cpm)	^{234}U (cpm)	^{232}U (cpm)	^{232}Th (cpm)	^{230}Th (cpm)	^{228}Th (cpm)
Mar 93	0.0005	0.0002	0.0011	0.0001	0.0005	0.0044
Jun 93	0.0006	0.0001	0.0010	0.0002	0.0006	0.0042
Sept 93	0.0004	0.0002	0.0019	0.0001	0.0006	0.0056
Oct 93	0.0001	0.0006	0.0020	0.0001	0.0002	0.0055
Dec 93	0.0001	0.0001	0.0022	0.0002	0.0001	0.0065
Apr 94	0.0005	0.0009	0.0013	0.0004	0.0006	0.0080
Jul 94	0.0004	0.0001	0.0023	0.0001	0.0002	0.0076
Oct 94	0.0005	0.0004	0.0038	0.0003	0.0001	0.0140
Jan 95	0.0008	0.0011	0.0107	0.0002	0.0013	0.0314
Apr 95	0.0009	0.0019	0.0109	0.0001	0.0013	0.0400

Table 4.2 Background counts (in cpm) of relevant isotopes on counter A from March 1993 to April 1995. Note the increase in the background counts after April 1994 associated with increased yields obtained using the Hallstadius (1984) electroplating method.

4.8.1. Errors associated with Alpha-spectrometric counting.

Nuclear decay is a random process and is described mathematically using an exponential decay derived from probability theory (Evans, 1955). Since the probability of decay is small and the number of observations large, the Poisson distribution (P_x) is used as a good approximation in nuclear statistics;

$$P_x = \frac{m^x}{x!} e^{-m} \quad \textbf{4.8}$$

where m is the true number of disintegrations whose measured value is x. It should be noted that this distribution is only valid when the observation time is short relative to t½

(Ivanovich and Murray, 1992). The standard deviation (σ^2) for the Poisson distribution of each measured quantity i.e. the ± error in a single measurement, is given by;

$$\sigma^2 = \pm\sqrt{m} \qquad \textbf{4.9}$$

The final error, R, is the sum of the standard deviations of individual measurements, thus;

$$R^2 = r_1^2 + r_2^2 + \ldots + r_n^2 \qquad \textbf{4.10}$$

where r_1, r_2, ...r_n are the standard deviations of the individual measurements.

In the measurement of a source countrate, s, a separate measurement of the background must be made first. The average countrate of source alone is determined thus:

$$S = s \pm \sqrt{(s/T_s + b/T_s + b/T_b)} \qquad \textbf{4.11}$$

where s is the measured countrate, T_s is the count time of the source, b is the background and T_b the count time of the background. Errors for background appear twice in equation (4.11), once for variation in measurement of s and b together and once for b alone. Alpha spectrometric dates and isotope ratios are therefore quoted with errors to one standard deviation (1σ) based on these counting statistics.

4.8.2. Errors associated with analytical processes.

Analytical errors may be incurred during the chemical separation of uranium and thorium in the laboratory as follows;

1) U and Th contamination of laboratory reagents.
2) Fractional losses of U and Th onto glassware during extraction.
3) Memory effects from isotopes on glassware.

4) Incomplete separation of uranium and thorium.

To check for reagent contamination possibilities 'reagent blank' experiments were conducted every few months. These experiments used only spike solution and normal extraction techniques for uranium and thorium. Alpha counting was then used to assess levels of contamination, taking into account counter background. No effects from contamination were noted in these reagent blank runs. Loss of isotopes onto glassware may occur if the pH rises >3.5. The two points at which this can happen are when U and Th are precipitated as iron hydroxide and also at the IPE stage. However, care was taken to maintain solutions at <pH 3.5 and copious quantities of acid were used to rinse glassware during extraction. Memory effects from isotope contamination of glassware are thought to be unlikely after cleaning in a chemical washer and rinsing in 9M HCl before each use. Incomplete separation of U and Th isotopes is thought most unlikely as each initial separation of isotopes from the 9M HCl supernate used fresh anion exchange resin. In addition, uranium forms strong anionic complexes in HCl acid solutions whereas thorium does not (Ivanovich and Harmon, 1992).

4.8.3 Errors associated with sample defects.

Low concentrations of uranium can cause problems in dating speleothem since alpha spectrometry normally requires a minimum of 0.05 ppm (Ivanovich and Harmon, 1992). To some extent the effects of low concentrations can be offset by using more sample but when quantities of material are limited this is not always possible. Low concentrations of uranium are especially problematic in young speleothems, where little allogenic ^{230}Th is present, resulting in increased counting errors. In this study Spanish stalagmite AG03 had uranium concentrations in the range 0.02 to 0.07 ppm which was below and close to the recognised limit. The highest concentrations of uranium were found in Spanish sample TR02 with a range of 1.1 to 1.8 ppm.

Detrital contamination, as discussed in section 4.4, was also problem found in most samples of this study. Stalagmite SC01 showed greatest levels of detrital

contamination with $^{230}Th/^{232}Th$ ratios of 0.8 to 1.6. As discussed in section 4.4.2, the top sample can be used as an estimate for the initial $^{230}Th/^{232}Th$ ratio thus allowing a correction to be made. Since many of the speleothems were active when collected this correction technique was considered valid in most cases. However, the errors associated with large detrital corrections were large but as the ages increased the percentage error in an individual date generally dropped since more radiogenic ^{230}Th was present.

4.9. Testing the leachate/leachate method on contaminated sub-samples.

In an attempt to check the dates obtained by standard U-series dating, several sub-samples containing high levels of detrital contamination were subjected to leachate/ leachate (L/L) analyses, as described in section 4.4.3.2. Although the use of the L/L method met with limited success in this study its potential for the dating of contaminated speleothems requires further assessment.

In this work the ^{230}Th, ^{234}U and ^{238}U isotope ratios of the detritus-free end-member were obtained using the isochron gradient of plots of $^{234}U/^{232}Th$ versus $^{230}Th/^{232}Th$ and $^{238}U/^{232}Th$ versus $^{234}U/^{232}Th$, commonly known as 'Rosholt-type' diagrams (Rosholt, 1976). In these diagrams the isotope-pair ratios of three (or more) co-genetic samples define a straight line whose slope determines the ^{230}Th, ^{234}U, ^{238}U detritus-free end-members. In general, the data for samples will not lie directly on a straight line but will scatter about it due to analytical errors.

The question arises of how to fit a line to such data taking into account the degree of scatter. Schwarcz and Latham (1989) for example, suggested that a line be fitted taking into account not the error of individual points but the scatter of the points about the least squares line. This was based on the assumption that the decreased activity of ^{232}Th equally affects the ordinate and abscissa. It does not account for the analytical errors in the measurement of each isotopic ratio. Luo and Ku (1991) suggested that since perfect fits to the least squares line were possible, resulting in zero scatter errors, the propagated error including individual counting errors of $^{230}Th/^{234}U$ and $^{232}Th/^{234}U$ in each

sample are used in combination with the scatter about the straight line. This approach does not assume error correlation between $^{230}Th/^{234}U$ and $^{232}Th/^{234}U$ when, in fact, ^{234}U and ^{232}Th are common to both plots.

A common method of line-fitting for stable isotope geochemistry uses a procedure that weights the data-points inversely according to their analytical errors and their error-correlations (Cumming *et al*, 1972). Determination of whether these analytical errors are likely to have caused the observed degree of scatter about the isochron are used to assign errors to the Uranium-series dates obtained from the regression line. The regression-line itself is fitted using either least-squares (York, 1969) or by maximum-likelihood estimation (Titterington and Halliday, 1979).

A paper by Ludwig and Titterington (1994) addressed the problems and additional statistical treatment required specifically when dealing with pairs of isochron diagrams. In stable isotope geochemistry, regression algorithms (Cumming *et al*, 1972; York, 1969; Titterington and Halliday, 1979; Kent *et al*, 1990) consider the case of correlated errors and assume that the analytical errors are the sole cause of scatter about the straight-line. Inverse weighting of each data point is achieved according to its analytical errors, error correlations and the iteratively defined slope and intercept of the regression line. It was noted that, in uranium-series isochron work two isochron diagrams are used to calculate the ^{232}Th-free isotope ratios ($^{234}U/^{232}Th$ vs. $^{230}Th/^{232}Th$ and $^{238}U/^{232}Th$ vs. $^{234}U/^{232}Th$). In addition, because the two plots share some of the same data, in this case $^{234}U/^{232}Th$, the normal error-weighted regressions are not valid. It was shown by Titterington and Halliday (1979) that the maximum likelihood estimation (MLE), originally applied to single X-Y isochrons could also be applied to a pair of X-Y isochrons allowing simultaneous regressions. The isochron-age errors are then calculated from the variances and covariance of the two regression slopes.

The MLE algorithm (Ludwig and Titterington, 1994) for calculation of ages and age errors from isochron data, is available as a Microsoft Quick Basic 4.5 program, UISO (Ludwig, 1993). UISO is for non-graphical output of isochron data and can be invoked from ISOPLOT (Ludwig, 1991) via a DOS shell. ISOPLOT itself can be used

for the graphical output of isochron data. For calculation of the sample age the program requires correct estimation of errors and error-correlations for each isochron data point. The following calculations are used for estimation of individual isotope ratio errors and error correlations. The isotope ratio errors on any particular isotope ratio of the same element are:-

$$s^2_{(a/b)} = s^2_a + s^2_b \qquad \textbf{4.13}$$

where $_a$ and $_b$ are the two isotopes (in our case ^{230}Th and ^{232}Th) and s is the percent counting error.

Since chemical yields of U and Th are not identical a spike is added to calculate ratios between unlike elements. The isotope ratio errors of two unlike isotopes (eg. ^{234}U/^{232}Th) are estimated thus;

$$s^2_{42} = s^2_4 + s^2_2 + s^2_{ThSpike} + s^2_{USpike} \qquad \text{for } ^{234}\text{U}/^{232}\text{Th} \qquad \textbf{4.14}$$

$$s^2_{82} = s^2_8 + s^2_2 + s^2_{ThSpike} + s^2_{USpike} \qquad \text{for } ^{238}\text{U}/^{232}\text{Th} \qquad \textbf{4.15}$$

where $_{42}$ = ^{234}U/^{232}Th, $_4$ = ^{234}U, $_2$ = ^{232}Th and $_{82}$ = ^{238}U/^{232}Th, $_8$ = ^{238}U, $_2$ = ^{232}Th.

In the Rosholt-type diagrams used in this study, a common isotope (^{232}Th) is found in both X and Y axes and thus the errors of X and Y values are correlated. The **error correlation** (ρ) of a pair of isotope ratio measurements where one of the pairs is for like-elements (i.e. ^{234}U/^{232}Th - ^{230}Th/^{232}Th) are calculated using:

$$\rho_{(42,02)} = \frac{s^2_2}{s_{42}s_{02}} \qquad \text{for } ^{234}\text{U}/^{232}\text{Th} - ^{230}\text{Th}/^{232}\text{Th} \qquad \textbf{4.16}$$

$$\rho_{(82,02)} = \frac{s^2_2}{s_{82}s_{02}} \qquad \text{for } ^{238}\text{U}/^{232}\text{Th} - ^{230}\text{Th}/^{232}\text{Th} \qquad \textbf{4.17}$$

where s_2 = error in ^{232}Th, s_{42} = error in $^{234}U/^{232}Th$, s_{82} = error in $^{238}U/^{232}Th$ and s_{02} = error in $^{230}Th/^{232}Th$.

For error correlations of an isotope pair where both contain isotopes of dissimilar elements the following is used;

$$\rho_{(82,42)} = \frac{s_2^2 + s_{USpike}^2 + s_{ThSpike}^2}{s_{82}s_{42}} \qquad \textbf{4.18}$$

4.9.1. Procedure and testing the L/L analysis using UISO.

Initial experimentation for the L/L method was performed on speleothem sub-samples from Mexican stalagmite SSJ2, kindly donated by Dr. C. Lean. The six samples 6B and C, 7B and C, 8B and C were homogenised by grinding, and divided into seven 20g assays for leaching. A calculated age would represent the mid-point of these sub-samples. Acids, HCl 0.2M, 1M, 4M, 9M, HNO_3 2M, 4M and 7M were used to dissolve the assays. A wide range of acid strengths and two acid types were used in order to isolate the ideal acid types and strengths and also to find the conditions giving the widest spread of data points, with isotope ratios reflecting the increased leaching of detrital isotopes into the leachate. The uranium-series results of individual L/L assays from SSJ2 are shown in Table 4.4. These results can be compared with samples from SSJ2 dated by standard uranium-series procedure in Table 4.5 (Lean, 1995). Table 4.4 shows that the samples leached in HNO_3 have similar $^{234}U/^{238}U$ ratios. In the HCl leached samples only sub-samples leached in 4M and 9M HCl show any overlap between $^{234}U/^{238}U$, at 1σ. This may indicate that variable DIF had occurred. For sub-samples leached in 0.2M and 1M HCl losses of thorium onto glassware or adsorption onto remaining detritus is also suspected, since the $^{230}Th/^{234}U$ and $^{230}Th/^{232}Th$ ratios suggest low levels of thorium. Bischoff and Fitzpatrick (1991) found this problem occurring at low acidities (using 0.1M HNO_3). They found that firing the samples at 900°C enhanced the carry over of thorium from detritus to leachate. In addition it reduced the effects of differential isotopic fractionation between like-isotopes.

Assay	Acid	$^{234}U/^{238}U$ (error)	$^{230}Th/^{234}U$ (error)	$^{230}Th/^{232}Th$ (error)	U Yield (%)	Th Yield (%)	U concentration (ppm)	Uncorrected age (ka)	Corrected age (ka)
1	HCl 0.2M	2.11 (±0.05)	0.006 (±0.004)	1.19 (±1.32)	90	84	0.09 (±0.002)	0.7 (±500)	-0.2 (±1.2)
2	" 1.0M	1.83 (±0.03)	0.012 (±0.003)	2.42 (±1.34)	69	41	0.19 (±0.004)	1.4 (±1.4)	0.5 (±0.7)
3	" 4.0M	1.95 (±0.02)	0.032 (±0.002)	2.86 (±0.44)	73	28	0.44 (±0.006)	3.5 (±0.3)	1.7 (±1.7)
4	" 9.0M	1.96 (±0.02)	0.036 (±0.002)	2.93 (±0.36)	72	56	0.41 (±0.006)	4.0 (±0.2)	2.0 (±0.4)
5	HNO_3 2.0M	1.99 (±0.02)	0.022 (±0.002)	4.89 (±1.32)	56	49	0.41 (±0.006)	2.4 (±0.2)	1.7 (±0.4)
6	" 4.0M	1.98 (±0.03)	0.022 (±0.002)	4.56 (±1.62)	56	51	0.43 (±0.006)	2.4 (±0.2)	1.6 (±0.4)
7	" 7.0M	1.99 (±0.03)	0.028 (±0.002)	2.46 (±0.36)	50	36	0.42 (±0.007)	3.1 (±0.2)	1.2 (±0.5)

Table 4.4. Isotope ratios and ages for leached samples from stalagmite SSJ2. Note that for all calculated dates a thorium correction ratio of 1.5 has been used. Errors are 1 sigma based on counting statistics.

Sample	234 U/238 U (error)	230 Th/234 U (error)	230 Th/232 Th (error)	U Yield (%)	Th Yield (%)	U concentration (ppm)	Uncorrected age (ka)	Corrected age (ka)
1C	1.91 (±0.05)	0.021 (±0.006)	3.25 (±1.73)	15.2	3.4	0.49	2.3 (±0.7)	1.2 (±1.2)
4B	2.03 (±0.07)	0.021 (±0.004)	6.22 (±3.83)	10.8	8.7	0.38	2.3 (±0.8)	1.8 (±0.8)
10B	1.90 (±0.06)	0.104 (±0.016)	6.38 (±2.46)	23.3	4.8	0.33	11.8 (±1.9)	9.1 (±2.8)
17B	2.07 (±0.05)	0.153 (±0.010)	28.8 (±7.6)	11.7	7.3	0.68	17.8 (±1.2)	-
17C	2.09 (±0.05)	0.138 (±0.010)	31.9 (±12.6)	14.2	5.8	0.63	15.9 (±1.2)	-

Table 4.5. Isotope ratios and ages for samples from stalagmite SSJ2 (After Lean, 1995). Samples used for L/Lanalysis in this stud were sub-samples 5,6 and 7; slices B and C (hence 'B' and 'C' suffix). Errors are 1 sigma and are based on counting statistics.

The $^{230}Th/^{232}Th$ ratio indicates detrital contamination. An increased detrital input to the leachate, due to increased leaching in stronger acids, should be revealed by a decreasing $^{230}Th/^{232}Th$ ratio. The HNO_3 leached sub-samples (Table 4.4) show that the $^{230}Th/^{232}Th$ ratios decrease from 4.89 ±1.32 (2M HNO_3) to 2.46±0.36 (7M HNO_3) as expected. However, $^{230}Th/^{232}Th$ ratios in HCl leached samples increase, although the 0.2M and 1M HCl samples are not considered reliable due to variable DIF and likely isotope losses. This increase is puzzling since it implies that with HCl as the leaching agent, less detrital thorium is carried over into the leachate at higher molarity. The reason for this may be due to variable DIF of ^{230}Th and ^{232}Th from the detritus which may only occur with HCl leaching. Due to this degree of uncertainty with the HCl leached samples, subsequent L/L experiments were performed with HNO_3.

Table 4.6 shows the relevant isotopic ratios, errors and errors correlations calculated from the SSJ2 HNO_3 leached assays, using the Ludwig and Titterington (1994) method. Figure 4.7 shows the isochron plots generated by ISOPLOT for these same data. UISO calculated a date of 2.1±0.3 ka for these three L/L data points. To check the validity of the regression line calculated, UISO uses the mean square of weighted deviates (MSWD). The MSWD is the degree to which the observed amount of scatter of the data points about the regression line can be explained by the calculated analytical errors and error correlations. The MSWD should average unity when the observed scatter about the regression line can be explained solely by the analytical error (Wendt and Carl, 1991).

The MSWD value for these SSJ2 data was 4.21×10^{-3}. According to the work of Wendt and Carl (1991) an MSWD of <0.3 indicates overestimation of the assigned analytical errors. However it should be noted that in our case there is effectively zero scatter about the regression line (r^2 =0.999). Luo and Ku (1991) suggest that perfect fits to the data are possible and appears likely in this case.

Acid	$^{238}U/^{232}Th$	1σ %error	$^{234}U/^{232}Th$	1σ %error	$^{230}Th/^{232}Th$	1σ %error	ρ 238/232-234/232	ρ 238/232-230/232	ρ 234/232-230/232
2M HNO_3	125.48	26.20	249.15	26.19	4.89	27.18	0.999	0.959	0.959
4M HNO_3	116.67	24.27	231.29	24.25	4.56	25.28	0.998	0.955	0.955
7M HNO_3	61.12	12.96	122.00	12.93	2.46	14.54	0.994	0.872	0.869

Table 4.6. Errors and error correlations (ρ) for HNO_3 leached SSJ2 samples calculated using equations 4.13 to 4.18 (shown in section 4.9).

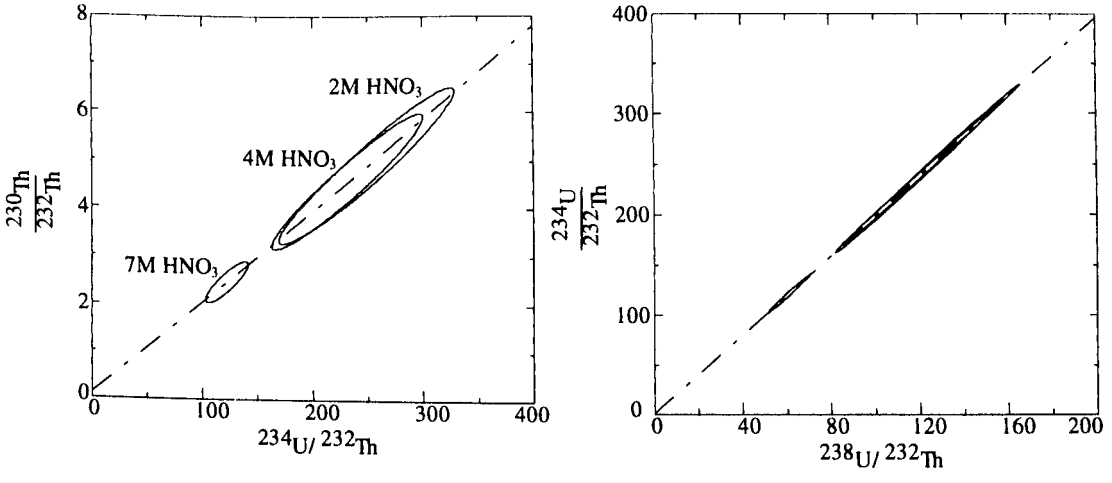

Figure 4.7. Isochron plots for the three assays of SSJ2 dissolved in 2, 4 and 7M HNO_3 respectively. Errors in both ordinate and abscissa are shown with ellipses, reflecting the highly correlated errors.

The date calculated by the MLE method compares well with those dates obtained by routine uranium-series analysis of SSJ2 and highlights an interesting property of this speleothem. The MLE date (effectively of sub-samples 7B and C) of 2.1±0.3 ka is in chronological sequence between normally dated sub-sample 4B at 1.8±0.8 ka and 10B at 9.1±2.8 ka (Table 4.5). This is, in itself, a fundamental test of the data obtained using the L/L method. Clearly, it also demonstrates that the growth rate of this speleothem has increased between sub-sample 10B and 7B.

Figure 4.8 illustrates the original dating of SSJ2 and the L/L date from this study. The original linear-least squares fit to these uranium-series data gave a growth rate of 0.02 mm/yr^{-1} making the SSJ2 basal age 18.9±2.2 ka and the top modern (solid best-fit line on Figure 4.8). The L/L date provides further evidence for at least one significant change in growth rate. As it was not known exactly where the change in growth rate took place, the midpoint of the L/L samples, effectively sub-sample 7B+C, was taken as the point of change. A new linear-least squares fit to sub-samples 1B, 4B and the L/L sub-sample midpoint gives a growth rate of 0.13 mm yr^{-1} for the upper section of SSJ2 (dotted line Figure 4.8). The best-fit to the dates of the lower sub-samples, including the L/L date, yields a growth rate of 0. 063 mm yr^{-1} and a basal age of 20.2±2.6 ka (dashed line Figure 4.8). This is within the 1σ errors of the original basal date.

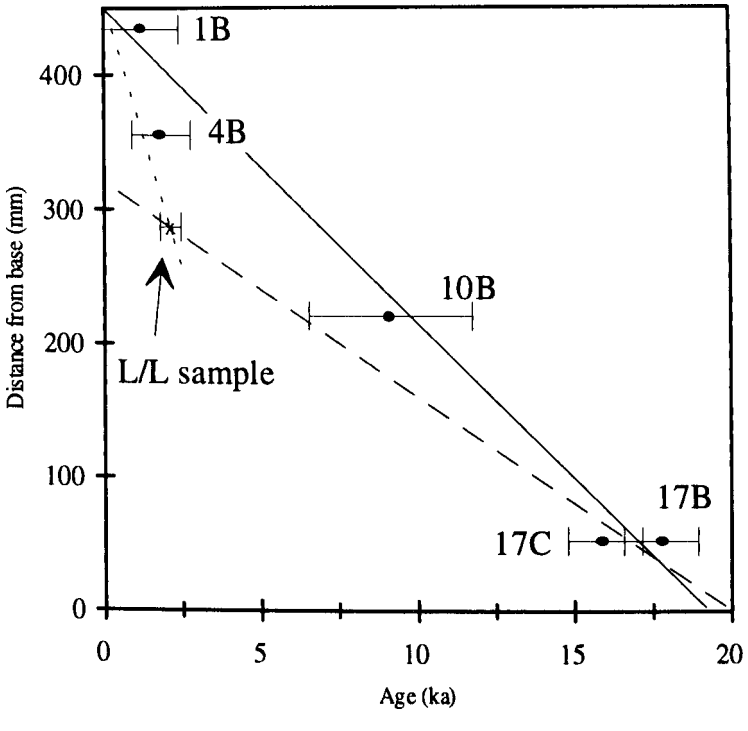

Figure 4.8. Age-height plot of dates obtained from uranium-series analysis of sub-samples from stalagmite SSJ2 (Mexico). The original linear-least squares fit is shown by the solid line and gave a basal age of 18.9±2.2 ka and a growth rate of 0.2 mm yr^{-1}. The L/L date, shown by X allows two growth rates to be identified. The best-fit to the upper samples (dotted line) gives a growth rate of 0.13 mm yr^{-1}. The fit to the lower dates gives a growth rate of 0.063 mm yr^{-1} and a basal age of 20.2±2.6 ka (dashed line).

These results illustrate one of the pitfalls of making a linear-least squares fit to all the data, in that changes in growth rate of this order are not detected with sampling of this resolution. Highest density sampling (i.e. smaller samples) is only possible when there is sufficient uranium concentration or when using mass-spectrometry. Table 4.4 also shows that in this case the thorium correction method used ($^{230}Th/^{232}Th$ =1.5) over-corrects individual uranium-series dates, producing dates that are increasingly younger than the L/L isochron age.

4.9.2. L/L analysis of samples from Chinese speleothems.

The Ludwig Titterington algorithm was used to calculate L/L dates for several trial sub-samples samples from the Chinese speleothems. The results are disappointing since, invariably, the MLE dates either did not fall within the linear fits to several standard uranium-series dates from single sub-samples and/or had larger associated errors. As a result only the L/L date calculated for PT04 was included in the overall dating of an individual speleothem. Figure 4.9 shows these data as isochron plots. Table 4.7 summarises the MLE dates obtained from the L/L method and compares them to linear least squares fits to normal U-series dates. Appendix K contains the U-series data plus errors and error correlations from L/L analysis of these sub-samples.

Speleothem	Sub-samples	MLE Date (ka)	U-series Date[1] (ka)	MSWD[2]	Probability of fit[2]
SC01	15+16B	2.6±4.2	4.8±0.7	0.039	0.962
PT02	21+22+23B	2.4±1.0	1.2±0.3	0.33	0.719
PT03	11+12B	-0.4±2.7	2.3±1.4	0.118	0.889
PT04	17+18B	1.9±1.5	2.6±0.5	0.305	0.737

Table 4.7. Comparison of dates obtained by L/L analysis with the MLE algorithm (Ludwig and Titterington, 1994) and with those obtained using standard U-series dating. [1]U-series date is based on a linear-least squares fit to dates of all sub-samples obtained by standard U-series analysis from each speleothem. [2]The MSWD (mean squared weighted deviation) and probability of fit show the statistical validity of the MLE regression line.

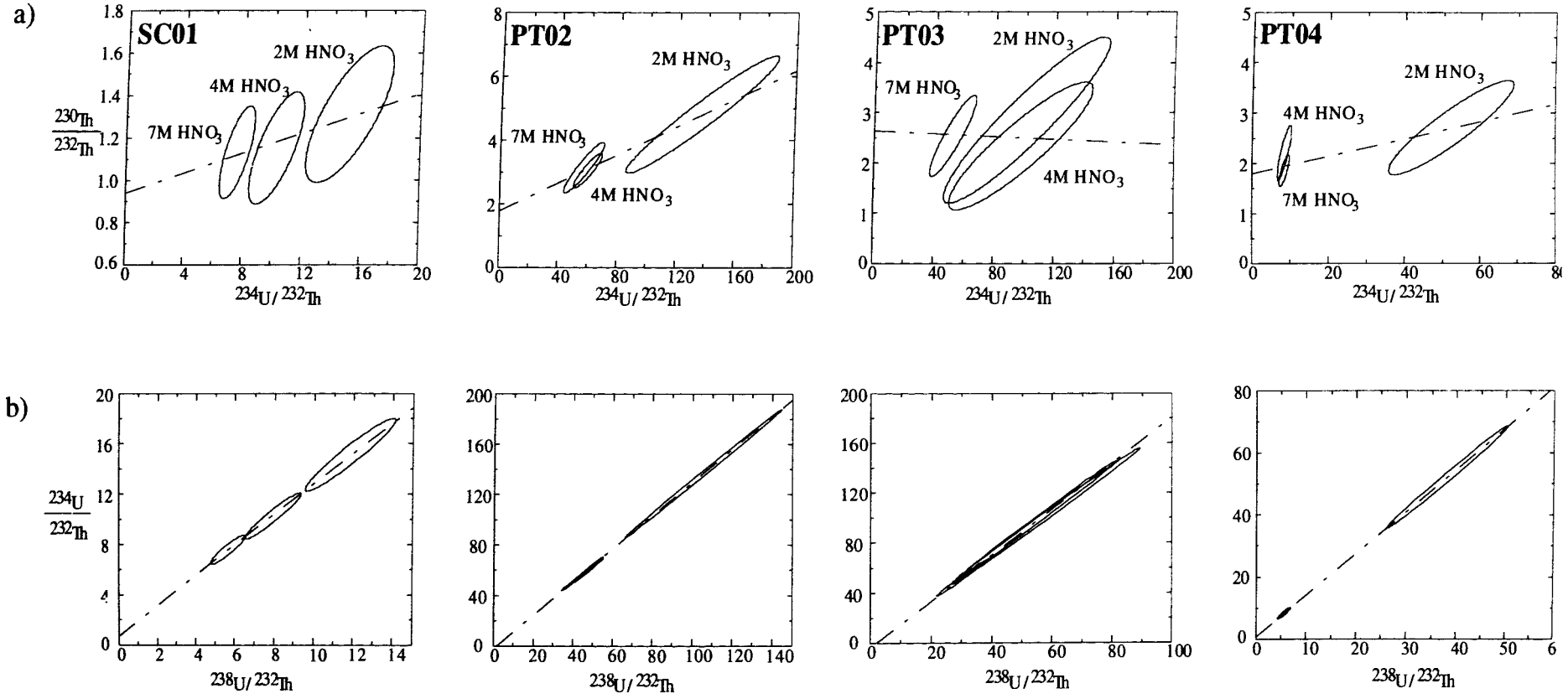

Figure 4.9 Isochron plots from ISOPLOT based on leachate / leachate data from Chinese speleothems SC01, PT02, PT03 and PT04. Errors are calculated using equations quoted in the text and are represented by error ellipses, reflecting the correlated errors.
a) $^{234}U/^{232}Th$ verses $^{230}Th/^{232}Th$ b) $^{238}U/^{232}Th$ verses $^{234}U/^{232}Th$

The low success rate for sub-samples subjected to L/L studies can be attributed to a number of possibilities. All speleothems had low uranium concentrations which, coupled with the young ages, have led to high counting errors especially for thorium. Figure 4.9a shows that most of the errors are associated with ^{230}Th or ^{232}Th resulting in large error ellipses. It is also apparent from Figure 4.9 that not all leaching experiments behaved as expected; in some cases increased strength of acid did not produce increased leaching of detrital isotopes to the leachate. For example, in PT03 the $^{230}Th/^{232}Th$ ratio for 2M HNO_3 was less than that for 4M HNO_3 (Figure 4.9a). The presence of variable DIF may be the cause of this non-sequential behaviour. The relatively poor spread of some datapoints may be attributable to the acids used to leach the samples. The acids used for leaching of the Chinese sub-samples were based on the initial experiments on SSJ2 outlined in section 4.9.1. From Figure 4.9 it is clear in the case of leached sub-samples of PT02, PT03 and PT03 that a wide spread of datapoints was not achieved. In fact some of the isotope ratios have widely overlapping error ellipses. The resulting poor spread of datapoints will result in a regression which yields more ambiguous MLE dates. For example, the MLE date calculated from PT03 (Table 4.7) for example was -0.4±2.7 ka and the errors on the MLE date of SC01 were six times that of the least-square fitted date errors (2.6±4.2 ka). Ku and Liang (1984) report that when leaching samples with two different strengths of $HN0_3$ a linear trend was not common. Bischoff and Fitzpatrick (1991) suggested that re-adsorption of isotopes onto detrital particles was possible in weak acids. Przybylowicz *et al* (1991) measured the molarity of the acid after leaching, using titration. They found that 7-5M HNO_3 had decreased to 6.5-3.5M after leaching. When leaching in 2M HNO_3 this decrease in molarity may make loss of isotopes a possibility.

Despite the fact that these were trial experiments it may have been possible to improve the leaching of sub-samples and to provide the MLE algorithm with better data. Firstly, further leaching by acid molarities in the range 2M to 7M HNO_3 and also beyond 7M HNO_3 may have assisted in producing a better spread of data. It may then have been possible to have sufficient data to reject suspect datapoints but the lack of large quantities of material made this difficult. In addition, for practical reasons it was not possible to leach more than three assays per coeval sub-sample. In further experiments,

leaching of more than 3 assays may help to achieve a better spread of data points on a more regular basis. However, it may have been possible to use a smaller range of acid molarities and still achieve a wide spread of data. For example, Przybylowicz *et al* (1991) leached their artificially produced samples in HNO_3 between 5 and 7M and achieved a sufficient spread of data to calculate dates. Secondly, further acid types or a variety of acids may be utilised despite the suggestion that HCl leaching was not generally successful in experiments on SSJ2 (section 4.9.1). For example, Hillaire-Marcel and Causse (1988) used acetic and hydrochloric acids for leaching of coeval samples. Thirdly, if as sometimes appears to be the case in the Chinese speleothems, variable DIF operates during leaching then the L/L method cannot be successful. The only method that is not affected by variable DIF is the TSD method (Bischoff and Fitzpatrick, 1991) as the detritus is dissolved with the carbonate member. The only requirement is that the detritus has a common $^{230}Th/^{232}Th$ ratio.

4.10. The ^{210}Pb dating method: a suitability trial on stalagmite PT03.

The ^{210}Pb dating method has been successfully used to date sediments and carbonates in the range 0 to 150 years (Druffel *et al*, 1990; Oldfield *et al*, 1989). Recently the method was used to date straw stalactites and stalactites from a cave in Texas, USA (Baskeran and Illife, 1993). This was the first use of this method in dating very young speleothems. The more usual method of U-Th dating is too imprecise over this time range and the ^{14}C dating method can suffer from contributions by 'fresh' and 'dead' carbon (Aitken, 1990). Potentially, the ^{210}Pb method has the ability to fill a gap in our ability to date very young speleothems. In this study the ^{210}Pb method has been used on stalagmite PT03 to obtain a comparison between the growth rates estimated using the U-Th method and those calculated with the ^{210}Pb method.

4.10.1. ^{210}Pb dating theory.

^{210}Pb ($t_{½}$ = 22.1 years) is the decay product of ^{226}Ra ($t_{½}$ = 1602 years) and initially diffuses into the atmosphere from soils via its gaseous intermediary ^{222}Rn ($t_{½}$ = 3.8 days).

^{222}Rn decays via a series of short lived isotopes to ^{210}Pb (Figure 4.1). ^{210}Pb remains in the atmosphere for up to a month after which it is removed by dry fall-out or precipitation. A percentage of this 'unsupported' ^{210}Pb, is adsorbed onto sediment particles deposited in surface waters. Subsequently, ^{210}Pb decays exponentially with depth in a sediment. Provided some estimate can be made of the initial ^{210}Pb activity then its activity at a particular depth can be used to determine the age of the sediment layer (Appleby and Oldfield, 1992). Therefore, the age or accumulation rate for a particular depth, assuming that ^{210}Pb and ^{222}Rn are immobile, is calculated from the unsupported ^{210}Pb activity (^{210}Pb unsupported = ^{210}Pb - ^{226}Ra) using the general decay equation:

$$C = C_0 e^{-\lambda t} \qquad \textbf{4.19}$$

where λ is the decay constant of the unsupported isotope (λ ^{210}Pb = 0.03114 yr^{-1}), C_0 is the initial excess and C the excess at time t. Thus, when plotted on a logarithmic scale the unsupported ^{210}Pb activity will decrease linearly with depth if the rate of supply and the rate of accretion remains constant. This has been termed the 'constant flux constant sedimentation rate' (CF-CS) model (Appleby and Oldfield, 1992).

In reality accumulation rates may change affecting the initial concentration of unsupported ^{210}Pb. In this case the ^{210}Pb profile will be non-linear with depth. Accretion rates can be calculated using two models assuming a) a constant initial ^{210}Pb concentration or b) a constant rate of supply. The first model, the CRS or 'constant rate of supply' model (Goldberg, 1963) assumes a constant transfer, ϕ, of ^{210}Pb to the accreting medium. Using this model, the supply rate of unsupported ^{210}Pb varies inversely with the accretion rate. The age t for a horizon at depth n is calculated from:

$$\sum(^{210}Pb - excess)_n = n_t(1 - e^{-\lambda 210 t}) \qquad \textbf{4.20}$$

where $\Sigma(^{210}$Pb-excess$)_n$ is the total excess ^{210}Pb activity from surface to depth n and n_t is the ^{210}Pb activity at a depth much older than 100 years. The second model assumes that the transfer function, ϕ, is directly proportional to the net accumulation rate. This allows the ^{210}Pb concentration to remain the same irrespective of changes in accretion rate and

is called the CIC or 'constant initial concentration' model (Pennington *et al*, 1976). The age difference between the surface and a particular depth *n* below the surface is given by:

$$t_n = \ln\left[(^{210}Pb-excess)_0 / {}^{210}Pb-excess)_n\right]\lambda_{210} \qquad \textbf{4.21}$$

where (^{210}Pb-excess)$_0$ and (^{210}Pb-excess)$_n$ are excess activities at surface and at depth *n* in dpm per gram of dry matter. For more detailed information on derivation of the CRS and CIC models refer to Appleby and Oldfield (1992).

In a cave system ^{222}Rn, incorporated into pore-waters from alpha-recoil of Rn atoms during decay of ^{226}Ra, will accompany unsupported ^{210}Pb into a speleothem. This provides two sources of ^{210}Pb; that supported from the decay of ^{222}Rn and that from atmospheric sources. By measuring the activity of ^{226}Ra, we can subtract the effects of the supported ^{210}Pb from the unsupported ^{210}Pb and thus calculate the accretion rate.

4.10.2. Sample preparation and counting.

Five samples were prepared from the top surface of PT03 by uniform scraping of successively deeper layers. Depth from surface was calculated by measuring the dimensions at key points on PT03 after each scraping. Each sample was weighed and placed inside an airtight glass vial.

The samples were counted on the gamma counter in the Environmental Radiation Laboratory at Liverpool University by Dr. P. Appleby. The advantages of gamma-counting are that it is non-destructive and consequently requires no spike, requires minimum sample preparation and allows assessment of other gamma-emitting isotopes simultaneously. Samples are excluded from environmental air for a minimum of two weeks before counting in order that any airborne ^{222}Rn activity reaches equilibrium with ^{226}Ra allowing its daughter ^{214}Pb to be used a proxy for ^{226}Ra. ^{226}Ra can be counted directly by gamma-spectroscopy but suffers from interference from ^{235}U whose energy levels overlap it. ^{214}Pb has a strong appearance in the gamma-spectrum allowing

detection limits as low as 0.4 mBq g^{-1}. Due to the low concentrations of ^{210}Pb, count times were in excess of three days for the oldest layers. Table 4.8 shows the isotope activities after counting and Figure 4.10 shows these activities as a function of distance from the stalagmite surface.

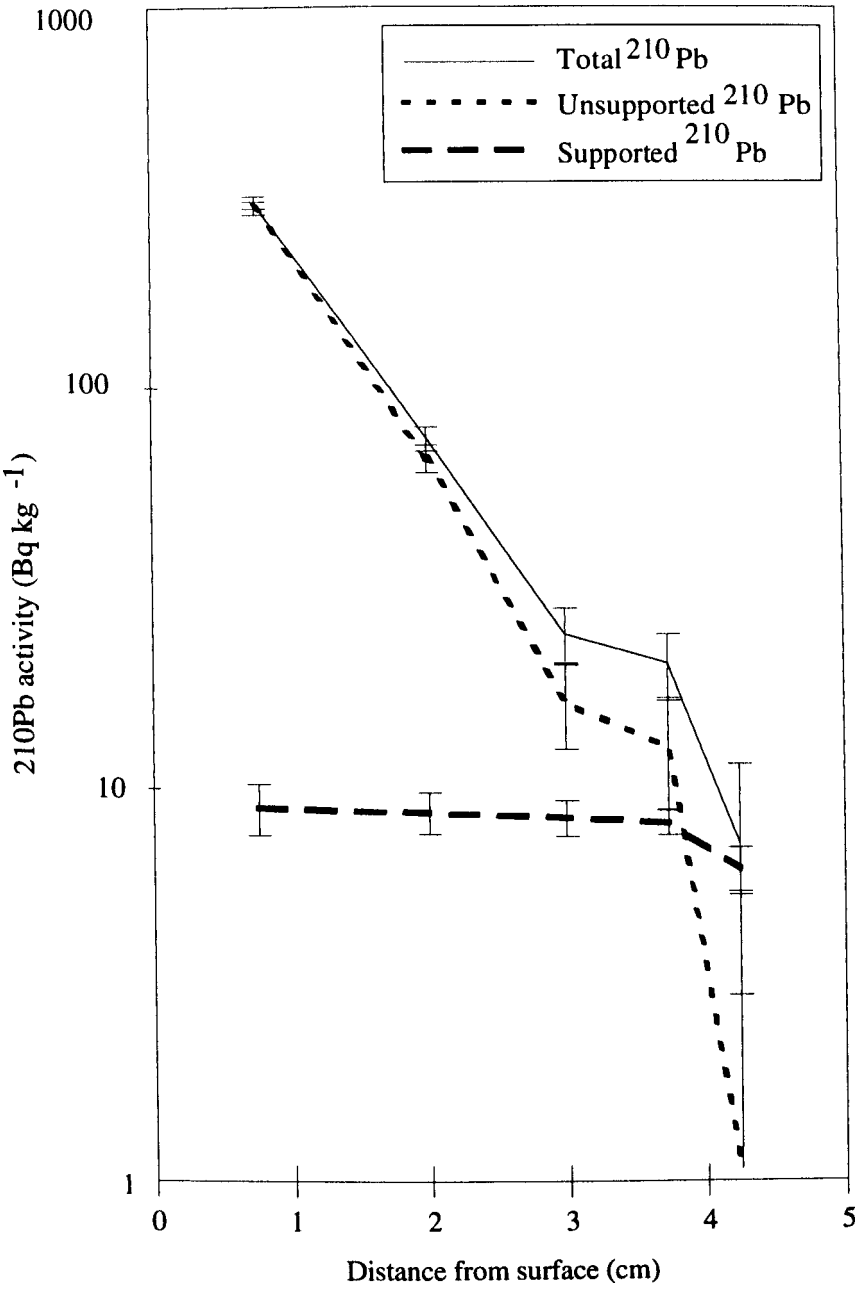

Figure 4.10. ^{210}Pb activity with distance from surface of stalagmite PT03. The growth rate is calculated from the linear decay of unsupported ^{210}Pb.

Sample	Depth (mm)	Mass (g)	Total ^{210}Pb conc. Bq/Kg	^{226}Ra conc. (^{214}Pb) Bq/Kg	Unsupported ^{210}Pb conc. Bq/Kg
PT03-A	0.76	1.7	315.54±11.31	9.07±1.39	306.47±11.40
PT03-B	2.0	1.55	80.08±5.63	8.86±1.08	71.22±5.73
PT03-C	2.99	1.50	25.61±4.04	8.59±0.91	17.02±4.14
PT03-D	3.73	1.56	21.51±4.02	8.40±0.60	13.11±4.06
PT03-E	4.24	1.48	7.44±4.43	6.37±0.88	1.07±4.52

Table 4.8. ^{210}Pb data for samples of PT03. Depth refers to the mean thickness, and hence depth from surface, of material from each scraping. Errors are to 1σ and are based on counting statistics.

From Figure 4.10 and Table 4.8 the activity of unsupported ^{210}Pb from the PT03-E, the deepest sample, is very low suggesting that at this depth equilibrium had been approached. It should also be noted that the decay of ^{210}Pb with depth is not constant especially below the 2.99 mm level. Despite this, the supported ^{210}Pb activity remains almost constant with depth suggesting that the non-linear ^{210}Pb decay was mainly due to incorrect depth measurement when sampling. Scraping over a wide area to get a sample for one depth interval was not the best way to prevent overlaps of material from one depth to another. In future using a small depth marked drill to extract over a fixed depth interval may be more accurate. The CRS and CIC models were used to calculate growth rates and ages of the samples from PT03. These data are presented in Table 4.9.

The mean growth rates from the CIC and the CRS models agree closely (0.024 and 0.028 mm yr^{-1} respectively). The mean growth rate based on the two models is 0.026 mm yr^{-1}. This growth rate is a little over half the growth rate of 0.048 mm yr^{-1} calculated from a linear-least squares fit to the U-Th dates (Chapter 6). It should be noted that, by its very nature, a linear-least squares fit on U-Th dates will smooth out any irregularities in growth rate and that the calculated rate is then a mean growth rate. Thus, U-Th dating will not generally pick out changes in growth rate over a period as short as 150 years. Moreover, the fact that at least 20g of sample was required in order to provide uranium in sufficient quantity for alpha-counting made sampling at higher resolutions impossible.

In addition, in speleothems such as PT03 where uranium concentration is low and detrital thorium contamination is high the associated age errors will also mask rapid changes in growth rate.

Model	Sample	Depth (mm)	Growth Rate (mm yr^{-1})	Age (years)
CRS MODEL		0.00		0
	PT03-A	0.76	0.026	29±2
	PT03-B	2.00	0.022	80±5
	PT03-C	2.99	0.025	123±12
CRS model equilibrium depth = 3.5 mm				
CIC MODEL		0.00	--	0
	PT03-A	0.76	0.028	27±1
	PT03-B	2.00	0.028	74±3
	PT03-C	2.99	0.028	120±8
CIC model equilibrium depth = 4.0 mm				

Table 4.9. ^{210}Pb ages and growth rates for PT03 calculated using the CRS and CIC models.

Despite these problems, the ^{210}Pb growth rate, when assumed to apply to the whole stalagmite, is comparable with that of the U-Th method. The basal age of 9.8±1.5 ka calculated from extrapolation of the ^{210}Pb data overlaps the U-Th basal age at the 1σ level. Figure 4.11 illustrates the differences between the age estimates of declination and inclination features in PT03 using the U-Th and ^{210}Pb methods for dating of individual sub-samples. Using the ^{210}Pb growth rate to date PT03 progressively increases the age of sub-samples down the stalagmite. In terms of comparison with other records from Xingwen, this slightly improves the fit of equivalent declination and inclination features in the range 0 to 3.0 ka but lessens the correlation below 3.0 ka. Figure 6.30 compares the U-Th dated record of PT03 with the other records from Xingwen. However,

extrapolating the ^{210}Pb growth rate over 9.8 ka based on the dating of 3.5 mm from the top of PT03 is hard to justify. In addition, the poor temporal resolution of PSV by PT03 did not warrant using the ^{210}Pb dating in preference to the U-Th dates, despite the errors associated with the latter.

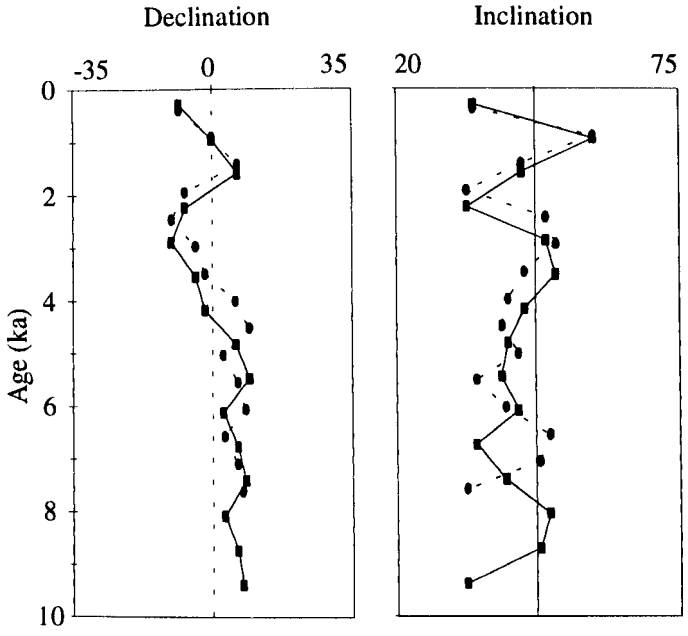

Figure 4.11. Declination and inclination of PT03 using U-Th dates (dotted line) and ^{210}Pb dates (solid line).

In summary, a direct comparison of the two dating methods may not be truly realistic in this case as each method applies over changes in growth rate of differing magnitudes. This exercise demonstrated that the ^{210}Pb method can be used effectively for dating the youngest surfaces of rapidly growing stalagmites. The ideal method would be to use a combination of dating methods with overlapping age ranges in order to a) precisely define young sample ages b) reduce the need for linear-least squares extrapolation below the effective dating range of the U-Th method and c) to resolve growth rate changes on a finer scale so at the very least several 'fits' can be made to the data according to its age.

5. Collection and preparation of speleothems.

This chapter aims to explain how speleothems form, how they are collected from the cave, how they are prepared and how their palaeomagnetic signal is measured and analysed. A brief account of previous work is also presented.

5.1. Speleothem growth and morphology.

Ground waters passing through limestones become saturated with calcium carbonate ($CaCO_3$) dissolved from the limestone. As this water enters the cave the partial pressure of CO_2 is greater than that of the cave air allowing degassing of CO_2. Degassing causes the water to become super-saturated forcing calcite to precipitate in a number of forms called speleothems (Ford and Williams, 1989).

Pore waters leaving fissures in the cave roof precipitate a thin ring of calcite which over time builds downwards forming a **straw stalactite**. If the central channel becomes blocked by calcite or detritus, water begins to flow down the sides of the straw, building up successive layers of calcite forming a **stalactite**. Water dripping from a straw or stalactite will strike the cave floor and if the substrate is suitable, a mound of calcite builds up eventually forming a columnar shaped **stalagmite**. Stalagmites and stalactites may join the roof or floor or each other forming a **column**. **Flowstones** are formed by laminar sheets of calcite deposited as water runs down a cave wall or along the cave floor. Figure 5.1 shows these types of speleothem deposits in a typical cave system.

Internally, a calcite speleothem grows by enlargement and coalescence of syntaxially deposited crystallites. These crystallites are columnar and may be parallel or radial, termed palisade (Kendal and Broughton, 1978). Often small voids remain between the crystallites trapping pore-waters (fluid inclusions) giving rise to a milky appearance. Changes in colour, texture and detrital content highlight the growth layers which can show variations in the deposition rate throughout the growth period. In an individual

speleothem colour may vary from layer to layer. Some of the colouration is thought to be caused by trace elements in the calcite matrix. Gascoyne (1979, 1977) showed that most colouration was from organic matter carried with the drip waters. Lauritzen *et al* (1986) confirmed that these organics were predominantly humic and fulvic acids of high molecular weight.

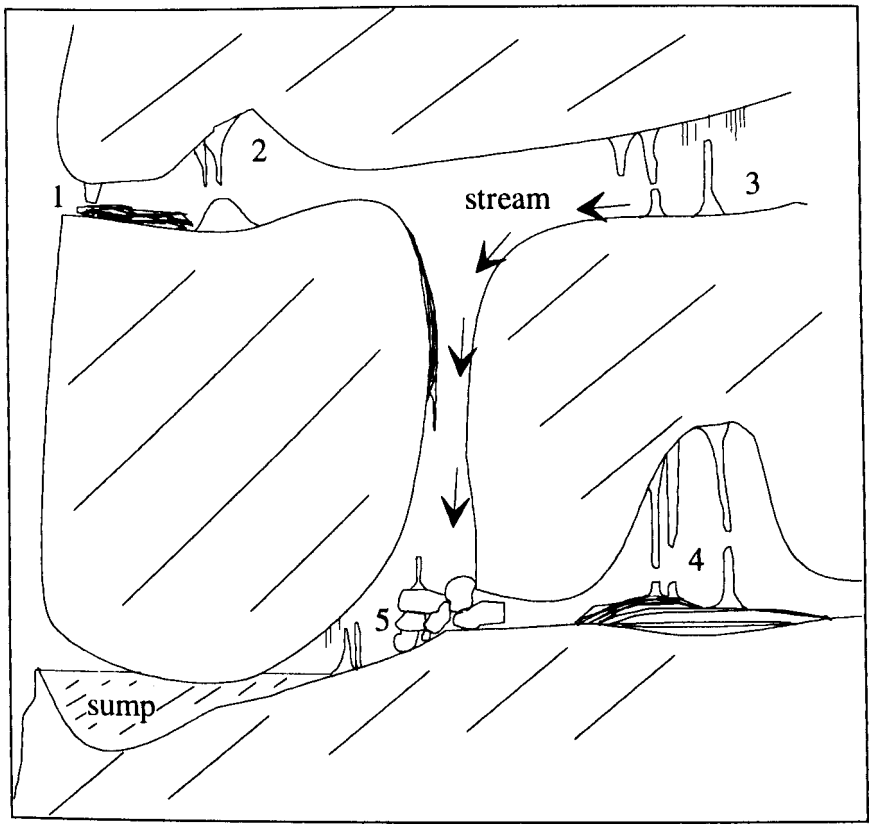

Figure 5.1. Cross-section through typical cave system showing the types of speleothem and their possible locations (After Latham and Schwarcz, 1992).

1. Entrance. High level abandoned entrance with rapid evaporation forming non-crystalline 'soft-calcite'. Formations contain large quantities of wind-borne detritus.
2. Near Entrance. Rapid degassing and some evaporation. Deposits are often massive and may be heavily weathered. Some wind-borne detritus.
3. Interior. High level formations. They contain no detritus unless flooded and are generally non-porous.
4. Deep Interior. Slow growth by degassing only. Older formations may contain detritus but are not currently active and are decaying.
5. Active streamway. Rapidly growing young speleothems are non-porous are seasonally flooded and contain large quantities of detritus. They form mainly by degassing but perhaps with some assistance from cave through-draughts causing evaporation.

The growth layers in a speleothem can show cessation of growth, usually by a clearly defined growth hiatus. Growth stoppages may occur when the drip waters are diverted, blocked by calcite or detritus in the fissures and if cold or arid conditions are in evidence. Submergence of the speleothem by flood waters or by rising sea-level will also stop growth. Seasonally flooded speleothems show alternating light and dark coloured sub-millimetre growth layers representing exposed and submerged conditions.

5.3. Previous speleothem work and the current state of research.

Latham led and pioneered the work on speleothem magnetism in a doctoral thesis (1981). In his initial work (Latham *et al*, 1979) the use of speleothems as recorders of PSV was justified. It was shown that speleothems could contain a weak but generally stable remanence, could sequentially record field behaviour, and could be reliably dated using the $^{234}U/^{230}Th$ method. A further far reaching possibility was the apparent lack of depositional errors (often associated with sedimentary PSV records; Verosub, 1977). This was demonstrated by sampling lateral samples, where growth layers dip almost vertically and by comparing their declination and inclination to coeval central samples. Agreement in both declination and inclination was within the α_{95} error limits. This was taken to indicate that the remanence was of chemical rather than detrital origin since depositional effects were thought likely to influence directions if a DRM was dominant. The absence of depositional errors was also confirmed in a study on Mexican and Canadian speleothems (Lean, 1995; Lean *et al*, 1995) and also in studies of UK stalagmites by Perkins (1993).

Subsequent work by Latham *et al* (1982, 1986, 1987 and 1989) has produced dated PSV records from speleothems in Mexico and Western Canada. These PSV records compared well with archaeomagnetic, sedimentary and modelled data for these areas. Tests for depositional errors again showed agreement between lateral and central samples despite the detrital load. In addition, the modern top of some speleothems allowed a comparison between the 'averaged' recorded field direction in the topmost

specimen and the present field direction. Directions were coincident indicating that the remanence was acquired instantaneously.

The question as to how the remanence is acquired is a point of great interest. Latham *et al* (1989) suggested that speleothem remanence was carried by CRM alone or a mixture of CRM and DRM. He pointed out that in speleothems with no visible detritus from England and Bermuda, with immeasurable NRMs, their high field IRMs showed the presence of single domain magnetite. It was presumed that this magnetite originated from the drip water. In two Canadian speleothems containing organics circumstantial evidence was seen for a CRM. In this case, iron complexed with organics upon calcite precipitation may have been released in a reduced state. In speleothems where the detrital content was high it was suggested that opportunity existed for grain alignment to occur before calcite precipitated or that a chemical remagnetisation occurred. However, the age of the remanence appears to be contemporaneous with the calcite matrix whether or not the NRM is a CRM or a CRM-DRM. Perkins (1993) suggested that equidimensional grains may align to the ambient field in surface depressions within the calcite matrix. He suggested that in each depression the depositional surface is effectively horizontal and that grains do not experience any depositional effect. This mechanism of remanence acquisition could operate up to the largest grains sizes reported in Mexican speleothems (Latham *et al*, 1989). However, upon calcite precipitation and de-watering of the depressions magnetic grains may be re-aligned. There has been no work on the associations between fluid inclusions and detritus trapped within them.

The reliability of speleothem PSV records have been tested using comparisons with other speleothem records of the same age and from the same area. Morinaga *et al* (1989) found comparable features of PSV in three SW Japanese speleothems. These records were dated by fitting them to archaeomagnetic records from Japan. The resulting correlations are described as 'tentative' and since no absolute dating was performed their ages, extrapolated up to 15 ka from the archaeomagnetic data, are debatable. Lean (1995) conducted a more thorough comparison of absolutely dated speleothem records from Canada and Mexico. Results indicated a reasonable degree of correlation between some of the speleothems but the quality of some of the speleothem records were

diminished by poor temporal resolution caused by slow growth rates. In this case the speleothem records were shown to be generally inferior to sedimentary records of higher resolution. Perkins and Maher (1993) found that stalagmite '90TS2' from Kingsdale Master Cave, Yorkshire, UK, correlated well with stalagmite 'TS' collected by Latham (1979) from the same cave, despite the uncertainties of a single basal date of 9.8 ka for 90TS2. Comparison with the PSV record for Britain for 0 to 10 ka (Turner and Thompson, 1981) was also favourable. Preliminary results from this study (Openshaw *et al*, 1993) showed good feature matching between four modern stalagmites from the same cave system in China.

PSV records from speleothems are most frequently dated using the uranium-series disequilibrium technique and the most popular detection method to date has been alpha-spectrometry due to ease of sample preparation and comparatively low cost. Typical dates produced using alpha-spectrometry have inaccuracies of 5-10% (Schwarcz, 1989). The main problem in using alpha-spectrometry for dating PSV in speleothems is that of avoiding the problem of detrital thorium contamination (Latham *et al*, 1989). Detrital thorium increases the dating uncertainties but a balance must be struck by having enough detritus to allow the NRM to be measurable. The use of mass-spectrometry can reduce the dating inaccuracies to <1% and can alleviate the detrital contamination problems since much smaller samples can be used (Lundberg, 1990; Li *et al*, 1989). Increased sensitivity extends the range of dating up to 500 ka. In cases where the extent of detrital contamination is severe various correction methods have now been proposed to produce isotopic activity ratios (Chapter 4). These methods are based on the use of so called isochrons and can be used for both mass and alpha-spectrometric dating providing sufficient material is available (Bischoff and Fitzpatrick, 1991; Schwarcz and Latham, 1989; Ku and Liang, 1984).

In summary, the main attractions of speleothems as recorders of PSV are that they grow continuously (with some exceptions), can be oriented prior to removal and do not appear to contain inclination errors. They also appear to record the ambient field instantaneously during crystallisation. The relative importance of CRM over DRM in the remanence acquisition process is still not fully resolved. It does appear however, that a

chemically precipitated magnetite, is sometimes present in apparently clean speleothems with no measurable NRM. In detritally rich speleothems the remanence is likely to be a combination of CRM and DRM, with the DRM dominating the palaeomagnetic signal. The process by which depositional errors are absent in detritus-rich speleothem continues to be uncertain. Speleothem PSV records can be dated absolutely, most commonly using the uranium-thorium disequilibrium method and alpha-spectrometry. This dating method is relatively rapid, inexpensive and methods have been developed to correct for contamination by allogenic isotopic components from detritus. There is, potentially, little difficulty in calculating dates for 'dirty' speleothems using the isochron methods and the inaccuracies in individual dates may be reduced further by the use of mass-spectrometry.

5.4. Sampling and preparation of speleothems for measurement.

5.4.1. Sampling criteria.

In order to collect speleothems that are most likely to yield measurable NRMs this study has used criteria based on personal experience and on the findings of previous workers (Latham, 1981; Latham, *pers comm*; Lean, *pers comm*).

1. Samples were not taken unless in-situ. Unlike most sediments (Verosub, 1977) speleothems are viable as absolute recorders of PSV as they have a fixed orientation and can be collected without disturbing magnetically aligned grains. PSV records from unoriented speleothems (those that are found knocked over for example) have been successfully produced (Lean, 1995) but yield only relative directions.

2. Only those speleothems found in active streamways and flood-prone areas were sampled. The flooding of a speleothem provides large amounts of detritus some of which becomes incorporated into the calcite matrix. From experience, this is the usual origin of a strong remanence. These types of speleothems are often covered by a mud coating and have a dirty appearance when surface mud is cleaned away. However, the

detritus will add detrital ^{230}Th to the isotopic inventory which may cause problems during dating. Speleothems in ancient high-level cave passages that are not flooded tend to have weak remanences since drip waters do not usually contain large quantities of detritus. However, Bull (1981) postulated that drip waters can carry detrital grains of up to 45μm although it is likely that fissures conveying the grains will become blocked quickly. This process would account for SD and PSD grains but fissures would filter out MD grains (Latham and Ford, 1993). This evidence alone was not thought sufficient to sample any high level speleothems for use in this study.

3. A speleothem with uniform width was taken as an indication of constant growth. Experience has shown that unusually shaped speleothems are often comprised of several periods of growth. In order to obtain records of maximum length and of uniform growth rate misshapen speleothems were avoided. In general, speleothems that were tallest and of narrowest diameter were taken as these were thought likely to offer the highest resolutions.

4. In order to obtain records of PSV to the present, active speleothems were sought where possible. This was indicated by a wet drip-cap.

5.4.2. Collection of speleothems from the cave.

When a suitable speleothem had been selected using the criteria set out above, it was oriented before removal. The apparatus used in this study was designed by Latham (1981) and modified by this author. The horizontal azimuth was taken by scratching two vertical marks on opposite sides of the speleothem with a scriber. Then, by aligning the sliding pointers on the aluminium frame, with the marks on the speleothem (figure 5.2a) a compass bearing was taken; the direction of orientation being marked with an 'A'. The procedure was repeated at least twice in order to minimise errors and to obtain a mean of all bearings. The degree of potential orientation error is discussed further in section 6.9.2.1. The 1993 International Geomagnetic Reference Field model values were used to correct for local deviation between geographic and magnetic north.

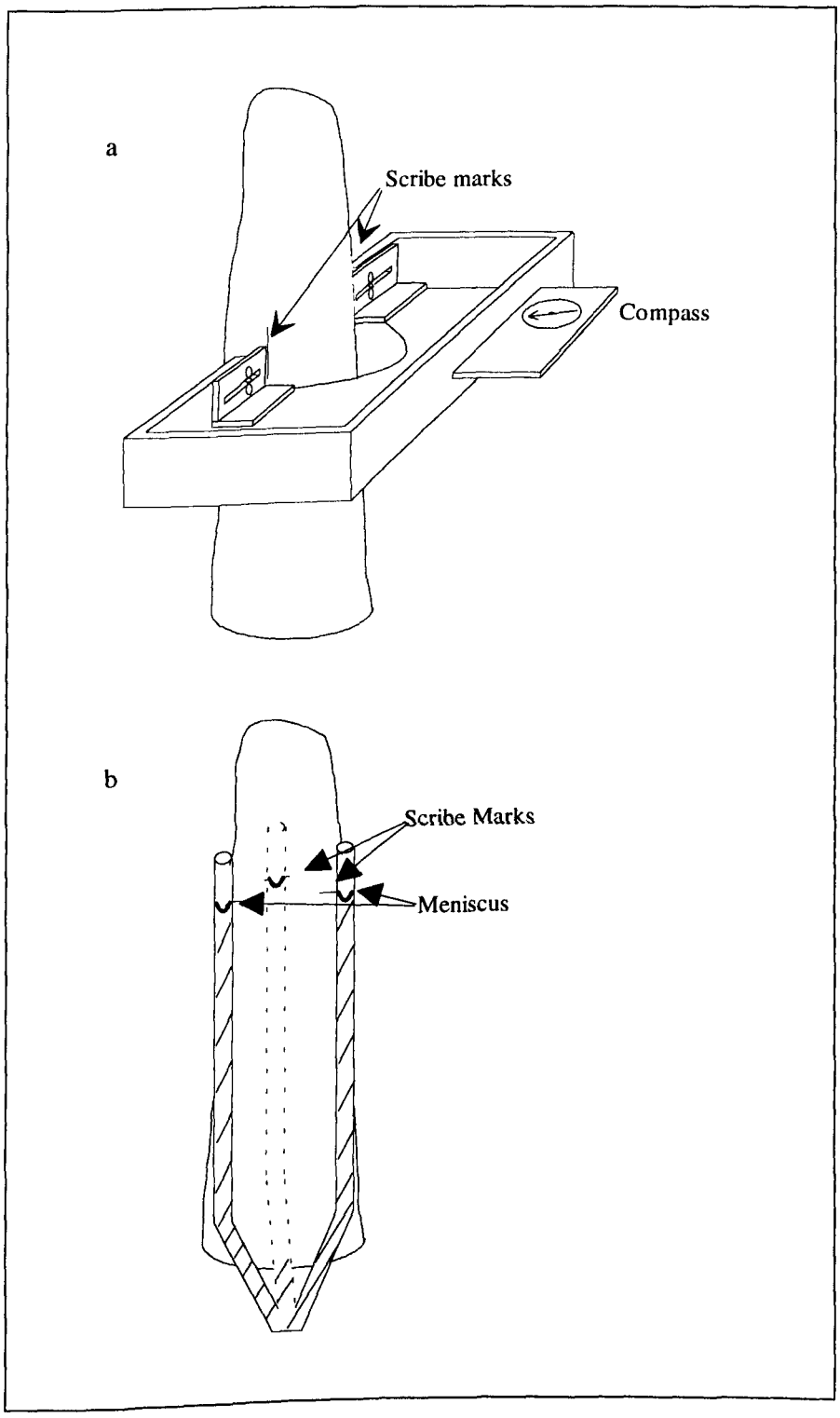

Figure 5.2. a) The aluminium frame used for horizontal (azimuthal) alignment. b) The 3-Arm U-tube used for orientation with respect to vertical.

Vertical orientation was accomplished using a 3-arm U-tube made from clear plastic, Figure 5.2b. The U-tube was filled with water before each collecting trip, using clamps to prevent the water escaping during transit. In this way the availability of water at the sampling site was not important. The U-tube was secured against the sides of the speleothem by two large rubber bands above and below the water line. The clamps were released and the levels in each of the arm's were marked on each side of the tubes, using a scriber. In some cases, where the sampling position was awkward, the tubes were shifted round a third of the diameter and another set of marks made. Estimating the accuracy of this method in the field is difficult but is discussed in section 6.9.2. Photograph 5.1 shows the sample orientation procedure for TR01 (Sistema de Cubija, Spain).

Photograph 5.1. Orienting stalagmite TR01 in the cave using the 3-Arm U-tube and aluminium frame.

After making notes on the sampling locality, such as height above water level and a description of the sampling site, the speleothem was removed from its plinth. Due to the crystalline nature of speleothems their removal in one piece was sometimes difficult. Using a chisel and lump hammer to cut a shallow ring around the base of the sample followed by one sharp 'tap' was sufficient for most samples. However some speleothems were, understandably, reluctant to leave the cave and required more aggressive persuasion, often breaking the speleothem into several pieces along its height.

5.4.3. Sample preparation.

In the laboratory, each sample was re-set in the vertical position using the 3-arm U-tube. Once vertical, plaster of Paris was moulded around the base to hold it in position until set. Once dry, the azimuthal scribe marks were aligned with a side of a box (Figure 5.3) and plaster was then poured in. This casting box was originally designed by Latham (1981) but was not satisfactory; it was redesigned by this author and kindly built by A.W.Openshaw. The new box was smaller than the original and allowed speleothems contained in a block of plaster to fit the clamping mechanism of a large diameter rock-saw. This saw was used to cut vertical slices from each speleothem. If a speleothem was too tall to fit the box it was broken and cast in two (or more) sections, each section aligned by relocating it on another before casting.

Vertical cut marks, 25 mm apart were marked through the drip-cap area of each section after casting for alignment during cutting on the rock-saw. The central vertical slice was sub-sampled using smaller rock saws available in the Geomagnetism Laboratory. Sub-samples were either 14 cm^3, or 7 cm^3 with the aim of sampling at the highest resolution. In this study speleothems were judged to be wide enough for only one vertical slice from the central drip-cap area and only one central sub-sample from the drip-cap of the vertical slice. Figure 5.4 shows the sampling methodology and markings used to identify sub-samples. The degree of orientation errors introduced at this stage are discussed in section 6.9.2. From the central slice only the 'B' sub-samples were used for obtaining palaeomagnetic directions. These sub-samples represented the fastest growth

portion of each speleothem and would recover the shortest time period of PSV. Lateral 'A' and 'C' sub-samples were used for rock magnetic, dating and for checks for the presence of depositional inclination errors.

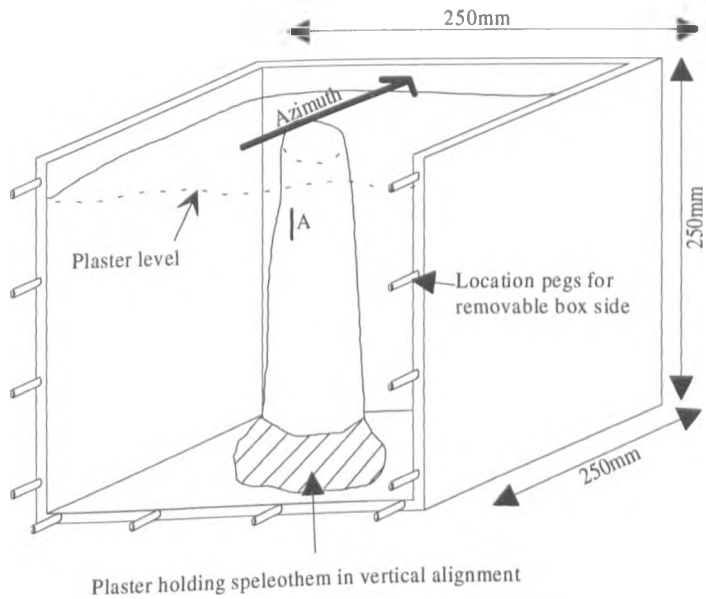

Figure 5.3. Equipment used for casting of oriented speleothems in plaster before cutting on the large diameter rock saw.

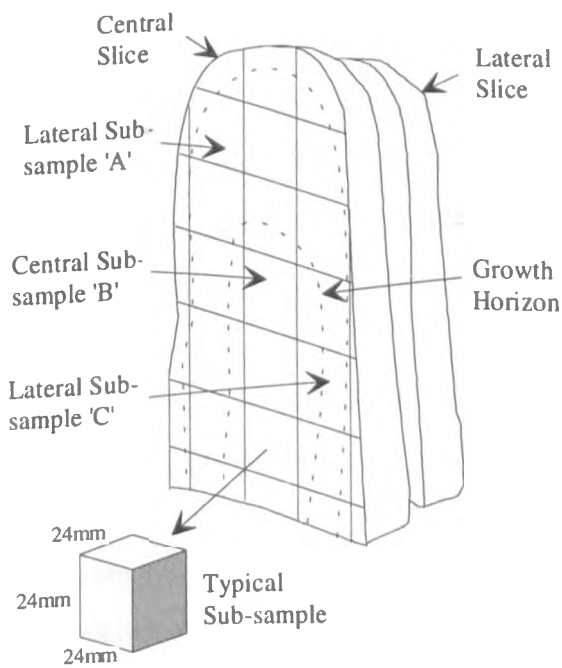

Figure 5.4. Sub-sample labelling scheme used for speleothem sub-samples.

5.5. Laboratory measurement of magnetic remanence.

Measurement of sub-sample remanences was performed on a Cryogenic Consultants Ltd. 3-axis cryogenic SQUID magnetometer, housed in a zero-field cage. This instrument is controlled by an IBM-PC which automatically writes the data to floppy disk as each sample is measured. To lessen any effects of instrument noise, drift and sample-holder contamination, each sub-sample was measured in four positions, each position consisting of four separate measurements. For each measurement cycle the sub-sample is measured twice within the sensing coils, with 90° rotation about the vertical axis between each measurement, and twice outside of the sensing coils to obtain background readings which are automatically subtracted from the total moment.

An important consideration when dealing with relatively weak sub-samples was the contribution of magnetometer background noise to each measurement. This noise would be a combination of magnetometer electronics noise, uncompensated ambient field and stray VHF radio emissions and effects from the sample holder. Any effect from the sample holder can be assumed to be constant since it was regularly cleaned in an ultra-sonic bath and AF demagnetised before each measuring session. In order to ascertain typical variations in background noise a series of 20 measurements were made over the space of a week in June 1994 with only the clean sample-holder in place. The results from these measurements showed the maximum contribution from noise over a typical period of measuring (Figure 5.5). A similar series of measurements were made in June 1995 to check for any longer-term variations in noise levels.

Figure 5.5a shows the stereographic projection for these data for June 1994 and Figure 5.5b shows the stereographic projection for June 1995. All measurements show a random scatter about the stereoplot indicating a lack of any systematic directional bias over time. Intensity measurements are shown in figure 5.5c. The maximum noise intensity for the combined measurements, made assuming a mass of 1.0g, was 6.0×10^{-8} $Am^2 Kg^{-1}$ with a mean noise level of 3.3×10^{-8} $Am^2 Kg^{-1}$. Samples in this study were approximately 25g or 13g, making the maximum background contribution 0.2×10^{-8} $Am^2 Kg^{-1}$ or 0.5×10^{-8} $Am^2 Kg^{-1}$ depending on sub-sample weight. These are the maximum

likely contributions to the magnitude of a sub-sample measurement. During demagnetisation the approach to this noise level was indicated increased scatter in the directions calculated for each sub-sample (Chapters 6 and 7).

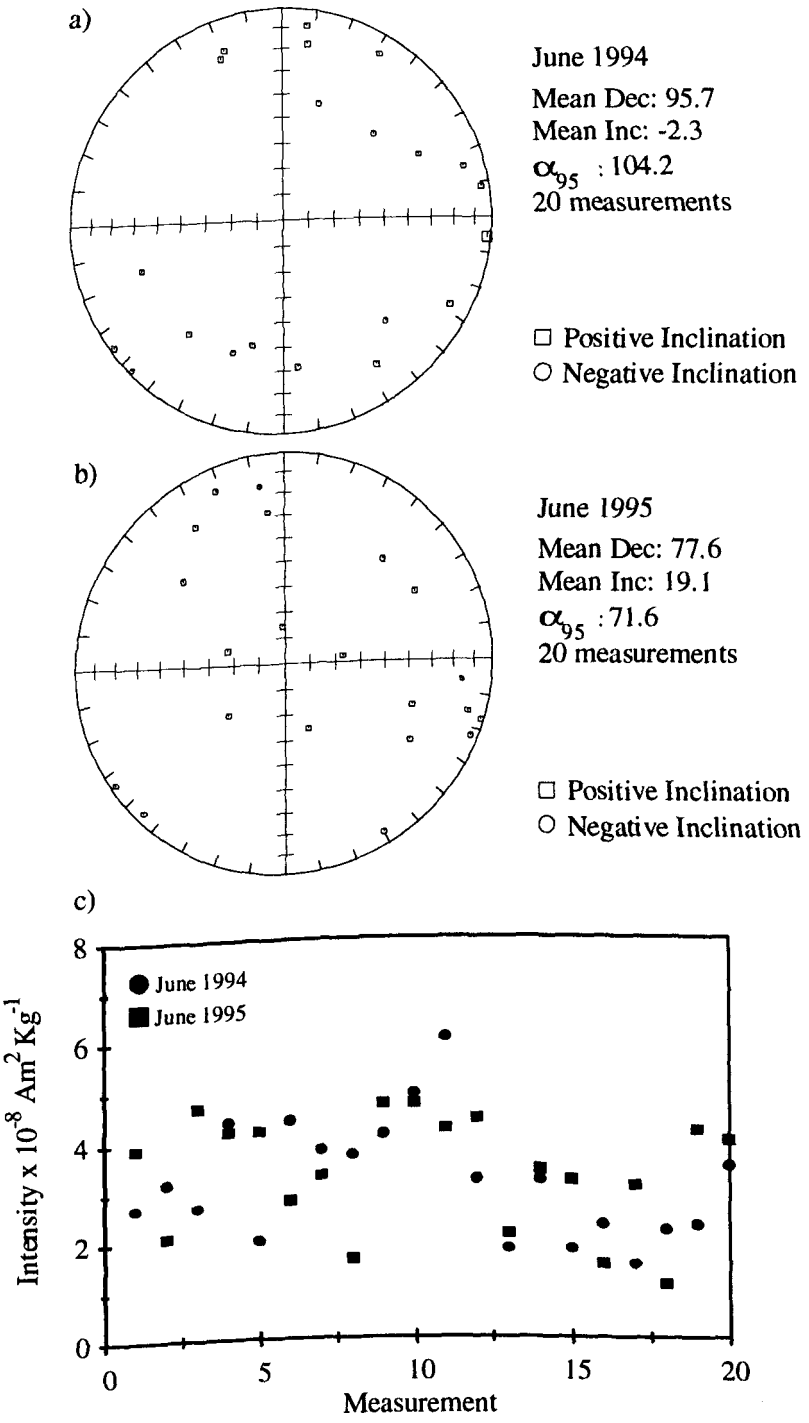

Figure 5.5 Magnetometer noise measurements a) June 1994 and b) June 1995. c) Combined intensity data for June 1994 and 1995. The maximum noise intensity was 6.0 x 10^{-8} Am^2 Kg^{-1} and the mean value was 3.3 x 10^{-8} Am^2 Kg^{-1}.

The accuracy of the individual sub-sample directions was determined using the standard measurement mean (smm). The smm represents the standard deviation of the X, Y and Z co-ordinates of each measurement and is calculated thus:

$$smm = \frac{((DX + DY + DZ)/3)^2}{INT_{total}} \qquad \textbf{5.1}$$

where DX, DY and DZ are the standard deviations of the X, Y and Z co-ordinate measurements and INT_{total} is the total intensity. When the smm of a sub-sample rose to 1.0 or above repeat measurements were made allowing calculation of mean X, Y and Z co-ordinates. If the smm increased beyond 5.0 or repeat measurements varied by more the 5° the sample was deemed immeasurable. This frequently occurred during the later stages of demagnetisation when remaining NRM was weak and influenced by magnetometer background noise.

5.6. Demagnetisation methods.

In palaeomagnetic studies involving large numbers of samples blanket demagnetisation is often used. In this method the stable remanence vector isolated in several pilot samples using stepwise AF or thermal demagnetisation is used a guide for the demagnetisation of the remaining samples at a single AF or temperature. Stalagmite SC01 was the only speleothem in this study to undergo blanket demagnetisation of its sub-samples after analysis of several pilot samples. Subsequently it was felt that more detailed demagnetisation information would be gained if stepwise demagnetisation was utilised throughout.

5.6.1. AF demagnetisation.

The majority of Chinese and Spanish speleothem sub-samples were subjected to stepwise AF cleaning in order to isolate primary remanence directions. The coercivities of the magnetic mineral assemblage within a sub-sample could also be assessed using this

technique. The AF demagnetiser at Liverpool consists of a tumbling sample holder set between demagnetising coils. The demagnetising coils close around the tumbling sample and the desired field (maximum 170 mT) was set before starting the AF demagnetisation cycle. Upon completion of the cycle the sample was placed in a Mu-metal pot and carried to the cryogenic magnetometer for measurement. The whole arrangement is surrounded by an orthogonal Helmholtz coil system adjusted to null the ambient field using a fluxgate magnetometer. This prevents the samples acquiring an ARM although this equipment can also be used to impart ARMs if required.

5.6.2. Thermal demagnetisation.

A selection of lateral sub-samples and in the case of AG03, central sub-samples were subjected to stepwise thermal demagnetisation which showed the T_c and blocking temperature spectrum of individual sub-samples. Thermal demagnetisations were performed in a Magnetic Measurements Ltd. thermal demagnetiser (MMTD) in steps of 50° or 100°C.

The major problem encountered during thermal demagnetisation was the destruction of some sub-samples due the expansion of air trapped in cavities within the calcite. Frequently samples would explode at temperatures of <300°C. When this occurred a small quantity of the sub-sample was always lost as powder and fragments but generally the sub-sample could be glued together using cyanoacrylate adhesive (tested for zero remanence). On subsequent heating the sample would again fall apart eventually becoming impossible to repair. Thus, accuracy was lost due to misalignment of the sub-sample sections during gluing and the continual loss of parts of the sub-sample. In the case of the weaker sub-samples the NRM decreased to the point where magnetometer noise had an effect on the measured directions before a stable remanence was defined by thermal demagnetisation.

Due to the problems encountered during thermal demagnetisation it was felt that AF demagnetisation was more suitable. In addition, the effects of heating on samples that

are used for uranium-series dating are poorly understood and in some cases can enhance the effect of any detrital isotopes present in a sample (Chapter 4). Although thermal demagnetisation is generally preferable to AF demagnetisation when high coercivity (haematite) minerals are concerned. However, AF demagnetisation of most sub-samples produced a linear trend on the Zijderveld plots (1967) to the origin and the primary remanence could be calculated using the method of Kirschvink (1980).

5.7. Data analysis and representation.

Directions from individual sub-samples have been calculated from **principal component analysis (PCA)**. Directional data from demagnetisation were represented on an **orthogonal vector plot (OVP)** commonly called a Zijderveld plot, where the change in the remanence vector between demagnetisation steps is plotted using the Cartesian co-ordinate system (Zijderveld, 1967). Thus, at each demagnetisation step the declination, inclination and intensity are represented as a **vector end-point (VEP)**. Removal of a single component of magnetisation is shown by a linear segment whilst two or more components are shown by further linear segments. If the coercivity or blocking temperatures of magnetic components overlap a curved vector segment can result. The linear segment that trends towards the origin is usually taken to be the primary remanence and the direction is estimated using the best fit line (Kirshvink, 1980). The maximum angular deviation (MAD) indicates directional precision.

Stereographic projections are utilised to indicate changes in inclination and declination during demagnetisation. In samples where there is a single magnetisation component (after removal of any viscous overprint) the vector end-points are tightly grouped. Samples that have two or more components show two distinct groupings. However, in some cases progressive movement of the VEPs along a great circle can occur as one of two overlapping components is partially removed at each demagnetisation step. Mean directions are calculated using Fisher (1953) statistics. Precision of the direction is assessed most often using the α_{95} parameter which is the angular radius of the cone of 95% confidence about the observed mean.

The normalised intensity plot can also be used to illustrate the coercivities, in the case of AF demagnetisation, or the blocking temperatures, in the case of thermally demagnetised samples. This allows immediate conclusions to be drawn on the relative 'hardness' of the magnetic mineral assemblage in AF demagnetised samples and of the types and thermal alteration of magnetic minerals in thermally demagnetised samples.

Directions were calculated for sub-samples, where possible, and were initially plotted against height in each speleothem. After dating was completed the age of each sub-sample was estimated from a linear least-squares fit to the dates obtained for a selection of sub-samples. It was not possible and not necessary to date each sub-sample. With each speleothem fixed to a timescale a fully dated PSV record was then produced allowing inter-speleothem comparisons. More extensive comparisons with other well-dated contemporaneous records were also made (Chapters 6 and 7).

6. Palaeosecular variation records and dating of speleothems from Xingwen, China.

This chapter describes in detail the palaeomagnetic and uranium-series data from each of the Chinese speleothems collected as part of this study. A short introduction to the geology and geomorphology of the Xingwen area and its caves precedes a field description of each speleothem. The demagnetisation behaviour, uranium-series dating and PSV of each speleothem are discussed prior to drawing comparisons between individual PSV records. Finally, the Xingwen records are compared with other contemporaneous records of PSV from China and Japan.

6.1. The caves and karst of Xingwen.

The village of Xingwen is located on a col in the dramatic limestone karst of western Sichuan Province, China (28.08°N 105.05°E). Figure 6.1 shows the geographical location of Xingwen. The limestones here have a thickness of 350m and are composed of the Permian Maokou and Qixa limestone units. These units are massive, pure limestones, which around Xingwen, are conformably overlain by Permian coal measures containing mudstones which, in turn are overlain by Triassic sandstones. Relief is rugged with surrounding mountains rising to 1400 m whilst the majority of caves lie in the limestone at the 700 m level. The main resurgence level is at 450 m a.s.l. 5 km to the south-east of Xingwen (Waltham and Willis, 1993).

The limestone in the Xingwen locality is characterised by well developed karren and pinnacle karst. In addition, cone (Fengcong) karst in various stages of development is found to the north of the village. Caves are common in these limestones and their active sinks feed the lower streamways ultimately passing to the main resurgence of Dong He 5 km distant. Sinkholes allow surface run-off from the bare limestone to quickly enter active cave systems during the wet season. In contrast to these active cave levels, older abandoned trunk routes of huge proportions (100 x 100 m) are common.

Access to the lower active levels is often possible via climbs and vertical pitches from these fossil passages (Waltham and Willis, 1993).

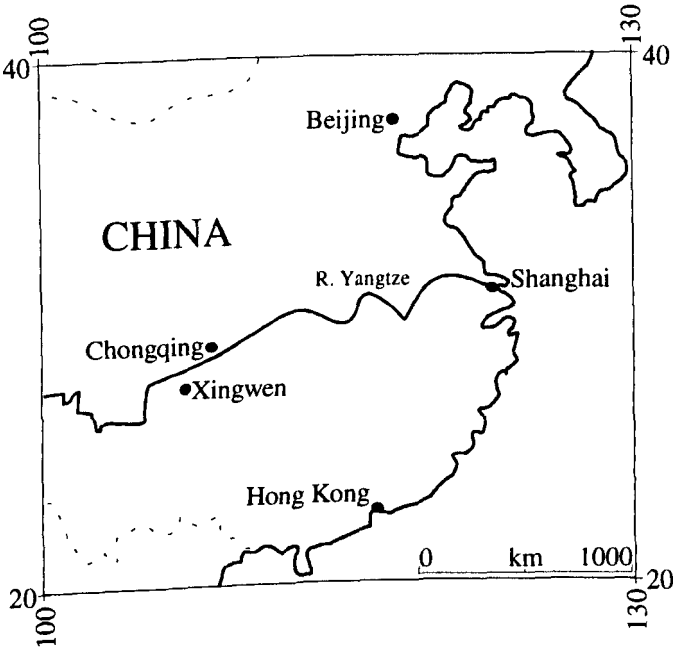

Figure 6.1. Map of China showing the location of Xingwen.

Speleothems were collected from the two longest caves in Xingwen. Both caves are part of the same hydrological network but are conveniently separated by a large doline. The active levels of Tiencuan Dong, the local show cave, yielded two speleothems from its active streamway. Zhucaojing (Pig Trough Well) was also visited, yielding a further four speleothems of which three were used in this study.

6.2. Speleothems from Tiencuan Dong (Show Cave).

Two speleothems were collected from the lower streamway in Tiencuan Dong (Figure 6.2). These samples were labelled SC01 and SC02. The passage at the sampling point was approximately 15 m across which, despite the dry-season, carried a large stream. Thick mud deposits on the exposed floor, walls and roof of the passage indicated that the passage filled completely during flood events.

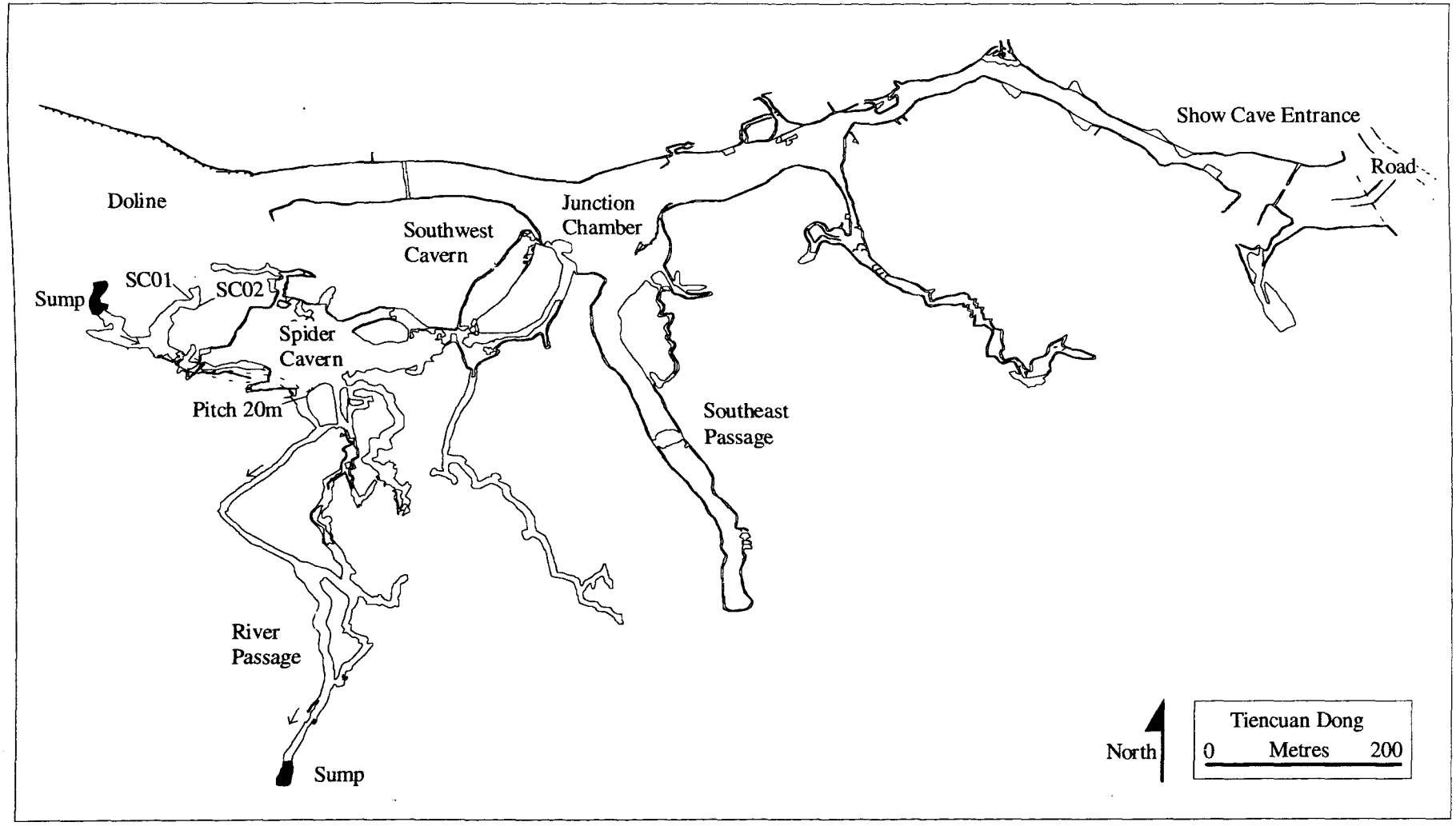

Figure 6.2. Sketch survey of Tiencuan Dong Show Cave showing locations of SC01 and SC02. From Waltham and Willis, 1993.

6.2.1. SC01 location and external/internal appearance.

This speleothem was a 635 mm high stalagmite taken from a narrow, steeply sloping alcove 4.2 m above the level of the streamway. When collected it was being dripped on indicating that it was presently growing. This satisfied one of the sampling criteria outlined in section 5.4.1. The entire outer surface of SC01 was covered in a 2 mm layer of red-brown mud, presumably from the detritus carried in the floods of the preceding wet-season. SC01 had a diameter of approximately 70 mm throughout its height except for the section below 155 mm from its base which was 55 mm wide.

SC01 was cast in three sections in the laboratory and one vertical slice was obtained from its centre using a large diameter rock-saw. Small cutting errors were inevitable during cutting and were corrected for during measurement. Internally SC01 was a dark grey colour with occasional darker banding. From 465 mm to 635 mm (top) the colour changed to a lighter tan. There were no visible hiatuses but growth layering was present on a $\leq$1 mm scale. Darker bands presumably represented seasonal flooding deposits cemented into the calcite matrix and the paler bands represented growth during the dry-season. There were three places at which the central drip-cap had offset with no growth stoppage; the areas around 106 mm, 442 mm and 539 mm. SC01 exhibited homogeneous crystal growth with no evidence for re-solution of the calcite matrix.

6.2.2. SC02 location and external/internal appearance.

The second speleothem collected from Tiencuan Dong was SC02. It was a 273 mm high stalagmite taken from a steeply sloping mudslope directly opposite SC01. The presence of a wet drip-cap showed that the top was modern. The base was 5.3 m above the current stream level and the stalagmite was covered in 1-2 mm of red-brown mud indicating the influence of seasonal flood events. SC02 had a constant diameter of 60 mm suggesting a relatively constant growth rate.

SC02 was cast in one piece in the laboratory and one vertical slice cut from its centre. Internally SC02 was an amber colour for much of its height excepting the top 30 mm which were almost white. Uranium-series dating (section 6.5.2) showed that there was less detrital contamination than in SC01. This was probably caused by less frequent flooding at this height above the streamway. Growth layering was on a ≤1 mm scale, evidenced by the spacing of the alternate dark and pale banding. There appeared to be no hiatuses within SC02 but there was a small area of vertical holes from 147 mm to 183 mm. Around these holes the calcite layering was concave upwards. Each hole was filled with detritus and may represent places of percussion erosion by detrital grains moving as they are hit by dripping water. These features have been termed 'work holes' by Latham (1981).

6.3. Speleothems from Zhucaojing (Pig Trough Well).

Four stalagmites were collected from two locations within Zhucaojing (Figure 6.3). Samples were labelled PT01 to PT04. All samples were collected from frequently flooded sites and all but PT01 were analysed in this study.

6.3.1. PT01 location and external appearance.

PT01 was a 700 mm high stalagmite collected from an undercut in the large chamber west of the Entrance Chamber. At this location, the stream occupied a flat sandy floor approximately 30 m across, whilst the chamber itself was 50 m across. Although the speleothems were collected during the dry-season, large quantities of mud and surface debris were evidence for seasonal flooding. The stream level was < 0.5 m below the base of PT01 indicating that only a small increase in discharge would inundate the stalagmite.

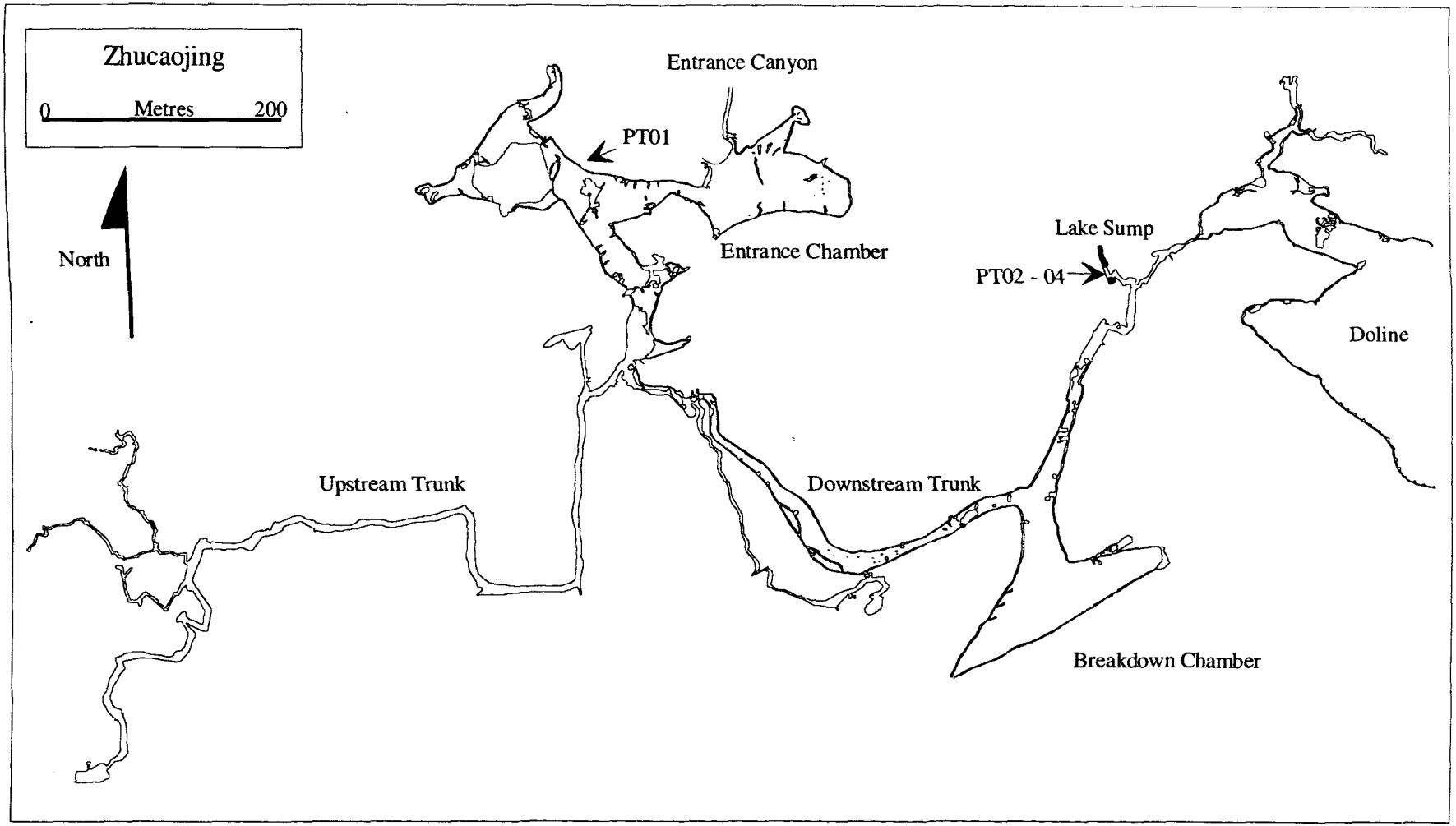

Figure 6.3. Sketch survey of Zhucaojing (Pig Trough Well) showing locations of speleothems PT01 to PT04.
From Waltham and Willis, 1993.

A parent stalactite and a wet drip-cap indicated that the stalagmite was growing at the present time. Although PT01 was approximately 80 mm diameter its outer surface was covered in 'cave popcorn' formed as feedwaters leave the speleothem via micro-fissures and evaporate slowly from the drop of water on the speleothem surface (Ford and Williams, 1989). In the case of PT01, it is suggested that further deposition of calcite over these small globular deposits had formed the highly irregular surface. PT01 was not used in this study because of the sampling problems likely to be met due to the highly irregular growth layering and also the possibility of some chemical alteration. PT01 was the first speleothem collected from Xingwen and after the discovery of the other speleothems it was felt that it should not have been taken.

6.3.2. PT02 location and external/internal appearance.

PT02 was a 531 mm stalagmite taken from 1.5 m above the streamway in the Lake Sump area of Tiencuan Dong. When collected, the top surface of PT02 was wet and a frequent drip emerged from a fissure in the roof; hence it was actively forming. The outer surface of PT02 was covered in 5-6 mm of black mud which required cleaning off in places before orientation marks could be made. The downstream sump lay 10 m from PT02 and copious quantities of mud in this area showed that water backed-up from this sump during the wet-season. PT02 had an average diameter of 85 mm for much of its height excepting the taper from 410 mm to the top at 531 mm.

PT02 was cast in three pieces in the laboratory and only one vertical slice was available from its centre. Cutting errors associated with using the rock-saw were judged from the closeness of the cut to the marked cutting lines and were corrected during measurement on the magnetometer. Once cut, PT02 was a grey, grey-cream colour with the usual <1 mm scale wet/dry-season banding. These wet-dry season markers were counted to see if a time scale could be applied. However, the bands were not clear in several areas making this method unreliable. There were several sections that contained thicker, dark bands and these may represent times when greater quantities of detritus have been cemented into the calcite matrix. These areas (279 mm to 338 mm and 374

mm to 434 mm) also showed evidence for drip-cap offset where the position of the drip has changed causing calcite precipitation to move laterally. Growth banding at these points was continuous and did not appear to be truncated (indicating erosion or re-solution) and are not thought to affect the fidelity of the PSV record. PT02 exhibited massive crystal growth with no work holes or dissolution.

6.3.3. PT03 location and external/internal appearance.

PT03 was collected from the surface of gently sloping flowstone 15 m above the sump at the top of Lake Sump chamber (Figure 6.3). The stalagmite was 375 mm tall and had a diameter of 85 mm at the base gradually tapering to 35 mm at its top. A 2 mm dark-grey mud-drape over the stalagmite and surrounding rocks demonstrated that seasonal flooding caused the sump to back-up inundating PT03. The top surface of PT03 was wet showing that it was presently growing.

Due to breakage during transit PT03 was cast in three pieces which could be re-fitted in the laboratory with no loss in orientation. During cutting of the single central vertical slice some cutting errors were introduced (up to 5°). A correction was applied to these cutting errors during palaeomagnetic measurement using the difference between the actual cut and the marked cutting lines as a guide. Internally PT03 had a banded dark-grey, pale-grey colouration due to varying quantities of detritus reflecting seasonal flooding. There were no hiatuses visible but there were four distinctly darker areas at 250, 330, 355 and 380 mm. As in PT02 these may show times when more detritus was incorporated into the calcite matrix. Re-solution of the calcite was not evident in PT03 and a single growth period was inferred.

6.3.4. PT04 location and external/internal appearance.

PT04 was growing on a rock bridge approximately 8 m above the streamway in the Lake Sump chamber. It was 638 mm in height and its width slowly tapered from 100

mm at the base to 65 mm at the top. The side of PT04 was covered with a 2 mm layer of light tan to brown coloured mud from flooding.

PT04 was cast in three pieces and one vertical slice was taken from its centre using the large diameter rock saw. The internal cream colour of PT04 was surprising since it was obviously flooded during the wet season. Uranium series dating showed PT04 to contain significant quantities of detritus by $^{230}Th/^{232}Th$ ratios of <<25. Whilst collecting PT04 splashing from water falling onto the other stalagmites in the group was noticeable. This splashing water may have washed the vast majority of mud from the sides of the speleothem after a flood subsided. In this way, comparatively little mud may remain to affect the colour of the speleothem whilst retaining sufficient quantities to affect the $^{230}Th/^{232}Th$ ratio.

The most noticeable growth features of PT04 were the numerous places where drip-cap offset had taken place. At 130 mm from base the drip-cap began to offset to the north and continued to do so up to 260 mm. The total lateral movement of calcite precipitation was 15 mm. From 260 mm to 290 mm it reverted to a southerly offset at which point vertical growth re-commenced. From 370 mm, a slow northerly offset continued to 540 mm, from which point, vertical growth resumed to 638 mm (top). Despite these offsets, there was no evidence for any cessation in the growth of PT04 which would otherwise be indicated by truncated growth layers. There was one work-hole from 110 to 130 mm containing large grains of [quartz?] detritus though with no dissolution of the surrounding calcite.

6.4. Palaeomagnetism and dating of SC01.

6.4.1. NRM and demagnetisation of SC01.

One vertical slice from the centre of SC01 yielded 26 central drip-cap sub-samples of 14 cm^3 labelled 1B to 26B. The NRM intensities in SC01 ranged from 50.1 to 635.8 x 10^{-8} Am^2kg^{-1} with an increase in sub-sample NRM intensity from top (1B) to

bottom (26B). Samples 1B to 8B, excepting 3B, had NRM intensities of less than 100 x 10^{-8} Am^2kg^{-1}. Pilot sub-samples 3B, 14B and 22B were stepwise AF demagnetised to ascertain the field required to reveal the primary remanence directions. AF was increased in steps of 5 mT up to 40 mT and subsequently in steps of 10 mT up to 160 mT. At 160 mT approximately 20% of the NRM intensity remained and median destructive fields (MDFs) of the order of 85 mT suggested the presence of magnetically hard (SD-like) remanence carriers.

Figure 6.4 shows relevant demagnetisation data for each pilot sub-sample. The removal of a viscous magnetisation in an opposing direction to the sub-samples primary remanence directions caused an initial increase in intensity of between 5% (14B) and 17% (22B) (Figure 6.4c, f and i). Removal of this viscous component allowed the isolation of a single remanence direction, (Figure 6.4a, d and g) which trended linearly towards the origin of the Zijderveld plots. This stable remanence direction was taken to be the primary remanence in all cases. An increase in the scatter of the directions after each AF step at the higher applied fields was thought to be due to the increased influence of the magnetometer backgound noise.

Mean directions from the pilot sub-samples were calculated from the Zijderveld plots using the method of Kirshvink (1980). The maximum angular deviations (MAD) of the pilot sub-samples ranged from 2.7° to 4.6° indicating good precision. Directions calculated from the stereographic projections for each of the sub-samples also had good precision with α_{95}'s ranging from 0.7 to 1.0 (Figure 6.4b, e and h). Mean directions calculated using the Zijderveld plots and the stereographic projections agreed closely. The agreement indicated that, although 20% of the NRM remained at 160 mT, a stable remanence vector had been accurately defined by AF demagnetisation. Since the viscous components of the pilot sub-samples were removed by an AF of 15 mT the remaining central sub-samples were demagnetised at 20 mT. This AF would remove any viscous overprinting whilst leaving a measurable remanence. Mean directions for the remaining sub-sample at 20 mT were calculated, from a minimum of three measurements, using Fisher statistics (Fisher, 1953).

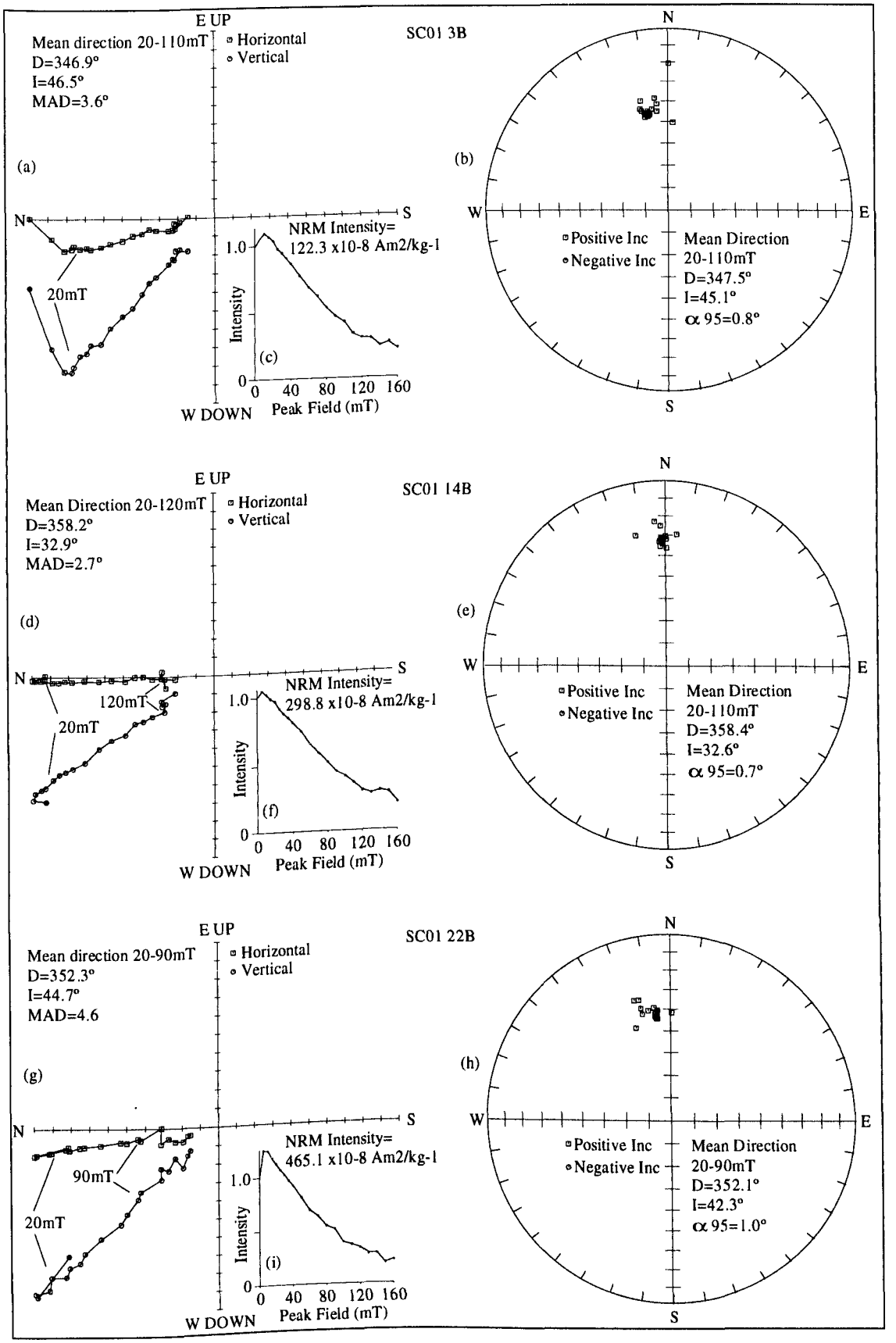

Figure 6.4. Demagnetisation data from SC01 sub-samples 3B, 14B and 22B.

Two lateral sub-samples were subjected to stepwise thermal demagnetisation in steps of 50° C up to 400° C and in 100° C steps up to a maximum temperature of 700° C. SC01 sub-samples did not appear to suffer as much from heating damage as did sub-samples from the other speleothems in this study. Figure 6.5 shows demagnetisation plots for sub-samples 4C and 18A. Removal of a viscous component of magnetisation by 150° C left a single stable remanence direction that trended towards the origin of the Zijderveld plots (Figures 6.5a and d). This was interpreted to be the primary remanence. The single component of magnetisation was also clearly seen on the stereographic projection (Figures 6.5b and e) as tightly grouped vector end-points (VEPs). Figures 6.5c and f show the decrease in NRM intensity with temperature. A loss of about 25% of NRM intensity between 100° and 150° C showed the unblocking of low T_b grains which appeared to hold the viscous remanence. The remaining unblocking spectra was seen to reduce to almost zero between 650° and 700° C. Magnetic mineralogy is discussed in detail in Chapter 8.

Previous workers have reported the absence of depositional inclination errors in speleothems (for example Lean *et al*, 1995; Perkins and Maher, 1993; Latham *et al*, 1986). Lateral sub-samples coeval with central sub-samples were used to test for inclination errors (Figure 6.6). Coeval sub-samples were chosen using the growth horizons which passed through central and lateral sub-samples as a guide. The agreement between inclinations and declinations of lateral and central sub-samples was good at the α_{95} confidence level, although all inclinations were shallower than those predicted by GADF model. However, this suggested that there were no systematic differences in the magnetic grain alignment processes between central sub-samples where the depositional surface is horizontal and the lateral sub-samples where the depositional surface dips steeply. It should be noted that sub-sample 18A was stepwise thermally demagnetised as a test to see whether thermal demagnetisation produced significantly different results from sub-samples that had been AF demagnetised. These data (Figure 6.6 and Table 6.1) suggested that there were no significant differences in directions in this case.

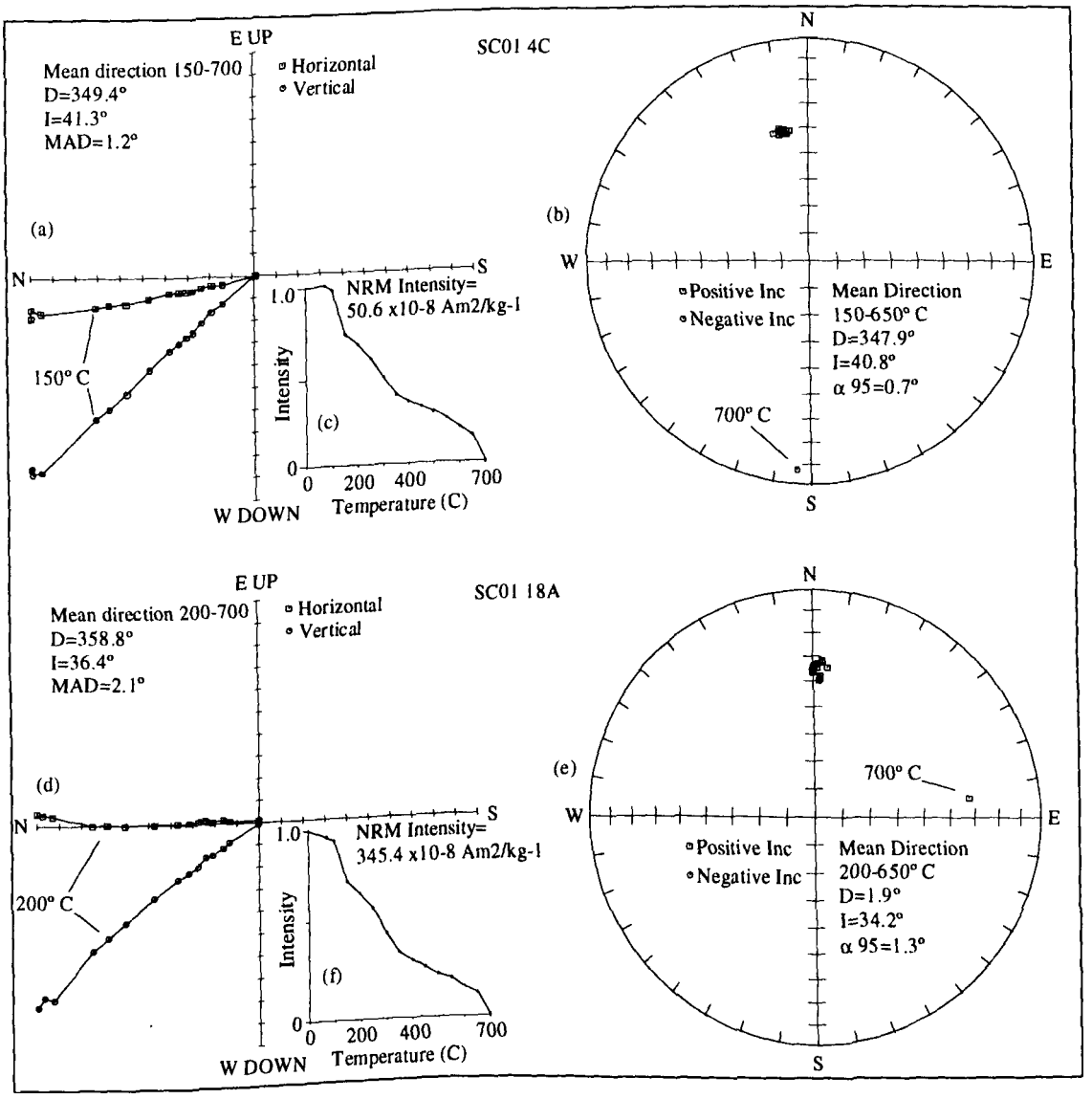

Figure 6.5. Thermal demagnetisation data for SC01 sub-samples 4C and 18A.

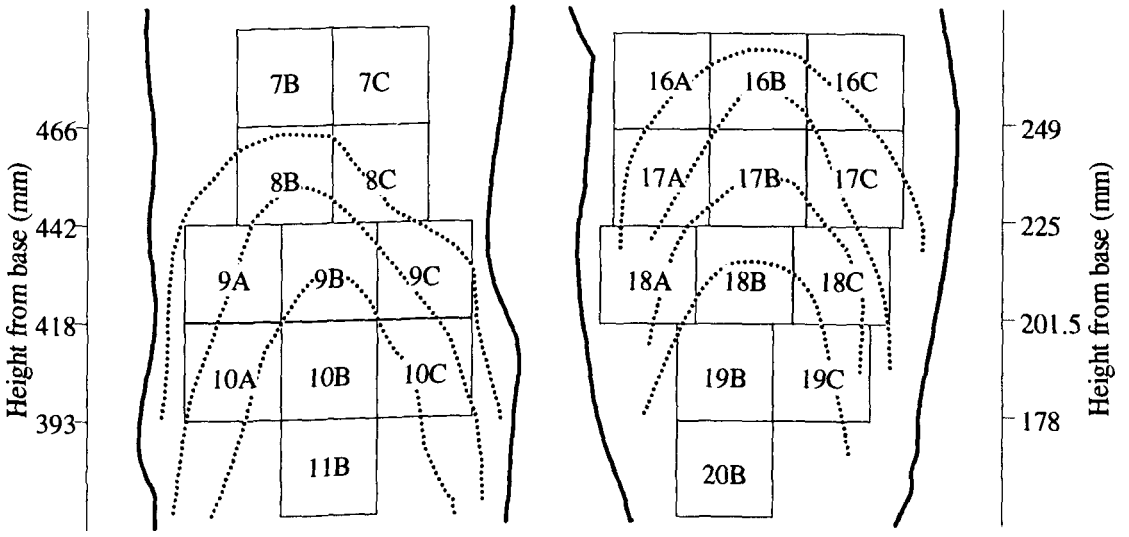

Figure 6.6. Cross-sections through SC01 central slice showing positions of sub-samples used for depositional inclination error tests. Dotted lines represent growth layers.

Sub-sample	Declination	Inclination	α_{95}
9A	340.1	46.0	1.2
8B	342.9	45.0	1.0
9C	342.7	44.0	1.8
10A	350.2	43.1	1.9
9B	348.7	44.0	1.1
10C	356.3	46.1	3.2
17A	352.7	42.3	2.1
16B	349.6	38.4	2.2
17C	351.9	40.3	1.3
18A	358.8	36.4	1.3
17B	1.05	38.9	1.8
18C	359.3	39.8	2.3

Table 6.1. Values of declination and inclination for coeval central and lateral sub-samples used for depositional inclination error tests. α_{95} is shown as a measure of precision.

6.4.2. Uranium-series dating of SC01.

The uranium-series data for SC01 are tabulated in Table 6.2. Sub-samples from SC01 all had high 1 sigma errors for a combination of reasons. Uranium concentrations were low (0.18 (13B) to 0.41 (1B) ppm) and, for many of the sub-samples, chemical recovery of U and Th was also low due to the inefficient electroplating method that was used in the laboratory at the time (discussed in Chapter 4). Uranium yields ranged from 9% to 26% (mean = 15.4%) whilst Th yields range from 3% to 52% (mean = 9%). Two dates (13B and 15+16B) obtained after the adoption of the Hallstadius technique, gave higher yields of Th but errors were not significantly improved as U yields remained low.

Detrital Th contamination, reflected by $^{230}Th/^{232}Th$ ratios in the range 0.81±0.51 (1B) to 1.61±0.30 (9B), also increased the dating uncertainties. As sub-sample 1B (top) was modern its $^{230}Th/^{232}Th$ value of 0.8 was used as an initial value to correct the remainder of the sub-samples for detrital thorium. Use of the MLE method on L/L data for combined sub-samples 15 and 16B, as discussed in section 4.4.3.2, gave a date of 2.6±4.2 ka (data in Appendix K). This method was attempted in order to increase dating precision and to check that the initial $^{230}Th/^{232}Th$ value of 0.8 was giving satisfactory dates. However, the MLE date for 15+16B was considered to be too imprecise to be of use in this case and was not used in calculating speleothem growth rate. Possible reasons for the poor MLE dates are discussed in Chapter 4.

Excluding the MLE date of 15+16B and the U-series date of 13B, which was out of stratigraphic order, a linear least squares fitting routine was used with the remaining corrected dates to obtain a best-fit growth line. Figure 6.7 shows the best-fit line on an age - height plot. From this plot it is clear that the high errors, the reasons for which are outlined above, have led to accurate but imprecise sub-sample ages. A top age of 0 ka and basal age of 8.4±1.2 ka were calculated from the best-fit data giving a constant growth rate of 0.075 mm yr^{-1}. The growth rate implied that each sub-sample represented a time-average of 335 years of recorded PSV. If a drift rate of 0.2°/yr^{-1} is considered then one complete rotation of the drifting field would be averaged by just under 6 sub-samples. This will produce a PSV record of reasonable, although not high, resolution.

Sub-sample	Concentration U (ppm)	U Yield (%)	Th Yield (%)	$^{234}U/^{238}U$	$^{230}Th/^{234}U$	$^{230}Th/^{232}Th$	Uncorrected age (ka)	Corrected age (ka)
1B	0.41±0.01	12	7	1.33±0.01	0.005±0.025	0.81±0.51	0.6±0.3	0.0
5B	0.36±0.01	12	7	1.32±0.03	0.039±0.005	0.87±0.14	4.3±0.6	0.8±1.0
7B	0.19±0.01	16	52	1.27±0.08	0.035±0.007	1.57±0.06	3.9±0.8	1.9±1.4
9B	0.39±0.01	18	3	1.33±0.03	0.058±0.008	1.61±0.03	6.5±0.9	3.3±1.5
13B	0.18±0.01	19	5	1.28±0.05	0.047±0.009	1.11±0.29	5.2±1.0	1.5±1.7
15/16B	0.18±0.01	17	38	-	-	-	-	2.6±4.2
17B	0.24±0.01	20	5	1.25±0.04	0.084±0.011	1.40±0.26	9.5±1.3	4.2±2.1
18B	0.35±0.02	15	3	1.38±0.06	0.124±0.015	1.28±0.02	14.3±1.8	5.6±2.9
19B	0.31±0.01	9	7	1.37±0.05	0.102±0.010	1.22±0.15	11.7±1.5	6.1±1.7
21B	0.23±0.01	26	8	1.30±0.03	0.014±0.012	1.01±0.12	16.4±1.5	7.0±2.4
23B	0.21±0.05	11	7	1.35±0.07	0.135±0.014	1.10±0.14	15.6±1.7	7.4±2.6
24B	0.20±0.01	9	5	1.19±0.06	0.139±0.017	1.11±0.17	16.2±2.1	7.8±3.2

Table 6.2. Uranium-series data for sub-samples of SC01 with resultant uncorrected and corrected ages. Errors are to one sigma and are based on counting statistics. Leached sub-samples 15/16B were dated using the isochron method (Schwarcz and Latham, 1989).

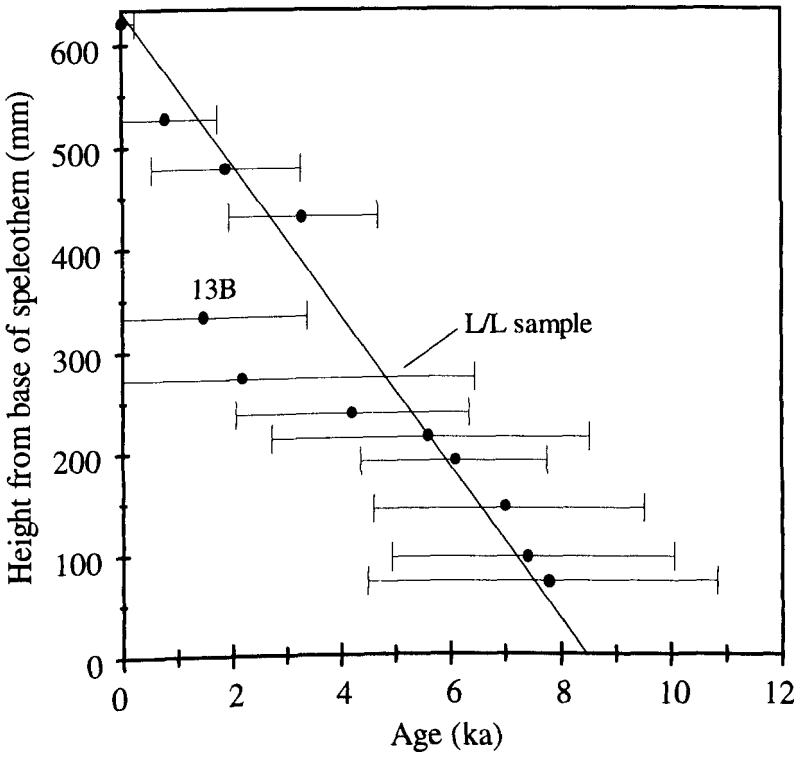

Figure 6.7. Speleothem SC01 uranium-series dates. The best-fit line is a linear least squares fit which ignores samples 13B and 15+16B (L/L sample) and assumes that the top was modern. Using these dates the basal age was 8.4±1.2 ka. Errors are to 1σ and are based on counting statistics.

6.4.3. The palaeomagnetic record of SC01.

The mean directions obtained from the AF demagnetised sub-samples of SC01 at 20 mT are presented in Appendix A. The variation in declination and inclination with height and age are shown in Figure 6.8. Declinations of central sub-samples for SC01 ranged from 342.8° (8B) to 2.8° (6B) and inclinations ranged from 27.4° (1B) to 46.3° (10B) with a mean declination of 354.5° and inclination of 39.4°. Declinations and inclinations from equivalent lateral samples are included in Figure 6.8 for comparison as are the present day declination and inclination for Xingwen as calculated from the IGRF model.

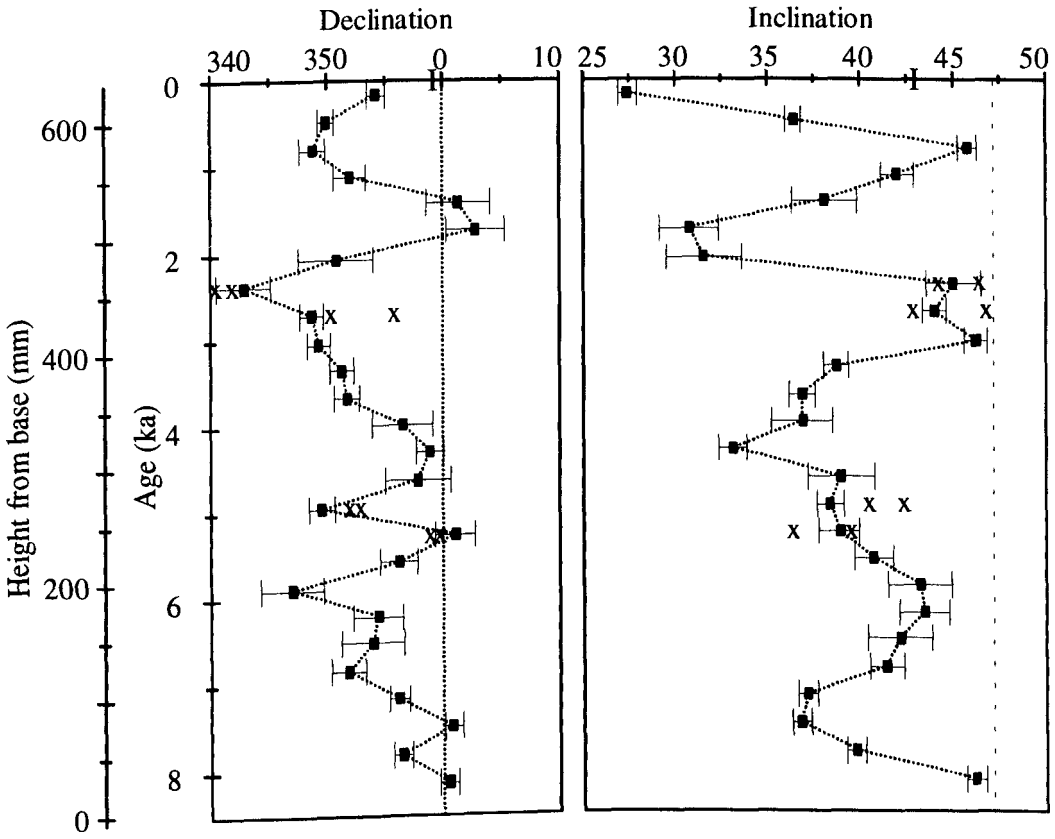

Figure 6.8 Declination and inclination of SC01 with time and height from base of stalagmite. Error bars show the α_{95} value for the mean direction of each sub-sample. Directions calculated from equivalent lateral sub-samples are shown by the X symbol with error bars omitted for clarity. The dotted line shows the GADF model for the site. The present day field calculated from the IGRF model is shown by 'I'.

The directional data were converted to equivalent virtual geomagnetic poles (VGPs) after being 3-point smoothed (Figure 6.9). The VGPs are mainly far-sided and follow an ill-defined flat anticlockwise loop from 8.1±1.1 to 4.3±0.6 ka followed by a linear easterly trend to 2.7±0.4 ka. A long clockwise loop continued to present-day. Clockwise and anti-clockwise looping of VGPs may indicate westward and eastward drift of the non-dipole field (Runcorn, 1959). Stationary non-dipole sources that have out-of-phase intensity variations may also cause such features (Creer and Tucholka, 1982).

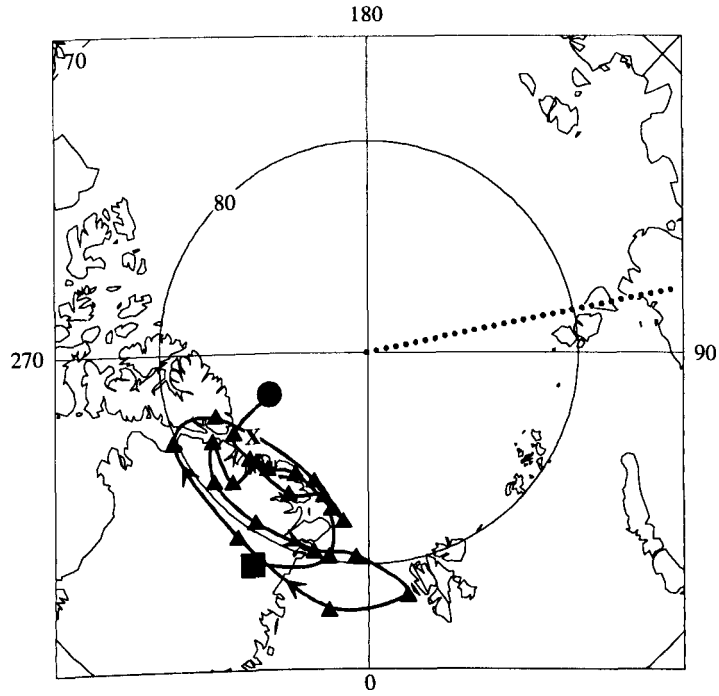

Figure 6.9. VGP progression through time for speleothem SC01. A 3-point smoothing filter has been applied to these data. The circle represents the start of the PSV record at 8.1±1.9 ka and the square represents the top which is modern. The site longitude is shown by a dotted line and the present VGP for Xingwen is shown by 'X'.

6.5. Palaeomagnetism and dating of SC02.

6.5.1. NRM and demagnetisation of SC02.

The single central slice of SC02 produced a total of 23 central drip-cap sub-samples which were used for palaeomagnetic work, labelled 1B to 23B. Most of the NRM intensities were low, ranging from 7.6 x 10^{-8} Am^2/kg^{-1} (21B) to 34.1 x 10^{-8} Am^2/kg^{-1} (15B). The two basal sub-samples, 22B and 23B, had the strongest NRM intensities; 151.7 x 10^{-8} Am^2/kg^{-1} and 817.7 x 10^{-8} Am^2/kg^{-1} respectively. All central drip-cap sub-samples were stepwise AF demagnetised in steps of 5 mT up to 30 mT and in steps of 10 mT up to a maximum of 170 mT. Median destructive fields were of the order 65 to 75 mT and approximately 20% of the NRM remained at 170 mT suggesting the presence of magnetically hard (SD-like) carriers of remanence.

Figure 6.10 illustrates representative AF demagnetisation behaviour for SC02. Due to the low NRM intensities, magnetometer noise introduced some scatter into each measurement. However, the stable unidirectional remanence vector can be clearly isolated in all cases as identified from the Zijderveld plots (Figure 6.10 a, d and g). A small viscous component of magnetisation was removed between 5 and 10 mT. A mean direction was calculated from the remaining data-points using the method of Kirschvink (1980).

Overall, the majority of sub-samples had MADs in the range 2.2° (22B) to 9.7° (2B) but two sub-samples (1B and 20B) had MADs of 11.0° and 11.3° respectively. Mean directions from the stereographic projections (for example Figure 6.10b, e and h) gave similar mean directions with α_{95}'s in the range 0.6° to 2.4°. The similarity indicated that the stable remanence had been adequately defined by AF demagnetisation.

Figure 6.11 shows demagnetisation data from two lateral sub-samples (13A and 13C) that were stepwise thermally demagnetised in steps of 50° C up to 700° C, excepting the 100° C step between 400 and 500° C. Both samples required reassembly after heating steps and this, combined with the weak NRM, introduced some noise into the results. This is especially apparent in the higher heating steps of sub-sample 13C (Figure 6.11d). A small viscous component of magnetisation was removed between 100 and 150° C leaving a single stable remanence direction. This was interpreted to be the primary remanence and could be identified up to 700° C where the vector lay close to the origin of the Zijderveld plot (Figures 6.11a and d). Stereographic projections of these data (Figures 6.11b and e) showed the single stable remanence, but also showed the degree of directional scatter resulting from sub-sample reassembly and from magnetometer noise. The decrease in NRM intensities during thermal demagnetisation are shown by Figures 6.11c and f. The sharp decreases in intensity between 100 and 150°C coincided with the removal of the viscous remanence, contained in low T_b grains. NRM intensity subsequently reduced, with a step between 350 and 400° C, to zero between 650 and 700° C.

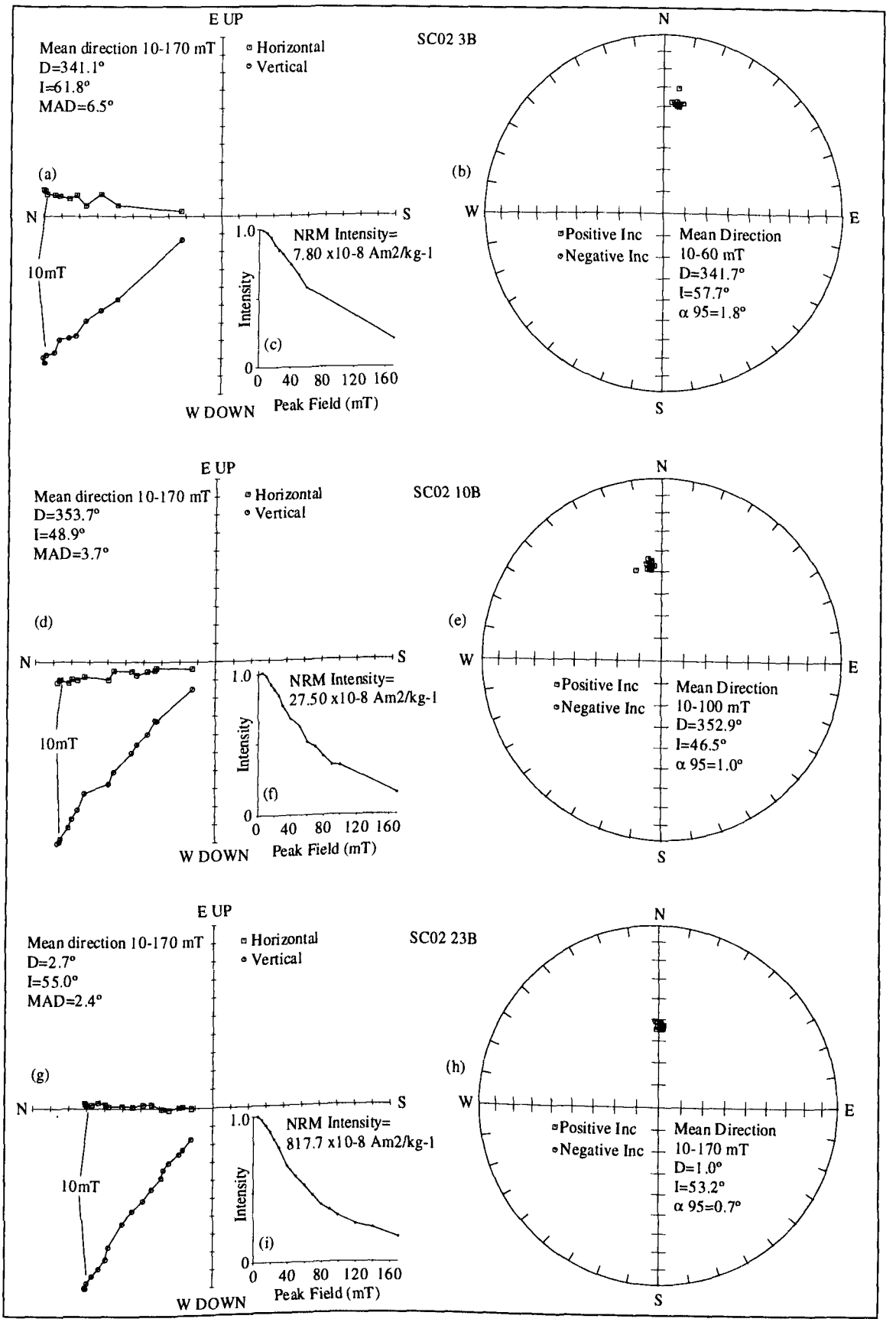

Figure 6.10. AF demagnetisation data from SC02 sub-samples 3B, 10B and 23B.

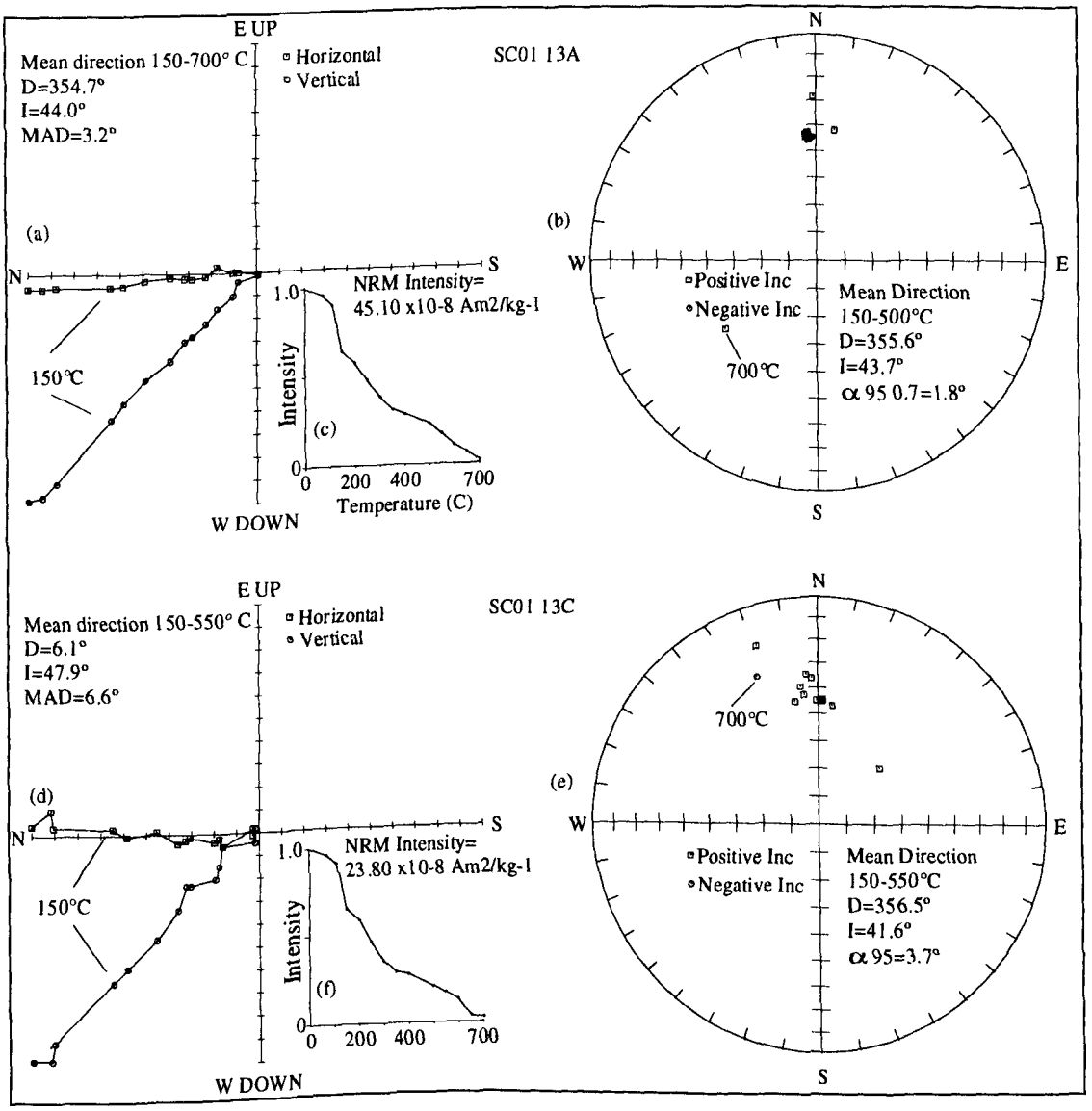

Figure 6.11. Thermal demagnetisation of SC02 lateral sub-samples 13A and 13C.

Table 6.3 and Figure 6.12 show the results of depositional inclination error checks made using comparisons between coeval central and lateral sub-samples. The position of prominent growth layers were used as a guide to the choice of coeval sub-samples. The inclinations agree within the MAD error parameter although both 16A and 16C have inclinations slightly steeper than their equivalent central sub-sample, 15B. These results illustrate that no systematic differences in remanence acquisition were apparent between central and lateral sub-samples.

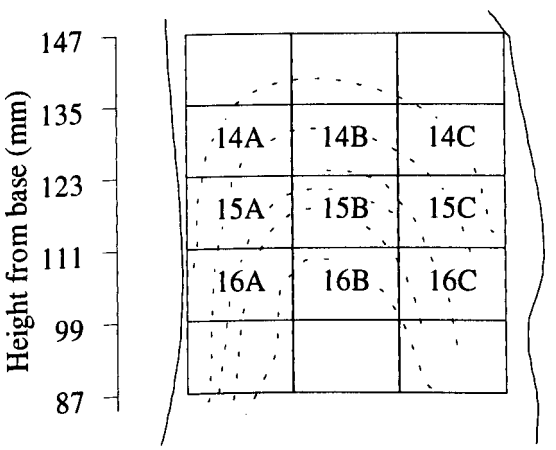

Figure 6.12. Cross-section through SC02 central slice showing positions of sub-samples used for depositional inclination error tests. Dotted lines represent growth layers.

Sub-sample	Declination	Inclination	MAD
15A	357.9	44.9	2.2
14B	356.5	43.3	2.8
15C	359.4	42.6	4.6
16A	358.4	44.6	5.3
15B	2.2	41.2	5.8
16C	3.8	43.0	6.1

Table 6.3. Values of declination and inclination for coeval central and lateral sub-samples used for depositional inclination error tests on SC02. MAD is shown as a measure of precision.

6.5.2. Uranium-series dating of SC02.

Uranium-series data from sub-samples of SC02 are presented in Table 6.4. Sub-sample dates suffered from a moderate to high degree of uncertainty with only 15B, 19B and 20B having age errors <10%. A combination of low uranium concentrations (0.38 to 0.64 ppm) and some low chemical yields of U and Th have contributed to these errors.

The persistent problem of detrital thorium contamination, indicated by $^{230}Th/^{232}Th$ ratios <<25, also increased the dating uncertainties. Sub-samples of SC02 had $^{230}Th/^{232}Th$ ratios in the range 2.6±1.7 (3B) to 20.5±7.5 (20B) which reflect the changes in contamination levels. The initial thorium correction ratio used in the dating program was maintained at 1.5 (after Gascoyne *et al*, 1981). The top of SC02 was assumed to be modern when collected since it was being dripped on. The date of sub-sample 1B (0.4±0.6 ka) reflects the young age indicating that the use of the initial thorium correction value of 1.5 was acceptable in this case. No attempt was made to correct the remaining dates using thorium ratio of sub-sample 1B as it would have made the date of 3B negative even though is was older than sub-sample 1B.

A linear-least squares fitting program was used to estimate the speleothem age. Those data used in the calculation are illustrated in Figure 6.13. The date of sub-sample 15B was ignored since it appeared unusually old. Possible reasons for anomalous ages are discussed in chapter 4 but in this case no single reason could be identified. Assuming that the top of SC02 was modern and that constant growth had occurred, a growth rate of 0.029 mm yr^{-1} was calculated. A top surface age of 0.1±0.1 ka and a basal age of 9.2±0.5 ka, were calculated giving a growth period of 9.1 ka. Based on this calculated growth rate a typical sub-sample of SC02 would represent a time-average of 400 years of PSV. This level of resolution of PSV is about as low as is useful for detailed records of PSV to be obtained. If we assume a drift rate of 0.2° yr^{-1} (Aitken *et al*, 1989; Yang *et al*, 1993; Hyodo *et al*, 1993) then only four sub-samples record just under one complete rotational cycle of the field. This is made worse, if we assume a drift rate of 0.3° yr^{-1}, to three sub-samples per rotation.

Sub-sample	Concentration U (ppm)	U Yield (%)	Th Yield (%)	$^{234}U/^{238}U$	$^{230}Th/^{234}U$	$^{230}Th/^{232}Th$	Uncorrected age (ka)	Corrected age (ka)
1B	0.64±0.02	20	15	1.31±0.04	0.007±0.002	3.29±3.52	0.7±0.3	0.4±0.6
2B	0.55±0.01	22	14	1.29±0.03	0.019±0.002	5.81±2.94	2.2±0.3	1.6±0.6
3B	0.38±0.01	38	5	1.29±0.03	0.017±0.006	2.57±1.71	1.8±0.6	0.8±1.2
5B	0.56±0.01	33	26	1.33±0.03	0.015±0.002	7.17±4.95	1.6±0.2	1.3±0.5
10B	0.39±0.01	73	65	1.29±0.02	0.048±0.003	5.48±1.46	5.3±0.4	3.9±0.7
15B	0.47±0.01	54	42	1.33±0.02	0.113±0.005	8.14±1.32	13.0±0.6	10.7±1.0
18B	0.61±0.01	48	14	1.29±0.02	0.065±0.005	17.60±8.80	7.3±0.6	6.7±0.9
19B	0.62±0.01	37	50	1.30±0.02	0.080±0.003	10.49±1.84	9.0±0.4	7.8±0.6
20B	0.60±0.02	10	45	1.34±0.04	0.074±0.003	20.49±7.49	8.3±0.4	7.7±0.7

Table 6.4. Uranium-series data for sub-samples of SC02 with resultant uncorrected and corrected ages. Errors are to 1 sigma and are based on counting statistics.

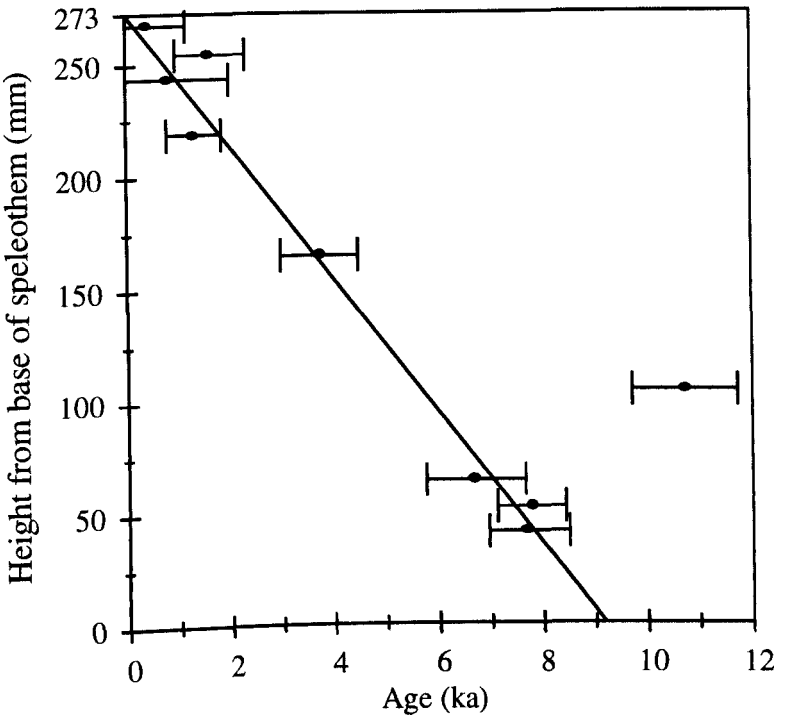

Figure 6.13. Speleothem SC02 uranium-series dates. Errors are to 1σ based on counting statistics. The best-fit line is a linear-least squares fit assuming the top is modern and ignoring sub-sample 15B. The top of SC02 is 0.1±0.1 ka and the base is 9.2±0.5 ka.

6.5.3. The palaeomagnetic record of SC02.

The mean directions calculated from central sub-samples of SC02 are tabulated in Appendix B. These inclination and declination data are shown in Figure 6.14. Declinations of central sub-samples ranged from 339.3° (8B) to 7.8° (6B) whilst inclinations ranged from 39.2° (20B) to 61.8° (3B). A mean declination of 354.5° and a mean inclination of 48.2° were calculated using Fisher statistics. The mean declination and inclination are close to the GADF model. It is interesting to note that the inclination and declination recorded by sub-sample 1B lie very close to the present day field at Xingwen (the 'I' symbols on Figure 6.14). This provides further evidence that the remanence is acquired instantaneously in speleothems as pointed out by Latham *et al* (1986). Figure 6.14 also includes the directional data from the coeval lateral sub-samples used for depositional inclination error experiments and illustrates their close agreement with corresponding central sub-samples.

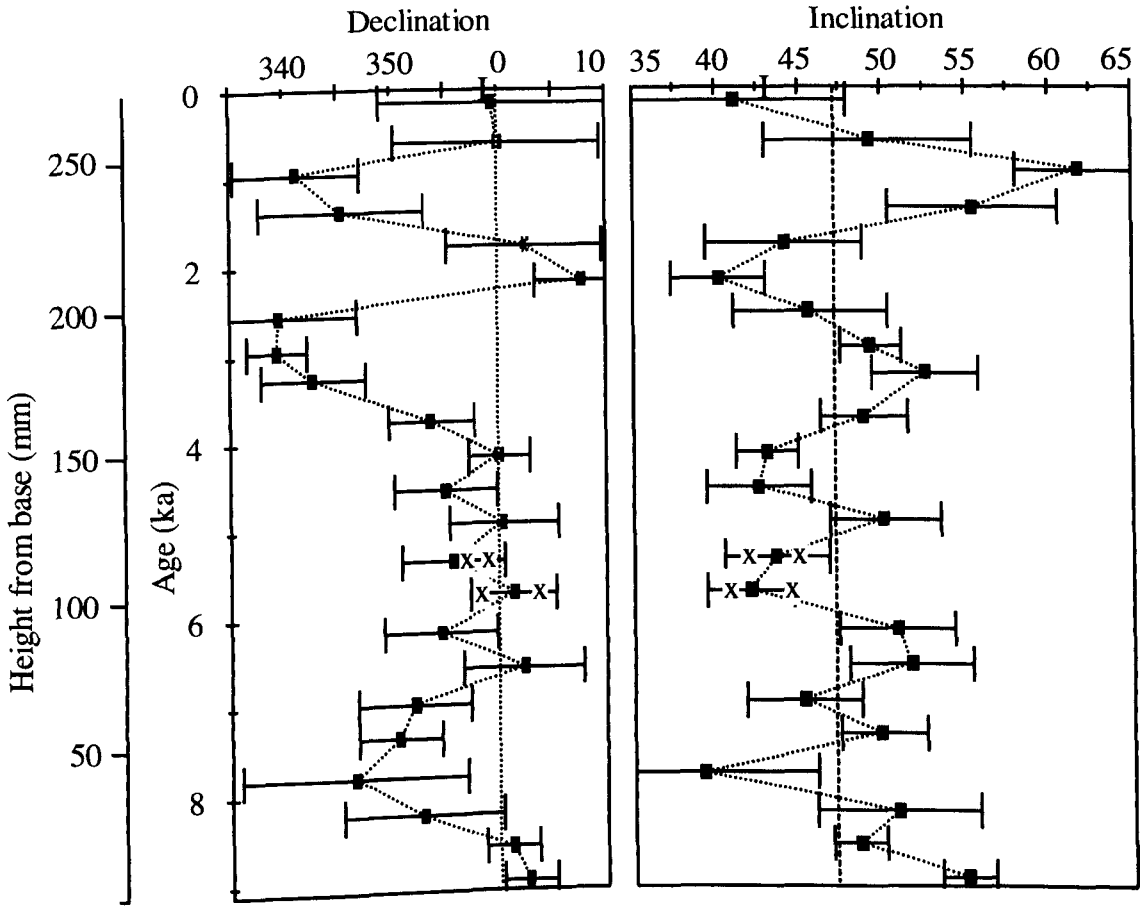

Figure 6.14. Declination and inclination of SC02 against sub-sample age and height from base of stalagmite. Error bars show the MAD value for each sub-sample. Directions calculated from equivalent lateral sub-samples are shown by X with error bars omitted for clarity. The dotted vertical line shows the GADF model for Xingwen and the 'I' symbol shows the present day field for Xingwen calculated from the IGRF model.

The directional data were converted to equivalent VGPs after the application of a 3-point smoothing filter (to reduce any noise in the data). Figure 6.15 shows the progression of the VGPs over time. From 9.2±0.5 ka to 6.6±0.3 ka the VGPs followed a north to south return path followed by an incomplete anticlockwise loop to 3.7±0.2 ka. A long clockwise loop was defined to 1.8±0.1 ka continuing with a vague indication of clockwise looping to the present day. It is worth noting that although the records of SC01 and SC02 are comparable in length and resolution that the VGPs lie in different quadrants. The VGPs of SC02 could be described as near-sided as opposed to far-sided in SC01. It is suspected that there was some loss in orientation during sample preparation. This is discussed at the end of this chapter.

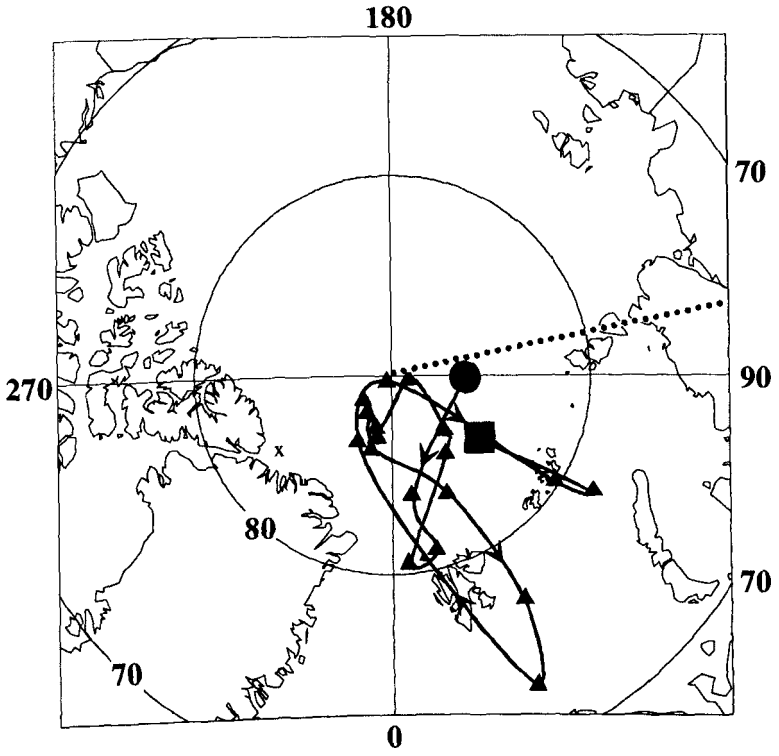

Figure 6.15 VGP progression through time for speleothem SC02. A 3-point smoothing filter has been applied to these data. The circle represents the start of the PSV record at 9.2±0.5 ka and the square represents the top which is modern. The site longitude is shown by the dotted line and the present VGP for Xingwen is shown by '**X**'.

6.6. Palaeomagnetism and dating of PT02

6.6.1. NRM and demagnetisation of PT02

The central slice of stalagmite PT02 produced 41 7 cm^3 central sub-samples for palaeomagnetic work; these were labelled 1B to 41B; sub-sample 35B was destroyed during the cutting-up process. NRM intensities ranged from 300 x 10^{-8} Am^2kg^{-1} (38B) to 5 x 10^{-8} Am^2kg^{-1} (12B) but the majority of sub-samples had intensities less than 80 x 10^{-8} Am^2kg^{-1}. Only the basal sub-samples (34B to 41B) had intensities over 100 x 10^{-8}

Am^2kg^{-1}. All central sub-samples were stepwise AF demagnetised in 5 mT or 10 mT steps depending on their NRM intensity to a maximum of 170 mT. No directions could be calculated from sub-samples 6B, 11B, 12B, 13B and 22B after AF demagnetisation. Repeat measurements of these sub-samples after each AF step failed to produce repeatable directions. It was considered that they were either unstable to AF demagnetisation or were too weak (NRM intensities 5 to 15 x 10^{-8} Am^2kg^{-1}). Other sub-samples became too weak to measure before complete demagnetisation but a direction could be calculated from the available data. Those sub-samples subjected to AF fields of 170 mT had 18 to 30% of their NRM intensity remaining. As in SC01 and SC02 this shows the presence of magnetically hard (SD-like) carriers of remanence.

Figure 6.16 shows representative demagnetisation behaviour of PT02 sub-samples. The weaker NRM intensities of some PT02 sub-samples introduced some noise in to each measurement on the SQUID magnetometer leading to more scattered directional data (Figure 6.16a and g). The effects of magnetometer noise were especially apparent after application of higher fields when little NRM remained. Despite noise it was still possible to isolate a single primary component of magnetisation.

The majority of sub-samples exhibited little, or no, apparent viscous remanent magnetisation. Figure 6.16a shows evidence for a small VRM in sub-sample 4B whilst Figure 6.16d shows the most significant VRM encountered in sub-sample 21B. After removal of the VRM, by a maximum AF of 15 mT, a linear trend to the origin of the Zijderveld plots could be isolated. This was inferred to be the primary remanence. Mean directions were subsequently calculated using the method of Kirschvink (1980). Sub-sample MADs were higher reflecting the effects of low NRM intensities and magnetometer noise and ranged from 1.5° (21B) to 9.6° (18B). Sub-samples 14B and 19B had MADs of 13.8° and 14.2° respectively but were not rejected as their directions were consistent with the other samples. The α_{95}s shown on the stereographic projections lay in the range 0.9° to 3.9° and but directions were similar to those calculated from the Zijderveld plots (Figure 6.16b, e and h for example). The stereographic projections clearly show the degree of directional scatter due to noise; directional grouping was tighter with samples having stronger NRMs.

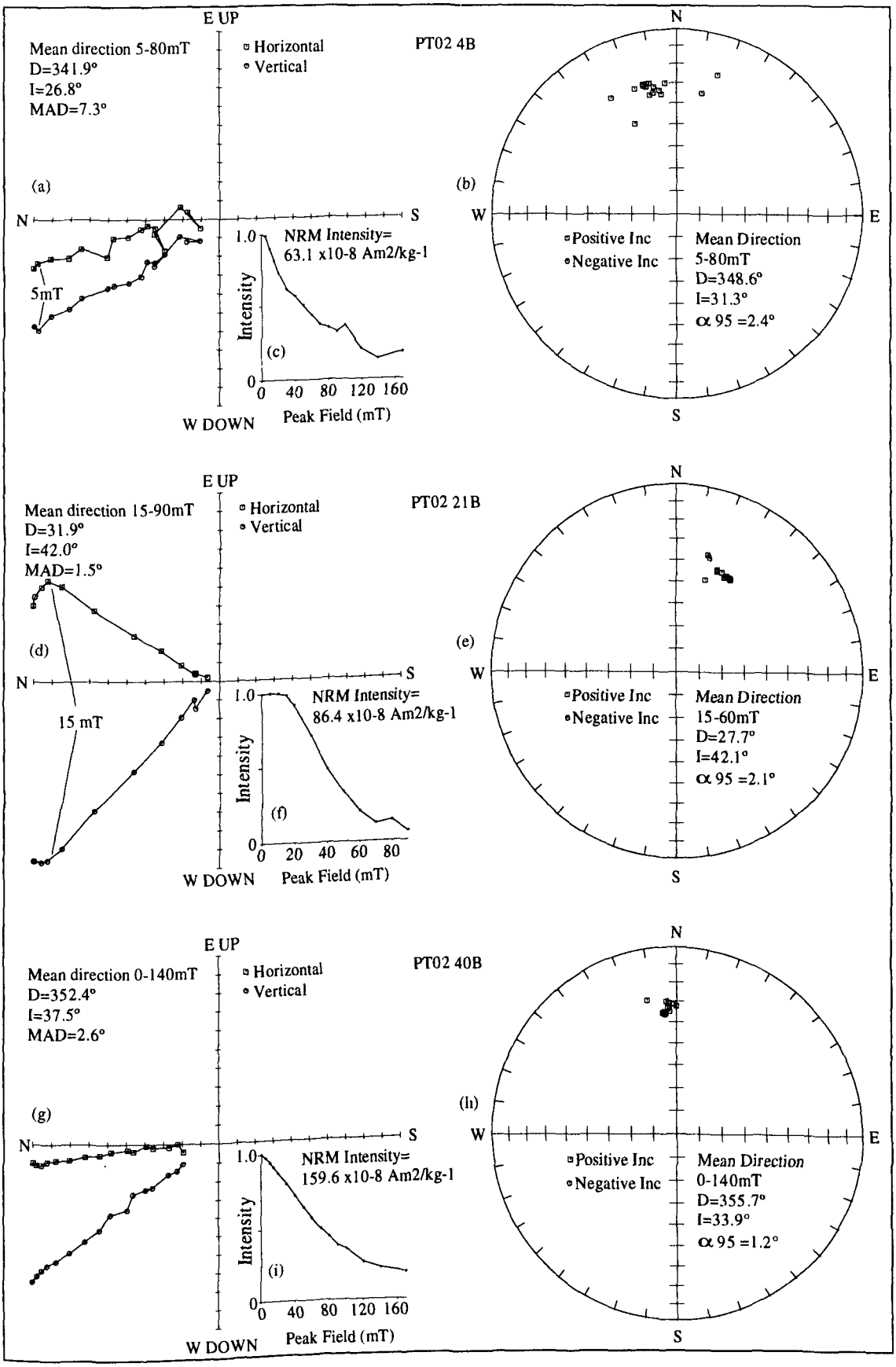

Figure 6.16 AF demagnetisation data from PT02 sub-samples 4B, 21B and 40B.

AF demagnetised sub-samples had MDFs in the range 36 to 80 mT and had two distinct groupings. MDFs were less than 60 mT above sub-sample 32B (from 129 mm from base to the top) and had values up to 80 mT from the base (41B) to 32B. This may indicate differences in the grain size distribution and concentration of the carriers of the NRM in PT02. However, rock magnetic experiments (chapter 8) indicated a constant mineralogy throughout the speleothem.

In order to assess the effects of thermal demagnetisation, lateral sub-samples 37A, 38A and 38C were stepwise thermally demagnetised in 50°C steps to 300°C, in 100°C steps to 500°C and in 50°C steps to 700°C. The results for 37A and 38C are shown in Figure 6.17. Sub-sample 37A had a small viscous component that was removed by 100°C. Subsequently the vector trended to the origin of the Zijderveld plot (Figure 6.17a) but appeared to pick up a small TRM between 400 and 500°C with a correspondingly small increase in intensity (Figure 6.17c). The stereoplot also showed this as two points away from the clustered VEPs (Figure 6.17b). This TRM may have been picked up after the sample was removed from the oven as it cooled to room temperature. The sub-samples used for thermal demagnetisation were heated simultaneously but no evidence for a TRM was seen in 38A or 38C. Thus, it was difficult to establish a cause although the effect of magnetometer noise cannot be ruled out as a possible reason. The equivalent coeval central sub-sample, 36B, had inclinations that matched within the MAD confidence limits although 36B had been AF demagnetised. Therefore a lack of depositional inclination errors was suggested by the absence of significant inclination discrepancies between the essentially horizontal central sub-samples and the steeply dipping lateral sub-samples.

Thermal demagnetisation of sub-sample 38C caused alteration which is best illustrated by the intensity plot (Figure 6.17e). Alteration occurred between 250 and 400°C which indicated the inversion of maghaemite to haematite. However, the incomplete removal of remanence by 700°C may illustrate the formation of titanomaghaemite by metastable oxidation (Thompson and Oldfield, 1986).

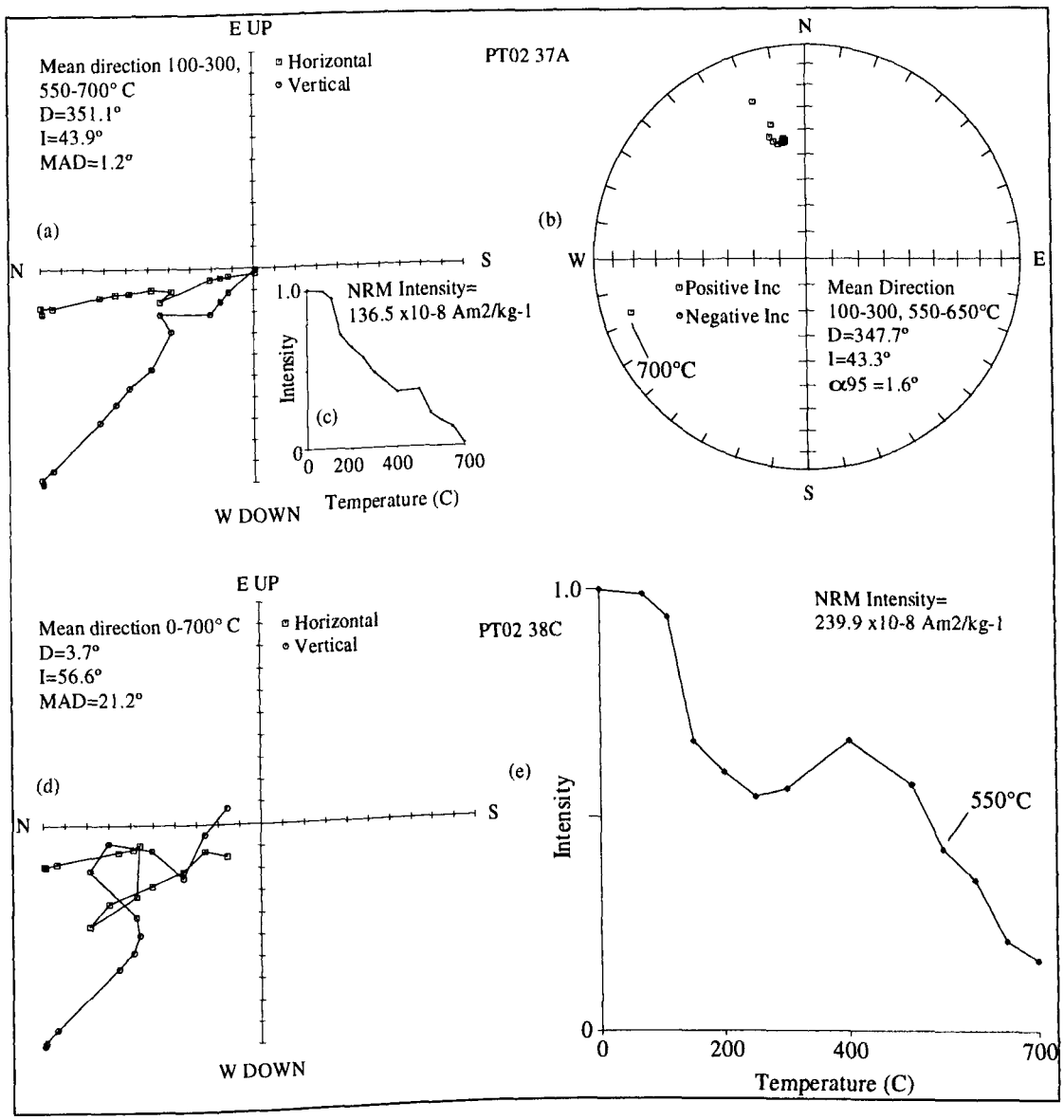

Figure 6.17. Thermal demagnetisation data for PT02 sub-samples 37A and 38C.

Insufficient and unsuitable lateral sub-samples made conclusive depositional inclination error checks difficult. The only data are for lateral samples 37A and 37C (discussed above) and 28A and 28C with their coeval central sub-sample 27B. After AF treatment inclination agreement was as follows:- 28A = 46.0° (MAD=2.3°), 27B = 49.0° (MAD=6.1°) and 28C = 46.4° (MAD=4.3°). These few results indicate that inclination shallowing was probably not significant between lateral and central samples but tests were not as rigorous as for SC01.

6.6.2. Uranium-series dating of PT02.

Table 6.5 shows that the uranium concentrations ranged from 0.49±0.01 (3B) to 0.79±0.01 ppm (5B). These were the highest uranium concentrations found in the speleothems from Xingwen. Chemical yields of PT02 were also consistently higher because the Hallstadius electroplating technique was used throughout. Uranium yields varied from 37% to 71% whilst thorium recoveries ranged from 12% to 64%. Both the higher uranium concentrations and the increased chemical yields helped to reduce the uncertainties for individual dates. All sub-samples, except 1B ($^{230}Th/^{232}Th$ ratio >1000) required a correction for thorium contamination. Thorium ratios of the remaining sub-samples ranged from 1.2±0.2 (5B) to 4.4±2.9 (3B) and an initial thorium correction ratio of 1.8 was used in the dating program as matches between the dated PSV records became more satisfactory. No estimate of the initial thorium ratio could be made from the clean top sample 1B. The corrected date from sub-sample 5B was -0.9±0.5 and was considered likely to have suffered from some unknown analytical error during preparation. A L/L date of 2.4±1.0 ka was obtained for combined sub-samples 21B, 22B and 23B using the MLE algorithm (Ludwig and Titterington, 1994).

Because the upper surface of PT02 was known to have been active when collected the date of 1B (1.5±0.3 ka) was ignored when estimating the ages of the remaining sub-samples. Comparison with the dated PSV records of other Xingwen speleothems also indicated that the date of 1B was likely to be anomalous. As a result of the generally poor dating control in PT02 two best-fits were attempted using combinations of sub-sample dates (Figure 6.18). The first fit was made to sub-samples 3B, 37B and 38B only and gave a top surface age of 0 and a basal age of 2.5±0.6 ka. The second fit was made to all sub-samples, excluding 1B and 5B, and gave an age range of 0 (top) to 3.1±0.4 ka (base). In terms of fitting the other PSV records from Xingwen, the former fit was considered more likely. This fit allowed a growth rate of 0.22 mm yr^{-1} to be estimated. Thus, each sub-sample of PT02 would record 58 years of PSV over the 2.5 ka growth period and it would require 31 sub-samples to record one complete rotation of the geomagnetic field (assuming a drift rate of 0.2° yr^{-1}). This was the highest resolution of all the speleothems in this study.

Sub-sample	Concentration U (ppm)	U Yield (%)	Th Yield (%)	$^{234}U/^{238}U$	$^{230}Th/^{234}U$	$^{230}Th/^{232}Th$	Uncorrected age (ka)	Corrected age (ka)
1B	0.77±0.01	71	12	1.25±0.02	0.003±0.003	>1000	1.5±0.3	-
3B	0.49±0.01	68	64	1.31±0.02	0.014±0.002	4.39±2.95	1.6±0.3	0.9±0.7
5B	0.79±0.01	47	45	1.28±0.02	0.014±0.002	1.15±0.20	1.5±0.2	-0.9±0.5
21-23B (L/L)	-	-	-	-	-	-	-	2.4±1.0
37B	0.63±0.01	37	26	1.28±0.02	0.048±0.003	2.93±0.44	5.3±0.4	2.1±0.8
38B	0.69±0.01	53	60	1.27±0.02	0.063±0.003	2.51±0.19	7.0±0.3	2.0±0.7
40B	0.75±0.01	46	51	1.24±0.02	0.051±0.003	4.27±0.60	5.6±0.3	3.3±0.6
41B	0.69±0.02	54	19	1.26±0.02	0.052±0.005	4.03±0.82	5.8±0.5	3.3±1.0

Table 6.5. Uranium-series data for sub-samples of PT02 with resultant uncorrected and corrected ages. Errors are to one sigma and are based on counting statistics. Leached sub-samples 21-23B were dated using the isochron method (Schwarcz and Latham, 1989)

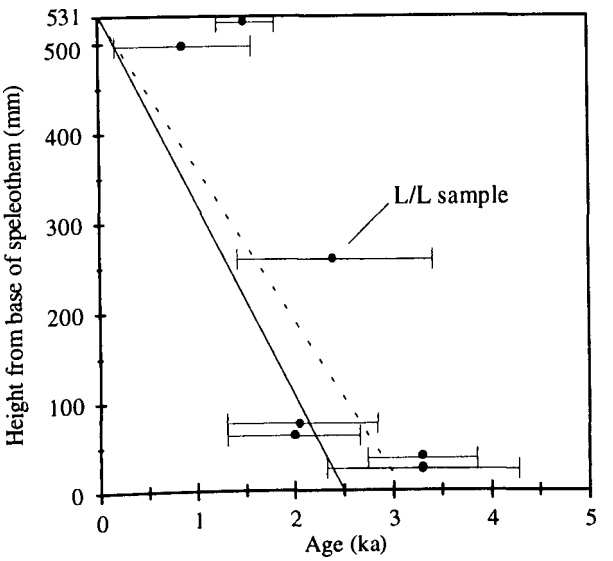

Figure 6.18. Speleothem PT02 uranium-series dates. Errors are to 1σ (based on counting statistics). The solid best fit line was calculated from sub-samples 3, 37 and 38B only. This growth period (2.5±0.6 to 0 ka) was considered the most likely after comparisons with the other Xingwen records. The dotted best-fit line (3.1±0.4 to 0 ka) was calculated from sub-samples 3B, the MLE date from 21-23B, 37, 38, 40 and 41B.

In hindsight, too few sub-samples from PT02 were dated. More dates would probably have helped to alleviate some of the ambiguities associated with the dating. In particular, a greater number of dates of sub-samples from the top and middle of PT02 would have been useful in constraining the upper age and in checking for changes in growth rate. However, because it was possible to match the record to the other dated Xingwen records these uncertainties are a little reduced. Despite this, the dating of PT02 should probably be considered preliminary and incomplete.

6.6.3. The palaeomagnetic record of PT02.

Appendix C contains the mean directions obtained from sub-samples of PT02. Figure 6.19 illustrates the variation in declination and inclination with height and age using the 0 to 2.5 ka best-fit estimate. Declinations for PT02 range from 330.2° (29B) to 31.9° (21B) with a Fisher (1953) mean of 350.3° while inclinations range from 22.8° (16B) to 64.2° (8B) with a mean of 44.0°.

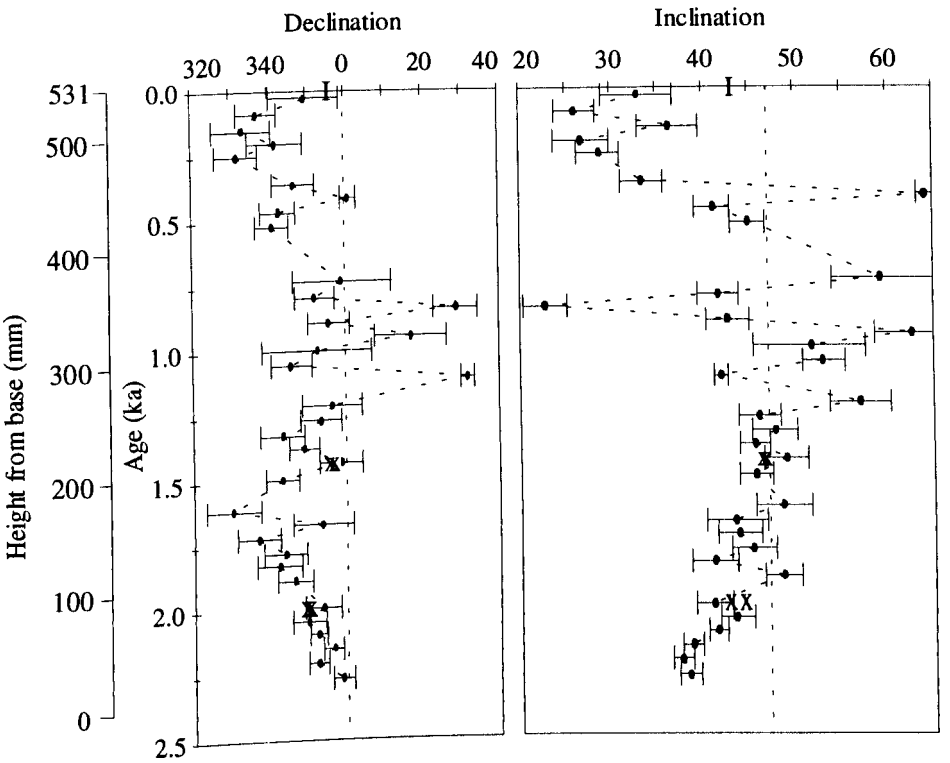

Figure 6.19. Declination and inclination of PT02 against sub-sample age and height from base of stalagmite. Error bars show the MAD value for each sub-sample. Directions calculated from equivalent lateral sub-samples are shown by X with error bars omitted for clarity. The dotted line shows the GADF model for the site and the 'I' symbol shows the present day field for Xingwen calculated from the IGRF model.

Most of these declinations were west of, whilst inclinations were slightly shallower than, the GADF (D=0°, I =47°). However, a growth period of 2.5 ka would not generally be considered long enough to average out PSV to the GADF (Merrill and McElhinny, 1983). Because PT02 was growing when collected the declination and inclinations in the upper sub-sample (1B) should be close to the present day field value for Xingwen. This is certainly the case for declination (Figure 6.19) as the present day declination is within the MAD calculated for sub-sample 1B. However for inclination there is a 6° difference between recorded and present day inclination. A possible cause would be that the very top of PT02 was not included in sub-sample 1B as it was trimmed during preparation. Overall, the PSV record from PT02 showed a higher amplitudinal variation compared to the other records and this was thought to reflect its higher resolution. Since each sub-sample represented 58 years, comparatively little smoothing of PSV has occurred during this period.

The declination and inclination data were smoothed using a 3-point smoothing filter to highlight the main trends and were converted to equivalent VGPs. Figure 6.20 shows the migration of the VGPs throughout the 2.5 ka growth period of PT02. The record began with a linear segment from 2.3±0.6 to 1.7±0.4 ka reflecting shallowing inclinations and westerly declinations. The path from 1.7±0.4 to 1.1±0.3 ka oscillated before migrating past the geographic pole. A flat clockwise loop followed by a larger anticlockwise loop can then be identified before the VGPs migrate back over the geographic pole. However, there is a lack of data in this region because it was not possible to calculate directions for sub-samples 11-13B thus inferences on field motion can not be made. No looping trend can be established in youngest section of the record (0.5 to 0 ka) but the VGPs migrate into lower latitudes due to a shallowing of the inclinations. Due to the shallowing of recorded inclinations the end of the record does not lie near the present day VGP (Figure 6.20; 'X').

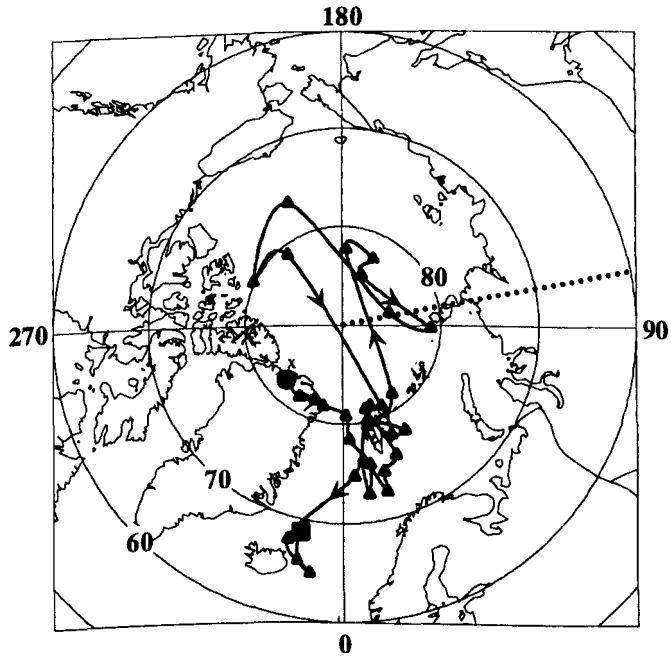

Figure 6.20. VGP progression through time for speleothem PT02. A 3-point smoothing filter has been applied to these data. The filled circle represents the start of the PSV record at 2.3±0.6 ka and the square shows the end of the record at 0 ka. The site longitude is shown by the dotted line and the present day VGP is shown by 'X'.

6.7. Palaeomagnetism and dating of PT03.

6.7.1. NRM and demagnetisation of PT03.

When cut PT03 yielded one central slice and 15 central sub-samples labelled 1B to 15B. NRM intensities were low and ranged from 18.4 x 10^{-8} Am^2kg^{-1} (1B) to 101.9 x 10^{-8} Am^2kg^{-1} (10B). All sub-samples were easily measured on the SQUID magnetometer. Stepwise AF demagnetisation was performed on all central sub-samples in steps of 10 mT to 170 mT, including a step at 15 mT. In line with other speleothems from Xingwen, sub-sample MDFs ranged from 40 to 75 mT and 13-20% of the NRM remained at 170 mT indicating the presence of magnetically hard (SD-like) carriers of remanence.

Representative AF demagnetisation characteristics for PT03 are illustrated in Figure 6.21a-f. Mean directions for sub-samples of PT03 were calculated from the Zijderveld plots after removal of any VRM (Figure 6.21a and d). After removal of VRMs by a maximum AF of 20 mT (Figure 6.21d for example) the majority of sub-samples exhibited a very stable primary remanence. Intensity plots (Figure 6.21c and f) showed a small increase in intensity as the opposing VRM was removed. Sub-samples 1B and 2B, which held the weakest NRMs (18.4 and 24.2 x 10^{-8} Am^2kg^{-1}) suffered some influence from magnetometer noise during demagnetisation; illustrated in figure 6.21a. Mean directions for these sub-samples were calculated from the Zijderveld plots using the method of Kirshvink (1980). Precision, as shown by the MAD of each sub-sample, was generally good but sub-samples 1B and 2B had MADs of 10.2° and 11.1° respectively. All remaining sub-sample MADs lay in the range 1.8° to 7.8°. Stereographic projections yielded mean directions that were close to those calculated from the Zijderveld plots (Figure 6.21b and e).

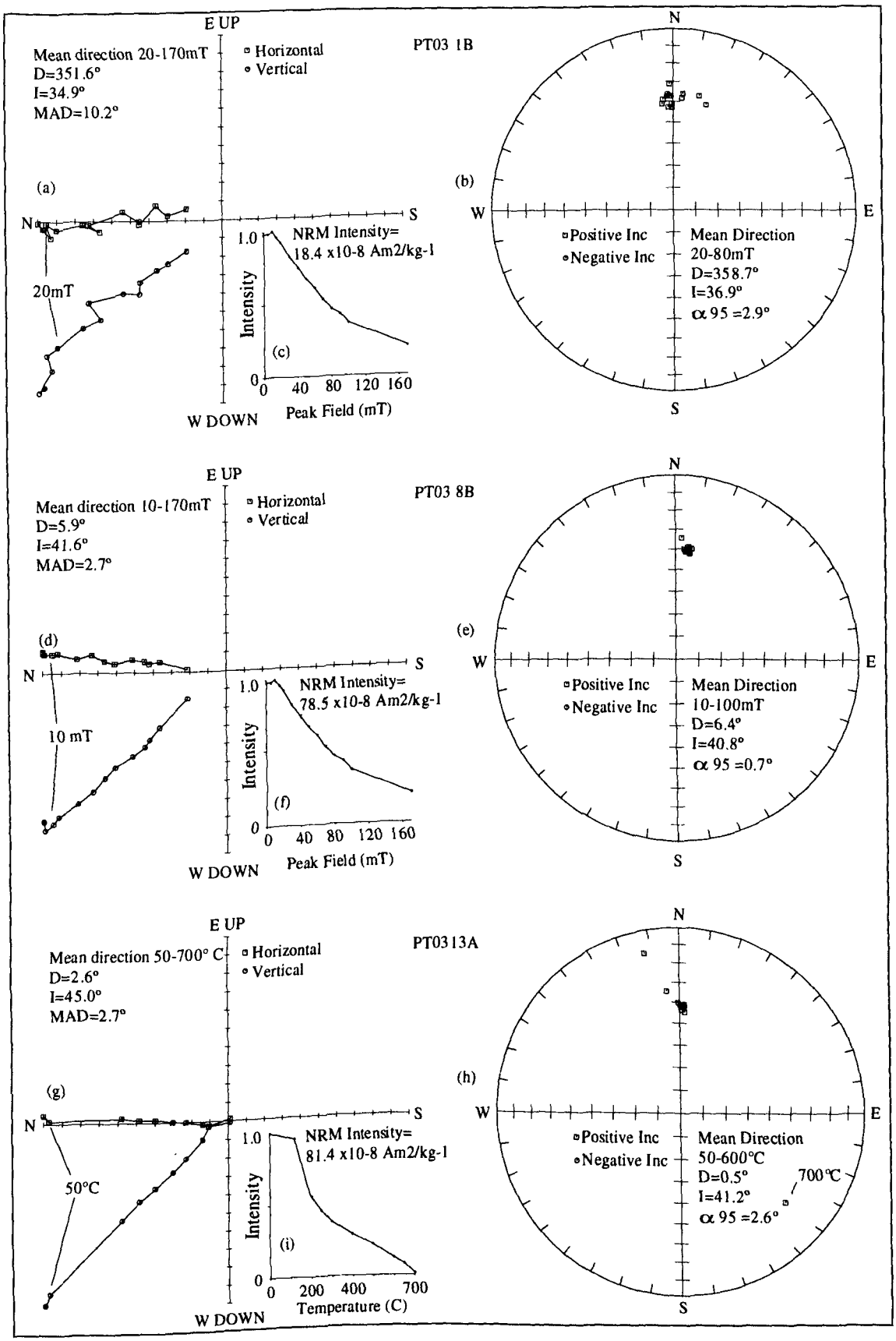

Figure 6.21. AF demagnetisation (a-f) and thermal demagnetisation (g-i) data for representative sub-samples from PT03.

Thermal demagnetisation was performed on two lateral sub-samples, 13A and 13B, in 100°C steps, to 700°C with additional steps at 350° and 650°C. These data for 13B are shown in Figure 6.21g, h and i. The Zijderveld plot clearly shows the complete removal of a small VRM by 50°C and the subsequent linear trend to the origin to 600°C interpreted to be the primary remanence. Some directional instability occurs between 650° and 700° possibly due to a combination of weak NRM and magnetometer noise. The stereographic projection (Figure 6.21h) also illustrates the tight grouping of the directional data. The intensity plot (Figure 6.21i) showed that NRM intensity reached zero between 650° and 700°C after removal of the VRM in low T_b grains by 150°C.

PT03 was too thin to obtain lateral sub-samples on which to perform detailed checks for depositional errors. However, thermally demagnetised lateral sub-sample 13A had a comparable inclination to its coeval central sub-sample 12B although the latter had been AF demagnetised. Inclinations of 12B and 13A were within MAD errors (13A Declination 2.6°, Inclination 45.0°, MAD 2.7° and 12B Declination 8.3°, Inclination 41.1°, MAD 2.6°). These discrepancies are probably due to inclusion of a small amount of non-coeval material in each sub-sample; the growth layers were simply used as a guide. Given the shortage of data these agreements should not be considered conclusive.

6.7.2. Uranium-series dating of PT03.

The dates from sub-samples of PT03 had large errors (Table 6.6). Low concentrations of uranium (0.11 to 0.14 ppm) and the generally low chemical yields of uranium and thorium partially contributed to the production of these uncertainties. Chemical yields of uranium ranged from 2% to 41% (mean 23%) whilst yields of thorium ranged from 2% to 52% (mean 14%). Only sub-sample 15B was electroplated using the Hallstadius technique which gave yields of 41% uranium and 52% thorium. The relatively high $^{230}Th/^{232}Th$ ratios also contributed significantly to the production of these age uncertainties. The $^{230}Th/^{232}Th$ ratios of PT03 sub-samples lay in the range 1.23±0.58 (1B) to 3.85±0.72 (15B) and decreased down the stalagmite suggesting less detrital contamination towards the base.

Sub-sample	Concentration U (ppm)	U Yield (%)	Th Yield (%)	$^{234}U/^{238}U$	$^{230}Th/^{234}U$	$^{230}Th/^{232}Th$	Uncorrected age (ka)	Corrected age (ka)
1B	0.13±0.01	30	7	1.73±0.05	0.015±0.005	1.23±0.58	1.7±0.6	0.0
2B	0.11±0.07	14	4	1.64±0.07	0.029±0.009	2.85±1.86	3.1±1.0	1.8±1.8
5B	0.14±0.04	32	2	1.86±0.05	0.151±0.026	3.29±1.23	17.6±3.3	11.6±5.4
6B	0.13±0.01	2	2	1.42±0.14	0.092±0.022	2.38±1.09	10.4±0.8	5.3±4.8
13B	0.14±0.01	20	19	1.70±0.05	0.094±0.007	3.38±0.49	10.6±0.8	7.0±1.3
15B	0.11±0.01	41	52	1.71±0.05	0.092±0.006	3.85±0.72	10.4±0.7	7.3±1.3

Table 6.6. Uranium-series data for sub-samples of PT03 with resultant uncorrected and corrected ages. Errors are to one sigma and are based on counting statistics.

As it was thought that sub-sample 1B was modern its $^{230}Th/^{232}Th$ ratio of 1.2 was used as an initial correction value for the remaining sub-samples. A MLE date (after Ludwig and Titterington, 1994) obtained from L/L analysis of sub-samples 11B and 12B was poor (-0.4±2.7 ka) due to non-linear isochrons (section 4.9.2). However, a comparison with other Xingwen speleothems suggested that the dates obtained using the correction procedure based on the thorium ration of sub-sample 1B were reasonable.

A linear-least squares fit was used to obtain a best-fit growth line for these dates (Figure 6.22). Sub-sample 5B was excluded as it lay outside the error limits of all other dates. A basal age of 7.7±2.5 ka and an upper surface age of 0.4±1.0 ka were calculated from the best-fit line. Despite the degree on uncertainty the modern top is reflected by the upper surface age estimate. Assuming a constant growth rate of 0.048 mm yr^{-1} each sub-sample had recorded a time-average of 517 years of PSV over 7.5 ka, although the dating errors make this an approximation. Thus, one global cycle of drift of the geomagnetic field would be recorded by just over three sub-samples. Resolution of this nature would only reveal the general trend of PSV over the growth period of PT03.

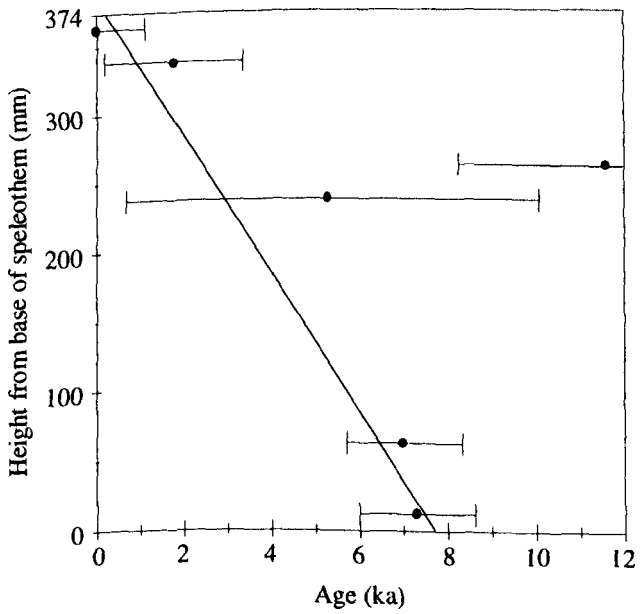

Figure 6.22. Speleothem PT03 uranium-series dates. Errors are to 1σ and are based on counting statistics. The best-fit line is a linear-least squares fit ignoring sub-sample 5B. The best-fit gives a basal age of 7.7±2.5 ka and an upper surface age of 0.4±1.0 ka.

6.7.3. The palaeomagnetic record of PT03.

The mean directions calculated from sub-samples of PT03 are shown in Appendix D. The PSV record is shown against age and height in Figure 6.23. Declination directions ranged from 349.8° (5B) to 9.2° (9B) with a Fisher (1953) mean of 1.7°. Inclinations ranged from 33.5° (15B) to 58.3° (2B) with a mean of 43.4°. These directions are close to those predicted by the GADF model. The amplitudinal variation of declination, in particular, was lower than that of the other Xingwen speleothems (±10°) probably reflecting the increased smoothing of PSV due to the slow growth rate of 0.048 mm yr^{-1}.

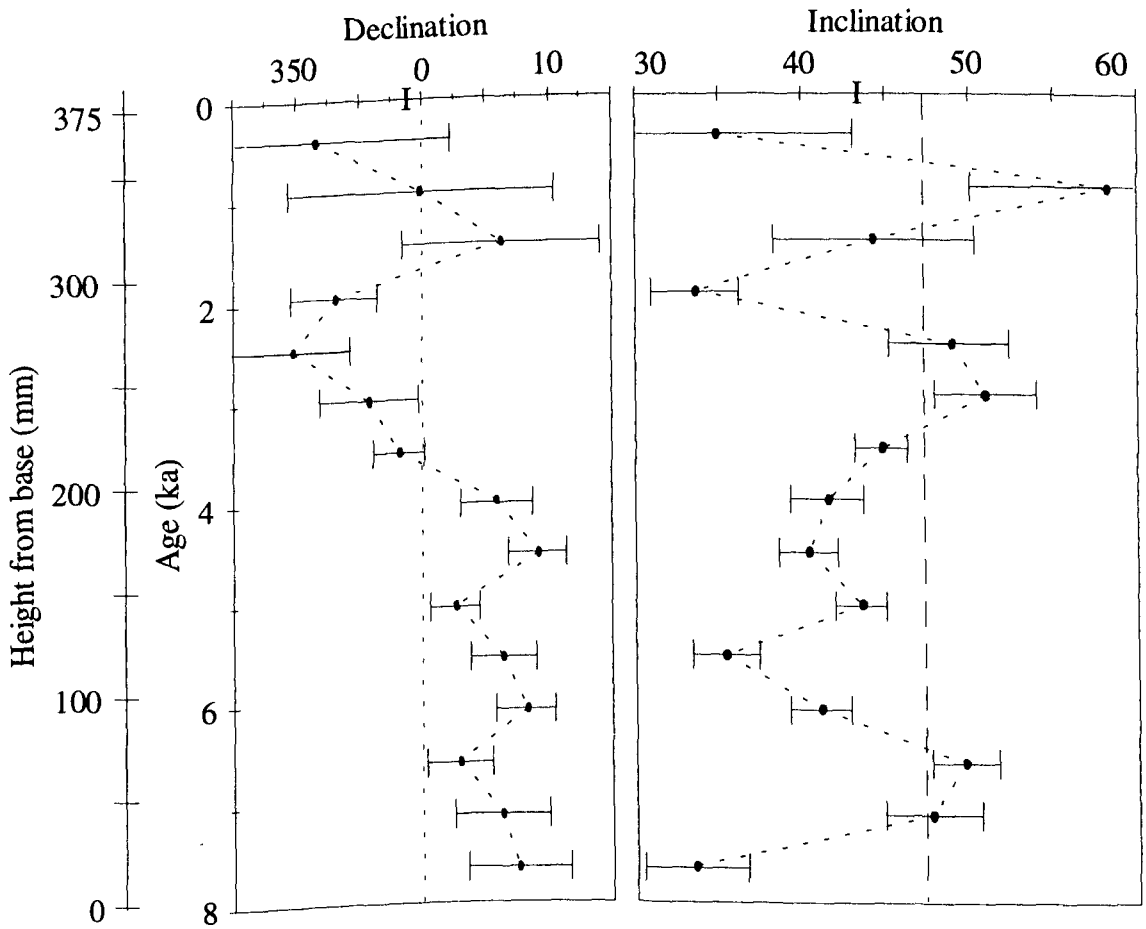

Figure 6.23. Declination and inclination of PT03 with age and height from base of stalagmite. Error bars represent the MAD of the mean direction calculated from each sub-sample. The dotted line shows the predicted GADF for Xingwen and the 'I' symbol is the present day field at Xingwen as calculated using the IGRF model.

Equivalent VGPs were calculated to show the progression of the VGP through time (Figure 6.24). The limited number of datapoints from PT03 showed only the general trend of VGP movement through time. The majority of VGPs were far sided as a result of the shallow inclinations. From 7.7±2.5 ka to 5.5±2.0 ka there was no clearly defined motion of the VGPs path. However, from 5.5±2.0 ka to the end of the record at the present day the VGPs follow one and a half clockwise loops. The end of the record at 0.4±1.0 ka lies close to the present day VGP for Xingwen..

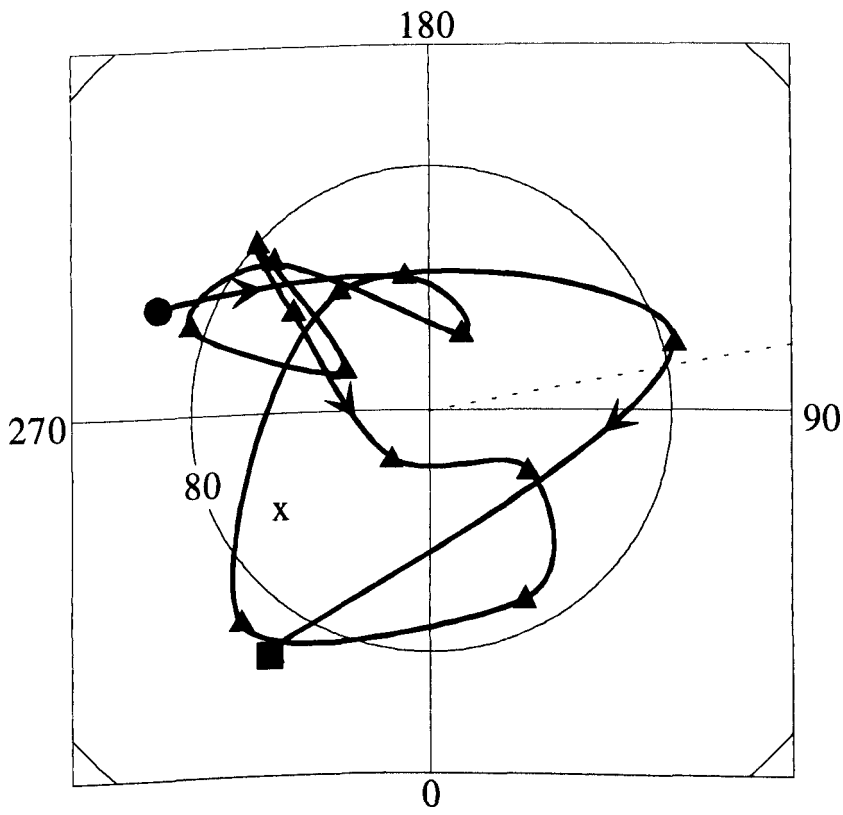

Figure 6.24. VGP progression through time for speleothem PT03. The filled circle represents the start of the PSV record at 7.7±2.5 ka and the filled square shows the position of the VGP at the top of the speleothem at 0.4±1.0 ka. The site longitude is shown by the dotted line and the present day VGP for Xingwen by an 'X'.

6.8. Palaeomagnetism and dating of PT04.

6.8.1. NRM and demagnetisation of PT04.

The central slice of PT04 was cut into 25 central drip-cap sub-samples of 14 cm^3 and labelled 1B to 25B. Lateral sub-samples from the central slice were prepared where the quantity of material either side of the central sub-samples allowed. NRM intensities ranged from 1.7 (2B) to 123.2 x 10^{-8} Am^2/kg^{-1} (25B) with a mean NRM intensity of 32 x 10^{-8} Am^2/kg^{-1}. Only sub-sample 25B had an NRM intensity >100 x 10^{-8} Am^2/kg^{-1}. There was a general increase in sub-sample NRM intensity from top to the base.

Stepwise AF demagnetisation was performed on all central sub-samples in 5 mT steps to 30 mT and subsequently in 10 mT steps up to the maximum applied field. MDFs of sub-samples ranged from 27 mT to 85 mT with a mean value of 68 mT suggesting high coercivity, possibly SD-like, remanence carriers. After application of the maximum available AF around 20% of the original NRM intensity remained. Typical sub-sample behaviours during AF demagnetisation are shown in Figure 6.25. Demagnetisation of some of the weaker sub-samples produced results as indicated by Figure 6.25 a-c. In these cases it appeared likely that a contribution to the signal from magnetometer noise had influenced the vector. Consequently the primary directions of these sub-samples identified from the Zijderveld plots had larger associated MADs. It was not possible to calculate stable primary directions for sub-samples 2B, 3B and 9B. However, the majority of sub-samples exhibited well-defined unidirectional behaviour after the VRM had been removed in fields <30 mT. This VRM took on two forms; a VRM contained within grains with a narrow coercivity band, for example that seen in sub-sample 4B (Figure 6.25d) or a VRM contained in a wider coercivity band, for example sub-sample 12B (Figure 6.25g). In the second form, greater overlap of the primary and viscous (secondary) remanence coercivities caused the vector to take on the direction of primary remanence over a greater number of AF steps and hence the curvature of the vector.

All sub-sample directions were calculated from the Zijderveld projections using the method of Kirshvink (1980). Sub-sample directions had MADs in the range 2.4° (17B) to 9.9° (7B) with a mean MAD of 5.7° indicating a reasonable degree of precision. However, sub-sample 1B had a MAD of 11.2° reflecting the increased contribution from magnetometer noise during demagnetisation.

Thermal demagnetisation results from two lateral sub-samples (11A and 24C) are shown in Figure 6.26. Two types of behaviour could be determined from these data. In the first case, illustrated by Figures 6.26a-c, a small viscous component was unblocked at temperatures less than 150° C after which a unidirectional primary remanence vector persisted before becoming slightly unstable at higher temperatures and weaker NRMs. The intensity plot (Figure 6.26c) showed a monotonic decrease in intensity after removal of the VRM between 100° and 150° C with no alteration apparent. A small break in slope between 550° C and 600° C indicated the unblocking of some magnetite as its T_c was reached. The remaining magnetisation was effectively removed between 650 and 700°C indicating the presence of haematite.

Figures 6.26 d-f shows the second type of thermal demagnetisation behaviour. This particular sub-sample, 24C, was unstable at higher temperatures after what appeared to be inversion of some maghaemite to haematite between 250 and 300°C. The primary remanence vector was identified as trending towards the origin of the Zijderveld plot (Figure 6.26d) and similarly, grouping of VEPs on the stereographic projection showed that a primary remanence had been isolated (Figure 6.26e). It is also possible that sub-sample 24C picked up a spurious TRM from an incompletely nulled field during the demagnetisation process although this does not explain why 11A was not affected as they were heated together.

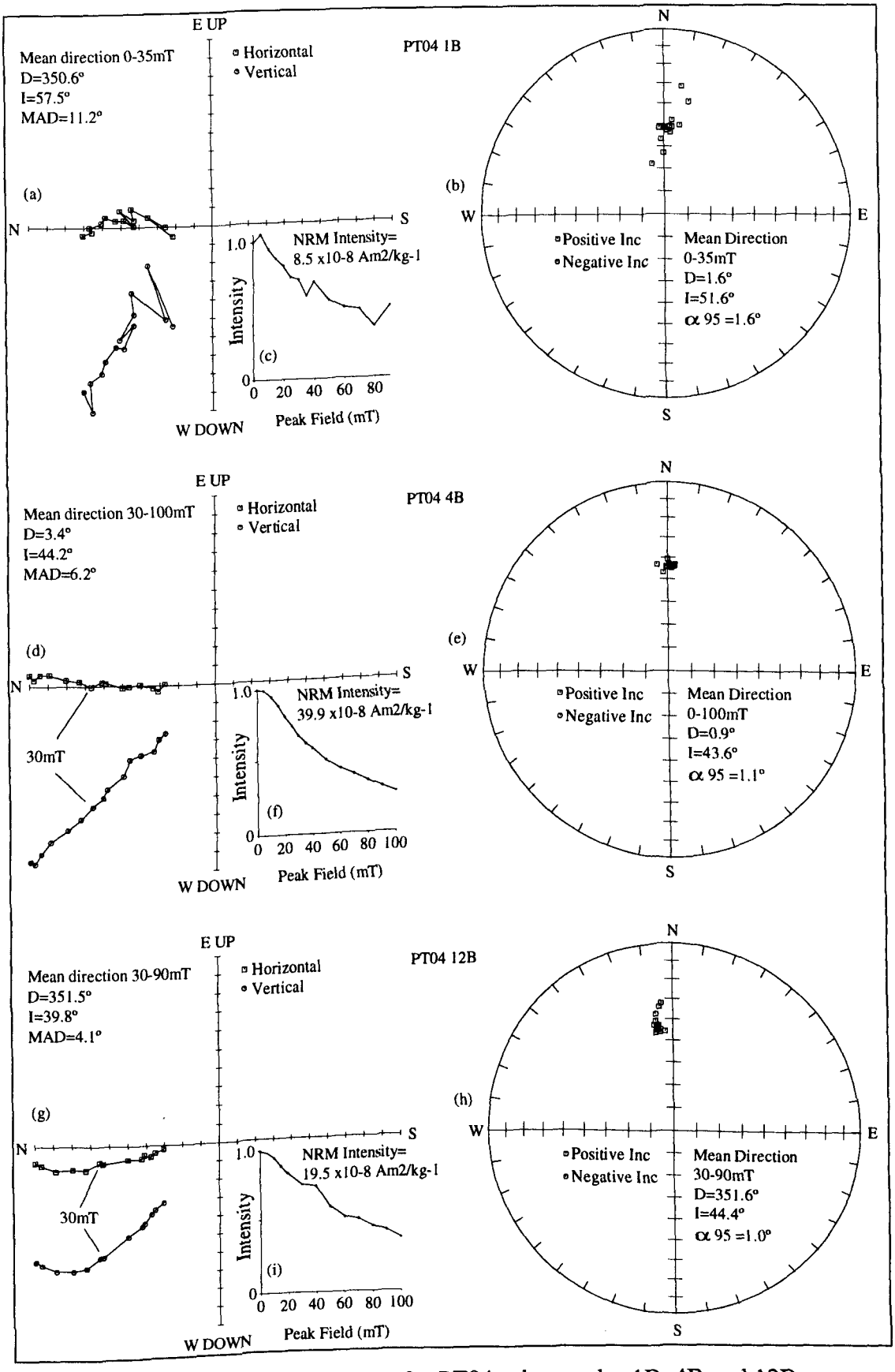

Figure 6.25. AF demagnetisation data for PT04 sub-samples 1B, 4B and 12B.

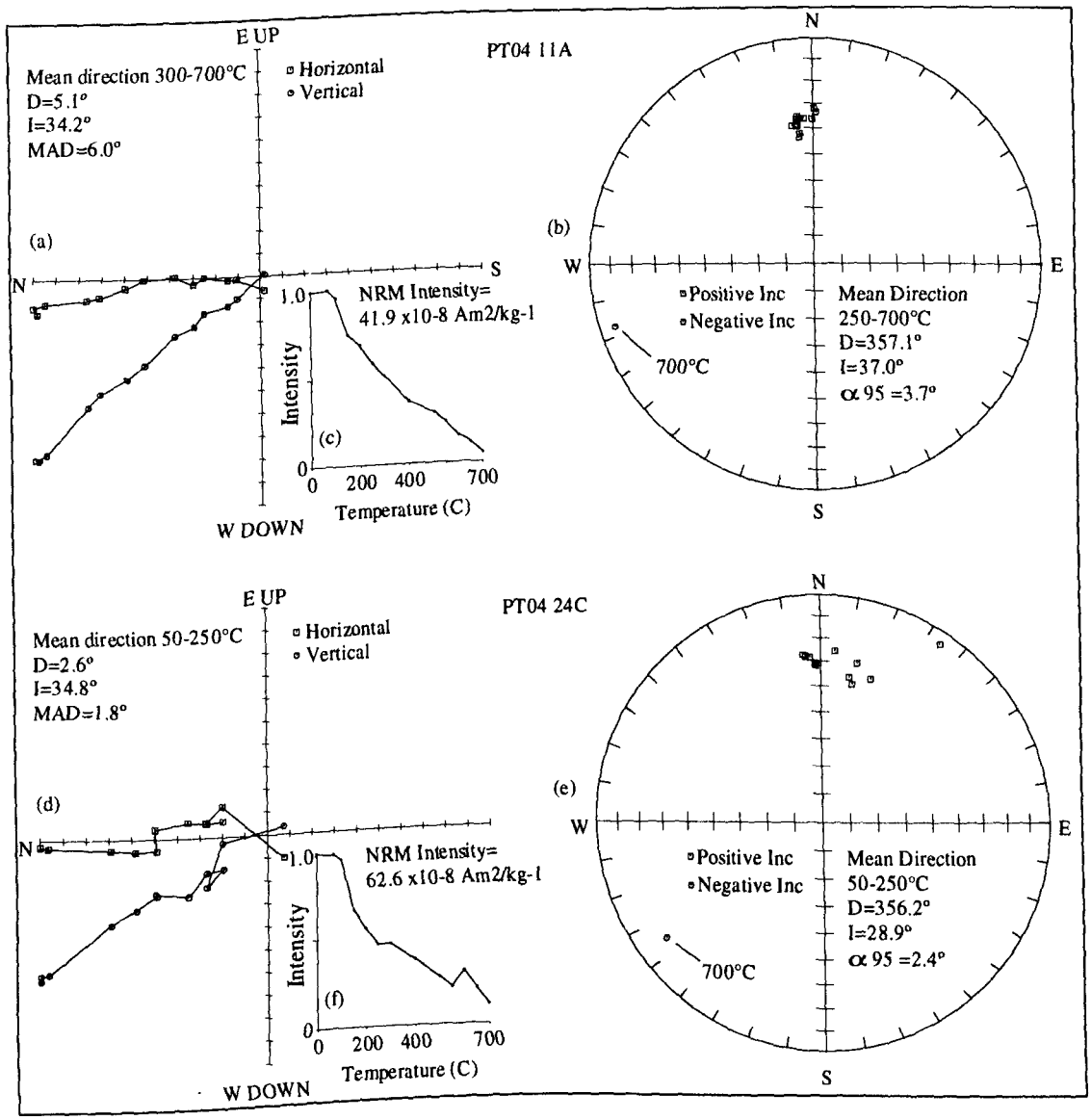

Figure 6.26. Thermal demagnetisation data for PT04 sub-samples 11A and 24C.

Excepting the base of PT04 there was insufficient lateral material from which to perform checks for depositional inclination errors. Lateral sub-samples 23A, 23C and 24A were stepwise AF demagnetised for comparison with their coeval central counterparts 22B and 23B. These sub-samples were chosen as coeval using the growth layers as a guide. Sub-sample 24A was also included in these checks but its directions had been calculated after thermal demagnetisation. Results are shown in Table 6.7.

Sub-sample	Declination (°)	Inclination (°)	MAD (°)
23A	359.2	38.2	3.6
22B	1.6	35.9	2.9
23C	2.8	33.4	1.6
24A	358.3	36.8	2.9
23B	9.1	34.0	2.6
24C*	2.6	34.8	1.8

Table 6.7. Values of declination and inclination after AF demagnetisation for coeval central and lateral sub-samples used for depositional inclination error tests. MAD shows the degree of precision. *Note that sub-sample 24C was thermally demagnetised.

Agreement between the inclinations of central and lateral sub-samples was good and all overlapped at the MAD confidence levels. There was, however, some discrepancy between the declinations of sub-samples 24A, 23B and 24C which did not overlap at the MAD limits. These limited results suggested that there were no systematic depositional errors which would imply that there are no differences between remanence acquisition processes of central and lateral sub-samples. The small discrepancies can be explained by the inclusion of some non-coeval growth layers in each sub-sample.

6.8.2. Uranium-series dating of PT04.

A total of six sub-samples of PT04 were dated using standard uranium-series methodology; a seventh date was obtained from a L/L analysis of two combined sub-samples using the MLE method after Ludwig and Titterington (1994). These data are tabulated in Table 6.8. Concentrations of uranium were low and ranged between

0.18±0.01 (24B) and 0.59±0.02 ppm (1B). Chemical yields were also low as the Hallstadius electroplating method had not be adopted at this time. Uranium yields ranged between 7% and 17% whilst thorium recoveries ranged between 2% and 10%. Detrital thorium contamination was at a high level for most sub-samples and this was reflected by $^{230}Th/^{232}Th$ ratios of 2.44±1.47 to 16.00±34.79. Despite these factors which affected the precision and accuracy of individual dates, all were in chronological sequence and an initial thorium correction value of 1.5 was maintained. Comparisons with features in the other PSV records from Xingwen also suggested that this value was acceptable. The L/L date from combined sub-samples 17B and 18B gave a date of 1.9±1.5 ka which was in chronological sequence with dates obtained using the conventional dating program. This again suggested that the initial correction ratio of 1.5 was a reasonable approximation.

Assuming that the upper surface was modern and that a constant growth rate had continued throughout the growth period, a linear-least squares fit was applied to these data (including the L/L sample) which gave a basal age of 3.6±0.8 ka and an upper surface age of 0 ka (Figure 6.27). During the 3.6 ka growth period of PT04 the growth rate was calculated to be 0.17 mm yr^{-1} with a typical sub-sample representing a time-average of 139 years of PSV. At this level of resolution a complete cycle of drift of the field assuming a drift rate of 0.2° yr^{-1} would be recorded in 13 sub-samples. The greater amount of detail in the PSV record of PT04 reflects the low degree of smoothing in each sub-sample.

6.8.3. The palaeomagnetic record of PT04.

The mean directions obtained from sub-samples of PT04 are plotted with height from base of speleothem and age in Figure 6.28. These data are also tabulated in Appendix E. Mean declinations ranged from 335.8° (13B) to 16.2° (24B) with a mean of 355.8° whilst inclinations ranged from 9.0° (10B) to 57.5° (1B) with a mean of 40.1°. Declination amplitude was of the order ±20° about the mean whilst inclinations had amplitudes of +16.8° to -31.1° about the mean due to some 'outlying' sub-sample directions.

Sub-sample	Concentration U (ppm)	U Yield (%)	Th Yield (%)	$^{234}U/^{238}U$	$^{230}Th/^{234}U$	$^{230}Th/^{232}Th$	Uncorrected age (ka)	Corrected age (ka)
1B	0.59±0.02	14	6	1.38±0.04	0.005±0.003	5.50±9.60	0.6±0.3	0.4±0.5
2B	0.40±0.02	8	3	1.59±0.06	0.010±0.006	2.25±2.13	11.0±0.6	0.4±1.2
9B	0.24±0.07	7	6	1.47±0.07	0.015±0.005	2.44±1.48	1.6±0.5	0.6±1.1
17/18B L/L	-	-	-	-	-	-	-	1.9±1.5
19B	0.29±0.01	9	2	1.43±0.06	0.028±0.001	16.00±34.79	3.1±1.1	2.8±1.7
23B	0.27±0.01	14	6	1.38±0.04	0.033±0.006	9.00±6.95	3.7±0.7	3.1±1.1
24B	0.18±0.01	17	10	1.32±0.04	0.053±0.007	5.85±2.48	5.9±0.8	4.4±1.4

Table 6.8. Uranium-series data for sub-samples of PT04 with resultant uncorrected and corrected ages. Note that the date for sub-samples17/18B is obtained by a maximum-likelihood estimation on L/L derived data(Ludwig and Titterington, 1994). All errors are to one sigma and are based on counting statistics.

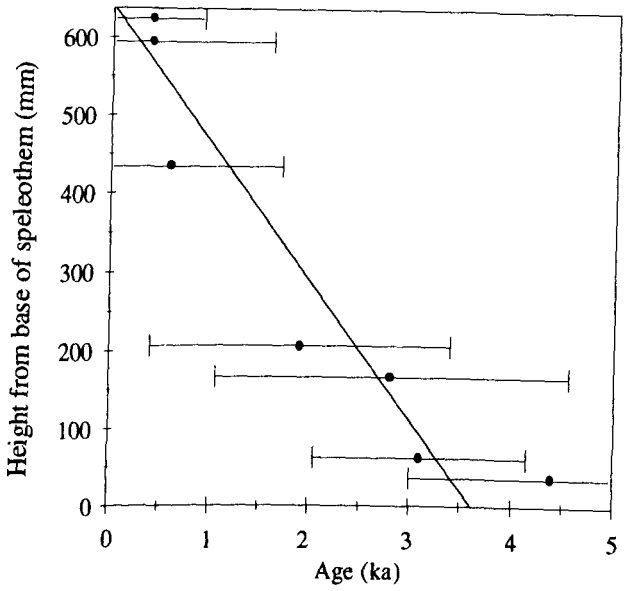

Figure 6.27. Speleothem PT04 uranium-series dates. Errors are to 1σ and are based on counting statistics. The best-fit line is a linear-least squares fit which gave an upper surface age of 0 ka and a basal age of 3.6±0.8 ka.

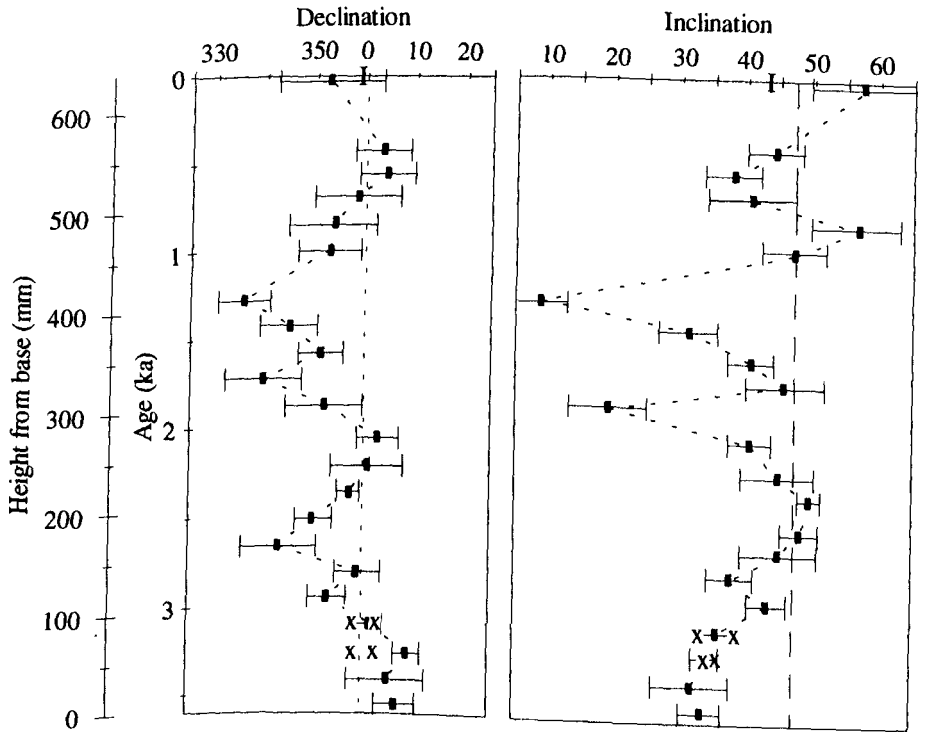

Figure 6.28. Declination and inclination of PT04 sub-samples with time and height from base of stalagmite. Error bars show the MAD value for each sub-sample. Directions calculated from equivalent lateral sub-samples are shown by X with error bars omitted for clarity. The dotted vertical lines represent the GADF for Xingwen and the 'I' symbol shows the present day field values as calculated using the IGRF model.

Declinations and inclinations where subjected to a three-point smoothing filter and were converted to equivalent VGPs in order to show any characteristic behaviour of the VGPs throughout the growth period (Figure 6.29). The VGPs are mainly far-sided and their motion over the growth period of PT04 can be summarised as two successive anti-clockwise loops with a linear return feature from 1.5 to 1.0 ka.

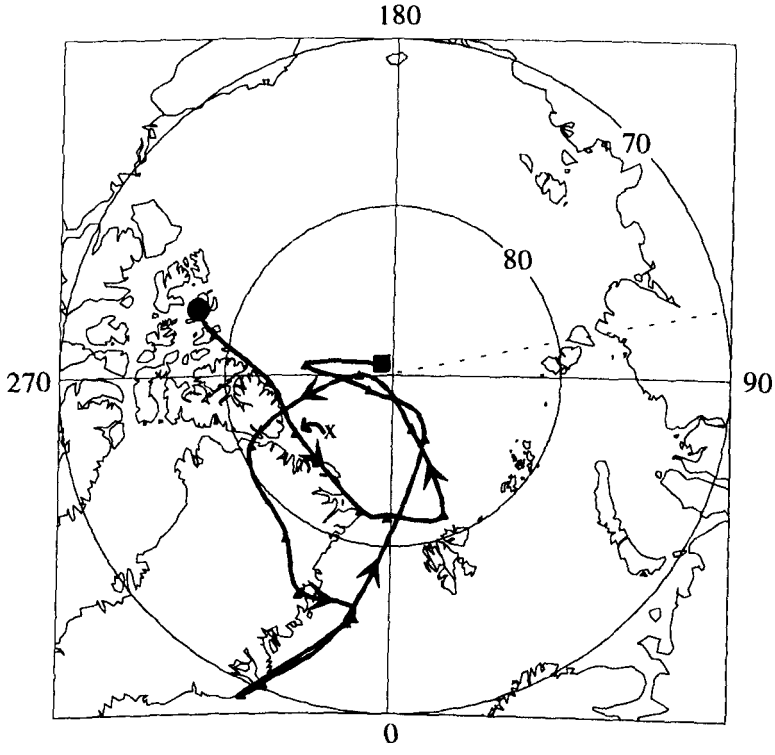

Figure 6.29. VGP progression through time for speleothem PT04. A 3-point smoothing filter has been applied to these data. The circle represents the start of the record at 3.5±1.5 ka and the square shows the end at 0.3±0.5 ka. The site longitude is shown by the dotted line and the present VGP for Xingwen is shown by '**X**'.

As the upper surface of PT04 was modern the recorded field values should lie close to the expected present day values if the speleothem has recorded the field instantaneously (Latham *et al*, 1986). From Figure 6.28 and Figure 6.29 we see that this is not the case. Declination lies within the MAD limits of the present day field but the inclination is much steeper (57.5°). The MAD value of 1B was high (11.2°) which indicates a direction with a low degree of precision which could explain this discrepancy.

6.9. Comparisons between the individual records from Xingwen.

6.9.1. Discordance in contemporaneous palaeosecular variation data.

There are several potential explanations for the differences in the recorded PSV signals between records from the same site. These may act singly or in combination:

1.) The same declination or inclination feature appears at different times in different speleothem records due to overall **dating inaccuracy**.

2.) Inability for dating to pick up subtle **changes in growth rate within a single record** leading to extension / compression of segments of each record. With little other evidence available, growth rate has always assumed to be constant in this study although this is not necessarily true as shown by the dating of SSJ2 (section 4.9.1).

3.) Differences in the growth rate of each speleothem leading to **variable resolution** and hence recording of different period PSV. Table 6.9 shows the resolution of sub-samples from each speleothem.

Speleothem	n	Mean declination (°)	Mean inclination (°)	$\propto_{95}$	Resolution (yrs)	Top age (ka)	Basal age (ka)
SC01	26	354.2	39.4	2.2	335	0.0	8.4±1.2
SC02	23	354.5	48.2	2.9	404	0.1±0.1	9.2±0.5
PT02	36	350.8	43.9	4.1	58	0.0	2.5±0.6
PT03	15	1.7	43.4	4.1	517	0.4±1.0	7.7±2.5
PT04	22	355.8	40.1	5.0	138	0.0	3.6±1.5

Table 6.9. Mean declination and inclination, $\propto_{95}$, sub-sample resolution and age range for the Xingwen speleothems.

In general, a sub-sample of 400 years resolution, for example, will not adequately resolve PSV with cyclical periods of less than about 1.6 ka (assuming a drift rate of

around 0.2° yr^{-1}). This resolution is made significantly worse if the drift rate is increased to, say, 0.3° yr^{-1} i.e. 3 samples per cycle. However, drift rates based on modern studies (Aitken *et al*, 1989; Hyodo *et al*, 1993) suggest a mean non-dipole field drift rate of between 0.1 to 0.2° yr^{-1}. Thus, samples that average PSV over 400 year intervals are just about adequate for obtaining details on at least the longer period features of PSV.

Problems 1 to 3 above, will be present in combination in all PSV records that have originated from a single site. When making comparisons with PSV in records from different sites, in different mediums and that have been dated using alternative techniques, the interpretation of individual records can become unavoidably complex.

6.9.2. Comparison of declination and inclination from individual records.

Bearing in mind the statements outlined in section 6.9.1, comparisons between records can be made. Figure 6.30 shows the variation of declination and inclination with time for each speleothem with the prominent features in declination marked 'a' to 'h' and in inclination 'i' to 'x'. Considering the dating uncertainties associated with each record the agreement between records is good suggesting that consistency exists in the recording of the local geomagnetic field and that each record represents a continuous record of PSV. The majority of features show slight differences in the timing of their appearances from one record to another. These differences are partly due to dating imprecision and the inability to pick out small growth rate changes, and also due to the differing rates of growth resolving PSV to a greater or lesser extent.

The amplitudes of declination and inclination changes appear to reflect the sub-sample resolution in each record (Table 6.9). For example, the highest resolution records, PT02 and PT04, exhibit the highest amplitudinal variation, of the order ±30° in declination and ±25° in inclination. This reflects the lesser degree of smoothing and the recording of shorter period PSV in their sub-samples which cover 58 and 139 years of field change respectively. Features 'iii' and 'iv', are only identified in the records of PT02 and PT04, and may represent this shorter period PSV.

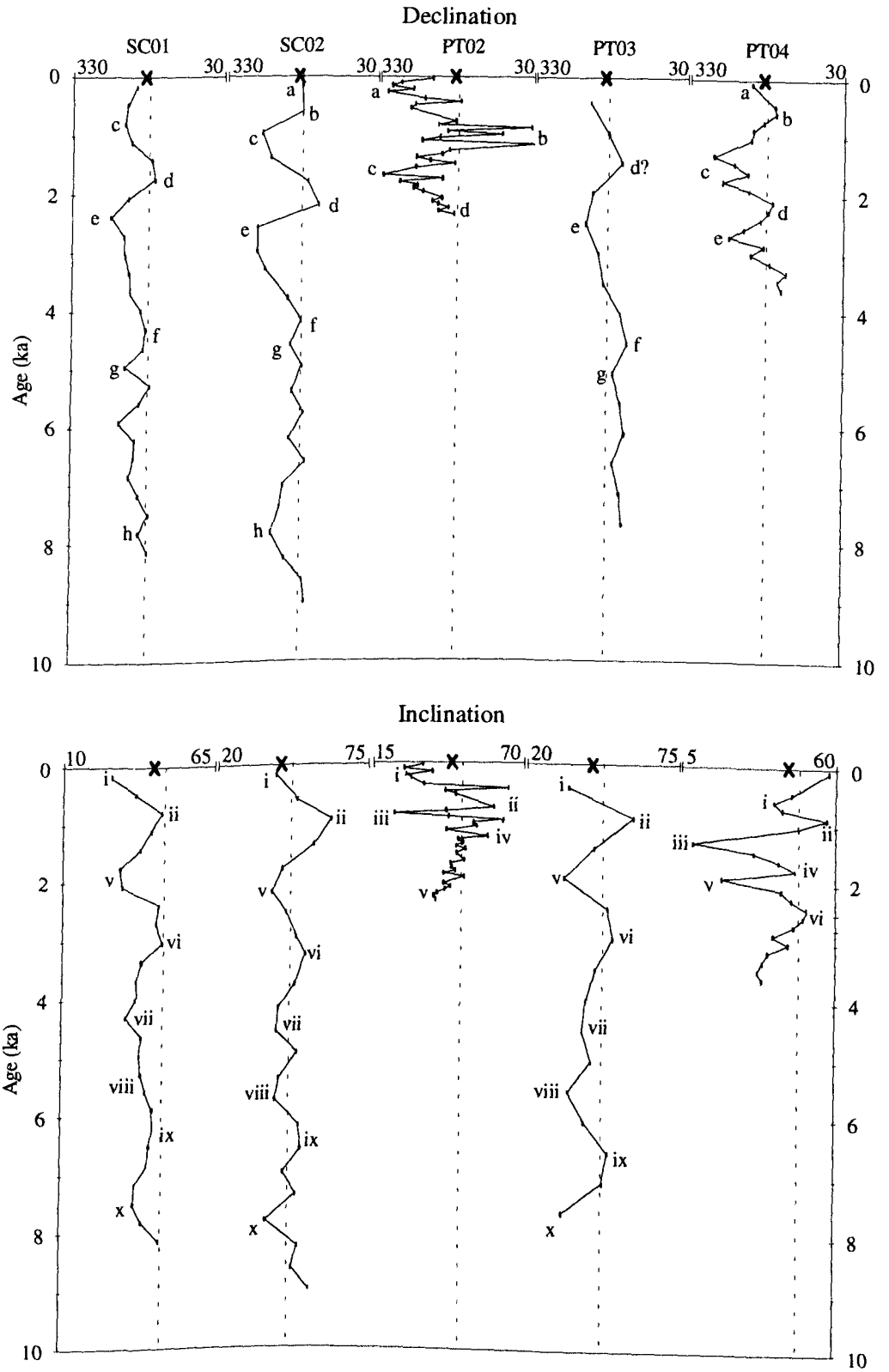

Figure 6.30. Comparison of declination (top) and inclination (bottom) data for each speleothem from Xingwen. The GADF is shown by the dotted line and the position of the present-day field by an 'X' recorded in the Xingwen speleothems. The dotted vertical lines represent the GADF position.

Conversely, in the record of PT03, whose sub-samples record an average of 517 years of PSV, a reduction in amplitude is noted, particularly in declination. In this speleothem, it is likely that only a general trend of PSV has been recorded as the effect of time-averaging would only partially resolve the shorter term features of PSV. The records of SC01 and SC02 are of intermediate resolution, their sub-samples resolving PSV over periods of 335 and 400 years respectively. The records of declination and inclination in SC01 and SC02 appear subdued before about 5.0 ka with amplitudinal changes in both declination and inclination reduced to ±15° about their means.

If the geomagnetic field at Xingwen was averaged to that of a geocentric axial dipole field over the period of our records, we would expect mean declinations to be zero and mean inclinations to be 47°. Calculation of the mean declination and inclination for each speleothem using Fisher statistics (Fisher, 1953) shows that all records have declinations with westerly bias, except PT03, and inclinations that are shallow with the exception of SC02 (Table 6.9). The maximum declination bias is 9° to the west in PT02 and the maximum deviance of inclination from the GADF value is -9° in SC01. As all records are shorter than the 10^4 ka normally taken as the period required to average out PSV to the GADF (Merrill and McElhinny, 1983) it is possible that these recorded declination and inclination offsets represent true field behaviour. However, some inconsistency is seen in the degree of these offsets. For example, the mean declination of PT03 overlaps the GADF direction at the 95% confidence level whilst its inclination is shallow. In contrast, the mean declination of SC02 is biased to the west, outside of the 95% confidence level, whilst its mean inclination straddles the expected inclination of the GADF.

Therefore, it is not possible to be certain whether these offsets represent undetected orientation and cutting errors imposed during sampling and sample preparation (Chapter 5) or a real long-term field bias. The potential reasons for these offsets are now discussed.

6.9.2.1. Sample orientation and preparation errors.

During sampling and sample preparation it is possible for orientation errors to be introduced by several means. The first is during the initial orientation of the sample in the cave by ill-positioning of the orientation frame, misreading of the compass and misreading / marking of the 3-arm U-tube. However, at least two readings of the compass were made using two sets of marks on the speleothem thus any error should be averaged out, unless the compass was permanently biased. [The compass was subsequently checked against a second compass and found to give the same reading ±1°] Likewise, when difficulty was encountered in reading the meniscus levels in the U-tube each arm was moved around and a second set of marks made. Thus, errors in orientation in the cave are likely to be random and should have averaged out.

The second area where orientation errors could be imposed was during casting of each speleothem in plaster prior to sectioning. It is possible that the azimuthal markings were poorly aligned and that vertical re-orientation was incorrect. This should also be a random error and again should have averaged out. When speleothems were cast in several sections there were thought to be no orientation errors because each section could be exactly repositioned on its lower section (Chapter 5).

The most likely area where errors were introduced was in the sectioning of each speleothem after casting in plaster. Sectioning consisted of two operations; cutting of a central vertical slice using a large diameter rock saw and sub-sampling of the central slice using a smaller rock saw. For cutting of the central section, cutting lines were marked on the plaster block using the side of the block parallel with the azimuthal orientation as a guide (Figure 5.3). However, when cutting it was frequently found that the vice on the large rock saw would allow the plaster block to slip. This resulted in central slices that were offset by up to 5°. In order to compensate, the degree of offset was measured. The offset equalled the difference between the cutting lines and the actual cut. Measuring the vertical and horizontal offsets, even with instruments, was likely to be prone to some degree of error due to the difficulty of alignment on the rough plaster surface and due to

the thickness of the cutting line and actual cut. The measured offset was taken into account automatically whilst measuring on the magnetometer.

Sub-sampling of the central vertical slice was not thought to add to any measurement errors. After marking out each sub-sample, the plaster, which was still attached to the central slice, was used to align each marked sub-sample with the cutting blade. Because the plaster represented orientation in the casting box there were no orientation differences. When measuring on the magnetometer, a sub-sample was aligned in the sample-holder on a face that was cut using the large diameter rock saw. Thus, no additional errors were likely to have been introduced during the sub-sampling stage.

Sub-sample miss-positioning in the magnetometer sample-holder was, for a typical sub-sample, ±1° (estimated by inserting a feeler gauge in the gap at the side of a sub-sample and measuring the maximum 'play' in degrees). This error will be random and will, over the large number of measurements required for stepwise demagnetisation, be averaged out.

In summary, if we assume sampling and preparation errors alone, the most likely reason for the differences between the Fisher mean (Fisher, 1953) directions and the GADF directions was the sectioning procedure used on the large diameter rock saw. Using the maximum offset of mean directions from the GADF it is possible to estimate the maximum degree of cutting error. From Table 6.9 the maximum in declination error would be 9.2° (PT02) and in inclination would be 8° (SC01). These sources of error above could explain some of the discrepancies between the mean directions and the GADF but do not explain why the declination offset appears to be mainly westward and the inclinations are generally shallower.

6.9.2.2. Effects from long-term bias of the local geomagnetic field.

The question remains as to what could the presence of the Mongolian anomaly have on local field directions over the period of the Xingwen PSV records? Could this be

an additional factor in accounting for the directional offsets? As pointed out in section 6.9.2. these offsets are a little inconsistent from record to record but the potential for local field influences requires discussion.

The Mongolian anomaly is an intense positive anomaly of the vertical component of the non-dipole field centred on 40°N 108°E over the Asian continent (Ren, 1980). In the last three centuries observatory measurements have shown that its intensity has increased threefold whilst its latitude and longitude have barely changed. Yukutake and Tachinaka (1969) concluded that the non-dipole field could be divided into standing and drifting components. They suggested that this division would account for some of the variations in the non-dipole field drift rate. In their early work they analysed the Gauss-Schmidt coefficients to approximate the Earth's standing and drifting non-dipole fields back into the 17th century. They concluded that a stationary source, such as the Mongolian anomaly, and passing drifting sources could account for the more complicated features of PSV. In a later paper (Yukutake, 1993) this relationship was refined using Japanese declination variations. It was shown that declinations biased to the east during the 16th century by a non-dipole anomaly to the east of Japan, swung to the west as this drifting feature moved to the west, passed Japan and migrated through the region of the standing non-dipole focus of the Mongolian anomaly during the 19th century. Field behaviour of this style has also been confirmed by Bloxham *et al* (1989). These observations are made over too short a period of time to say with any confidence that this is the cause of westerly declination bias and shallow inclinations throughout the Xingwen records. However, processes similar to these may have applied over longer periods of time.

It would also be instructive to assess what the effects would be from the Mongolian anomaly alone if the drifting non-dipole field is ignored. The Mongolian anomaly is presently located is some 12° latitudinally north and 3° to the east of Xingwen (Ren, 1980). According to work compiled by Yukutake (1993), a site to the west of a stationary positive anomaly should have easterly biased declinations. Inclinations would be a maximum (+ve) in the anomaly's centre but the effect would also be to steepen recorded inclinations away from the focus. Observatory data on the magnitude and

position of the Mongolian anomaly is only available for the past 400 years (Yukutake, 1993). However, if we consider that over the period of the Xingwen records the Mongolian anomaly has changed in form and magnitude it is possible to suggest that it has been more often than not to the west of Xingwen. This could help to explain the mainly westerly declinations but does not explain the shallow inclinations. Gubbins and Kelly (1993) by modelling the radial dipole components of the field found that the Mongolian anomaly may have been present 'in some form' during the past 2.5 Ma.

To conclude, the small directional bias in the PSV records could be caused by sampling induced errors or by one, or more, geomagnetic field anomalies. However, considering the causes discussed above, it seems that sampling and orientation errors are the most likely candidates. However, the shallow inclinations are not thought to have arisen from post-depositional effects. The results from previous work (Lean *et al*, 1995; Perkins, 1993; Latham *et al*, 1986) and results from this study suggest that speleothems are not subject to depositional effects. It would be more satisfactory if it were possible to confirm or dismiss these offsets by further sampling in this region. Until it is possible to determine with greater probability which process is responsible for the biases, the directions of each speleothem have been normalised about the GADF as an interim measure for the purposes of comparison with other records. In the near future it may be possible to collect some further speleothems from the Peoples Democratic Republic of Laos, located 17°45'N 104°50'E; directly south of Xingwen. Interesting comparisons may be possible as this site may be close enough record the same features of PSV as in Xingwen but sufficiently far away to have been influenced differently by the Mongolian anomaly.

6.10. Comparisons with alternative contemporaneous records.

Speleothem records that could offer the most direct comparisons with this study are those from Japan (Morinaga *et al*, 1989 and 1986) and South China (Liu *et al*, 1990). Unfortunately no absolute dating was performed on these speleothems providing little basis for comparison. Alternative records available for comparison are a

sedimentary record from the Yellow River mouth, China (37.8°N 119.43°E) by Cong and Wei (1989); archaeomagnetic results from China (Wei *et al*, 1983); SVJ2, a deconvoluted lake and marine sediment composite record from Japan (35.8°N 136.3°E) by Hyodo *et al*, (1993) and the compiled archaeomagnetic data of Hirooka (1983) from south-west Japan (34°N 136°E). These contemporaneous records are compared to our speleothem records in Figures 6.31a and b. In making comparisons we have omitted the record of PT03 since its low resolution makes it unable to resolve PSV with a frequency less than 1.0 ka and in this study we are more concerned with higher frequency PSV.

For the purposes of comparison the records SC01 and SC02 were normalised to the GADF for Xingwen, stacked, and values of declination and inclination were taken from a cubic spline which fitted the data best with knots at 50 year intervals. This was possible because of the similar resolution in each of these records. These values were then nine-point smoothed to time-average the values over a period of 200 years which was close to the overlap period of the stacked records. The remaining records of PT02 and PT04 were normalised about the GADF.

The main features of declination and inclination in Figures 6.31a and b have been labelled using the notation of Figure 6.30. For declination the most striking resemblance's are in the characteristic variations labelled 'c' to 'g' (4.2 to 1.1 ka) and in the timing of feature 'a' seen in the records covering the most recent times. The declination feature labelled 'b' is also seen in the records but suffers from larger age-lags of up to 0.7 ka across the records. Comparisons of inclinations also shows reasonable agreement. The inclination variations labelled by 'ii' to 'vii' are seen in all records although they too suffer from age lags. The Yellow River record shows the greatest amplitudinal variation of ±40° in both declination and inclination, perhaps a result of the depositional or sampling induced errors associated with sedimentary records. The record of Japanese sediments (Hyodo *et al*, 1993) also appears subdued especially in inclination possibly for the same reason. However, this record has also been mathematically deconvoluted which may have, in this case, reduced the amplitudinal variation of recorded PSV. Compared over the same period as the Japanese arachaeomagnetic data (Hirooka, 1983) this Japanese sedimentary record also appears more subdued. Over the

period 8.5 to 5.0 ka the subdued nature of our SC composite record makes correlation of declination and inclination with the Japanese sedimentary record difficult. For this reason we can only infer tentative correlation of declination feature 'h' and inclination features 'vii' to 'x'.

The lags in the appearance of equivalent features could be explained by a combination of the following; inexact dating associated with each record, the assumption of a constant rate of growth or accumulation introducing stretching and compression of records and post-depositional effects in the sedimentary records. It should also be noted that the longitudinal separation between the sites in China and Japan of between 15° and 35° may contribute to lags in the appearance of features if we consider the effects of drifting non-dipole sources and their changing geometry over time.

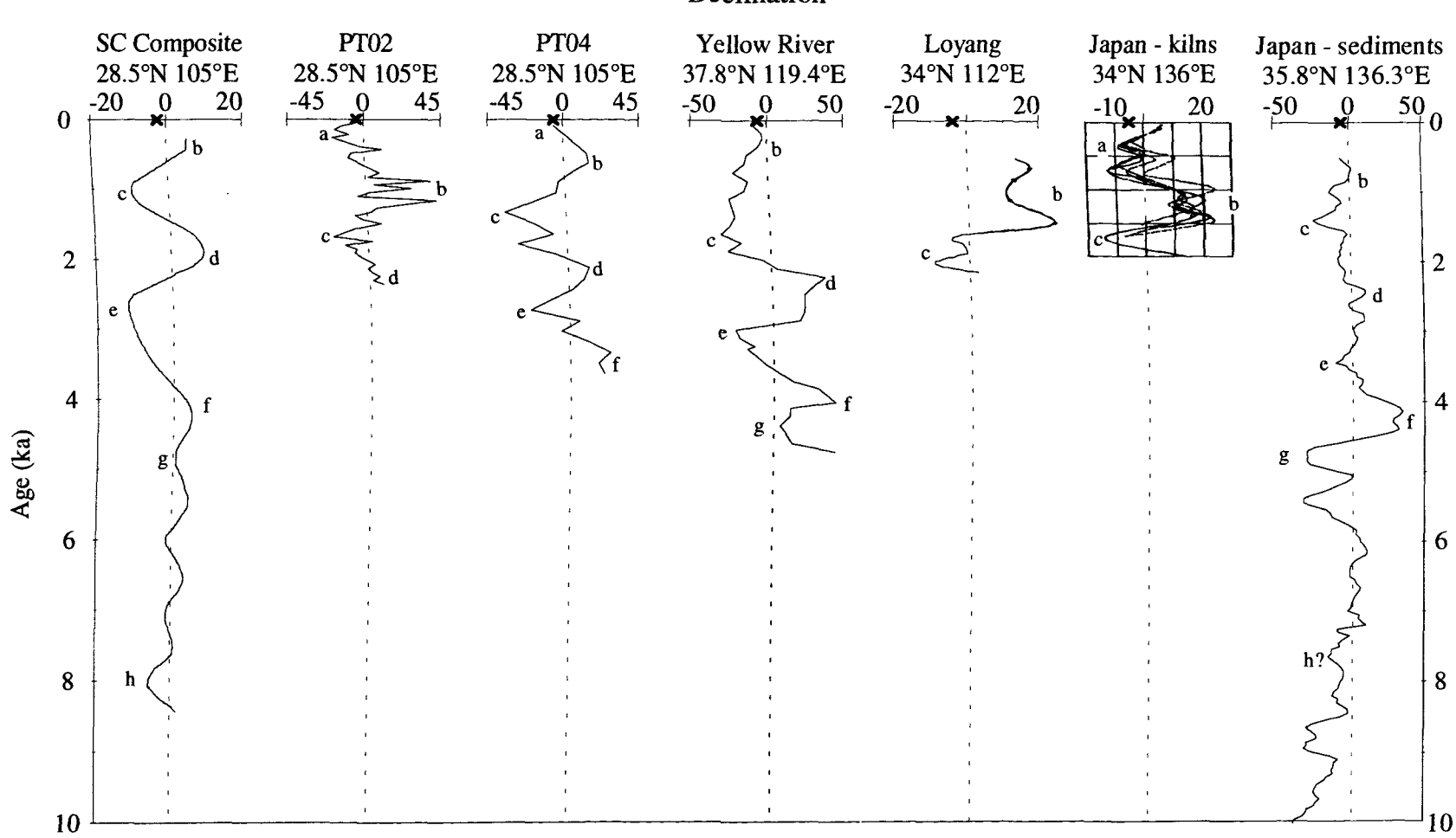

Figure 6.31a. Comparisons of the Xingwen declinations with those from China and Japan. From left to right; SC composite record; PT02; PT04; Yellow River sediments; archaeomagnetic data from Loyang, China; archaeomagnetic data from S.W.Japan; sedimentary data from Japan. The present day field at each site is shown by 'X' and the GADF by the dotted vertical line.

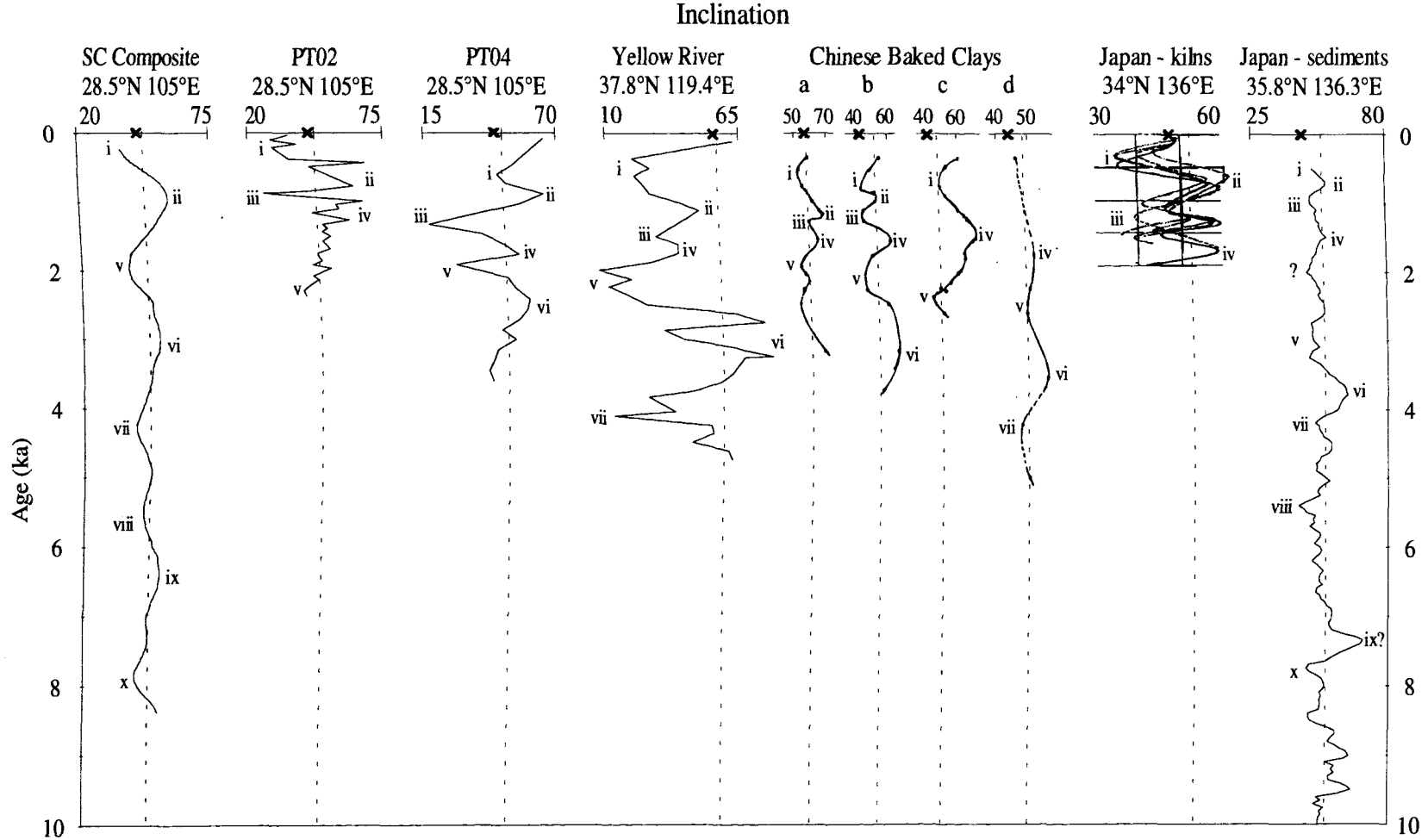

Figure 6.31b. Comparisons of the Xingwen speleothem inclinations with those from contemporaneous records from China and Japan. From left to right; SC composite curve; PT02; PT04; Yellow River sediments; Chinese archaeomagnetic data from a) Beijing b) Shanxi c) Henan d) Hubei provinces; Japanese archaeomagnetic data; a composite sedimentary record from Japan. References for these data are indicated in the text. The modern field at each site is shown by 'X' and the GADF by the dotted vertical line.

7. Palaeosecular variation records and dating of speleothems from Matienzo, Cantabria, Spain.

This chapter describes the palaeomagnetic and uranium-series data from four Spanish speleothems collected during this study. A short introduction to the geology and geomorphology of the Matienzo area and its caves precedes a field description of each speleothem. The demagnetisation behaviour and uranium-series dating are discussed when possible, even though the weak magnetisation of many sub-samples made for poor records of PSV.

7.1. The caves and karst of Matienzo.

Matienzo (43.2°N 3.4°E) lies 25 km to the south-east of Santander (Figure 7.1). The enclosed depression is formed in pure Cretaceous limestones with a maximum thickness of 600m in the surrounding mountains. Generally, the limestones are thinly bedded (~1m) with some massive bedding in the Urgonian facies. Occasionally, thin sandstone and marl horizons break up the succession. Underlying the limestones are marls which are exposed in parts of the depression floor where the hinge of an east to west trending anticline is intersected. These marls provide an impermeable layer forcing surface drainage to flow across the depression floor to the main sink at approximately 150 m a.s.l. The main resurgence from the depression is in the Secadura valley 3.5 km to the north-east and 100 m below the main sink (Waltham, 1981).

The depression itself was not subject to full glacial conditions during the Pleistocene and the limit of glacial advance is marked by terminal moraines in the head of the Ason valley 15 km to the south. The absence of limestone pavement also shows the lack of glacial action but limestone rubble indicates that periglacial conditions were in existence. This limestone rubble is covered with a thin regolith which supports a sparse vegetation on the mountain sides. Fertile soils are found only in the valley floor and originate from flooding of the valley during the wetter months (Waltham, 1981).

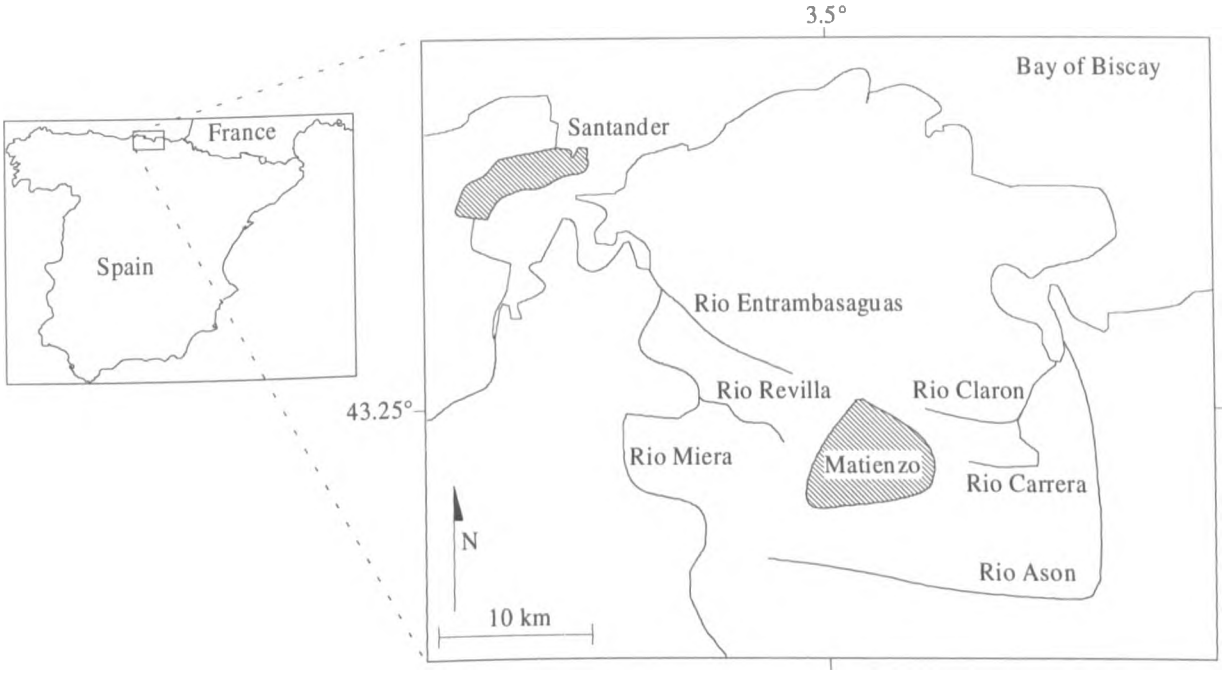

Figure 7.1. Sketch map showing the location of the Matienzo depression and its surrounds.

The cave systems in Matienzo are represented by both active and abandoned development levels. Many old fossil levels occur at 400 m a.s.l. with a second concentration of fossil levels at the 200 m a.s.l. level. These older segments of passage are often linked to the active development levels by deep shafts which intersect lower levels of passage development. These lowest development levels carry drainage waters just below the valley floor in vadose systems. However, in some notable exceptions large phreatic passages have formed deep beneath the valley floor on or around the level of the former water table. The Torca Regaton section of the Sistema de Cubija is an example of this type of development.

Eight speleothems were collected from numerous caves in the depression. The weak nature of the NRMs in the first four speleothems did not warrant further work on the remaining speleothems. Speleothems providing data in this study consisted of two stalagmites from Cueva del Agua, one of the major valley floor conduits and two stalagmites from the Torca Regaton part of the Sistema de Cubija.

7.2. Speleothems from Cueva del Agua.

Two of the stalagmites (AG02 and AG03) collected from the streamway of Cueva del Agua were analysed. Figure 7.2 shows the original locations of these samples.

7.2.1. AG02 location and external/internal appearance.

AG02 was a 408 mm stalagmite taken from the east side of the streamway 0.5 m above the current water levels. AG02 had a width of 55 mm throughout its height and it was one of a group of four stalagmites all of which appeared to be actively growing as indicated by a wet surface. A regular drip of water was observed falling onto AG02 and there was also considerable spray from the nearby streamway which may also have served to wet the speleothem surface. The upper surface appeared fresh suggesting that the drip was sufficient to wash it clean of most surface detritus. The outer surface was covered by 3 mm layer of mud which had to be scraped off to make orientation marks.

AG02 was cast in two sections in the laboratory and one vertical slice was obtained from its centre using a large diameter rock-saw. Internally, AG02 showed no evidence of hiatuses that would indicate growth stoppage. Growth layers were well defined as either cream or dark grey layers.

7.2.2. AG03 location and external/internal appearance.

AG03 was a 678 mm stalagmite obtained from an alcove on the west side of the Agua streamway 0.25 m above the present water levels. There was no drip onto the upper surface but the top appeared fresh. The stalagmite was a constant 60 mm diameter excepting the topmost 100 mm which tapered towards the upper surface.

AG03 was cast in three sections in the laboratory and one vertical slice was cut from its centre. Measurable cutting errors, estimated using the original cut lines, were of

the order ±2° and were corrected during measurement on the magnetometer. The effects of these cutting errors are discussed in section 6.9.2.1. Prominent growth layering was visible in the central slice; this was highlighted by dark brown and cream colouration. These dark brown layers are thought to represent the inclusion of detrital material in to the calcite matrix as calcite precipitation resumed after flooding.

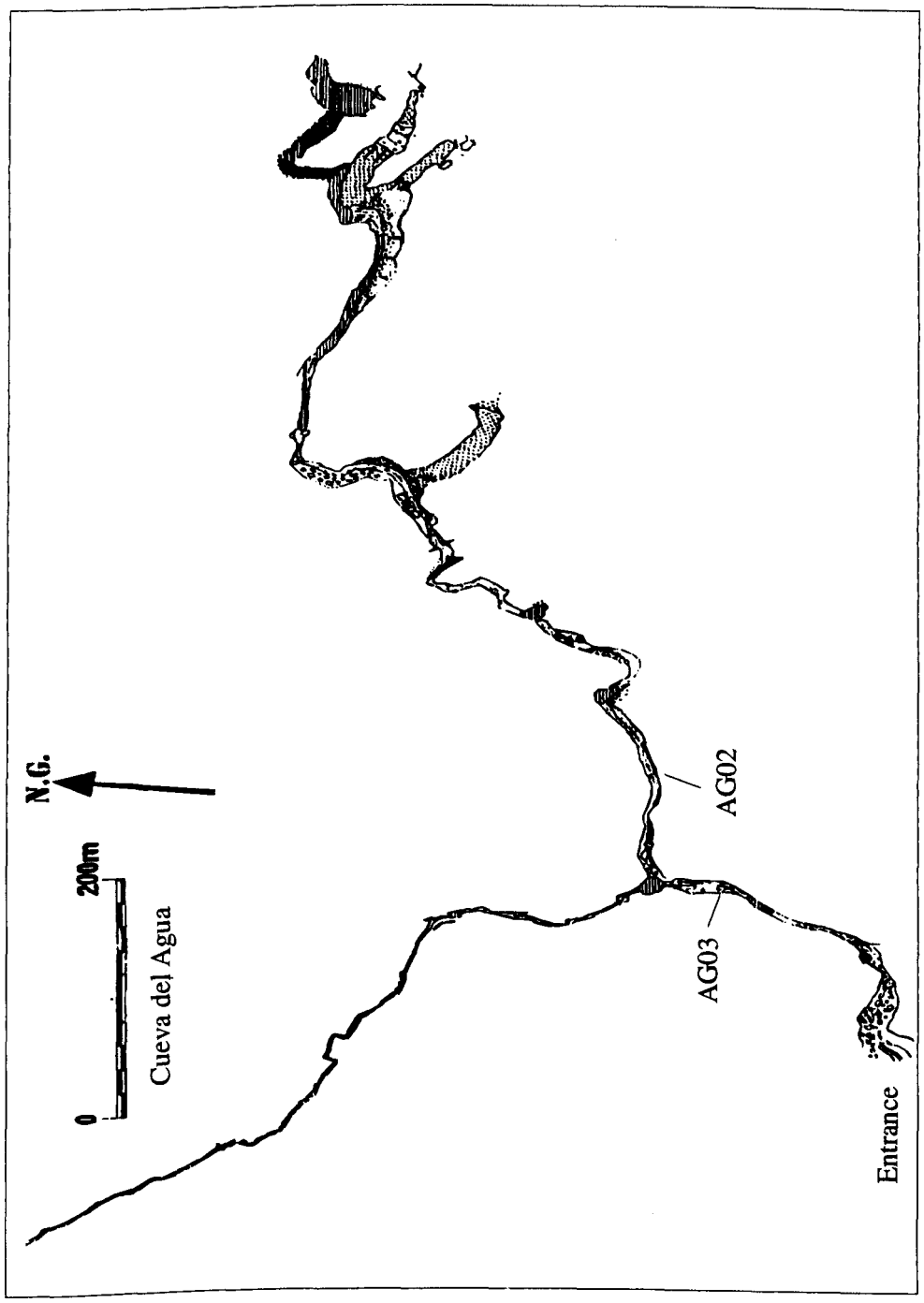

Figure 7.2. Survey of Cueva del Agua, Matienzo, showing locations of speleothems AG02 and AG02.

7.3. Speleothems from Sistema de Cubija.

Two stalagmites (TR01 and TR02) collected from Sistema de Cubija were subjected to palaeomagnetic and U-series analysis (Figure 7.3).

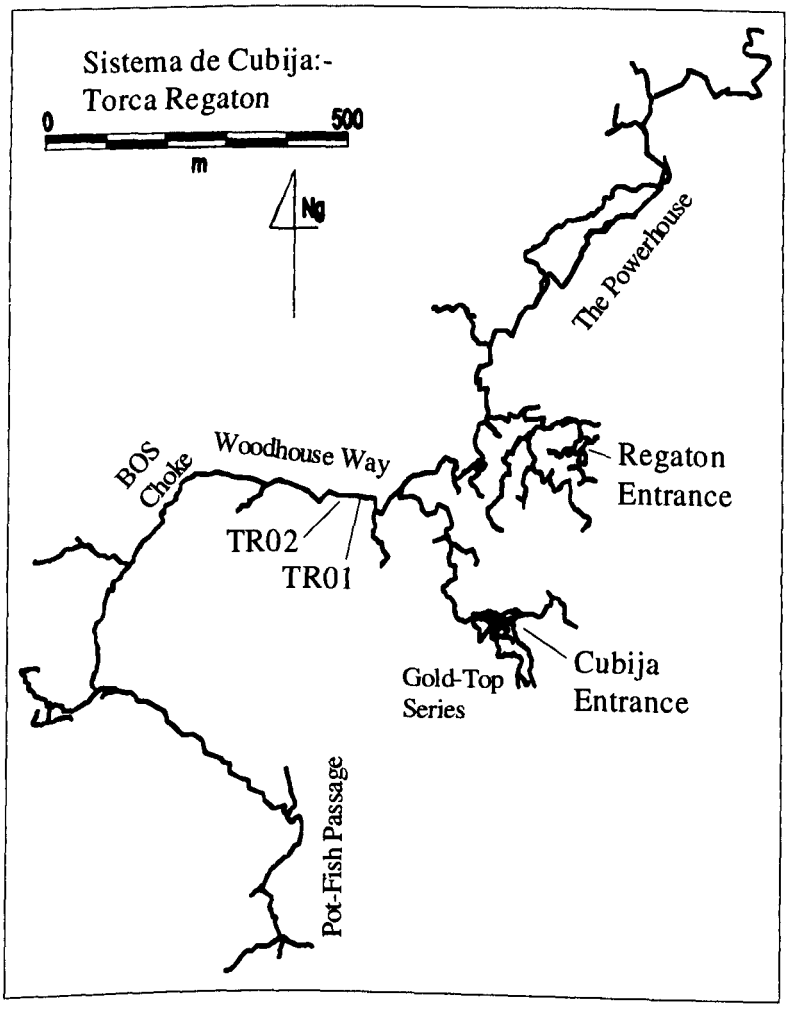

Figure 7.3. Survey of Torca Regaton, part of the Sistema de Cubija, showing the location of speleothems TR01 and TR02. Copyright Matienzo Caving Expedition, 1995.

7.3.1. TR01 location and external/internal appearance.

TR01 was a 510 mm stalagmite collected from a sloping ledge 300 mm above the streamway of the Torca Regaton section of Sistema de Cubija (Figure 7.3). The upper surface of TR01 appeared fresh but no drip was observed for the period prior to

sampling. The outer surface of the stalagmite was covered with a thin layer of mud (<1 mm) from the preceding winters floods. TR01 was a constant 50 mm in diameter throughout it height with slight tapering towards the upper surface.

In the laboratory TR01 was cast in plaster of Paris in three sections and one central vertical slice was obtained using a large diameter rock saw. The cutting lines were followed accurately; thus it was estimated that there were no cutting errors. Internally, the growth layers colour ranged from dark tan/tan to cream presumably reflecting detrital contamination from flooding during growth. Each layer was approximately 0.25 mm thick (estimated using a hand lens). There was no evidence for any growth stoppage, as would be indicated by the lack of growth layer hiatuses; these growth layers were evenly distributed throughout TR01.

7.3.2. TR02 Location and external/internal appearance.

The second stalagmite taken from Sistema de Cubija was TR02 which was 600 mm in height. It was taken from a flowstone plinth in the centre of the streamway 10 m downstream of TR01 (Figure 7.3). It was one of a group of four stalagmites and appeared to have a fresh upper surface. No mud coated the outside of TR02 but during flooding it would have been submerged as indicated by flood debris in the roof 2 m above. During flooding a fast water flow may have prevented the accumulation of mud on the stalagmite sides. The base of TR02 was 110 to 130 mm in width up to 300 mm from its base. The stalagmite then rapidly narrowed to 70 - 80 mm in width and remained within this range up to the upper surface. Despite one of the criteria for the selection of suitable speleothems being a relatively constant diameter, it was decided to collect it anyway. A neighbouring stalagmite had joined with the basal section of TR02 and this was thought to be the main influence for the widening of this section rather than a separate period of growth.

Casting of TR02 was performed in three sections and one central vertical slice was cut using the large diameter rock saw. Internally TR02 was a dark tan/tan to cream

colour which highlighted the 1 mm scale growth layering. The change in width at 300 to 325 mm from the base was clearly highlighted by the growth layers. As expected the drip cap decreased in width from 55 mm to approximately 25 mm over this same interval. Throughout the period of narrowing no growth hiatuses were observed indicating that the growth rate was likely to have remained constant.

7.4. Palaeomagnetism and dating of AG02.

7.4.1. NRM and demagnetisation of AG02.

The central vertical slice from AG02 was sufficient for the preparation of 32 7 cm^3 sub-samples and these were labelled 1B to 32B. However, sub-sample 20B was destroyed during the cutting process. The NRM intensities were low and in the range 10.0 x 10^{-8} Am^2/kg^{-1} (7B) to 314.6 x 10^{-8} Am^2/kg^{-1} (13B) with most intensities less than 30 x 10^{-8} Am^2/kg^{-1}. Only sub-samples 11B, 13B, 28B and 30B had NRM intensities greater than 100 x 10^{-8} Am^2/kg^{-1} representing only 13% of the total number of sub-samples. In order to magnetically clean each sub-sample AF demagnetisation was used in steps of 5 mT to 30 mT and then in 10 mT steps to a maximum applied AF of 170 mT. Only the samples with the strongest NRM intensities could be demagnetised to this AF before becoming too weak to measure. Median destructive fields lay within the range 12 to 38 mT but at the highest applied AFs 15 to 20% of the NRM intensity remained. This indicated that the remanence may have been carried by a mixture of low and high coercivity minerals.

Representative plots for the demagnetisation of 3 sub-samples are shown in Figure 7.4. The magnetically strongest sub-samples (for example 30B which had an NRM of 112 x 10^{-8} Am^2kg^{-1}; Figure 7.3 a-c) exhibited a stable remanence direction with little scatter after removal of a small VRM by 10 mT. Some weaker sub-samples (for example 4B which had an NRM intensity of 22 x 10^{-8} Am^2kg^{-1}; Figure 7.3 d-f) also exhibited stable remanence directions but these were less well defined with greater signal to noise ratios. In several instances, sub-samples which were not necessarily the weakest

(for example 2B which had an NRM intensity of 31.8 x 10^{-8} Am^2kg^{-1}; Figure 7.3 g-i) were unstable during demagnetisation. It was either not possible to calculate directions from these sub-samples or they had high MAD values associated with the calculated direction. Stable remanence directions were calculated after removal of any VRM (by a maximum AF of 15 mT) from the Zijderveld plots using the method of Kirschvink (1980). Directions were calculated from all sub-samples except 2B, 6B, 10B, 11B 12B, 13B, 28B and 32B which were rejected for the reasons outlined above.

In order to assess the effects of thermal demagnetisation, and to see if there were any significant differences in the data obtained by thermal and AF means, lateral sub-samples 23A and 29B were stepwise thermally demagnetised (Figure 7.5). Demagnetisation was undertaken in steps of 100°C to 700°C with 50°C steps at 50, 550 and 650°C. Of the two sub-samples, directions could only be calculated for sub-sample 23A in which a stable remanence was defined (Figure 7.5a). In this case, a small VRM was removed by 100°C and the vector subsequently trended towards the origin. This was interpreted to be the primary remanence.

It was not considered possible to calculate a direction for sub-sample 29A even though its NRM intensity was relatively strong at 101 x 10^{-8} Am^2kg^{-1}. The Zijderveld plot and the stereo plot (Figure 7.5d and e) show that there may be three magnetisation components within this sub-sample although the data are noisy.

There was insufficient lateral material for depositional inclination errors tests to be performed. However, the direction obtained after thermal demagnetisation of sub-sample 23A (declination = 3.7°, inclination = 64.4°, MAD = 0.9°), was within the directional errors of its coeval central sub-sample 22B (declination = 4.1°, inclination = 62.9°, MAD = 6.0°). In the case of AG02 it was not possible to draw conclusions on the presence or absence of inclination errors based on this single result.

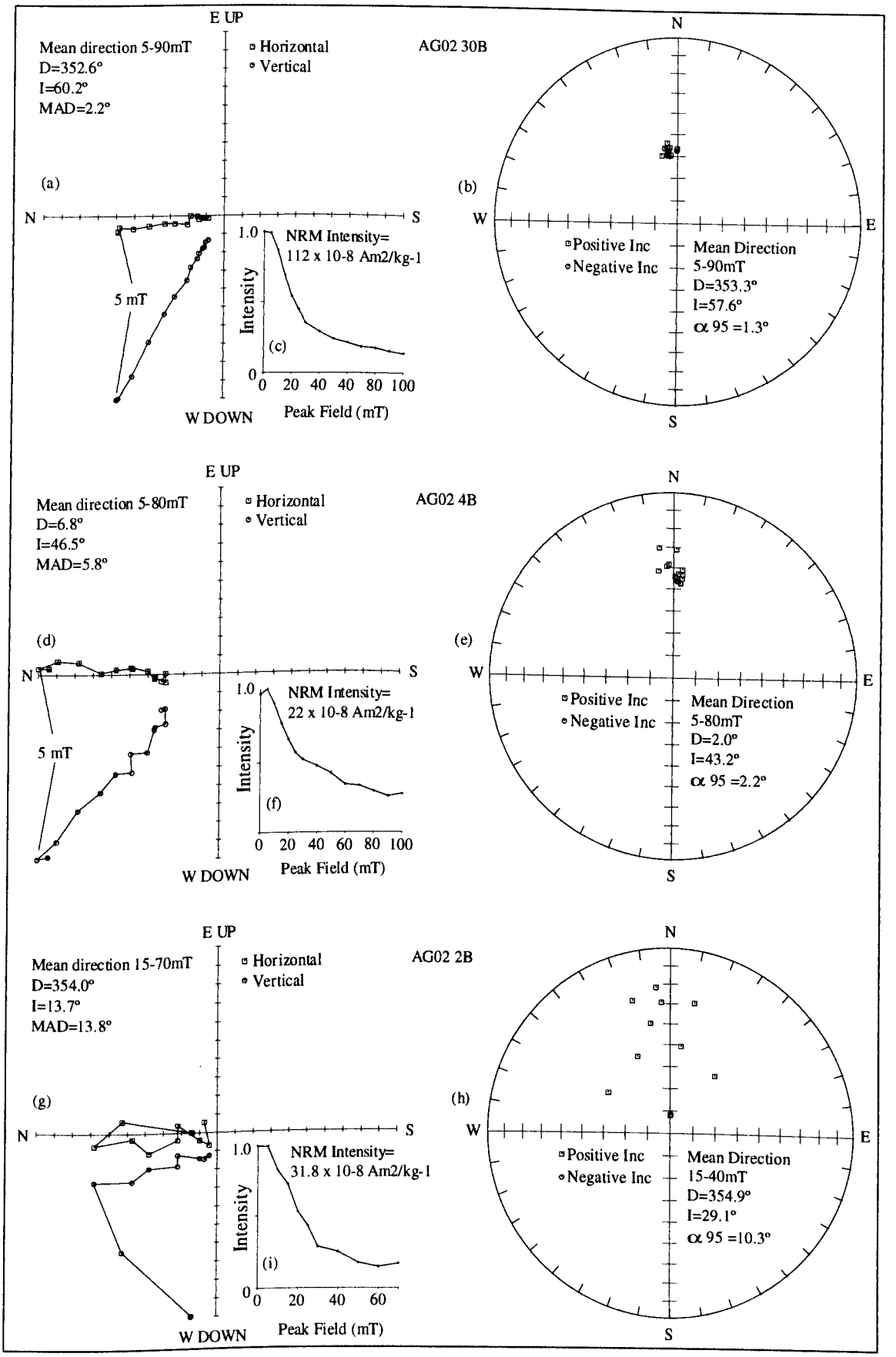

Figure 7.4. AF demagnetisation data from AG02 sub-samples 30B, 4B and 2B.

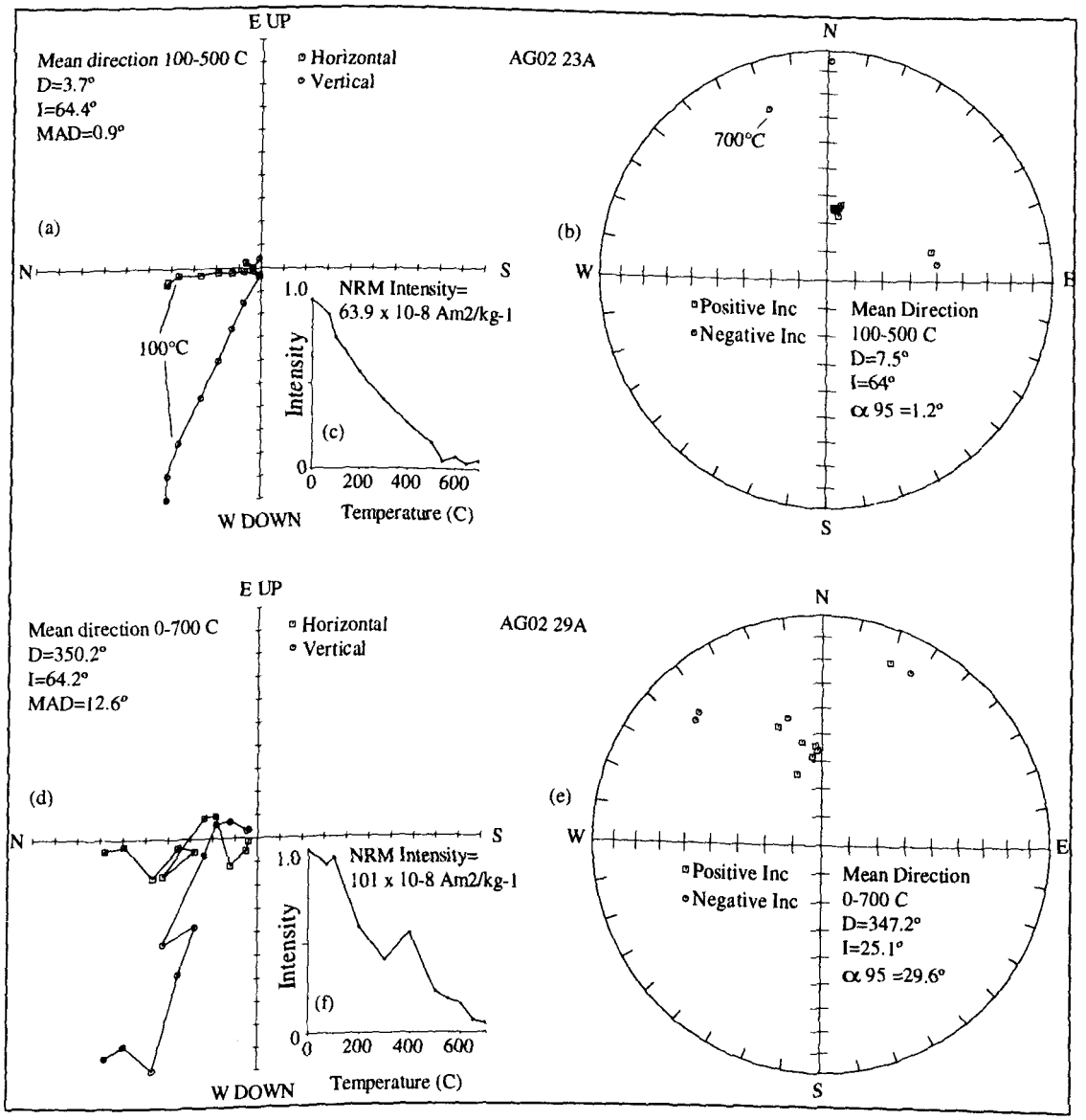

Figure 7.5. Thermal demagnetisation data for AG02 sub-samples 23A and 29A.

7.4.2. Uranium-series dating of AG02.

The uranium-series data for AG02 are tabulated in Table 7.1. The $^{230}Th/^{232}Th$ ratio of sub-sample 1B ($^{230}Th/^{232}Th$ = 2.13) was used to correct the ages of the remaining sub-samples as the upper surface of AG02 was being dripped on when collected. The corrected dates were vastly different from the uncorrected dates and so do not inspire confidence. Even so, most dates, excepting those from the base of AG02, were in stratigraphic order and lay on a straight line on an age-height plot. The date calculated from sub-sample 3B was negative and could only be made to lie in stratigraphic order by guessing its initial $^{230}Th/^{232}Th$ ratio; it was consequently ignored.

Overall, the high age errors are most likely due to a combination of low U concentrations and detrital contamination. Uranium concentrations were particularly low in sub-samples of AG02 and ranged from 0.02 (30B) to 0.14 ppm (2B). Low concentrations of U increase the associated errors in counting the uranium and thorium isotopes of interest. In fact, uranium concentrations such as these are close to or below the required limit (0.05 ppm) for alpha-spectrometry (Ivanovich and Harmon, 1992).

The Hallstadius electrodeposition method was used throughout the uranium-series dating of AG02, resulting in high chemical yields of U and Th. Therefore, yields were considered to have had minimal effect on the precision of each date possibly excepting the dates of 15B and 28B whose U yields were low. Sub-sample 30B had an anomalous $^{234}U/^{238}U$ ratio of 4.64 but gave a comparable age to the remaining dates. $^{230}Th/^{232}Th$ ratios changed little down the speleothem (1.68±0.62 to 2.68±0.19) indicating that detrital contamination remained relatively constant.

The age of AG02 was estimated using linear-least squares fitting ignoring the date of 3B (Figure 7.6). Assuming that the top surface of AG02 was modern and that a constant rate of growth had occurred, an estimated growth rate of 0.037 mm yr^{-1} was calculated giving an upper surface age of 0.0 ka a basal age of 10.9±6.0 ka. Over the 10.9 ka period of growth each sub-sample would time-average 351 years of PSV. These dates are considered approximate due to the magnitude of imprecision.

Sub-sample	Concentration U (ppm)	U Yield (%)	Th Yield (%)	$^{234}U/^{238}U$	$^{230}Th/^{234}U$	$^{230}Th/^{232}Th$	Uncorrected age (ka)	Corrected age (ka)
1B	0.09±0.05	46	72	1.16±0.05	0.087±0.012	2.13±0.58	9.9±1.4	0.0
2B	0.14±0.01	25	35	1.17±0.05	0.036±0.074	2.34±1.10	3.9±0.8	0.4±2.4
3B	0.11±0.01	75	87	1.19±0.46	0.056±0.011	1.68±0.62	6.2±1.3	-0.7±3.1
5B	0.07±0.04	22	65	1.28±0.08	0.089±0.013	2.25±0.89	10.0±1.6	1.6±4.5
15B	0.12±0.13	4	26	1.33±0.17	0.201±0.024	2.66±0.41	24.2±3.2	5.3±6.6
27B	0.09±0.10	11	52	1.18±0.10	0.337±0.028	2.56±0.30	44.2±4.6	8.8±9.9
28B	0.11±0.01	7	73	1.21±0.13	0.461±0.039	2.68±0.19	65.7±7.9	17.6±14.2
30B	0.02±0.01	19	58	4.64±0.56	0.324±0.024	2.46±0.28	40.4±3.5	6.8±8.3

Table 7.1. Uranium-series data for sub-samples of AG02 with resultant uncorrected and corrected ages. Errors are to 1 sigma and are based on counting statistics.

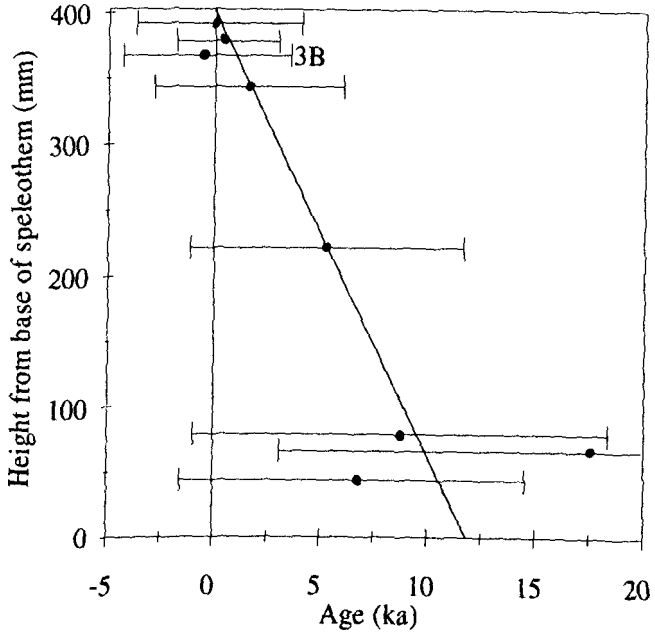

Figure 7.6. Speleothem AG02 uranium-series dates. Errors are to 1 sigma and are based on counting statistics. The best fit line is a linear least squares fit assuming that the top is modern. The top age was estimated to be 0.0 ka and the basal age to be 10.9±6.0 ka.

7.4.3. The palaeomagnetic record of AG02.

The variations in declination and inclination for sub-samples where a primary remanence direction could be identified are shown in Figure 7.7 (Appendix F). Declinations ranged from 340.0° (31B) to 12.2° (9B) whilst inclinations ranged from 43.5° (5B) to 67.5° (15B) with a mean declination of 1.8° and mean inclination of 56.4° (Fisher, 1953). The mean inclination was shallower than that the 61° calculated using the GADF model but was within the α_{95} errors of the mean.

These declination data had amplitudinal variations of the order ±10° although the directions of 27B and 31B were 15 and 20° west respectively. From the base of the record the declinations had a general trend from west to east with a westerly swing over the period 7.5 to 5.2 ka. The amplitudinal variation of inclination was of the order ±15° about the mean and had two consecutive cycles of shallowing followed by steepening (8.8 ka to 5.2 ka and 5.2 to 1.6 ka (mean period 3.6 ka)). Considering the magnitude of

the errors associated with each direction this pattern of PSV is not well-constrained in time. However, the topmost values of declination and especially inclination are close to the present day field at Matienzo, estimated using the IGRF model (D = 1.8° west, I = 59°), helping to confirm that AG02 was growing when collected.

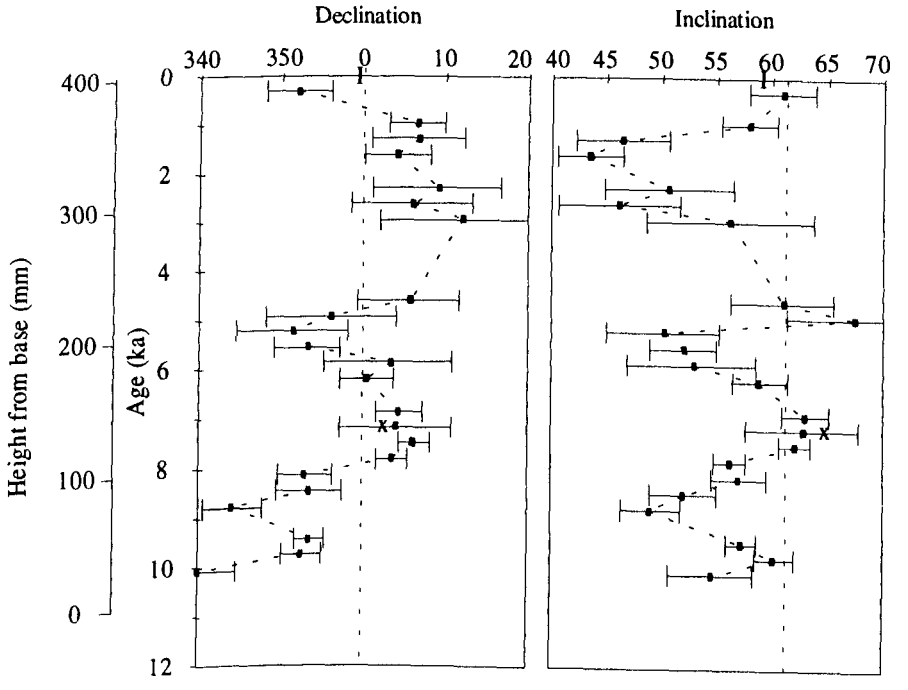

Figure 7.7. Declination and inclination of AG02 against estimated sub-sample age and height from base of stalagmite. Error bars show the MAD value for the direction of each sub-sample. The direction calculated from lateral sub-sample 23A is also shown with MAD errors omitted for clarity and the 'I' symbol shows the present day field for Matienzo as calculated from the IGRF model.

These data were converted into equivalent VGPs after being three-point smoothed (Figure 7.8). Over the period 10.9±6.0 ka to 0.0 ka the VGPs are far sided, due to their shallow inclinations. Progression of the VGPs through time defines a tight clockwise loop (7.8 to 6.3 ka) followed by a large open anti-clockwise loop from 6.3 ka to the present. This may be indicative of westward and eastward drift of the non-dipole field (Runcorn, 1959). However, stationary sources with out-of-phase intensity variations may also cause such looping (Creer and Tucholka, 1982).

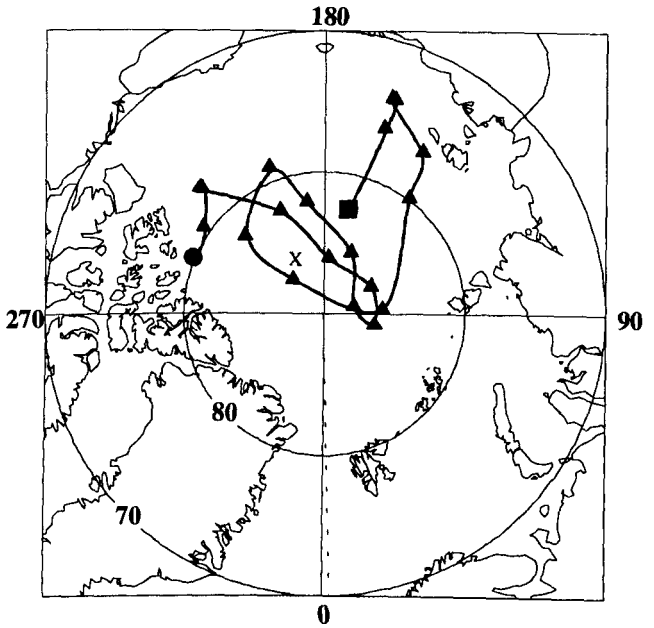

Figure 7.8. VGP progression through time for speleothem AG02. A 3-point smoothing filter has been applied to these data. The filled circle (square) represents the start (end) of the record at 10.9±6.0 ka (present-day). The present day VGP position for Matienzo is shown by 'X' and the dotted line shows the site longitude.

7.5. Palaeomagnetism and dating of AG03.

7.5.1. NRM and demagnetisation of AG03.

AG03 was into cut into one central vertical slice which yielded 23 14 cm^3 sub-samples, labelled 1B to 23B. The NRM intensities lay in the range 45 to 2.9 x 10^{-8} Am^2kg^{-1} and sub-samples were subjected to thermal demagnetisation in steps of either 50 or 100°C. Between 300 and 400°C the majority of weaker sub-samples had intensities that reached the same magnitude as the background noise of the magnetometer.

Representative plots of demagnetisation behaviour for three sub-samples are shown in Figure 7.9. The strongest sub-samples (for example 23B with an NRM intensity of 30.4 x 10^{-8} Am^2kg^{-1}; Figure 7.9a-c) yielded a stable remanence direction after thermal demagnetisation and showed no sign of a VRM. At temperatures of 550°C

approximately 90% of the NRM had been unblocked indicating the presence of magnetite or titanomagnetite as a carrier of magnetic remanence. The remaining magnetisation unblocked between 650 and 700°C (for example Figure 7.9c) Weaker sub-samples (such as 7B; NRM intensity 14.0 x 10^{-8} Am^2kg^{-1}; Figure 7.9d-f) also showed unidirectional decay towards the origin of the Zijderveld plots but had much higher signal to noise ratios which imparted a greater degree of directional scatter. However, 13 of the 23 sub-samples were too magnetically weak for directions of remanence to be estimated (for example 8B; NRM intensity 2.9. x 10^{-8} Am^2kg^{-1}; Figure 7.9g-i).

7.5.2. Uranium-series dating of AG03.

Table 7.2 contains the uranium-series data from sub-samples of AG03. Standard alpha-spectrometry requires a minimum of 0.05 ppm of uranium in order to accurately measure isotope activities above the level of detector background (Ivanovich and Harmon, 1992). Sub-samples of AG03 had uranium concentrations in the range 0.02 to 0.07 ppm; close to and below this detection limit. Coupled with the level of detrital contamination ($^{230}Th/^{232}Th$ ratios 2.0 to 2.5) calculated dates are considered to be nothing more than rough estimates. An initial thorium correction value of 1.5 was used throughout the dating of AG03 after Gascoyne *et al* (1981). Although a large degree of imprecision was associated with each date, they were in stratigraphic order. A linear least-squares fit to these imprecise data (Figure 7.10) indicated that AG03 had probably grown sometime between 35 ka and the present day; an approximate growth rate of 0.03 mm yr^{-1} was calculated. Within the growth period, sub-samples have averaged out PSV over periods of 841 years. If we consider a westward drift rate of the geomagnetic field to be 0.2° per year then one complete global cycle will be resolved by just over two sub-samples. Averaging of this degree will give no more than a general idea of geomagnetic field behaviour and is of little use in PSV studies.

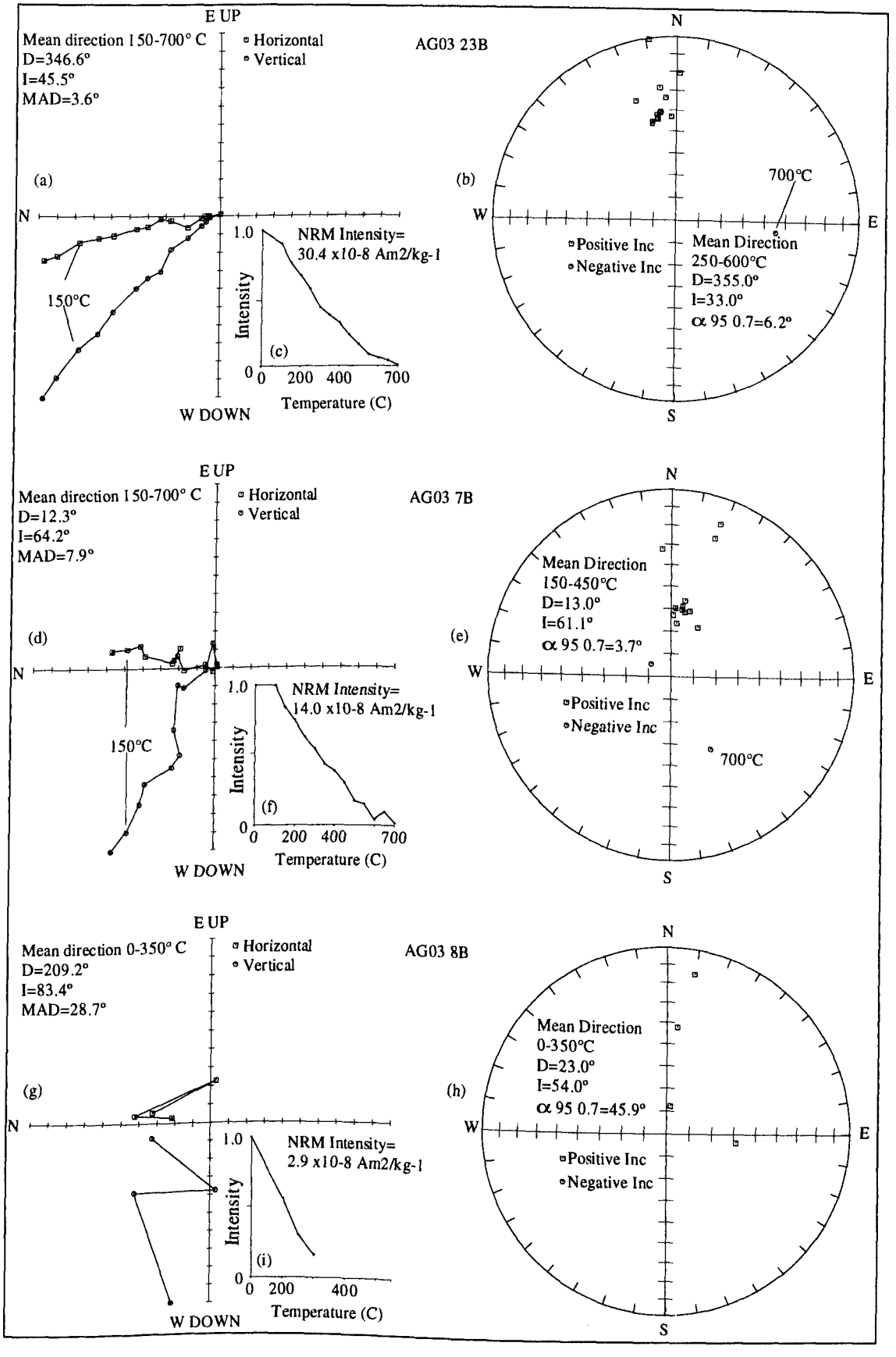

Figure 7.9. Thermal demagnetisation data for AG03 sub-samples 23B, 7B and 8B.

Sub-sample	Concentration U (ppm)	U Yield (%)	Th Yield (%)	$^{234}U/^{238}U$	$^{230}Th/^{234}U$	$^{230}Th/^{232}Th$	Uncorrected age (ka)	Corrected age (ka)
3B	0.02±0.03	26	75	1.08±0.08	0.221±0.023	2.01±0.38	26.9±3.3	7.5±7.0
11B	0.07±0.03	49	72	1.14±0.05	0.021±0.017	2.47±0.45	24.9±2.4	10.6±4.9
24B	0.07±0.03	45	34	1.15±0.03	0.301±0.015	2.26±0.19	38.6±2.4	14.6±4.5
31B	0.07±0.02	60	33	1.07±0.03	0.467±0.023	2.28±0.18	67.7±4.6	28.2±8.1

Table 7.2. Uranium-series data for sub-samples of AG03 with resultant uncorrected and corrected ages. Errors are to 1 sigma and are based on counting statistics.

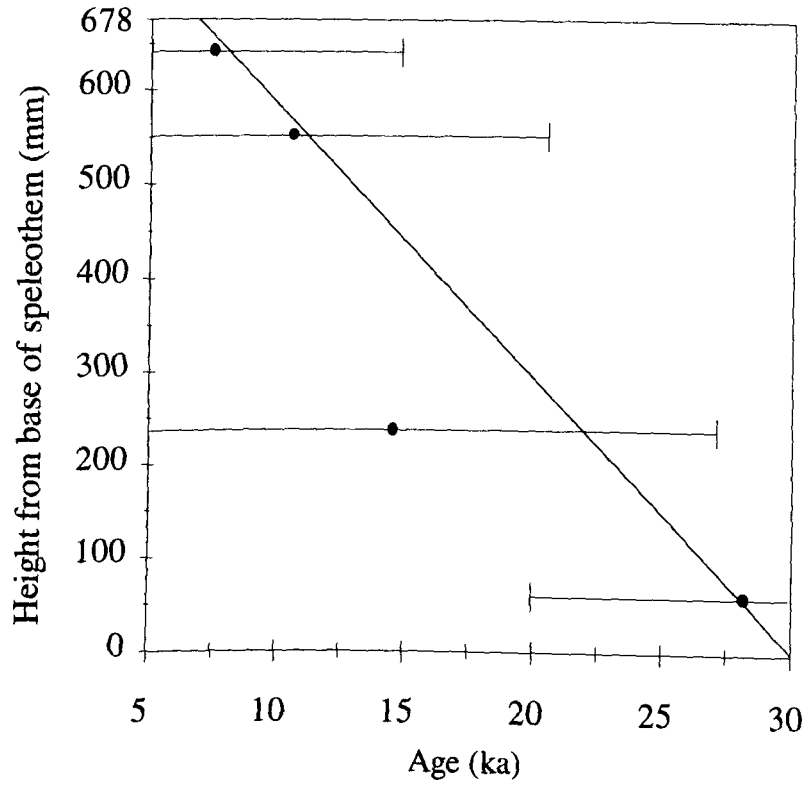

Figure 7.10. Speleothem AG02 uranium-series dates. Errors are to 1σ and are based on counting statistics. The best-fit line is a linear-least squares fit using dates of four sub-samples. The speleothem appears to have grown some time between 35 ka and the present day.

7.5.3. The palaeomagnetic record of AG03.

The few sub-samples that yielded directions have their inclination and declination values shown against age and height from the base in Figure 7.11. These directions are tabulated in Appendix G. Conclusions on the pattern of PSV over the growth period cannot be made as these data were too sparse and dating too imprecise. Using Fisher statistics (Fisher, 1953) the mean declination was 2.6° and the mean inclination was 51.6° (10° shallower than that predicted by the GADF).

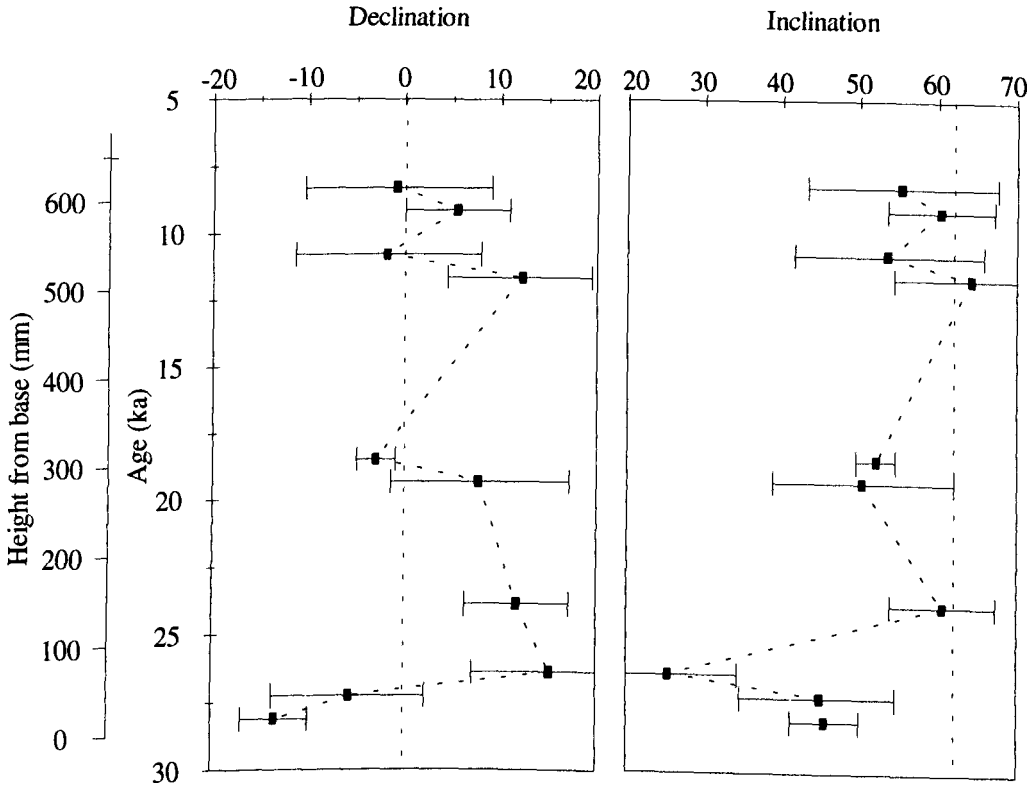

Figure 7.11. Declination and inclination for sub-samples of AG03 against sub-sample age and height from base of stalagmite. Error bars represent the MAD for each sample calculated as an indication of precision. The dotted vertical lines are the GADF model values for Matienzo.

7.6. Palaeomagnetism and dating of TR01.

7.6.1. NRM and demagnetisation of TR01.

The central slice of TR01 was cut into 40 7 cm^3 sub-samples labelled 1B to 40B. Of these sub-samples, six had NRMs that were measurable on the SQUID magnetometer. NRM intensities for these sub-samples ranged from 12 to 28 x 10^{-8} Am^2kg^{-1}. The remaining 34 sub-samples were close to the noise level of the magnetometer and the NRM directions of repeat measurements were inconsistent. Attempts to increase the NRM to measurable levels by stacking sub-samples in pairs was

unsuccessful and repeat measurements continued to give disparate directions. No further attempts were made to obtain palaeomagnetic information from TR01.

7.6.2. Uranium-series dating of TR01.

Uranium series data for sub-samples of TR01 are presented in Table 7.3. The dating of TR01 serves to illustrate the high degree of accuracy that can be achieved using alpha-spectrometry on detritally free and uranium-rich samples.

Uranium concentrations lay in the range 0.99 to 1.10 ppm and $^{230}Th/^{232}Th$ ratios (25.43 to 104.78) were such that an initial thorium correction was not required for any sub-sample. Chemical yields of U and Th were generally high. However, in two cases where yields were low (U in 6B and U and Th in 39B; Table 7.3), the high concentrations of U outweighed the poor recoveries and dating errors were not significantly increased. Percent error of each date ranged from 2 to 6%; in some cases smaller than the quoted 'typical' errors of alpha-spectrometry (5-10%; Schwarcz, 1989). Due to the precise dating of sub-samples of TR01 all ages were in stratigraphic order.

A linear-least squares fitting procedure was used to estimate the age of the speleothem (Figure 7.12). It was assumed that TR01 grew continuously throughout its height for the purposes of this calculation. From the line of best-fit to these individual dates an upper surface age of 3.6±0.1 ka and a basal age of 9.7±0.3 ka were calculated giving a growth period of 6.1 ka and a growth rate of 0.08 mm yr^{-1}. Each sub-sample would, therefore, average PSV into periods of 146 years. The tightly controlled dating suggested that TR01 was not growing at the present as originally thought. Thus, the belief that a surface is active, as judged by its 'fresh' appearance, is not always borne out. The dating of TR02 shows that without the effects of low uranium concentration dating accuracy can be greatly increased (the low degree of detrital contamination will also have assisted in the age error reduction). However, as TR01 demonstrates, low concentrations of detritus may provide an unreliable or immeasurable palaeomagnetic signal.

Sub-sample	Concentration U (ppm)	U Yield (%)	Th Yield (%)	$^{234}U/^{238}U$	$^{230}Th/^{234}U$	$^{230}Th/^{232}Th$	Uncorrected age (ka)	Corrected age (ka)
6B	1.06±0.04	10	31	2.14±0.06	0.037±0.002	44.74±26.79	4.1±0.2	-
8B	1.10±0.15	79	63	2.24±0.02	0.041±0.001	54.63±33.06	4.6±0.1	-
21B	1.08±0.12	71	46	2.14±0.18	0.058±0.002	25.43±6.15	6.4±0.2	-
35B	1.09±0.14	49	69	2.28±0.02	0.081±0.002	79.64±31.14	9.1±0.2	-
39B	0.99±0.04	7	10	2.29±0.06	0.087±0.05	104.78±77.61	9.8±0.6	-

Table 7.3. Uranium-series data for sub-sampes of TR01with resultant ages. No correction for detrital thorium was required. Errors are to 1 sigma and are based on counting statistics.

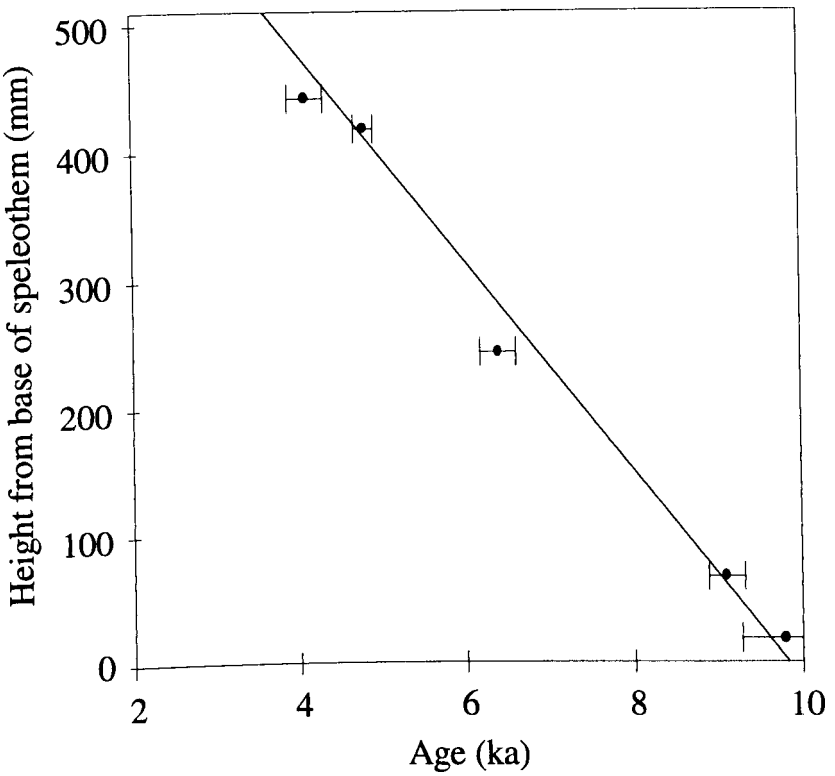

Figure 7.12. Speleothem TR01 uranium-series dates. Errors are to one sigma, based on counting statistics. The best-fit line is a linear-least squares fit assuming a constant rate of growth. The upper age estimate is 3.6±0.1 ka and the basal age estimate 9.7±0.3 ka.

7.7. Palaeomagnetism and dating of TR02.

7.7.1. NRM and demagnetisation of TR02.

The central vertical slice of TR02 was, in places, of sufficient width to allow pairs of coeval sub-samples to be cut from its drip-cap area. A total of 24 'B' sub-samples, labelled 1B to 24B, and 11 'C' sub-samples, labelled 13B to 19B and 21B to 23B, were cut, each being 14 cm^3 in size. NRM intensities were weak (21 to 0.7 x 10^{-8} Am^2 kg^{-1}) with the majority less than 10 x 10^{-8} Am^2 kg^{-1}. Several of these sub-samples had NRMs close to the noise level of the magnetometer (0.24 x 10^{-8} Am^2 kg^{-1}). Of sub-samples whose NRM intensities were above the magnetometer noise level, NRM directions

obtained from repeat measurements were disparate. It was considered unlikely that any reliable palaeomagnetic data could be obtained from further demagnetisation of TR02.

7.7.2. Uranium-series dating of TR02.

Table 7.4 shows the uranium-series data obtained from sub-samples of TR02. Sub-samples had uranium concentrations in the range 1.13±0.01 to 1.80±0.02 ppm. These concentration were the highest encountered during this study.

The $^{230}Th/^{232}Th$ ratios of sub-samples from TR02, which indicate a detrital contribution, were greater than those in TR01. This may reflect their differing locations within the streamway. TR01 was located above the streamway and would only have been affected by more severe flooding. Conversely TR02 was growing in the streamway and may have been inundated by the more frequent, lesser flooding events. The $^{230}Th/^{232}Th$ ratios were sufficiently high in 2B, 5B and 11B for a correction of 1.5 to be applied (after Gascoyne *et al*, 1981).

Despite the adoption of corrections for thorium contamination in these three cases, the resulting dates are considered precise. They are well within, and in some cases smaller than the quoted 5-10% accuracy for alpha-spectrometrically derived dates (Schwarcz, 1989). The percentage error of individual dates ranges from 1.2% (7B) to 6.3% (2B) and were the lowest dating errors achieved during this study.

In estimating the age of TR02 a linear-least squares fit was made to these five dates (Figure 7.13). Due to the high degree of precision of individual dates the best fit line lies just outside of the 1 sigma errors of sub-samples 2B, 11B and 15B. In fact, a linear regression would probably suffice as errors are small and are therefore [almost] insignificant. By rejecting the date of 11B the linear-least squares fit would have overlapped all the remaining dates but considering the dating accuracy this would not offer a significant improvement in the overall dating.

Sub-sample	Concentration U (ppm)	U Yield (%)	Th Yield (%)	$^{234}U/^{238}U$	$^{230}Th/^{234}U$	$^{230}Th/^{232}Th$	Uncorrected age (ka)	Corrected age (ka)
2B	1.31±0.01	83	67	2.32±0.01	0.017±0.006	10.37±1.85	1.8±0.1	1.6±0.1
5B	1.13±0.01	55	80	2.54±0.02	0.026±0.001	23.54±5.37	2.9±0.1	2.7±0.1
11B	1.80±0.02	59	83	2.57±0.02	0.049±0.001	23.90±3.25	5.5±0.1	5.2±0.2
15B	1.55±0.02	52	69	2.56±0.02	0.070±0.001	26.00±1.94	7.8±0.1	-
20B	1.17±0.02	36	31	2.53±0.02	0.090±0.002	116.68±36.77	10.2±0.3	-

Table 7.4. Uranium-series data for sub-samples of TR02 with resultant uncorrected and corrected ages. Errors are to one sigma and are based on counting statistics.

Using all dates a growth rate of 0.05 mm yr^{-1}, an upper surface age of 0.98±0.08 ka and a basal age of 12.1±0.4 ka were estimated. Thus, TR02 appears to have ceased growing approximately 1.0 ka before present. Based on this growth rate each sub-sample of TR02 would have averaged PSV over periods of 466 years. Thus, if the non-dipole drift rate of 0.2°/yr (Hyodo *et al*, 1993) is considered each sample would record just under a quarter of each global cycle (0.45 ka). A PSV record of this resolution would not be sufficient to resolve the shorter period features of field change.

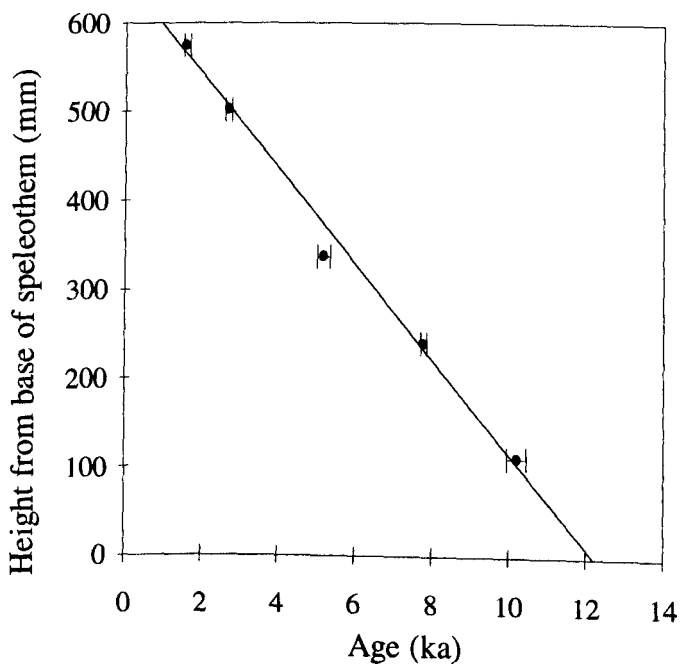

Figure 7.13. Speleothem TR02 uranium-series dates. The best-fit line is a linear-least squares fit assuming a constant rate of growth. Errors are to one sigma and are based on counting statistics. The upper surface age was estimated to be 0.98±0.08 ka and the basal age was estimated to be 12.07±0.36 ka.

7.8 Comparisons with contemporaneous records.

In Figure 7.14 the AG02 declination and inclination records are compared to the UK lake sediment record of Turner and Thompson (1981). The UK lake sediment record offers excellent resolution of PSV and has tight dating control making it the standard record for comparisons of Holocene PSV in the European region.

Figure 7.14 shows that the AG02 record appears to resolve most of the highest amplitude features of PSV despite being of low resolution (351 years of averaged PSV per sub-sample). The comparison between the declination records (Figure 7.14a) shows a striking similarity in the amplitude and timing of declination maxima and minima. These declination features have been labelled according to the scheme of Turner and Thompson (1981). With the exception of features 'b' and 'c' declination features 'a' to 'j' can be identified in the record from AG02.

In comparison with the inclination record, the AG02 record has a higher amplitudinal variation (±10° about the mean) compared to ±5° in the UK record (Figure 7.14b). This may indicate that the UK record has undergone some depositional smoothing effects during or after accumulation or may have been disturbed during the coring / sampling process. As discussed in chapter 6, depositional inclination errors in speleothems appear to be absent although it was not possible to test for this in the case of AG02. However, it is possible that the greater amplitudinal variation of inclination in AG02 could be attributed to inclination errors in the absence of any test data.

Inclination features in AG02 are more difficult to correlate over time. Over the period 10.9 to 5.0 ka the UK record has two consecutive shallowing to steepening cycles labelled 'ν' to 'ι' on the UK record. There appears to be a discrepancy in the timing of these features in the record of AG02 allowing two possible comparisons to be made ('λ' to 'ϑ' and 'ν' to 'κ'; Figure 7.14b). The latter comparison appears more likely as a better relative position is observed for feature 'λ' as it is steeper than the GADF at this point in both records. Interpretations must consider the errors associated with the dating of AG02, resulting from low uranium concentrations and detrital contamination. These errors allow the timespan of AG02 to be shifted relative to the UK record which may provide a better overall fit. However, on the basis that age shifts would also introduce lags into declination data no such shifting has been attempted. The detail of the AG02 PSV record was not considered sufficient for further attempts at improving the correlation.

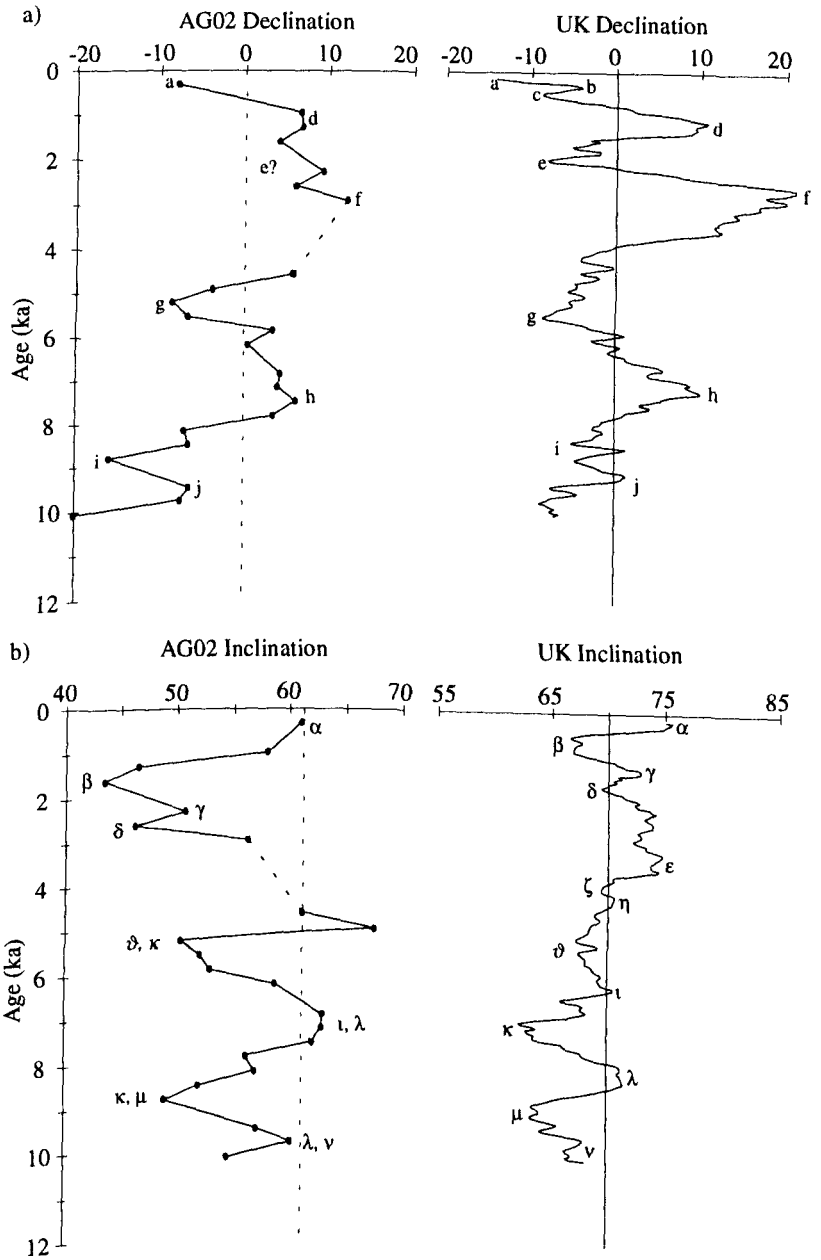

Figure 7.14. Comparison of the a) declination and b) inclination of AG02 and the UK lake sediment record of Turner and Thompson, (1981).

In summary, the speleothems from Matienzo, excepting AG02, were of little use for studies of PSV. They were magnetically too weak for accurate measurement on the SQUID magnetometer. Additionally, in the cases of AG02 and AG03 the concentration of uranium was extremely low (sections 7.4.2 and 7.5.2) and this contributed significantly to the dating uncertainties. However, the feature-to-feature correlations

between the PSV record from AG02 and the UK master curve of Turner and Thompson, (1981) shows promise and indicates that other speleothems from Matienzo are likely to yield good records of PSV. Further sampling in Torca Regaton, for example, may yield a stalagmite that has both high uranium concentrations and a strong, measurable remanence. This would potentially allow further very accurately dated records of PSV to be produced. The question remains of why do the speleothems from Torca Regaton (TR01 and TR02) have much higher uranium concentrations? One potential source for uranium is from a shale parting, or horizon, in the strata directly above this section of the cave passage. Shales, particularly black shales, can contain uranium in concentrations of up to 1300 ppm (Ivanovich and Harmon, 1992). It would be interesting to see if other speleothems from the Sistema de Cubija had such high uranium concentrations.

8. Rock magnetism of Chinese and Spanish speleothems.

8.1. Introduction.

Rock magnetic tests were carried out in order to determine the nature of the magnetic mineral phases that contributed to the remanence in each speleothem. Due to the low concentrations of magnetic material and hence the very weak magnetisations, the variety of rock magnetic tests that could be performed were limited by the sensitivity of the equipment available. These low concentrations of magnetic minerals were somewhat surprising as field evidence suggested frequent flooding which would provide a relatively high detrital loading leading to a DRM with relatively strong NRM intensities. Inspection of the speleothems did show detritus within the growth layers. The most informative rock magnetic tests were found to be those based on acquisition of isothermal remanent magnetisation (IRM). A synopsis of these methods are given in each section prior to their results.

8.2. Magnetic susceptibility.

The measurement of magnetic susceptibility (χ) is a measure of the ease by which a magnetic material can be magnetised and is dependent on the type(s) of mineral phases present and also on their concentration and grain size. Room temperature susceptibility is a good starting point for rock magnetic study as it can also suggest which other rock magnetic tests will or will not be effective (Thompson and Oldfield, 1986). Room temperature susceptibility was measured on a Bartington MS1 susceptibility meter using the low frequency (0.47 Hz) setting. For each measurement the background drift was subtracted as it was of a similar magnitude as the sample susceptibility.

Calcite, composing the matrix of each sub-sample, is weakly diamagnetic with a susceptibility of -0.5×10^{-8} m^3kg^{-1}. When dealing with low concentrations of magnetic

minerals the negative susceptibility of the matrix tends to swamp the susceptibility of the magnetic phases. As a consequence, the majority of susceptibilities measured in this study were either negative or low (of the order -2.0 to 3.0 x 10^{-8} m^3kg^{-1}) and repeat measurements were not always in agreement (the maximum difference between repeat measurements was ±1.5 x 10^{-8} m^3kg^{-1}). It may be possible to subtract the effects of the calcite matrix from the susceptibility of the magnetic phases but the widely variable measured susceptibilities suggested that this could not be achieved with any degree of accuracy. Sub-sample susceptibility measurements are included in Appendices A to I.

8.3. Acquisition of isothermal remanent magnetisation (IRM).

An IRM is imparted along one axis of a sample by application of a direct field at a constant temperature; usually at room temperature (Thompson and Oldfield, 1986). The magnetisation of grains whose coercivities are less than the applied field will align parallel to the applied field. Coercivity is dependent upon the type of magnetic mineral(s) present and is greatest for SD size material; the energies required to change the axis of magnetisations of SD grains are higher than those for larger MD grains in which domain wall movement occurs (Thompson and Oldfield, 1986). The magnitude of the IRM is dependent on the applied field and will increase to a maximum value in successively higher applied fields. This maximum is termed the saturation isothermal remanent magnetisation (SIRM). At Liverpool the IRM equipment was not capable of producing the high fields required to saturate some magnetic minerals such as haematite. In these instances, the SIRM represents the highest magnetisation that can be induced using laboratory equipment (Thompson and Oldfield, 1986). In a natural material there may be a variety of magnetic minerals with a range of grainsizes and consequently a range of coercivities. These ranges of coercivity are known as a coercivity spectrum and may identify the mineral phase(s) within a particular sample.

8.3.1. Laboratory method.

From each speleothem, sub-samples were selected from the top and base in order to check whether any intra-speleothem compositional differences could be identified using IRM acquisition. IRM acquisition was performed on sub-samples, after AF demagnetisation of their NRMs, using an MM9P pulse magnetiser. The pulse field was increased in increments to a maximum of 4T and the IRM intensity was measured on a Molspin spinner magnetometer within 10 seconds of each field application. In order to impart IRMs in the range 0 to 4T the pulse magnetiser was supplied with a 25 mm diameter coil. Sub-samples required 'trimming' before they would fit the sample holder for this coil. To avoid trimming, the Spanish sub-samples were subjected to a maximum field of 2T using a larger 40 mm diameter coil (used for inducing IRMs over the range 0 to 2T).

8.3.2. Results from the Chinese speleothems.

Figures 8.1a-e show representative normalised plots of IRM acquisition performed on sub-samples from SC01, SC02, PT02, PT03 and PT04. SIRMs lay in the range 28.23 to 0.82 x 10^{-5} Am^2kg^{-1} at 4T. All curves show a similar form with an initial steep increase in IRM intensity with 76 to 85% of the SIRM acquired by 300 mT, the maximum coercivity of pure magnetite (O'Reilly, 1984). Above 300 mT a further 24 to 15% of the total SIRM was acquired and the curves began to flatten. However, saturation was not reached by the maximum applied field of 4T. This indicated the presence of a high coercivity mineral such as haematite or goethite which would require fields of around 5 and 7 T respectively for saturation to occur (O'Reilly, 1984; Rochette and Fillion, 1989; Lowrie, 1990). These IRM acquisition curves show that the coercivities of the mineral phases present within one speleothem remained relatively constant. The only significant difference in form was observed between the curves of sub-samples from PT04. The base of PT04 may contain a greater concentration of SD sized magnetic grains which required greater energy to impart the IRM.

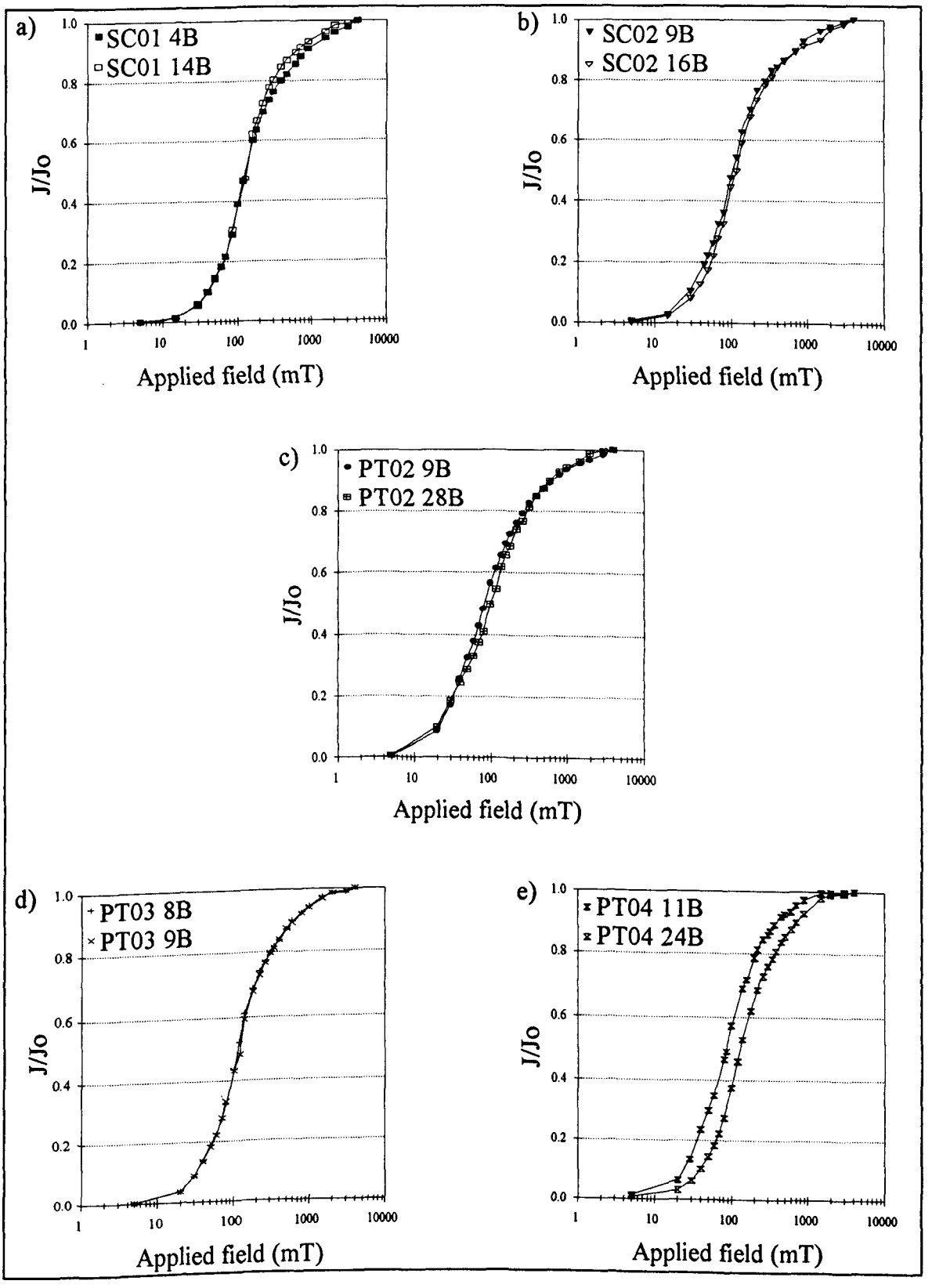

Figure 8.1. Incremental acquisition of IRM to a maximum applied field of 4T for sub-samples from a) SC01, b) SC02, c) PT02, d) PT03 and e) PT04.

8.3.3. Results from the Spanish speleothems.

Figures 8.2 a-d show representative IRM acquisition curves for sub-samples of Spanish speleothems TR01, TR02, AG02 and AG03. In these cases, sub-samples were subjected to a maximum pulse field of 2T which was adequate to highlight the coercivities of the magnetic minerals contained therein.

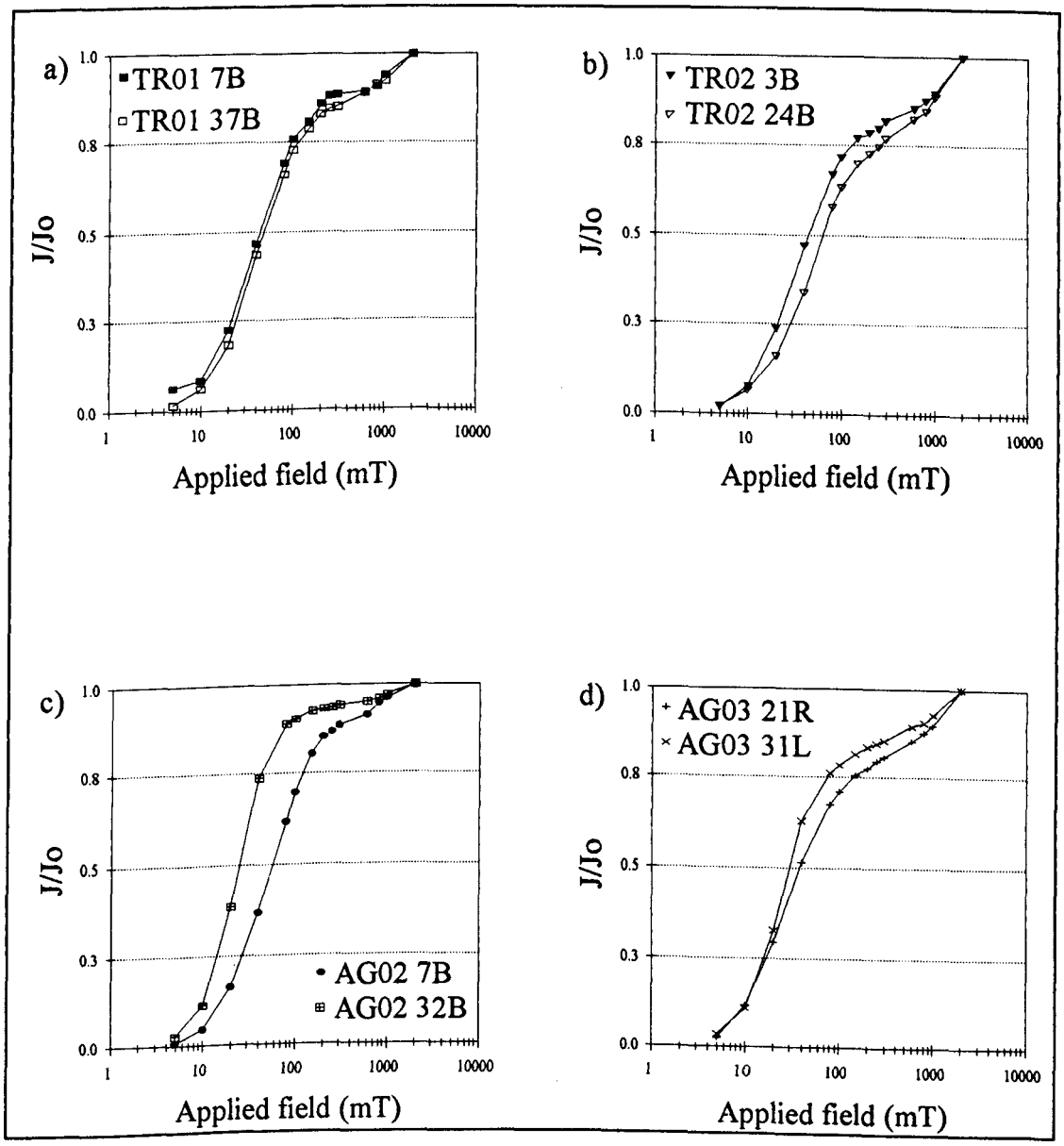

Figure 8.2. Incremental acquisition of IRM to a maximum applied field of 2T for sub-samples from a) TR01, b) TR02, c) AG02 and d) AG03.

Evidence for the presence of a magnetic minerals with distinct coercivity ranges was seen in the sub-samples of the Spanish speleothems. Curves for sub-samples from the top and bottom (centre and bottom for AG03) within each speleothem show that there may be some differences in the relative proportions of magnetic minerals with coercivities less than ~1T. This is suggested by the divergence of the acquisition curves (Figure 8.2b,c,d). However, by 300 mT, 80 to 95% of the SIRM was reached suggesting that magnetite/maghaemite was dominant. Magnetite/maghaemite would saturate by 300 mT (O'Reilly, 1984). Above 300 mT the curves continued to climb but less steeply. In the case of TR01 7B and AG02 32B (Figures 8.2a and c) the curves almost, but do not completely flatten out, which would indicate saturation. However, a jump in the IRM intensity of all sub-samples between 0.8 and 2T suggested the presence of a mineral, such as haematite or goethite, whose coercivity range is quite distinct and relatively unaffected until these higher applied fields. At an applied field of 2T the SIRM of these sub-samples lay in the range 0.73 to 96.56 x 10^{-5} Am^2kg^{-1}.

8.4. Identification of magnetic minerals using a log-gaussian approach.

A more quantitative method for the identification of magnetic minerals making up the components of a SIRM was proposed by Robertson and France (1994). They noted that for a single magnetic mineral an IRM acquisition curve can be represented by a cumulative log-gaussian function of the applied field. In a sample that contains a number of different mineral components their acquisition curves should amalgamate in a linear fashion. This approach has been utilised on the Chinese and Spanish speleothem sub-samples by modelling the gradient of the IRM acquistion curve. The relative amount and mean coercivity of each component can be calculated from the gradient of the IRM acquisition curve after fitting a log-gaussian distribution over several coercivity ranges.

8.4.1. Procedure.

In this study a FORTRAN program, IRMGRAD, written by Dr. T. Rolph was used in the modelling process. The gradient of the IRM acquisition curve, after being

normalised to the maximum gradient was plotted against the natural Log of the applied pulse field (i.e. Ln(field (mT)). This coercivity spectrum was then fitted with a curve by varying the following parameters for each of the chosen log-gaussian distributions; a) the centre field, which equals the mean coercivity of remanence, BO_{CR} b) the relative height and c) the standard deviation of the distribution. The percentage contribution to the total remanence of each fitted distribution was then calculated from the area under each curve. In fitting each curve it was found that 3 log-gaussian distributions gave a reasonable degree of fit. The parameters used to fit each distribution were maintained at similar values throughout the experiments so that intra- and inter-speleothem comparisons were possible. There may well be a further component represented by goethite which has high coercivities and generally does not saturate in fields < 4T (Lowrie, 1990; Eyre, 1994).

8.4.1. Results from the Chinese speleothems.

Using the log-gaussian technique for three components, fits were made to IRM acquisition data obtained from sub-samples of SC01, SC02, PT02, PT03 and PT04 (Figure 8.3a-e). Table 8.1 contains the relative amount, mean field and standard deviation calculated from the fit of each log-gaussian component. Overall there was reasonable intra- and inter-speleothem consistency between the fitted components. Because these speleothems were collected from hydrologically connected caves no distinction was made between the fitted components to the Chinese sub-samples.

Component 1 (Figure 8.3a) contributed between 8.4 and 22.0% of the SIRM and had a mean IRM coercivity of 31 mT. This value compares well with published data on the coercivity of remanence of SD magnetites which infer values between 15 and 40 mT (Thompson and Oldfield, 1986; Dunlop, 1986 and Maher, 1988). Component 2 (Figure 8.3a) contributed between 54.5 and 74% of the total SIRM and had a mean IRM coercivity of 126 mT (PT04 11B had a mean IRM coercivity of 100 mT; in this case Figure 8.1e also suggests a higher predominance of lower coercivity grains).

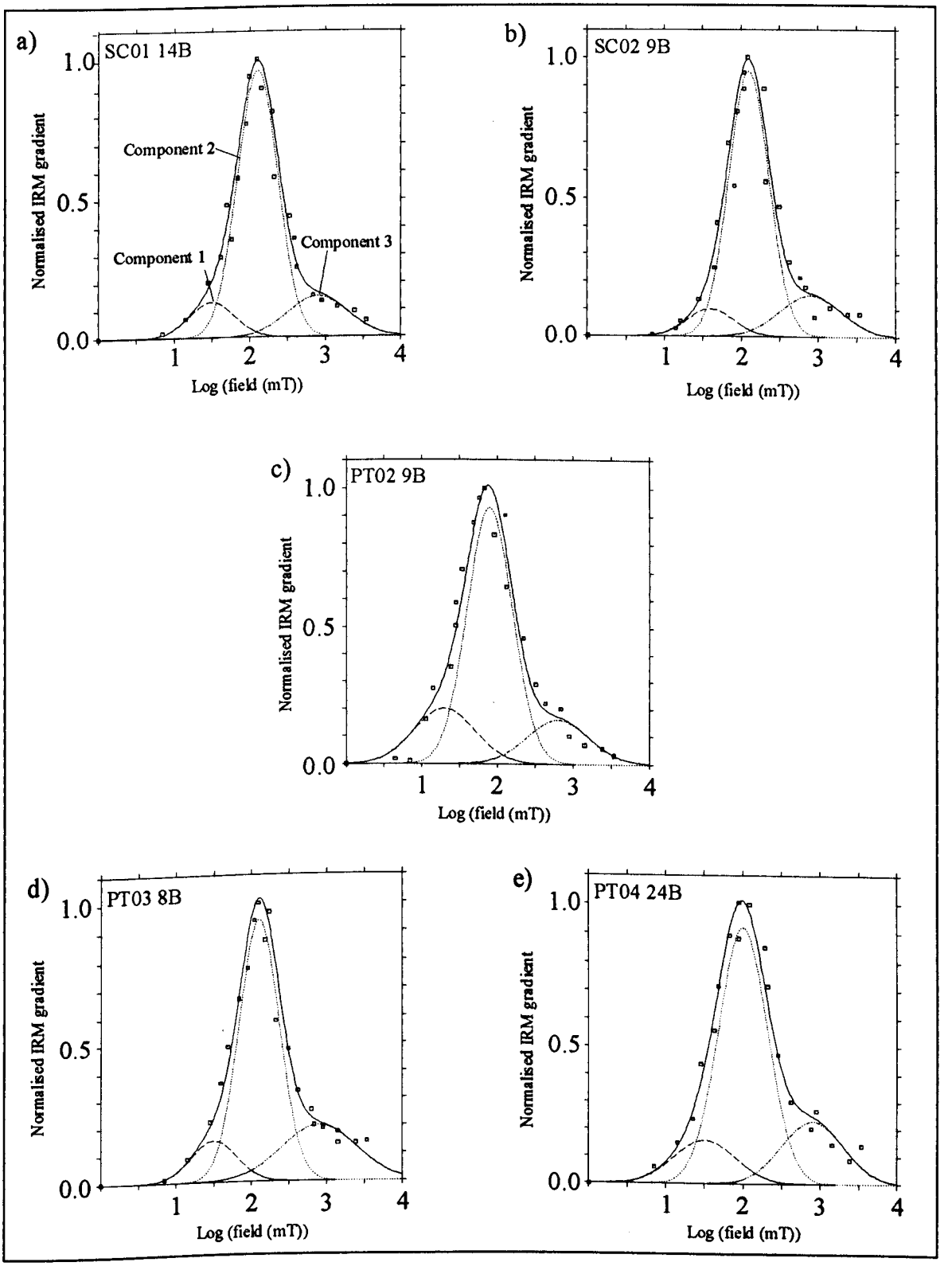

Figure 8.3. IRM coercivity spectra and log-gaussian fits to sub-samples from a)SC01, b)SC02, c)PT02, d)PT03 and e)PT04.

sub-sample	Component 1			Component 2			Component 3		
	mean field (mT)	standard deviation	% SIRM	mean field (mT)	standard deviation	% SIRM	mean field (mT)	standard deviation	% SIRM
SC013B	31.6	0.3	8.7	126	0.3	74.0	794	0.4	17.3
SC01 4B	31.6	0.3	10.9	126	0.3	66.6	630	0.4	22.4
SC01 14B	31.6	0.3	10.9	126	0.3	72.4	794	0.4	16.8
SC01 20B	31.6	0.3	10.0	126	0.3	72.7	630	0.4	17.3
SC01 22B	31.6	0.3	11.1	126	0.3	74.0	794	0.4	14.8
SC024B	31.6	0.3	11.9	126	0.3	72.3	794	0.4	15.8
SC02 9B	31.6	0.3	14.6	126	0.3	68.1	794	0.4	17.2
SC02 14B	39.8	0.3	8.8	126	0.3	72.3	794	0.4	18.2
SC02 16B	31.6	0.3	14.5	126	0.2	61.1	794	0.4	24.4
PT02 4B	20.0	0.4	18.9	126	0.3	66.0	631	0.4	15.1
PT02 9B	25.0	0.4	21.9	126	0.3	54.5	630	0.4	23.6
PT02 28B	31.6	0.4	22.0	126	0.3	56.0	630	0.4	22.0
PT02 40B	31.6	0.4	10.8	126	0.3	62.2	630	0.4	27.0
PT03 8B	31.6	0.3	11.1	126	0.3	64.1	794	0.5	24.7
PT03 9B	31.6	0.3	13.0	126	0.3	60.5	794	0.5	26.5
PT04 6B	31.6	0.4	12.4	126	0.4	68.6	794	0.4	19.0
PT04 11B	31.6	0.4	14.2	100	0.3	65.4	794	0.4	20.4
PT04 24B	31.6	0.3	8.4	126	0.3	69.2	794	0.4	22.4

Table 8.1. Results of individual log-gaussian fits to IRM coercivity spectra of sub-samples from SC01, SC02, PT02, PT03 and PT04.

Component 2 fell midway between the remanent coercivities of SD magnetite and haematite (Thompson and Oldfield, 1986) and could represent either a high coercivity magnetite phase due to low temperature weathering or a low coercivity haematite phase (O'Reilly, 1984). Component 3 (Figure 8.3a) contributed between 14.8 and 27.0% of the total SIRM and had IRM coercivities in the range 630 to 794 mT. These values were within the quoted remanence coercivity values for fine grained (SD) haematite of between 500 to 820 mT (Thompson and Oldfield, 1986; Dunlop, 1981; Dankers, 1981).

8.4.2. Results from the Spanish speleothems.

Log-gaussian fitting to the IRM spectra of sub-samples from TR01, TR02, AG02 and AG03 again allowed the identification of 3 coercivity distributions (Figure 8.4a-d). Table 8.2 contains the relative amount, mean field and standard deviations calculated from the fit of each log-gaussian component. No major differences existed between the fitted IRM coercivities despite the fact that Torca Regaton (TR01 and TR02) and Cueva del Agua (AG02 and AG03) are fed by different hydrological networks.

Component 1 (Figure 8.4a) contributed a small amount to the total SIRM (2.5 to 5.8%) and had a mean IRM coercivity of 6.3 mT. The coercivity of remanence of MD magnetite is quoted as around 15 mT (Thompson and Oldfield, 1986) but the low values from this study may be due to a lack of data in the <10 mT range. Component 2 (Figure 8.4a) contributed between 68 and 87% of the total SIRM and had IRM coercivities in the range 25.1 to 52.4 mT (mean 40 mT). This value is comparable to the quoted values of SD magnetites of between 15 and 40 mT (Thompson and Oldfield, 1986; Dunlop, 1986 and Maher, 1988). Component 3 (Figure 8.4a) was clearly identified as a hard magnetic mineral such as haematite, with a very distinct coercivity range. These IRM coercivities lay in the range 0.79 to 1.25T (mean 1.07T) which are somewhat higher than the quoted coercivity of 0.7T in haematite (Thompson and Oldfield, 1986; Dunlop, 1981). However, because the applied fields were to only 2T there may be some inaccuracy in the inferred coercivity ranges. Taking this in to account, component 3 contributed up to 26.2% of the total IRM. There is some possibility that this component

includes goethite which would not saturate at 2T. Therefore, it may have been useful to apply a 4T field to these sub-samples to highlight this component 3 more completely. However, further tests (section 8.5) suggested that goethite was not present.

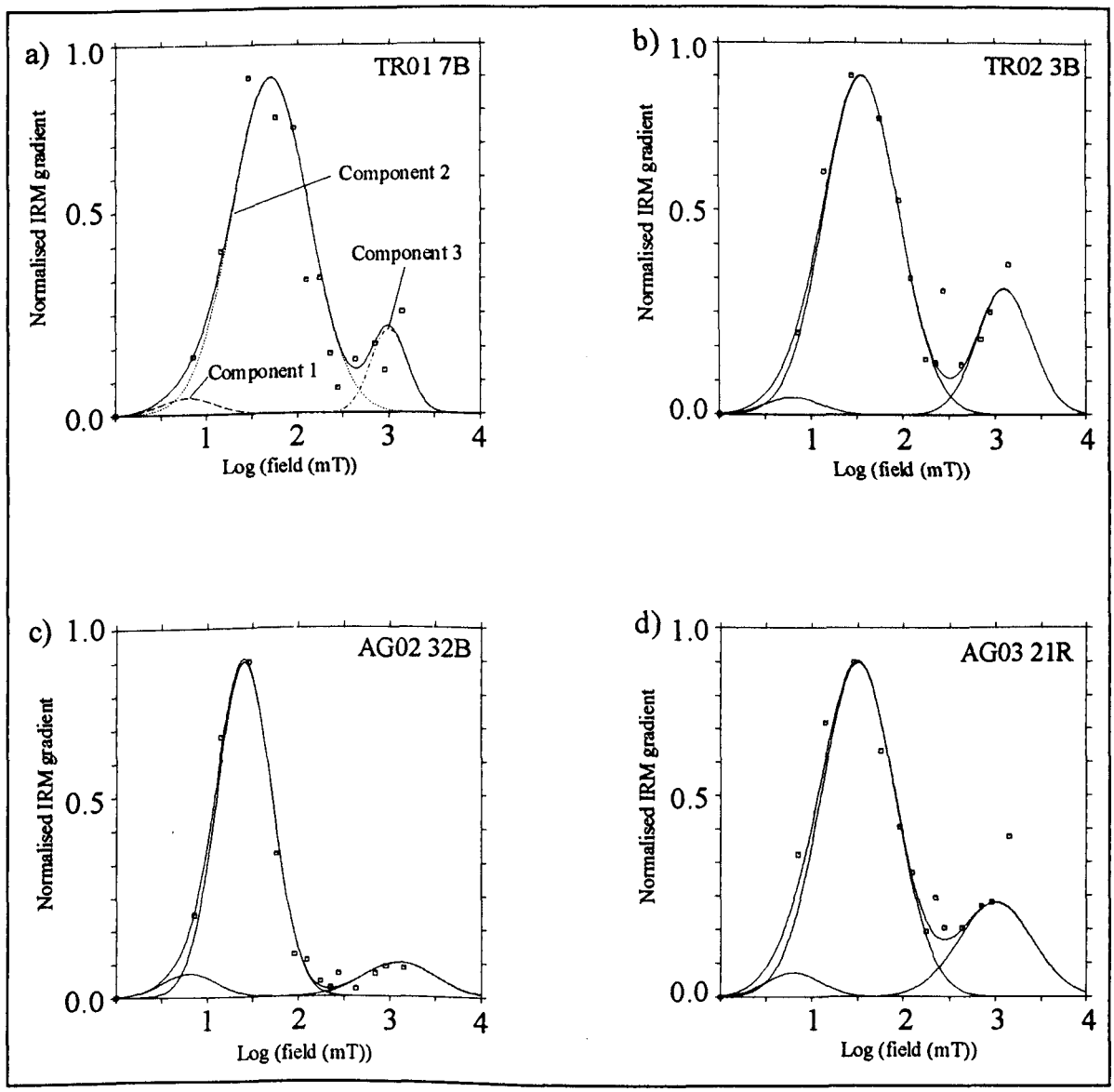

Figure 8.4. IRM coercivity spectra and log-gaussian fits to sub-samples of a)TR01, b)TR02, c)AG02 and d)AG03.

sub-sample	Comp. 1			Comp. 2			Comp.3		
	mean field (mT)	standard deviation	% SIRM	mean field (mT)	standard deviation	% SIRM	mean field (mT)	standard deviation	% SIRM
TR01 7B	6.3	0.3	3.1	50.1	0.4	86.6	1000	0.2	10.3
TR01 37B	6.3	0.3	3.1	50.1	0.4	86.6	1000	0.2	10.3
TR02 3B	6.3	0.3	2.9	35.5	0.4	76.0	1258	0.3	21.1
TR02 24B	6.3	0.3	5.8	50.1	0.3	68.0	1258	0.3	26.2
AG02 7B	6.3	0.3	4.4	52.4	0.4	83.2	794	0.4	12.5
AGO2 32B	6.3	0.3	5.8	25.1	0.3	83.1	1258	0.4	11.1
AGO3 21R	6.3	0.3	3.9	31.6	0.3	75.1	1000	0.4	21.0
AG03 31L	6.3	0.3	2.5	25.1	0.3	77.9	1000	0.4	19.6

Table 8.2. Results of individual log-gaussian fits to IRM coercivities of sub-samples from TR01, TR02, AG02 and AG03.

8.5. Thermal demagnetisation of a three component IRM.

Having identified the types of magnetic minerals present on the basis of their coercivity it seems appropriate to confirm their presence on the basis of their blocking temperatures. Lowrie (1990) found that three IRM coercivity fractions could be isolated in a cubic sample by using successively smaller applied fields on each axis. In this way the first (strongest) field remagnetises grains in a single direction, the second (smaller) field remagnetises grains with coercivities less than the second field in a perpendicular direction to the first and the third (weakest) field applied on the remaining axis remagnetises the lowest coercivity grains. By using stepwise thermal demagnetisation Lowrie (1990) found that detailed information on the blocking temperatures within each coercivity fraction could be obtained by plotting out the (demagnetised) values of each axis separately.

8.5.1. Laboratory method.

Three coercivity fractions were isolated using applied fields of 4T (2T for Spanish samples), 0.3T and 0.1T. It was hoped that fractions isolated in each field would include those components identified using the log-gaussian fits in section 8.4. After application of the final, 0.1T field, sub-samples were measured on a SQUID magnetometer (necessary to measure the weak magnetisations remaining after the higher stages of thermal demagnetisation). Stepwise thermal demagnetisation was undertaken in stages to 700°C and after each stage the values of the three orthogonal components of magnetisation were noted.

8.5.2. Results from the Chinese speleothems.

Figures 8.5a-c illustrate the thermal decay of each coercivity fraction during demagnetisation. These three IRM components have been normalised to their initial (room temperature) value for the purposes of inter-speleothem comparison.

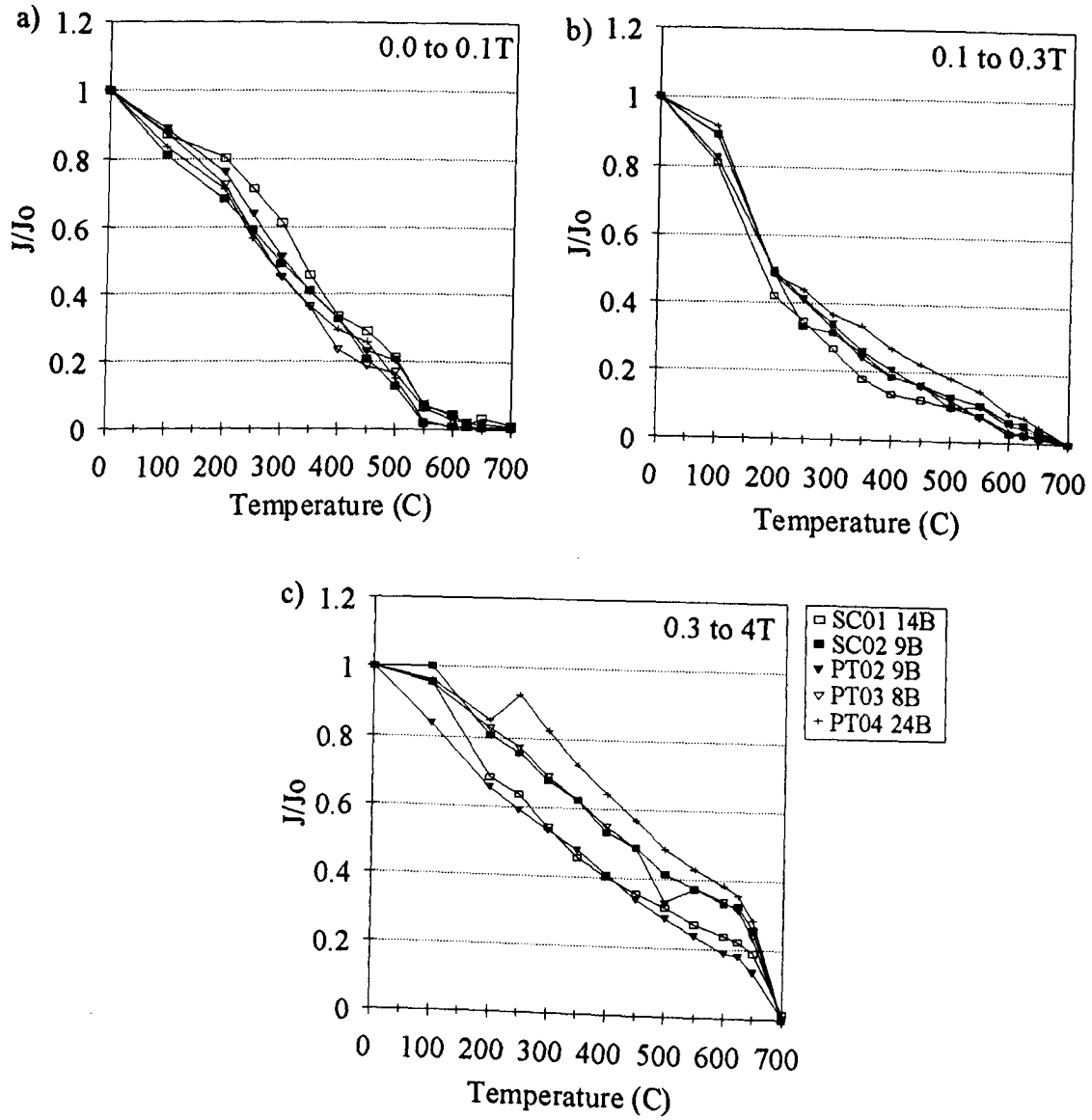

Figure 8.5. Chinese speleothems. Thermal demagnetisation of orthogonal IRMs produced by a) a 0.1T field b) a 0.3T field and c) a 4T field.

The 0 to 0.1T fractions (Figure 8.5a) decay almost linearly and complete unblocking occurs mostly between 500 and 550°C. This is indicative of titano-magnetite as a significant contributor to this fraction. The slight inflection in the curve between 100 and 300°C may indicate the inclusion a small percentage of maghaemite. Maghaemite completes its inversion to haematite around 350°C with a decrease in magnetisation (O'Reilly, 1984; Thompson and Oldfield, 1986).

The 0.1 to 0.3T fraction (Figure 8.5b) appears to include a greater percentage of maghaemite than the 0 to 0.1T fraction. This was illustrated by the significant decrease in intensities between 100 and 200°C and also the lesser decreases between 200 and 350°C as maghaemite inverted to haematite. From 350 to 550°C the component decays in a gentle curve until an inflexion between 550 and 600°C. This suggests the presence of magnetite as the predominant contributor to the remanence of this fraction. Unblocking is completed between 600 and 700°C indicating that haematite is present which may originate from the inversion of maghaemite.

The 0.3 to 4T fractions show a linear decay in intensity and unblock completely between 650 and 700°C. This indicates that haematite carries the largest proportion of the remanence of this fraction as there is no evidence to suggest the presence of goethite. Goethite would most likely be illustrated by unblocking and decreases in the IRM intensity between 60 and 170°C.

8.5.3. Results from the Spanish speleothems.

The decay of each coercivity fraction with temperature is shown in Figure 8.6a-c in which each IRM fraction has been normalised to its SIRM value. The three orthogonally applied fields were 2T, 0.3T and 0.1T. In hindsight it would have been better to use a smaller third field of perhaps 0.05T to isolate the low coercivities identified in section 8.4.2 more effectively.

The lowest coercivity fraction 0-0.1T (Figure 8.6a) exhibited a gentle curve to complete unblocking between 500 and 600°C. This fraction includes components 1 and 2 identified in section 8.4.2. The unblocking temperatures indicate the presence of a (titano-) magnetite phase.

The intermediate coercivity fraction of 0.1-0.3T (Figure 8.6b) shows almost monotonic decay and completes its unblocking between 550 and 650°C. It is thus likely to be a magnetite phase and indicates that a fourth log-gaussian component with mean

field of around 125 mT could have been fitted to some of the coercivity spectra (Figure 8.4). The IRM coercivity spectra for AG02 32B in Figure 8.4c did not suggest that a component was present in the 125 mT region. During thermal demagnetisation of AG03 32B (Figure 8.6b) its decay is somewhat less rapid when compared with other sub-samples and its blocking temperature is between 600 and 650°C. This coercivity fraction in AG02 32B may therefore include some accessory maghaemite that inverts to haematite over 350°C. Alternatively this sub-sample may contain a greater proportion of higher coercivity/higher blocking temperature cation deficient magnetite.

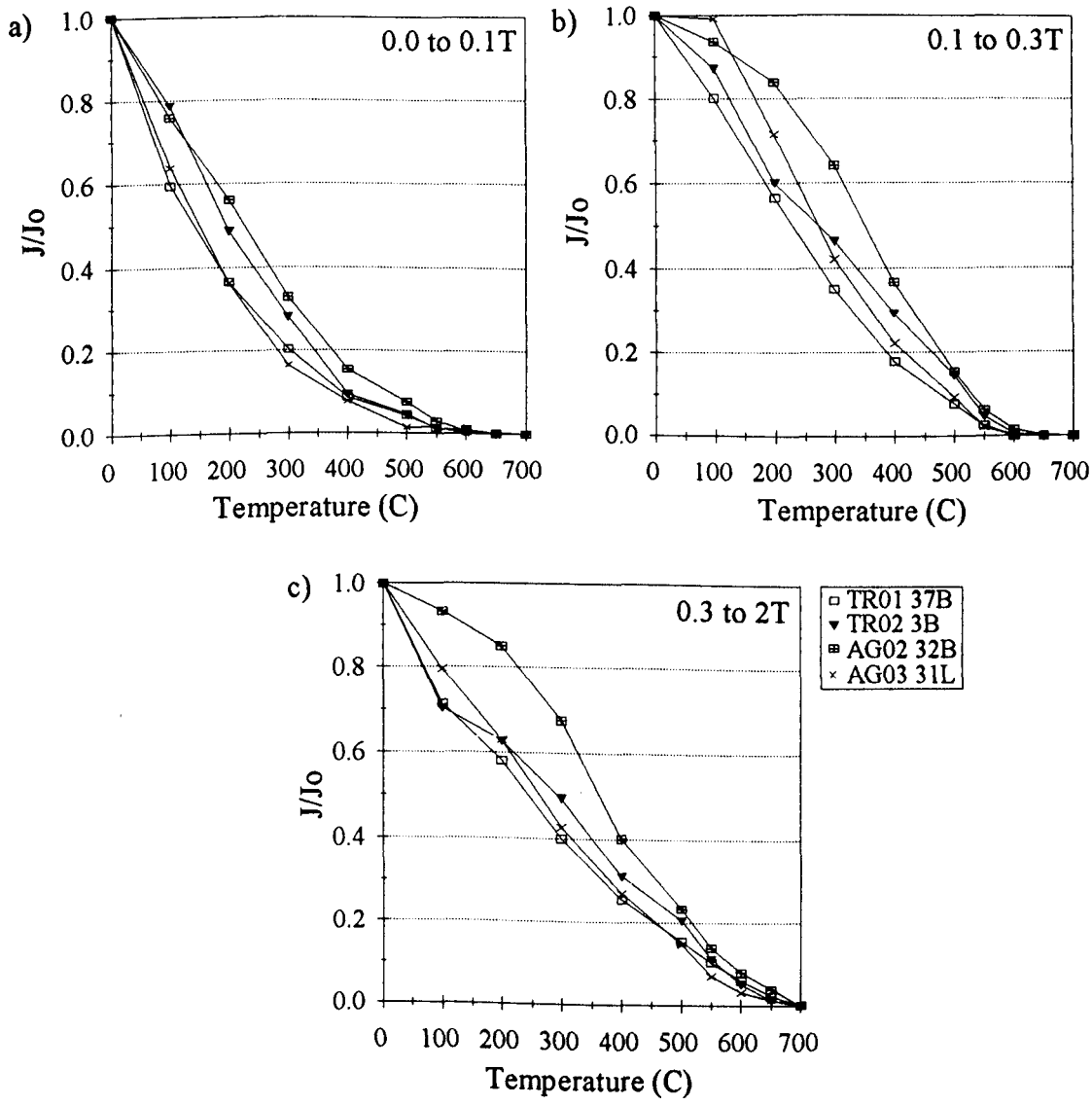

Figure 8.6. Spanish speleothems. Thermal demagnetisation of orthogonal IRMs produced a) a 0.1T field b) a 0.3T field and c) a 2T field.

The coercivity fractions of 0.3 to 2T exhibited maximum blocking temperatures greater than 650°C identifying haematite as a notable contributor to these fractions. Again, the remanence in sub-sample AG02 32B decays less rapidly as it contains greater overlap of components 2 and 3 identified in section 8.4.2 and therefore contains a greater proportion of higher coercivity ferrimagnetic minerals which unblock at lower temperatures.

8.6. Magnetic extract experiments.

In order to concentrate the magnetic minerals from each speleothem and thus make magnetic measurements on the Curie balance and VSM, magnetic extracts were taken using methods similar to that of Freeman (1986) and of Perkins (1993). The method involved the dissolution of the carbonate matrix of several sub-samples using acetic acid (buffered to pH4). After several days the remaining 'slurry' was centrifuged and washed with distilled water, in order to rinse away the remaining acid, and the residue was subsequently dried. The residue was then diluted in distilled water with Calgon, which was added as a dispersive agent. This mixture was pumped continuously from a reservoir through tubing including a semi-horizontal glass bulb held between the poles of a strong (300 mT) magnet. The magnetic material left in the bulb after several hours was flushed out using distilled water and acetone and then dried naturally in a Teflon beaker.

This technique was attempted on several lateral sub-samples but with little success. Even after extraction, the quantities of magnetic material were small and barely visible and it remained impossible to measure magnetic properties of combined extracts from a number of sub-samples with any degree of precision using either the VSM or the Curie balance. Using a similar technique, Perkins (1993) has reported extraction of 70-85% of ferrimagnets but only 15-35% of the canted anti-ferromagnets (based on pre- and post-extraction IRM moments). However, there were uncertainties associated with these calculated extraction efficiencies arising from losses during the extraction procedure, the effects of grain interactions and from reagent contamination.

Because of these problems, there must also be some question as to the validity of assessing the magnetic properties of a material when not all fractions of the original magnetic population remain or are not collected. Eyre (1994) has shown that magnetic extraction, using these and other similar methods, preferentially concentrates the ferrimagnetic fractions. A comparison between the results from log-gaussian fitting for IRM acquisition data from extracts and whole samples would provide some idea as to the coercivity fractions lost during extraction procedure. This was not attempted in this study as the rock magnetic tests outlined in sections 8.3 to 8.5 were thought to adequately represent the magnetic mineral assemblage in each speleothem.

By measuring the wt% of HNO_3 acid insoluble detritus remaining after dissolution during routine uranium-series analysis, a comparison with the original sub-sample NRM intensity was possible. It was thought that this would give an indication as to the importance of detrital magnetic fractions. A contribution to the magnetisation of speleothems from chemically derived magnetic carriers have been suggested by several authors (Latham and Ford 1993; Latham *et al*, 1989; Lean, 1995 and Perkins and Maher, 1993). The suggestion is that the weak magnetisation in clean speleothems results from a CRM and the contribution from a CRM to the NRM in dirty (detritally loaded) speleothems is, usually, small. The relationship between weight % of undissolved material and the NRM intensity should therefore be linear in the presence of a predominantly detrital magnetic fraction. A suite of samples from a single locality would be expected to have an NRM intensity that increased in proportion to the quantity of [magnetic] detritus (Noel, 1990; although he suggested an 'approximate' relationship).

The weight % of detritus remaining in the Chinese speleothems was between 0.01 and 0.29% and in the Spanish speleothems was between 0 and 0.02%. Figures 8.7a and b shows the relationship for Chinese and Spanish sub-samples. There is a clear relationship between weight % acid insoluble detritus and NRM intensity for the majority of Chinese sub-samples (Figure 8.7a) as shown by regression coefficients, 'r', in the range 0.84 to 0.99. The weight % of detritus from PT03 sub-samples had a weak relationship with their NRM intensity.

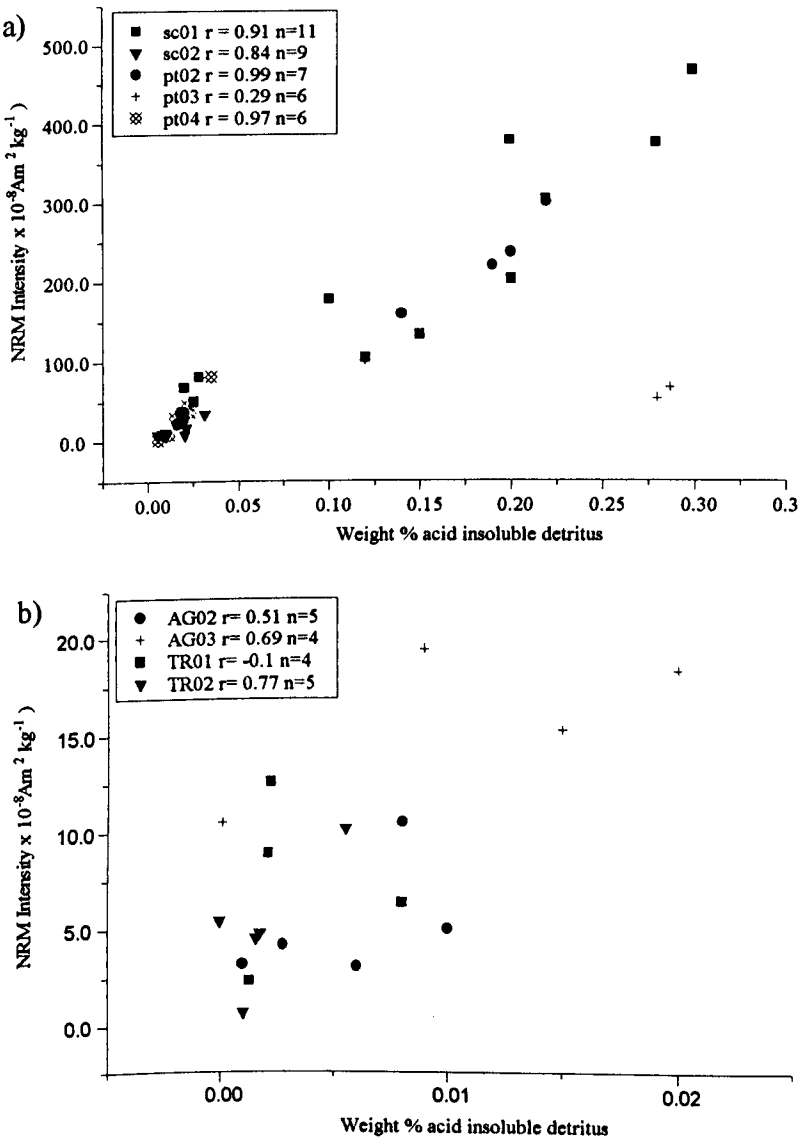

Figure 8.7. Relationship between sub-sample NRM intensity and weight % 7M HNO_3 insoluble detritus for a) Chinese sub-samples and b) Spanish sub-samples.

Therefore, in the majority of these Chinese speleothems the positive relationship between their detrital loading and NRM intensity suggests that the remanence is dominated by detrital magnetic fractions; a DRM. The same relationships for Spanish sub-samples were less clearly defined; regression coefficients ranged from -0.1 to 0.77 (Figure 8.7b). This was probably due to a more uniform distribution of detrital material. It would also be easy to say that the weak NRMs of these Spanish speleothems was

predominantly due to a CRM which bears no relation to the quantity of detritus. However, visual inspection showed that the Spanish speleothems did contain detritus. Thus, there is some ambiguity in this hypothesis and more substantial work is needed to decrease the uncertainties.

We should take some care in the interpretation of these results. The acids normally used for dissolution during uranium-series dating are more aggressive than the usual acids used for extracting magnetic phases. Freeman (1986), for example, used acetic acid buffered to pH 4.0. The effect of 7M HNO_3 acid on the magnetic phases in this case are unknown. The remaining undissolved fraction will also include non-magnetic minerals, such as quartz. Thus, erroneous inferences can be made about the weight % of magnetic fractions using data which also includes non-magnetic fractions.

8.7 Summary.

Performing a wider range of rock magnetic measurements was difficult with such low concentrations of magnetic minerals in these speleothems. An indication as to these concentrations was gained from the small (<0.3 wt%) quantities of detritus remaining after dissolution of sub-samples. The inclusion of a significant proportion of antiferromagnetic minerals has undoubtedly compounded the measurement problems.

Despite using tests based only on IRMs (IRM acquisition, log-gaussian fitting to IRM acquisition and thermal demagnetisation of orthogonal IRMs) these experiments served to highlight the predominant magnetic mineralogy of both Chinese and Spanish speleothems.

The Chinese speleothems contained magnetite for the most part, with haematite as a secondary but also important carrier of remanence. Remanence properties, illustrated using IRM acquisition and thermal demagnetisation of orthogonal IRMs, suggested that the intermediate coercivity (126 mT) component (component 2) carried the majority of remanence (54 to 74%). This component unblocked completely between

550 and 600°C which compared well with unblocking temperatures associated with magnetite (T_c=575°C; Thompson and Oldfield, 1986; O'Reilly, 1984). Coercivities in component 2 were higher than those commonly quoted for SD magnetite which suggested that some low temperature oxidation had occurred. Maghaematised rims can form on magnetite during low temperature weathering processes (O'Reilly, 1984). Component 1 (0-0.1T coercivity fraction) also had the coercivities and Curie temperatures characteristic of SD magnetite. We can conclude that partially oxidised magnetites of component 2 are accompanied by relatively unweathered magnetites of component 1. The high coercivity fraction (0.3 to 4T; component 3) had coercivities in the range 630 to 794 mT and unblocked at temperatures indicative of haematite (T_c=675°C; O'Reilly, 1984). This high coercivity (SD) haematite appears to carry a significant proportion of the SIRM (15 to 27%) and probably accounts for the 20% or so of the NRM not removed by AF cleaning at 170 mT (Chapter 6). Thermal cleaning of the NRMs up to 700°C showed that both magnetite and haematite carried the primary remanence (Chapter 6). Maghaemite has also been identified in accessory amounts from alteration characteristics during thermal demagnetisation (section 8.5.2). The presence of goethite was not indicated during thermal demagnetisation suggesting that the lack of saturation in 4T applied fields was predominantly due to haematite.

The magnetic mineral assemblages within the Spanish speleothems were composed in the main from magnetite and to a lesser, but significant extent, from haematite. Maghaemite was detected from its inversion to haematite during thermal demagnetisation. Component 2 (0.1 to 0.3T fraction) carried the majority of the SIRM and displayed the characteristic thermal properties of magnetite (T_c=575°C). Component 1 (0 to 0.1T fraction) was not particularly well defined using the log-gaussian fitting technique (section 8.4.2) and the orthogonal field applied (section 8.5.3) probably activated some grains of component 2. However, thermal demagnetisation behaviour showed that some titanomagnetite was present in this fraction as unblocking temperatures of <575°C were noted. The low IRM coercivities of this component also appeared to suggest the presence of some MD magnetite which contributed to this fraction. Component 3 (0.3 to 2T) was perhaps most interesting. The IRM log-gaussian fitting technique showed that its coercivity range was both distinct and relatively narrow.

Although the maximum applied field was only 2T, the fitted curves did not appear to illustrate the presence of goethite, at least in this coercivity range. Through thermal decay of the 0.3 to 2T fraction, component 3 was clearly identified as haematite. There was no evidence to suggest the presence of goethite which would [partially] be included in the fraction and would unblock at temperatures between 60 and 170°C (O'Reilly, 1984). The remanence coercivity of haematite is generally quoted as around 0.7T but the log-gaussian fitting experiments suggested values up to 1.25T. The cause for haematites high coercivity is uncertain but may result from stress in the basal plane (O'Reilly, 1984; Stacey and Banerjee, 1974). The high MDFs encountered during AF demagnetisation and the incomplete removal of the NRM at high AFs can be attributed to the presence of this haematite fraction.

The potential for distinguishing between a DRM and a CRM within a speleothem has been illustrated in section 8.6. These initial results suggest that this may be a valid method to classify the dominant type of remanence in future speleothem studies. The relationship between NRM intensity and weight % undissolved detritus is very clear in the case of the Chinese speleothems. However, the correlation is positive, but less clear in the case of the Spanish speleothems. Future work may also examine the relationship between IRM intensity and weight % undissolved detritus which may indicate the relative contribution to the NRM, if any, from high coercivity fractions such as haematite. It would also be interesting to see the effects of different acid strengths on the NRM-weight % relationship. For the different magnetic minerals this may indicate the degree of resistance to acid attack. If this method is coupled with the identification of the magnetic fractions using the log-gaussian fitting function and their blocking temperature spectra then we have a method to characterise the magnetic properties of the DRM fraction alone. If the DRM contribution can be subtracted then we have some method, as yet untested, to calculate the contribution to the NRM from a CRM.

9. Conclusions and the potential for future work.

9.1. Introduction.

This study has successfully produced contemporaneous records of PSV from Chinese speleothems, and somewhat less successfully, from Spanish speleothems. The high degree of inter-correlation between the Chinese records and other contemporaneous, non-speleothem records have unequivocally shown that speleothem PSV records reflect true palaeomagnetic field behaviour. As previous studies have concentrated on producing individual speleothem records, the specific analysis of multiple speleothems from single localities has remained incompletely explored. To quote Latham (1981);

'A full assessment.. will only be finalised with the production of other overlapping or contemporaneous (speleothem) *records'*.

Thus, this study has probably gone some way to further promote the value of speleothem PSV records as a viable alternative, and as a compliment, to records derived from sediments. Although sediments frequently suffer from depositional and sampling effects speleothems do not and their freedom from depositional effects has been demonstrated again in this study. However, the records produced from especially the Spanish speleothems illustrate again the main problem in using speleothems to gain information on PSV. This is the problem of low magnetic mineral concentrations giving rise to weak and immeasurable magnetic remanences. Nevertheless, the one reasonable record produced from Spanish speleothem AG02 compared well with the UK lake sediment master curve of Turner and Thompson (1981). Thus, there continues to be some luck associated with collecting suitable speleothems for both palaeomagnetic and uranium-series dating work. However, in these cost conscious days, sampling of speleothems for studies on PSV is faster and requires much less logistical support when compared with most sediment coring (cavers are usually cheap and run on alcohol!). However,

speleothem PSV records will never entirely replace sedimentary records because the latter are generally longer, often have higher resolution and are often selected prior to sampling on the basis of approximately known age. We must also be aware that speleothems are objects of great beauty and large scale sampling should only be undertaken after careful consideration of the aesthetic impacts on the cave environment.

9.2. Uranium-series dating.

9.2.1. Dating problems: causes and effect.

The accuracy of uranium-series dates from the speleothems in this study, excluding those from TR01 and TR02, were generally low. The percent errors associated with individual sub-sample dates ranged from 8 to 187% and the majority were much less than the quoted accuracy of 5-10% for alpha-spectrometry (Schwarcz, 1989). In contrast, the dates for individual sub-samples from TR01 and TR02 had percent errors of between 1 and 6%. In many ways TR01 and TR02 could be described as ideal samples on which to perform uranium-series analysis because they had high concentrations of uranium and low quantities of detrital contamination. Several reasons appear to have acted in combination to produce these larger inaccuracies, discussed as follows.

All of the Chinese and two of the Spanish speleothems (AG02 and AG03) had uranium concentrations that were on the whole less than an order of magnitude greater than the normal limit recommended for alpha-spectrometry (0.05 ppm; Ivanovich and Harmon, 1992). In fact, some sub-samples from AG03 had uranium concentrations less than 0.05 ppm which has increased the isotope counting errors. These errors have also been compounded by the low quantities of ^{230}Th, a result of the young ages. In addition, $^{230}Th/^{232}Th$ ratios were typically $<<5$ and sometimes <1 indicating that detrital contamination levels were high. Thus, a large degree of uncertainty was introduced when differentiating authigenic ^{230}Th from detector background and allogenic uranium and thorium isotopes. In fact, for sub-samples of SC01 the $^{230}Th/^{232}Th$ ratio of 0.8 in the uppermost sub-sample indicated that there was more detrital thorium than allogenic

thorium. For each sub-sample the overall effect was to increase the counting errors of each isotope, particularly for ^{230}Th. Finally, the chemical yields of uranium and thorium were initially very low; typically <10% for thorium and <20% for uranium. This situation was improved considerably after adopting the modified Hallstadius method for electrodeposition of planchets (section 4.5.4). Despite yields being consistently higher the decreases in the dating uncertainties were not as marked as one would have liked and in this study the accuracy of an individual sub-sample date seems to be almost yield independent. The effects of chemical yields on dating uncertainties are detailed later.

Which of these problems outlined above has had the greatest effect? If we look at the results from TR01 and TR02 whose sub-samples, generally, had high chemical yields, high uranium concentrations and low detrital contamination we may see the following:

1) Sub-samples from TR01 had relatively high chemical yields excepting sub-sample 39B which had low yields of both U and Th (7% and 10% respectively; Table 7.3). The percent age error for 39B was 6% compared to the lowest error of 2% in sub-sample 8B which had the highest chemical yields. The age error of 39B was also within the normal 5-10% accuracy of alpha-spectrometry (Schwarcz, 1989). Sub-sample 6B which had a U yield of only 10% but had a higher Th yield of 31% similarly had percent age errors of only 5%. Thus, in these cases, the lower yields appear to have only marginally affected the percent age errors, although admittedly this suggestion is based on only two results.

2) The dates from TR01 required no correction for detrital contamination. In contrast, TR02 required a correction to three of its five dated sub-samples (Table 7.4). Even though a correction was applied to the youngest three sub-samples, where the effect from detrital contamination would be greatest, the corrected dates had errors of between 4 and 6% (Table 7.4). The percent errors of the dates not requiring correction (15B and 20B) were between 1 and 3%; not significantly different. It is difficult to calculate the effect of detrital contamination alone in the Chinese speleothems because all required a correction and all had relatively low uranium concentrations.

3) Compared with the other speleothems in this study, uranium concentrations in both TR01 and TR02 were constantly high at 1.0 to 1.8 ppm and at best were 36 times greater than the minimum required for alpha spectrometry (Ivanovich and Harmon, 1992). All dates calculated from sub-samples with these high uranium concentrations had percent age errors that were low (<10%).

Thus, in both Chinese and Spanish speleothems, it appears likely that low uranium concentrations and high levels of contamination have had the greatest effect in lowering the precision of a given date. The effects of chemical yield variation upon age errors after the adoption of the Hallstadius method are thought to be minimal. This is reinforced by preliminary work (Dr. C. Lean, unpublished work) which shows that yields greater than about 30% do not significantly reduce specific dating errors. The largest percent age errors are, generally, associated with the youngest ages (Figure 9.1).

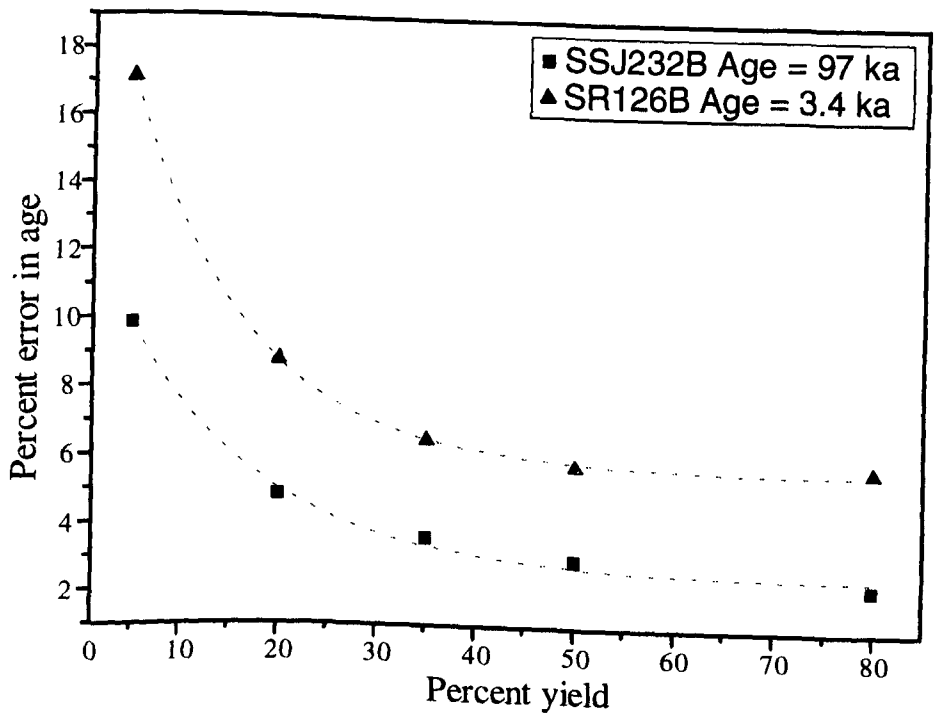

Figure 9.1. The effect of variation of the chemical yield on the percent age errors of speleothem sub-samples of intermediate and young ages. a) SSJ3 2B, 97 ka and b) SR1 26B, 3.4 ka. Both speleothems are from Mexico (17°N 268°E). The dotted lines are intended to suggest a trend in the data of each speleothem. Unpublished data from C. Lean.

The results in Figure 9.1 were derived from back-calculation of a standard uranium-series analysis to simulate the percent age errors associated with differing chemical yields. These samples had no measured detrital thorium contribution and had uranium concentrations of >0.5 ppm. Thus, the influence of chemical yield alone could be assessed. In each case, the simulated yields of uranium and thorium have been maintained at the same level for each calculation and thus, the isotope ratios remain unaltered. It is possible to see that yield increases above 30% decrease the age errors by only a few percent. For example, the differences in percent age errors between chemical yields of 35 and 80% for SSJ3 32B and SR1 26B are 1.3 and 0.7% respectively. The difference in age errors between chemical yields of 5 and 35% are 6 and 10% respectively; a change that could become significant in young samples. Thus, in this study the initial increases in dating accuracy achieved by changing from the initial electroplating method to the Hallstadius method (sections 4.5.3 and 4.5.4) were probably significant. However, as yields were generally maintained above 35% using the Hallstadius method any effect on the accuracy of a sub-sample date from yields alone was likely to be negligible.

The accepted lower working detection limit for alpha-spectrometry is 5 ka (Schwarcz, 1980). Below this age the ability to resolve the lower counts of isotopes over background diminishes. This is especially the case when dealing with samples of low uranium concentration as found in the Chinese speleothems and in AG02 and AG03 from Matienzo. However, this problem has been greatly improved in the Liverpool U-series laboratory by the use of low background, high resolution 'PIPS' detectors. These detectors can resolve the ^{228}Th and ^{224}Ra backgrounds (section 4.7.1) and allow separate corrections to be made to the corresponding uranium and thorium spectra. Thus, reliable dates can be produced in samples <5 ka and this is particularly the case for samples with high uranium concentrations such as TR01 and TR02.

9.2.2. Electroplating.

A comparison between two electroplating procedures illustrated the major source of yield loss during chemical separation of uranium and thorium (section 4.5). Tests

using the original electroplating method suggested that no immediate improvement to chemical yields could be made (section 4.5.3). The modification and subsequent adoption of the Hallstadius method (Hallstadius, 1984) in April 1994 dramatically increased yields from <10% for thorium and <20% for uranium to between 40 and 90% for both isotopes. The modified Hallstadius method is now part of the routine uranium-series procedure in the Liverpool laboratory. The improvement in chemical yields means that the sample count rates are easily distinguishable above counter background thus satisfying the criteria of Komura and Sakanoue (1964). They suggested that the detection limit is four times the standard deviation of the background count rate i.e. $4(b/T)^{½}$ where b is the background countrate and T is the count time of the blank run.

9.2.3. The L/L method and implications for routine U-series analysis.

Dates of selected Chinese sub-samples calculated using the MLE data treatment technique of Ludwig and Titterington (1994) were disappointing. The reasons and potential remedies for these poor results have already been discussed (4.9.2). Despite these problems the potential of the method is such that L/L analysis should almost certainly be undertaken routinely when dealing with heavily contaminated samples. The L/L method, with dates calculated using the MLE algorithm can considerably reduce the doubt attached to a series of ages corrected using only an estimated initial thorium ratio. Despite the dating inaccuracies of sub-samples in this study, the correlations between similarly aged features in a) the individual Chinese records (Figure 6.30) and b) in other contemporaneous records (Figures 6.31a and b; Figure 7.14) corroborates the overall dating accuracy.

These limited L/L results, particularly those from analyses of SSJ2 (section 4.9.1) suggested an interesting possibility that may arise during routine uranium-series analysis of young (<10 ka) and contaminated sub-samples. If a sub-sample has a $^{230}Th/^{232}Th$ ratio of <25 then it is deemed to be detritally contaminated. A routine uranium-series date is normally obtained from a single sub-sample and in effect, this represents a single leach. If the sub-sample is detritally contaminated then the acid used for dissolution will affect the

quantity of detrital thorium and uranium carried over into the leachate. This in itself will increase the $^{230}Th/^{234}U$ ratio and produce an apparently increased age. Because detrital contamination is independent of the authigenic isotopes any changes in the measured $^{230}Th/^{232}Th$ ratio will result in differing degrees of correction throughout a series of 'dirty' samples. Figure 9.2 shows this effect using a plot of $^{230}Th/^{234}U$ versus $^{230}Th/^{232}Th$ from L/L analyses of coeval sub-samples from SSJ2 (section 4.9.1).

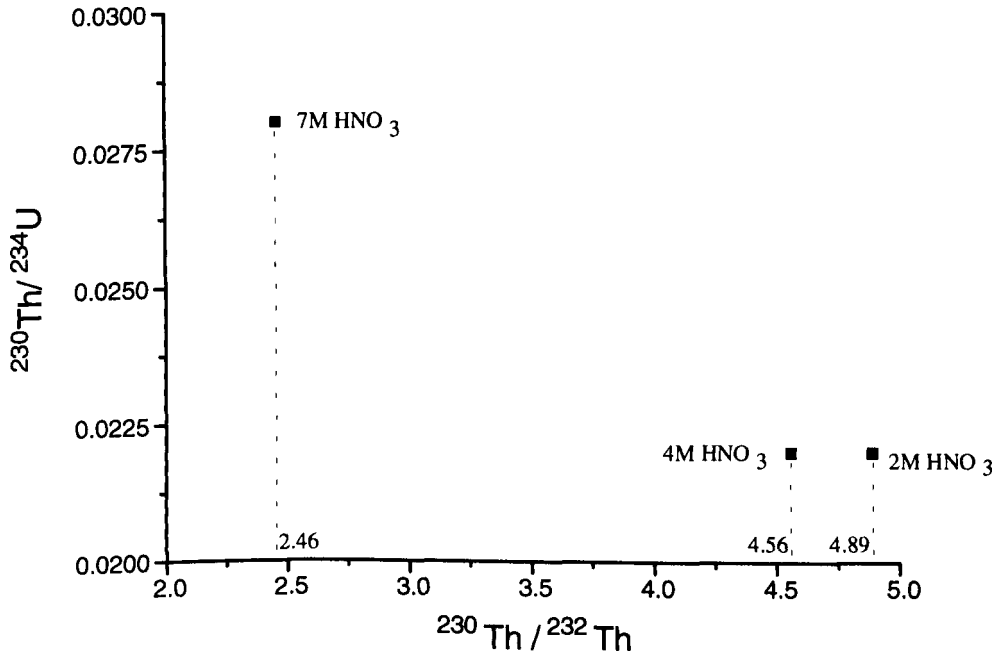

Figure 9.2. Effects of different acid strength on the measured $^{230}Th/^{232}Th$ ratio of three coeval samples from Mexican speleothem SSJ2. Despite each sample being coeval the changing $^{230}Th/^{232}Th$ ratio produces differing correction factors and subsequently different calculated dates (Table 4.4)

In the case of SSJ2, for each of the HNO_3 leaches (deemed to be more reliable than the HCl leaches in this case; section 4.9.1) the $^{230}Th/^{232}Th$ ratio decreased with increasing acid strength (the $^{230}Th/^{234}U$ ratio increased because of the increased input of detrital thorium). Thus, in a routine uranium-series procedure the $^{230}Th/^{234}U$ and $^{230}Th/^{232}Th$ ratios (and hence the age) observed in analyses of single sub-samples would be dependant upon the strength of the acid used. For example, Table 4.4 shows that the uncorrected date from each coeval leach from SSJ2 becomes older with more detrital

leaching, as expected. Despite all samples being coeval, corrections using an initial thorium ratio of 1.5, produced dates that varied between 1.7±0.4 ka (when using 2M HNO_3) and 1.2±0.5 ka (when using 7M HNO_3). These dates are equal within the 1σ confidence limits but examination of Table 4.4 shows that the dates are increasingly reduced with increased acid strength. Thus, at the very least the acid used for dissolution during routine uranium-series analysis should be of constant molarity.

Thus, a PSV record dated from 'dirty' samples with no assessment of the effects on age from the detrital isotopes (using the L/L or some other method) and dated using standard uranium-series procedure, could suffer from age-shifting by at least several hundred years. In the absence of further dates, such as those produced using the L/L method which takes contamination into account, this shift in age remains unknown. In actual fact, the dates from individual SSJ2 leaches were all over-corrected using an initial thorium ratio of 1.5 according to their MLE date of 2.1±0.3 ka (Table 4.4).

9.3. ^{210}Pb dating and its potential for dating young speleothems.

The results from the ^{210}Pb dating were promising (section 4.10). The technique has the potential to measure accurately the short-term growth rates over periods of, perhaps, as little as 2-3 years by careful sampling of growth layers. In addition, it can demonstrate whether a speleothem has grown during the past 150 years. Thus, estimates on growth rate based on ^{210}Pb would compliment and, perhaps, replace in some cases those estimated from U-Th dating over this time range. Even with precise U-Th dates the identification of growth rate changes, or even stoppages, less than 200 years are unlikely. For example, using U-Th disequilibrium the lowest age errors achieved for individual sub-samples in this study were ±0.1 ka (TR01).

In part, the non-linearity in unsupported ^{210}Pb activity in the older growth layers of PT03 (Figure 4.10) could be explained by the imprecise method of sampling these layers. Thus, the time periods covered by the material from each scrape may not have been equal. In future work the use of small dental drills (as used in oxygen isotope work)

may prove a more accurate method of sampling especially when growth layers are on such a fine <1 mm scale. The mismatches in the growth rates of PT03 calculated from U-Th and ^{210}Pb dating reflect the low U concentrations and detrital contamination. Thus, it would be interesting to compare the growth rates obtained using the ^{210}Pb method and the U-Th methods on a clean speleothem with high uranium concentrations. This would indicate the validity of extrapolation of ^{210}Pb growth rates over long periods of time.

9.4. Secular variation in speleothems.

9.4.1. Errors in speleothem orientation.

As discussed in section 6.9.2.1 the most likely cause for the westerly declination biases and shallow inclinations in the Chinese speleothems appears to be cutting errors imparted during the preparation of the central vertical slice on the large diameter rock saw for which no effective correction could be applied. Of the Spanish speleothems, only one reasonable PSV record was obtained from AG02. Its inclinations were also slightly shallow at 56.4° but was within the α_{95} confidence limits of the GADF inclination value of 61°.

For the Chinese speleothems, it is also possible that over the periods of their growth the field in Xingwen was biased to the west and was shallower than the GADF due to the influence of the Mongolian anomaly. This possibility is thought to be less likely than cutting errors as there have been no such long term biases reported in other (non-speleothem) records from China or Japan (the sedimentary record of Hyodo *et al* (1993) was not oriented and declination and inclination were centred about their means). Experiments in this study (Chapters 6 and 7) and in other studies (Latham *et al*, 1989, 1986 and 1981; Lean *et al*, 1995; Perkins, 1993) have shown that speleothems are free from the effect of depositional errors so an inclination error seems an unlikely explanation for these shallow inclinations.

9.4.2. Accuracy of the individual records of PSV.

The NRM intensities of both Spanish and Chinese speleothems were low. These low NRM intensities are common in speleothems and have been reported by several workers (Latham *et al*, 1986, 1989; Perkins and Maher, 1993; Lean *et al*, 1995 amongst others). The NRM intensity will be a function of the type(s) of magnetic mineral and of their concentrations. These increased errors (derived from magnetometer noise and incompletely nulled field during measurement and demagnetisation) coupled with the measurement of the low NRM intensities have decreased the precision of the directions obtained from some sub-samples. In this study precision was indicated by the MAD (α_{95} in the case of SC01). It was noted that an increase in directional scatter occurred during demagnetisation of the weakest sub-samples and during the later stages of demagnetisation in the stronger sub-samples. Despite this directional scatter the majority of directions trended towards the origin of the Zijderveld plots after the removal of any VRM. This was interpreted to be the primary remanence in each case.

Unfortunately, none of the Chinese speleothems were of sufficient width to allow double sub-sampling i.e. two parallel vertical slices. This method of sample preparation would allow at least two adjacent coeval sub-samples to be taken from the drip-cap of one central vertical slice (Figure 5.4). A second set of coeval sub-samples could be taken from the drip-cap of the second slice (a method used by Latham *et al*, 1989 for example). Thus, four directions may be obtained per horizon. Records produced from sampling in this fashion would have allowed a) inter-central slice comparisons b) intra-horizon directional consistency checks and c) a potential reduction in the measurement errors by allowing directions to be combined using Fisher statistics (Fisher, 1953). Limited double sub-sampling of this nature was possible with TR02. The second set of sub-samples were taken from the single vertical slice where the drip-cap was of sufficient width. Unfortunately, because of the weak magnetic signal no reliable directions were obtained.

Tests for the presence of inclination errors within the Chinese and Spanish speleothems were not exhaustive, primarily due to a lack of sufficient lateral material after sub-sampling. However, the tests performed (Chapters 6 and 7) indicated that there

were no differences in the directions recorded by central and lateral sub-samples. This suggests that errors due to surface effects were less the measurement errors. Differences in the directions obtained from coeval central and lateral sub-samples may be explained by the inclusion of some non-coeval material. However, despite the directional similarity between coeval sub-samples, the majority of Chinese records exhibited mean inclinations that were shallower than the GADF. The cause of this shallowing was thought originate from the cutting of each speleothem on the rock saw as discussed previously.

Good correlations existed between the individual speleothem PSV records (Figure 6.30) and with other contemporaneous records (Figures 6.31a and b). This illustrates that each speleothem has recorded PSV with reasonable accuracy. In some respects the fact that the individual PSV records from the Xingwen speleothems compared closely made up for the inability to obtain directions from multiple sub-samples from each horizon. In addition, this study has shown that the time resolution of recorded PSV is affected by speleothem growth rate. This relationship is shown in Figure 9.3 by comparing the sub-sample resolution against growth rate and VGP dispersion.

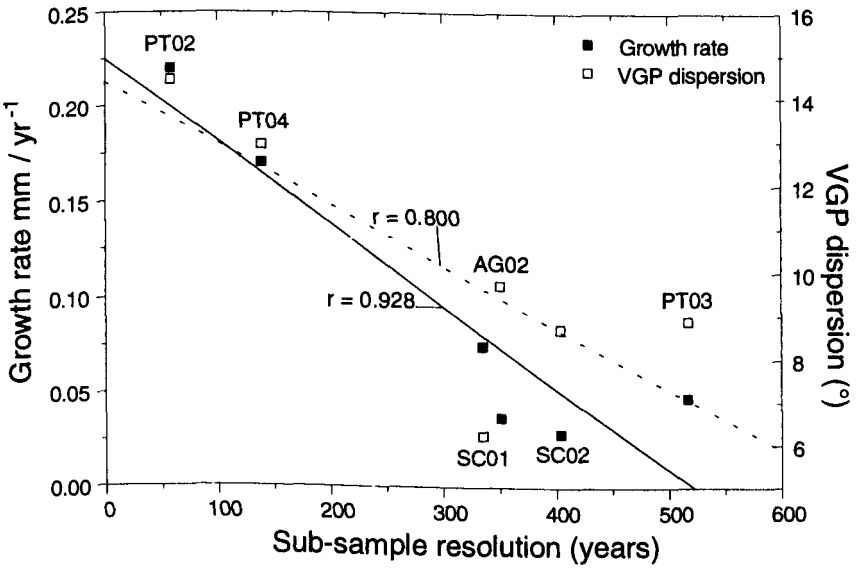

Figure 9.3. The relationship between sub-sample resolution, speleothem growth rate and VGP dispersion.

The effects of time averaging on the PSV signal should also be illustrated in records which are contemporaneous but which have differing sub-sample resolutions. Thus, the detail in a high resolution record should be represented in a lower resolution record but with the latter having decreased amplitude and detail. In order to assess the effects of a slower growth rate and hence a lower resolution of recorded PSV, the higher resolution records of PT02 and PT04 have been smoothed using a cubic spline approximation and then time-averaged over 400 year intervals using a 9-point smoothing filter. This has the effect of lowering the resolution of PSV recorded in sub-samples of PT02 and PT04 to approximately that in SC01 and SC02 (respectively 335 and 404 years per sub-sample). From Figure 9.4 the time-averaged data of PT02 and PT04 compare reasonably well in detail, amplitude and timing of recorded directions, particularly in declination. However, feature v in the inclination record of PT04 is more difficult to correlate with the other records and appearing approximately 0.5 ka earlier. However, these comparisons suggest that SC01 and SC02 are indeed recording the same features of PSV as PT02 and PT04 but with a lower resolution.

Figure 9.4 also compares the 1995 IGRF model values of declination and inclination at latitude 28°N taken at intervals of 20° in longitude as if the present day field at this latitude had drifted westwards past Xingwen at a rate of 0.13° yr^{-1} equivalent to one full cycle of westward drift. This rate of non-dipole drift is similar to those reported by several authors for Asia (Hyodo *et al*, 1993; Yang *et al*, 1993 and Aitken *et al*, 1989). Thus, the topmost values of declination and inclination of the IGRF in Figure 9.4 are the present day values at Xingwen. The agreement between directions of these records are good particularly for declination. The amplitudes of variation in the IGRF record are of the same order of magnitude as the speleothem records (±~25°) and the timing of recorded features are quite close considering dating inaccuracies associated with each speleothem record. This suggests that some features of declination and inclination result from the passage of non-dipole sources which have drifted westward past Xingwen.

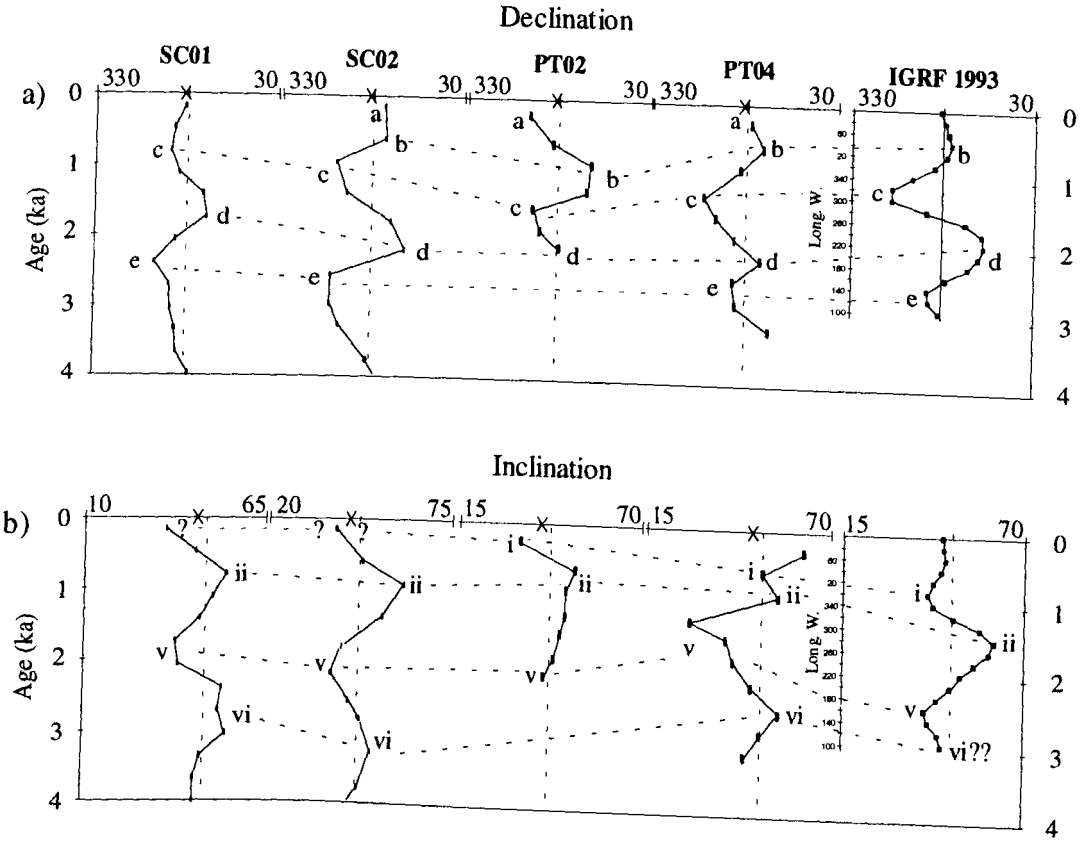

Figure 9.4. The effects of time-averaging on recorded PSV over the same period a) declination and b)inclination. The records of PT02 and PT04 were time-averaged to approximately the same resolution as SC01 and SC02. Also shown are the 1993 IGRF model values at latitude 28°N taken at intervals of 20° longitude as if the present day field were drifting westwards at a rate of 0.13° yr^{-1}.

A comparison with the drifted IGRF model has also been made for the Spanish record of AG02 (Figure 9.5). The PSV record also matches the general pattern of the IGRF model values at 43°N however, the correlation is less convincing than for the equivalent comparison using the Chinese speleothems. This is partly due to the lack of detail in the record of AG02 and also partly due to the lack of data from Matienzo in general. Greater difficulty was also encountered in comparing the UK master curve (Turner and Thompson, 1981) especially in inclination. There are also significant shifts in the timing of what appear to be the same features in the UK record and in the AG02 record and the IGRF construction. This is most likely to be due to the ~10° latitudinal separation between Matienzo and the UK. Clearly, when more records are available from Matienzo a better interpretation may be possible.

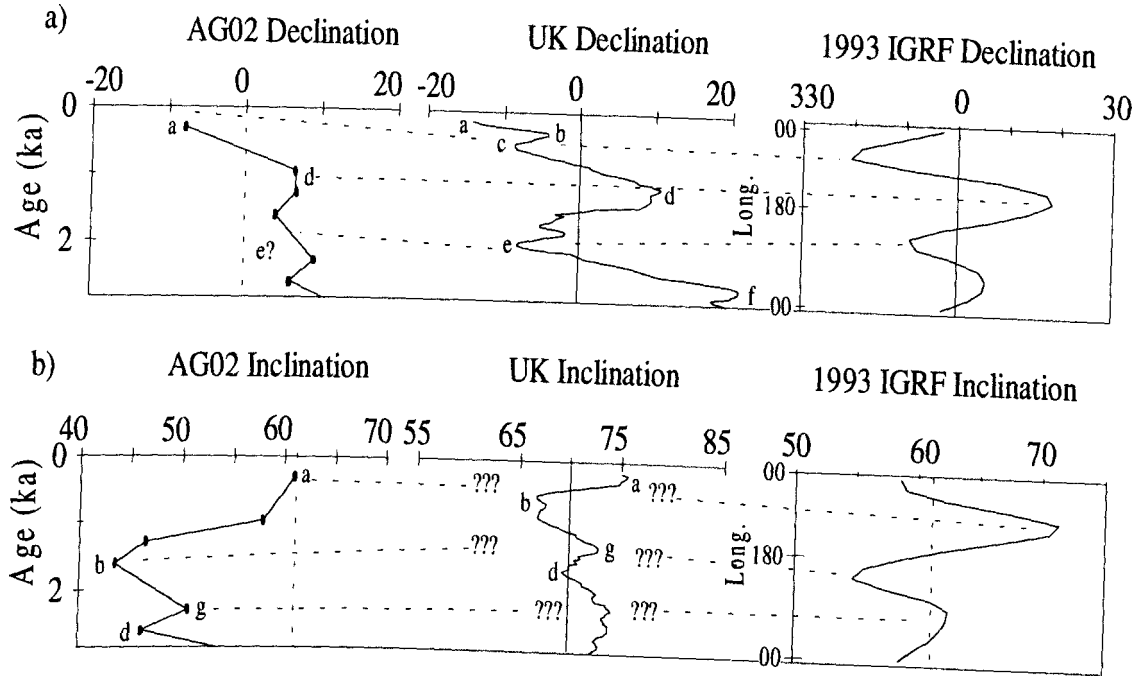

Figure 9.5. A comparison between the PSV record of AG02 (43°N 3°E), the UK master curve (~52°N 0.0°E) and the IGRF field values at latitude 43°N taken at intervals of 20° longitude as if the present day field were drifting westwards at a rate of 0.13° yr^{-1}.

9.5. Rock magnetism and remanence acquisition.

9.5.1. Rock magnetism.

In both the Spanish and Chinese speleothems there appears to be a mixture of SD ferrimagnetic [magnetites] and antiferromagnetic [haematite] grains (Chapter 8). It is also likely that a small proportion of MD magnetite are present. These magnetic minerals have been inferred from IRM acquisition and thermal demagnetisation. Magnetic properties of such mixtures have been studied only in superficial detail, one of the difficulties being that of separating out the frequently overlapping properties of each mineral. Many, previous studies have concentrated on exclusive blends of either magnetite or haematite and have not produced artificial mixtures of both with known proportions, grain sizes or domain state (Dankers, 1981; Maher, 1988).

Mixtures of ferri- and antiferromagnets were studied by Robertson and France (1994). They suggested that the cumulative log-gaussian fitting method gave the clearest picture of the relationships between IRM coercivities of ferri- and antiferromagnetic minerals within sample matrices. In this study, it has been more instructive to model the gradient of the IRM acquisition using a number of log-gaussian distributions (Eyre, 1994). This method has allowed the magnetic mineral coercivities identified in each sample to be compared to coercivities of known domain states. In addition, the percentage contribution to the total remanence [of the SIRM] from each coercivity distribution can be calculated. The thermal demagnetisation of orthogonal IRMs (Lowrie, 1990) provides a complementary method to determine the T_c of selectively activated minerals.

The magnetic mineralogy of these Chinese and Spanish speleothems are comparable to the magnetic carriers identified in previous speleothem studies, except for the greater contribution from haematite reported here. For example, ferrimagnetic phases were shown to be dominant in speleothems studied by Lean, 1995; Lean *et al*, 1995; Perkins, 1993 and Latham *et al*, 1982, 1986, 1987 and 1989. These previous studies have also shown presence of canted antiferromagnetic grains (i.e. haematite) as an accessory component in varying quantities. In some speleothems in this study up to 27% of an SIRM has been held by haematite (section 8.4). Haematite has been identified as the main carrier of remanence only once previously, in a speleothem collected from Cueva de la Capellania, Guatemala (Lean, 1995).

In this study, the constant magnetic mineralogy within speleothems from the same site is clearly seen in the IRM experiments. Small changes in the ranges of coercivity components are thought to reflect nothing more than the natural variation expected from within a small catchment and do not reflect major changes in mineralogy that would be associated with, for example, an increased input from a distal source and/or climate changes. There is some evidence to suggest that sediments from the Sistema de Cubija, Matienzo, are from a different catchment area but a full magnetic analysis has yet to be conducted (Quin, 1995).

9.5.2. Remanence acquisition.

There continues to be uncertainty as to the mode of acquisition of speleothem remanence. This arises from the inability to differentiate between CRM and DRM components that contribute to the NRM. The relationship between weight % acid insoluble detritus and NRM intensity is discussed in section 8.6. This method requires further systematic work but may have the potential to distinguish between a DRM or a CRM remanence.

All speleothems in this study have been taken from flood-prone streamways. In both Matienzo and Xingwen, large scale flooding occurs on a yearly basis. The results of these floods are seen within each speleothem as finely laminated, alternating light and dark growth layers. These dark layers represent growth immediately after a flood which cements detritus into the calcite matrix. The light layers represent growth after flood detritus has been cemented in to the calcite matrix prior to the next flood. Therefore, the primary source for magnetic minerals within the calcite matrix is likely to be from direct deposition of magnetic minerals onto the speleothem surface from flood events; a DRM. Unfortunately, no material was taken from the cave floors in either Matienzo or Xingwen. It has, therefore, not been possible to compare the magnetic properties of the cave floor sediments to the detritus within the speleothems.

A second possible source for detrital material within the speleothems was from the drip-waters. Bull (1981) suggested that fissures within the overlying limestone, which carry the drip-waters, can carry grains of up to 45μm. However, over the long periods required for speleothem growth it is likely that these fissures become blocked and will subsequently filter-out MD grains (Latham and Ford, 1993). In the future, examination of the magnetic properties of surface soils above known speleothems and their drip waters may go some way to illustrate which magnetic grain types and sizes are carried by this mechanism. Latham (1981) found that the overlying soils were the source for iron oxyhydroxides within speleothems in some caves.

A third potential source of magnetic minerals in these speleothems is from organic compounds (humic and fulvic acids) which chelate iron (II) and iron (III) giving rise to a CRM. These compounds release iron in a reduced state upon calcite crystallisation to form SD magnetite (Latham and Ford, 1993). However, the processes of de-chelation and production of authigenic magnetite in caves have not been studied fully (Perkins, 1993; Latham and Ford, 1993). However, in this study, the relationship between the quantity of undissolved detritus and the NRM intensity (section 8.6) particularly in the case of the Xingwen speleothems, does suggest that a DRM is primarily responsible for the remanence. That is not to say a CRM does not also exist but rather that its presence may be masked by the greater contribution from a DRM.

9.6. Future studies on speleothems.

Many suggestions for future work have been discussed in their relevant chapters but those with the most potential are mentioned here. This study probably represents the most complete series of PSV records of speleothems from a single locality. The results suggest that similar sampling schemes in other areas could yield similar suites of results which may expand the global coverage of speleothem PSV data.

Because the potential exists for detrital contamination to affect the ages of young 'dirty' samples (section 9.2.3) the L/L method should be undertaken as a matter of routine. Should time and facilities allow, the TSD method (section 4.4.3.3) should be used in preference to the L/L method. However, the frequent lack of sufficient coeval material in the case of speleothems means that these methods are often not possible when using alpha-spectrometry. The surest way to undertake L/L analysis on contaminated speleothems would be with mass-spectrometry primarily because of its increased measurement accuracy. In addition, smaller samples of <1 gram can be used which would allow many coeval leaches to be performed. Thus, the accuracy of any fitted isochron would be increased.

The U-Th method and also the ^{210}Pb method, have been shown to be effective in dating modern speleothems with active drip-caps. However, below 5 ka the lower limits

of the U-Th method are being approached and, with the presence of contamination, the errors in measurement are increased especially with low uranium concentrations. Thus, it would be interesting to attempt to fill the gap in dating between the ^{210}Pb and U-Th methods using another method, such as ^{226}Ra excess dating, which is unaffected by detrital contamination (Ivanovich and Harmon, 1992; Latham *et al*, 1986). The ^{226}Ra excess method can be used for samples up to ~10 ka (Ivanovich and Harmon, 1992) and within this age range any ^{226}Ra produced from decay of ^{230}Th is negligible. However, it is assumed that the specific activity of ^{226}Ra down the stalagmite remains the same as the measured value in the youngest (top) sample. In active speleothems, ^{210}Pb ages obtained from gamma counting of the upper surface of a speleothem could confirm its modernity. The measured ^{226}Ra activity from this upper layer sets the activity at $t=0$. Thus, ^{226}Ra activity of further samples down the speleothem can be calculated using the following equation:

$$t = (1602 / \ln 2).\ln(A_0 / A_x) \qquad \textbf{9.1}$$

where A_0 is the activity of ^{226}Ra in the top layer (i.e. $t=0$) and Ax is the ^{226}Ra activity in a layer distance x down the stalagmite. Thus, depending on the sampling density, it ought to be possible to resolve growth rate changes on a fine scale. Age concordancy checks could also be performed using U-Th disequilibrium dating over the entire age range (errors permitting). The use of the ^{210}Pb and ^{226}Ra methods would also save a great deal of time as they require minimal sample preparation, no spike, and depending on the isotope concentrations, require less than five days for the gamma counting process.

The method outlined in section 8.6 to determine whether or not the NRM is carried predominantly by a DRM or a CRM using weight % of undissolved detritus requires additional testing. There have been many speleothem studies and a little co-operation between the various workers in supplying speleothem off-cuts from a wide variety of localities would allow this work to be achieved without the need for further sampling from caves.

References

Adam, N.V., Ben'kova, N.P., Orlov, V.P. and Tyrumina, L.O. (1964). Western drift of the geomagnetic field. *Geomag. Aeron.*, **4**, 434-441.

Aitken, M.J. (1990) Science-based dating in archaeology. *Longman archeaology series*, 274pp.

Aitken, M.J., Adrian, A.L., Bussell, G.D. and Winter, M.B. (1989). Geomagnetic intensity variation during the last 4000 years. *Phys. Earth Planet. Ints.*, **56**, 49-58.

Appleby, P.G. and Oldfield, F. (1992). Application of Lead-210 to sedimentation studies. In: *Uranium-series disequilibrium: Applications to Earth, Marine, and Environmental Sciences.* Second Edition. (Eds. Ivanovich, M. and Harmon, R.S.) Clarendon Press, Oxford. pp 899.

Banerjee, S.K. (1971). New grains size limits for palaeomagnetic stability in haematite. *Nature.*, **232**, 15-16.

Barbetti, M.F. and McElhinny, M.W. (1972). Evidence of a geomagnetic excursion 30,000 yr BP. *Nature*, **239**, 327.

Baskeran, M., and Iliffe, T.M. (1993). Age determination of recent cave deposits using excess ^{210}Pb - A new technique. *Geophys. Res. Lett.*, **20**, 603-606.

Bauer, L.A. (1895). On the distribution and the secular variation of terrestrial magnetism, No. III. *Amer. J. Sci.* **50**, 314.

Bischoff, J.L. and Fitzpatrick, J.A. (1991) U-series dating of impure carbonates: An isochron technique using total-sample dissolution. *Geochim. Cosmochim. Acta.*, **55**, 543-554.

Blackwell, B. and Schwarcz, H.P. (1986). U-series analyses of the Lower Travertine at Ehringdorf, DDR. *Quaternary Research*, **25**, 215-222.

Bloxham, J., Gubbins, D. and Mankinen, E.A. (1989). Geomagnetic secular variation. *Phil. Trans. Roy. Soc. Lond.*, **329**, 415-502.

Bull, P.A. (1981). Some fine-grained sedimentation phenomena in caves. *Earth Surf. Proc. Landf.*, **6**, 11-32.

Bullard, E.C., Freedman, C., Gellman, H., Nixon, J. (1950). The westward drift of the earth's magnetic field. *Phil. Trans. Roy. Soc. Lond. A*, **243**, 67-92.

Burlatskaya, S.P., Nechaeva, T.B. and Petrova, G.N. (1965). The westward drift of the secular varation of magnetic inclination and variations in the earth's magnetic moment according to archaeomagnetic data. *Izv. Akad. Nauk SSSR. Fizika Zemeli*, **6**, 31.

Campbell, E.E. and Moss, W.D. (1965). Determinations of plutonium in urine by anion exchange. *Health Phys.*, **11**, 737-742.

Chapman, S. (1951). Some phenomena of the upper atmosphere. *Proc. Phys. Soc. London*, **B64**, 833

Chapman, S. and Bartels, J. (1940, 1962). *Geomagnetism,* Vols. 1 and 2 (1940); 2nd edition (1962), Oxford University Press, Oxford, 1049pp.

Chen, J.H., Edwards, R.L. and Wasserburg, G.J. Mass spectrometry and application to uranium-series disequilibrium. In: *Uranium-series disequilibrium: Applications to Earth, Marine, and Environmental Sciences.* Second Edition. (Eds. Ivanovich, M. and Harmon, R.S.) Clarendon Press, Oxford. pp 899.

Cherdyntsev, V.V. (1971). Uranium-234. *Israel Program for Scientific Translations, Jerusalem.*

Cong, Y.Z. and Wei, Q.Y. (1989). Study of secular variation (2000 BC-1900 AD) based on comparison of contemporaneous records in marine sediments and baked clays. *Phys Earth Planet. Ints.*, **56**, 69-75.

Cox, A (1982). Magnetostratigraphic Time scale, In: *A Geologic Time Scale,* ed W. B. Hartland, Cambridge University Press, Cambridge, 55pp.

Cox, A. and Doell, R.R. (1964). Long period variations of the geomagnetic field. *Bull. Seismol. Soc. Am.*, **54**, 2243-2270.

Creer, K.M. (1983). Computer synthesis of geomagnetic palaeosecular variations. *Nature*, **304**, 695-699.

Creer, K.M. (1989). The Lac du Bouchet palaeomagnetic record: its reliability and some inferences about the character of geomagnetic secular variations through the last 50000 years. In: *Geomagnetism and Palaeomagnetism.* (Eds.) Lowes, F.J., Collinson, D.W., Parry, J.H., Runcorn, S.K., Tozer, D.C., Soward, A. NATO ASI Series C262, Kluwer Academic Publishers, Dordrecht. pp 71-89.

Creer, K.M. and Ispir, Y. (1970). An interpretation of the behaviour of the geomagnetic field during polarity transitions. *Phys. Earth Planet. Ints.*, **2**, 283.

Creer, K.M. and Tucholka, P. (1982). Secular variation as recorded in lake sediments: a discussion of North American and European results. *Phil. Trans. R. Soc. Lond., A*, **306**, 87-102.

Cumming, G.L., Rollet, J.S., Rosotti, F.L.C., and Whewell, R.J. (1972). Statistical methods for the computation of stability constants, I. Straight-line fitting of points with correlated errors. *J. Chem. Soc., Dalton Trans.*, 2652, 2658.

Dankers, P. (1981). Relationship between median destructive field and remanent coercive forces for dispersed natural magnetite, titanomagnetite and haematite. *Geophys. J. R. astr. Soc.*, **64**, 447-461.

Dekkers, M.J. and Linssen, J.H. (1989). Rockmagnetic properties of fine-grained natural low-temperature haematite with reference to remanence acquisition mechanisms in red beds. *Geopys J. Int.*, **99**, 1-18.

Denham, C.R. and Cox, A. (1971). Evidence that the Laschamp polarity event did not occur 13 300-30 400 years ago. *Earth Planet. Sci. Lett.*, **13**, 181.

Dodson, R.E. (1979). Counterclockwise precession of the geomagnetic field vector and westward drift of the non-dipole field. *J. Geophys. Res.* **84**, 637.

Druffel, R.M., King, L.L., Belastock, R.A., Buesseler, K.O. (1990). Growth rate of a deep-sea coral using ^{210}Pb and other isotopes. *Geochim et Cosmochim Acta*, **54**, 1493-1500.

Dunlop, D. J. (1990). Developments in rock magnetism. *Rep. Prog. Phys.* **53**, 707-792.
Dunlop, D.J. (1971). Magnetic properties of fine-particle haematite. *Annales de Geophysique*, **27**, 269-293.

Dunlop, D.J. (1981). The rock magnetism of fine particles. *Phys. Earth Planet. Ints.*, **26**, 1-26.

Dunlop, D.J. (1986). Coercive forces and coercivity spectra of submicron magnetites. *Earth Planet. Sci. Lett.*, **78**, 288-295.

Eighmy, J.L. (1991). Archaeomagnetism: new data on the south-west U.S.A. master virtual geomagnetic pole curve. *Archaeometry*, **33**, 201-214.

Evans R.D. (1955). The Atomic Nucleus. *McGraw-Hill, New York*, pp. 988.

Eyre, J.K. (1994). *Magnetic mineralogy of Chinese Loess*. Unpub. Ph.D. thesis, University of Liverpool, UK.

Fisher, R. (1953). Dispersion on a sphere. *Phil. Trans. R. Soc. Lond.*, **A, 306**, 295-305.

Ford, D.C. and Williams, P.W. (1989). *Karst geomorphology and hydrology*. Unwin Hyman Ltd., London. pp. 601.

Freeman, R.(1986). Magnetic mineralogy of pelagic limestones., *Geophys. J. R. astr. Soc.*, **85**, 433-452.

Gascoyne, M. (1977). Trace element geochemistry of speleothems. *Proc. 7th Int. Spelo. Congr.*, 205-207.

Gascoyne, M. (1979). Pleistocene climates determined from stable isotope and geochronologic studies of speleothem. *Unpublished Ph.D. thesis, Dept. of Geology, McMaster University, Ontario, Canada.* 467pp.

Gascoyne, M., Ford, D.C., Schwarcz, H.P. (1981). Late Pleistocene chronology and palaeoclimate of Vancouver Island determined from cave deposits. *Can. J. Earth. Sci.*, **18**, 1643-1652.

Goldberg, E.D. (1963). Geochronology with ^{210}Pb in radioactive dating. *IAEA, Vienna*, 121-131.

Griffiths, D.H., King, R.F., Rees, A.I. and Wright, A.E. (1960). The remanent magnetisation of some recent varved sediments. *Proc. Roy. Soc. Lond.* **A, 256**, 359-383.

Gubbins, D. (1987). Mechanism for geomagnetic reversals. *Nature*, **326**, 167-169.

Gubbins, D. (1991). Dynamics of secular variation. *Phys. Earth. Planet. Int.*, **68**, 170-182.

Gubbins, D. (1994). Geomagnetic polarity reversals: A connection with secular variation and core-mante interaction. *Rev. Geophys.*, **32**, 61-83.

Gubbins, D. and Kelly, P. (1993). Persistent patterns in the geomagnetic field over the past 2.5 Myr. *Nature*, **365**, 829-832.

Gubbins, D. and Sarsen, G. (1994). Geomagnetic field morphologies from a kinematic dynamo model. *Nature*, **368**, 51-55.

Gubbins, D., Masters, T.G. and Jacobs, J.A. (1979). Thermal evolution of the Earth's core. *Geophys. J. R. Astr. Soc.*, **59**, 57-99.

Hagee, V.L. and Olsen, P. (1991). Dynamo models with permanent dipole fields and secular variation. *J. Geophys. Res.*, **96**, 11673-11687.

Halley, E. (1692). An account of the cause of the change of variation of the magnetic needle; with an hypothesis of the structure of the internal part of the Earth. *Phil. Trans. Roy. Soc.* **17**, 563-578.

Hallstadius, L. (1984). A method for the electrodeposition of actinides. *Nucl. Instr. Meth.*, **223**, 266-267.

Hillaire-Marcel, C., and Causse, C. (1989). Chronologie Th/U des concrétions calcaires des varves du lac glaciaire de Deschaillon (Wisconsinien inférieur). *Can. J. Earth Sci.* **26**, 1041-52.

Hirooka, K. (1983). Archaeomagnetism of baked clays, Results from Japan. In: *Geomagnetism of baked clays and recent sediments.* (eds) Creer, K.M., Tucholka, P. and Barton, C.E. pp150-157. Elsevier, 1983.

Hoffman, K.A. (1986). Transitional field behaviour from southern hemisphere lavas: evidence for two stage reversals of the geodynamo. *Nature,* **320**, 228-232.

Hutchings, A. (1967). Computation of the behaviour of two- and three-axis rotating systems. In: *Methods in Palaeomagnetism* (eds) D.W. Collinson, K.M. Creer and S.K. Runcorn, Elsevier, Amsterdam, 222-236.

Hyodo, M., Itota, C. and Yaskawa, K. (1993) Geomagnetic secular variation reconstructed from magnetisations of wide-diameter cores of Holocence sediments in Japan. *J. Geomag. Geoelectr.*, **45**, 669-696.

Ivanovich M. and Harmon, R.S. (Eds). *Uranium-series disequilibrium: Applications to Earth, Marine, and Environmental Sciences.* Second Edition. Clarendon Press, Oxford. pp 899. 1992.

Ivanovich M. and Murray A. (1992). Spectroscopic Methods. In: *Uranium-series disequilibrium: Applications to Earth, Marine, and Environmental Sciences.* Second Edition. (Eds. Ivanovich, M. and Harmon, R.S.) Clarendon Press, Oxford. pp 899.

Ivanovich, M, and Warchal, R.M. (1981) Report on second uranium-series intercomparison project workshop, Harwell, June 1980, *A.E.R.E. Rep.*, **10044**.

Jacobs, J.A. (1984), *Reversals of the Earth's magnetic field.* Adam Hilger, Bristol, 230pp.

Karlin, R., Lyle, M. and Heath, G.R. (1987). Authigenic magnetite formation in suboxic marine sediments. *Nature*, **326**, 490-493.

Kaufman, A. (1993). An evaluation of several methods for determining ^{230}Th/U ages in impure carbonates. *Geochim. et Cosmochim. Acta*, **57**, 2303-2317.

Kaufman, A. and Broecker, W. (1965). Comparison of ^{230}Th and ^{14}C ages for carbonate materials from Lakes Lahontan and Bonneville. *J. Geophys. Res.* **70**, 4039-4054.

Kendal, A.C. and Broughton, P.L. (1978). Origin of fabrics in speleothems composed of columnar calcite crystals. *J. Sed. Petr.*, **48 (2)**, p 519-538.

Kent, J.T., Watson, G.S. and Onstott, T.C. (1990). Fitting straight lines and planes with an application to radiometric dating. *Earth Planet. Sci. Lett.*, **97**, 1-17.

King, J.W. and Channell, J.E.T. (1990). Sedimentary magnetism, environmental magnetism and magnetostratigraphy. *Rev. Geophys. Suppl.*, U.S. national report to I.U.G.G. (1987-1990), 358-370.

King, R.F. (1955). Remanent magnetism of artificially deposited sediments. *Mon. Notic. Roy. Astron. Soc., Geophys. Suppl.* **7**, 115-134.

Kirschvink, J.L. (1980). The least squares line and plane and the analysis of palaeomagnetic data. *Geophys. J. R. astr. Soc.*, **62**, 699-719.

Komura, K and Sakanoue, M. (1964). Studies on the dating methods for Quaternary samples by natural alpha-radioactive nuclides. *Sci. Rep. Kanazawa Univ.*, **12(1)**, p21.

Kovacheva, M. (1980). Summarised results of the archaeomagnetic investigation of the geomagnetic field variation for the last 8000 years in south-eastern Europe. *Geophys. J. R. astr. Soc.*, **61**, 57-64.

Ku, T.-L, Bull, W.E., Freeman, S.T. and Knauss, K.G. (1979). $^{230}Th/^{234}U$ dating of pedogenic carbonates in gravelly deserts of Vidal Valley, *Southwestern California. Bull. Geol. Soc. Am.*, **90**, 1063-73.

Ku, T.-L. and Liang, Z.C. (1984) The dating of impure carbonates with decay series isotopes. *Nucl. Instr. Meth.*, **223**, 563-571.

Laj, C., Mazaud, D., Weeks, A., Fuller, M., Herrero-Bervera, E. (1991). Geomagnetic reversal paths. *Nature*, **351**, 447.

Lally, A.E. (1992). Chemical procedures. In: *Uranium-series disequilibrium: Applications to Earth, Marine, and Environmental Sciences.* Second Edition. (Eds. Ivanovich, M. and Harmon, R.S.) Clarendon Press, Oxford. pp 899.

Langereis, C.G., van Hoof, A.A.M., Rochette, P. (1992). Longitudinal confinement of geomagnetic reversal paths as a possible sedimentary artefact. *Nature, 358*, 226-230.

Latham, A.G. (1981). *Palaeomagnetism, rock magnetism and U-Th dating of speleothem deposits.* Unpub. Ph.D. thesis, Dept. of Geology, McMaster University, Ontario, Canada. 507pp.

Latham, A.G. and Ford, D.C. (1993). The palaeomagnetism and rock magnetism of cave and karst deposits. In: *Applications of palaeomagnetism to sedimentary geology.* **SEPM Sp. Pub. 49.**

Latham, A.G. and Schwarcz, H.P. (1992) Carbonate and Sulphate Precipitates. In: *Uranium-series disequilibrium: Applications to Earth, Marine, and Environmental Sciences.* Second Edition. (Eds. Ivanovich, M. and Harmon, R.S.) Clarendon Press, Oxford. pp 899.

Latham, A.G., Ford, D.C., Schwarcz, H.P. and Birchall, T. (1989). Secular variation from Mexican stalagmites: their potential and problems. *Phys. Earth Planet. Ints.*, **56**, 34-48.

Latham, A.G., Schwarcz, H.P. and Ford, D.C. (1986). The palaeomagnetism and U-Th dating of Mexican stalagmite, DAS2. *Earth Planet. Sci. Lett.*, **79**, 195-207.

Latham, A.G., Schwarcz, H.P. and Ford, D.C. (1987). Secular variation of the earth's magnetic field from 18.5 to 15.0 ka BP as recorded in a Vancouver Island stalagmite, *Can. J. Earth Sci.*, **24**, 1235-1241.

Latham, A.G., Schwarcz, H.P., Ford, D.C. and Pearce, G.W. (1979). Palaeomagnetism of stalagmite deposits. *Nature*, **280**, 383-1995.

Latham, A.G., Schwarcz, H.P., Ford, D.C. and Pearce, G.W. (1982). The palaeomagnetism and U-Th dating of 3 Canadian speleothems: evidence for the westward drift, 5.4-2.1 ka. *Can. J. Earth Sci.*, **19**, 1985-1995.

Lauritzen, S.E., Ford, D.C. and Schwarcz, H.P. (1986). Humic substances in speleothem matrix. *Comm 9th Int. Speleo. Congr. Barcelona*, 77-79.

Lean, C. (1995). *The palaeosecular variation of North and Central America*, Unpub. Ph.D. thesis, University of Liverpool, Liverpool, U.K. 310pp.

Lean, C.B., Latham, A. and Shaw, J. (1995). Palaeosecular variation from a Vancouver Island stalagmite and comparison with contemporary North American records. *J. Geomag. Geoelectr.*, **47**, 71-87.

Leaton, B. R. and Malin, S.R.C. (1967). Recent changes in the magnetic dipole moment of the earth. *Nature*, **213**, 1110.

Levi, S. and Banerjee, S. (1990). On the origin of inclination shallowing in redeposited sediments. *J. Geophys. Res.*, **95**, 4383-4390.

Levi, S. and Karlin, R. (1989). A sixty thousand year palaeomagnetic record from Gulf of California sediments: secular variation, late Quaternary excursions and geomagnetic implications. *Earth Planet. Sci. Lett.*, **92**, 219-233.

Li, W. -X., Lundberg, J., Dicken, A.P., Ford, D.C., Schwarcz, H.P., McNutt, R. and Williams, D. (1989). High precision mass spectrometric uranium-series dating of cave deposits and implications for palaeoclimatic studies. *Nature*, **339**, 534-536.

Liu, Y., Morinaga, H., He, J., Rao, H., Kusakabe, M. and Yaskawa, K. (1990). Study on earth's palaeo-environment using speleothem from South China. *J. Speleol. Soc. Japan*, **15**, 47-55.

Lovely, D.R., Roden, E.E., Philips, E.J.P. and Woodward, J.C. (1993). Enzymatic iron and uranium reduction by sulphate-reducing bacteria. *Marine Geology*, **113**, 41-53.

Lowrie, W. (1990). Identification of ferromagnetic minerals in a rock by coercivity and unblocking temperature properties. *Geophys. Res. Lett*, **17**, 159-162.

Ludwig, K.R. (1991). ISOPLOT- a plotting and regression program for radiogenic-isotope data. *U.S.G.S. Open file report*, **91-445**.

Ludwig, K.R. (1993). UISO- a program for calculation of ^{230}Th-^{234}U-^{238}U isochrons. *U.S.G.S. Open file report*, **91-531**.

Ludwig, K.R. and Titterington, D.M. (1994). Calculation of $^{230}Th/U$ isochrons, ages and errors. *Geochim. et Cosmochim. Acta*, **58 (22)**, 5031-5042.

Lund, S.P. (1983). Late Quaternary secular variations recorded in Central North American wet lake sediments. In: *Geomagnetism of Baked Clays and Recent Sediments.* (Eds.) K.M. Creer, P. Tucholka, and C. E. Barton, Elsevier, 324pp.

Lund, S.P. and Banerjee, S.K. (1985). Late Quaternary palaeomagnetic field secular variation from two Minnesota lakes. *Earth Planet. Sci. Letts.*, **122**, 331-341.

Lundberg, J. (1990). *U-Series dating of carbonates by mass spectrometry with examples of speleothem, coral and shell.* Unpub. Ph.D. thesis, McMaster University, Hamilton, Ontario, Canada. 271pp.

Luo, S. and Ku, T-L. (1991). U-series isochron dating: A generalised method employing total-sample dissolution. *Geochim. et Cosmochim. Acta*, **55**, 555-564.

Maher, B.A. (1988). Magnetic properties of some synthetic sub-micron magnetites. *Geophys. J.*, **94**, 83-96.

Maher, B.A. and Taylor, R.M. (1988). Formation of ultrafine-grained magnetite in soils. *Nature*, **366**, 368-370.

McElhinny, M. and Senanayake, W. (1982). Variations in the geomagnetic dipole 1: the past 50 000 years. *J. Geomag. Geoelectr.*, **34**, 39.

McIntosh, G. (1993). Postdepositional detrital remanent magnetisation in Chinese Loess: Preliminary results of laboratory experiments. *Geologica Carpathica,* **44, 5**, Bratislava, October 1993, 335-358.

Mercanton, P.L. (1926). Inversion de l'inclinaison magnétique terrestre âux ages géologiques. *Terr. Magn. Atmos. Elect.*,**31**, 187-190.

Merrill, R and McElhinny, M. (1983). *The Earth's Magnetic Field; Its History, Origin and Planetary Perspective.* Academic Press, London, 401pp.

Merrill, R.T. (1970). Low-temperature treatments of magnetite and magnetite-bearing rocks. *J. Geophys. Res.*, **75**, 3342-3349.

Morinaga, H., Inokuchi, H. and Yaskawa, K. (1986). Magnetisation of a stalagmite in Akiyoshi Plateau as a record of the geomagnetic secular variation in West Japan. *J. Geomag. Geoelectr.*, **38**, 27-44.

Morinaga, H., Inokuchi, H. and Yaskawa, K. (1989). Palaeomagnetism of stalagmites (speleothems) in SW Japan. *Geophys. J.*, **96**, 519-528.

Moskowitz, B.M, Frankel, R.B., Bazylinski, D.A., Jannasch, H.W. and Lovely, D.R. (1989). *Geophys. Res. Letts.*, **16 (7)**, 665-668.

Mothersill, J.S. (1979). The palaeomagnetic record of the Late Quaternary sediment of Thunder Bay. *Can. J. Earth. Sci.*, **16**, 1016-1023.

Nagata, T. (1965). Main characteristics of recent geomagnetic secular variation. *J. Geomag. Geoelectr.* **17**, 263.

Needham, J. (1962). Science and Civilisation in China. Vol. 4, *Cambridge University Press*, p.434.

Noel, M. (1990). Palaeomagnetic and archaeomagnetic studies in the caves of Guangxi, *Cave Science*, **17 (2)**, 73-76.

O'Reilly, W.O. (1984). *Rock and mineral magnetism.* Blackie and Son Ltd. London. 220pp.

Oldfield, F., Maher, B.A., Appleby, P.G. (1989). Sediment source variations and the ^{210}Pb inventories in recent Potomac Estuary sediment cores. *J. Quat. Sci.*, **4**, 189-200.

Olsen, P. (1981). A simple physical model for the Terrestial Dynamo. *J. Geophys. Res.*, **86, No. B11**, 10875-10882.

Opdyke, N.D., Kent, D.V., Lowrie, W. (1973). Details of magnetic polarity transitions recorded in a high deposition rate deep-sea core. *Earth Planet. Sci. Lett.*, **20**, 315-324.

Openshaw, S.J., Latham, A.G., Shaw, J. and Xuewen, Z. (1993). Preliminary results on recent palaeomagnetic secular variation recorded in speleothems from Xingwen, Sichuan, China. *Cave Science*, **20 (3)**, 93-99.

Ozima, M. and Ozima, M. (1964). Aquisition mechanism of TRM-Low temperature characteristics of TRM and magnetisation of some granites. *Ann. Prog. Rep. Rock Magn. Res. Group Japan.*, 21-29.

Peng, L. and King, J.W. (1992) A late Quaternary geomagnetic secular variation record from Lake Waiau, Hawaii and the question of the Pacific non-dipole low. *J. Geophys. Res.*, **97**, 4407-4424.

Pennington, W., Cambrey, R.S., Eakins, J. and Harkness, D.D. (1976). Radionuclide dating of the recent sediments of Blelham Tarn. *Freshwater Biol.*, **6**, 317-331.

Perkins, A.M. (1993). *Magnetic studies of speleothems*, Unpub. PhD thesis, University of East Anglia, 244pp.

Perkins, A.M. and Maher, B.A. (1993). Rock magnetic and palaeomagnetic studies of British speleothems. *J. Geomag. Geoelectr.*, **45**, 143-153.

Petrova, G.N. and Pospelova, G.A. (1990). Excursions of the magnetic field during the Brunhes Chron. *Phys. Earth Planet. Int.*, **63**, 135-143.

Prévot, M and Camps, P. (1993). Absence of preferred longitude sectors for poles from volcanic records of geomagnetic reversals. *Nature*, **366**, 53-57.

Przybylowicz, W., Schwarcz, H.P. and Latham, A.G. (1991). Dirty Calcites 2: Uranium series dating of artificial calcite-detritus mixtures. *Chem. Geol. (Isotope Geosci section).*, **86**, 161-178.

Quin, A. (1995). Morphological links between distinct cave systems, as revealed by the magnetic properties of cave sediments. *Studies in Speleology*, **5**, 5-19.

Ren, G.T. (1980). Study on East-Asia continental magnetic anomaly. *Reports of Institute of Geophysics, Academica Sinica*, 17-29.

Robertson, D.J. and France, D.E. (1994). Discrimination of remanence carrying minerals in mixtures, using isothermal remanent magnetistion acquisition curves. *Phys. Earth Planet. Ints*, **82**, 223-234.

Rochette, P. and Fillion, G. (1989). Field and temperature behaviour of remanence in synthetic goethite: palaeomagnetic implications. *Geophys. Res. Lett.*, **16**, 851-854.

Rogers, J.J.W. and Adams, J.A.S. (1969). Uranium. In: *Handbook of geochemistry. Ed. KPH. Wedepohl.* **Springer-Verlag, Berlin**.

Rosholt, J.N. (1976). $^{230}Th/^{234}U$ dating of travertine and caliche rinds. *Geol. Soc. Amer. Abstr. Prog.* **8**, 1076.

Runcorn, S.K. (1959). On the theory of geomagnetic secular variation. *Ann. Geophys.*, **15**, 87-92.

Schwarcz, H.P. (1980). Absolute age determination of archaeological sites by uranium series dating of travertines. *Archaeometry*, **22**, 3-24.

Schwarcz, H.P. (1989). Uranium-series dating. *Quat. Int.*, **1**, 7-17.

Schwarcz, H.P. and Latham, A. G. (1989). Dirty Calcites 1: Uranium series dating of contaminated calcite using leachates alone. *Chem. Geol. (Isotope Geosci section)*, **80**, 35-43.

Sidhu, P.S. (1998). Transformation of trace element-substituted maghaemaite to heamatite. *Clays Clay Min.*, **36(1)**, 31-38.

Skiles, D.D. (1970). A method of inferring the direction of drift of the geomagnetic field from palaeomagnetic data. *J. Geomag. Geoelectr.* **22**, 441-462.

Stacey, F.D. and Banerjee, S.K. (1974). *The Physical Principles of Rock Magnetism: Developments in Solid Earth Geophysics*, vol 5, Elsevier Scientific Publishing Co., New York. 195 pp

Talvitie, N.A. (1972). Electrodeposition of actinides for alpha spectrometric determination. *Anal. Chem.*, **44**, 280-283.

Tarling, D. (1983). *Palaeomagnetism; Principles and Applications in Geology, Geophysiscs, and Archaeology*. Chapman and Hall, London, 379pp.

Tauxe, L. and Kent, D.V. (1984). Properties of a detrital remanence carried by haematite from study of modern river deposits and laboratory redeposition experiments. *Geophys. J. R. astr. Soc.*, **77**, 543-561.

Thellier, E and Thellier, O. (1959). Sur l'intensite du champ magnetique terrestre dans la passe historique et geologique. *Ann. Geophys.*, **15**, 285-376.

Thellier, E. (1981). Sur la direction du champ magnetique terrestre, en France, durant les deux derniers millenaires. *Phy. Earth Planet. Ints.*, **24**, 89-132.

Thompson, R. (1975). Long period European geomagnetic secular variation confirmed. *Geophys. J. R. astr. Soc.*, **43**, 847-859.

Thompson, R. and Oldfield, F. (1986). *Environmental magnetism*. Allen and Unwin, London. 227pp.

Thouveny, N., Creer, K.M. and Blunk, I. (1990). Extension of the Lac du Bouchet palaeomagnetic record over the last 120,000 years. *Earth Planet. Sci. Letts.*, **97**, 140-161.

Titterington, D. M. and Halliday, A.N. (1979). On the fitting of parallel isochrons and the method of maximum likelihood. *Chem. Geol.*, **26**, 183-195.

Tric, E., Laj, C., Jéhanno, C., Valet, J-P., Kissel, C., Mazaud, A., Iaccarino, S. (1991). High-resolution record of the Upper Olduvai transition from Po Valley (Italy) sediments: Support for dipolar transition geometry. *Phys. Earth Planet. Ints.*, **65**, 319-336.

Turner, G.M. and Thompson, R. (1981). Lake sediment record of the geomagnetic secular variation in Britain during Holocene times. *Geophys., J. R. astr. Soc.*, **65**, 703-725.

Verosub, K.L. (1977). Depositional and postdepositional processes in the magnetisation of sediments. *Rev. Geophys Space. Phys.*, **15 (2)**, 129-143.

Verwey, E.J.W. and Haayman, P.W. (1941) Electronic conductivity and transition point in magnetite. *Physics*, **8**, 979-982.

Vestine, E.H., LaPorte, L., Lange, I., Cooper, C., Hendrix, W.C. (1947). Description of the earth's main magnetic field and its secular change, 1905-1945. *Washington: Carnegie Institution Publ. no.* **578**.

Waltham, A. C. and Willis, R.G. (Eds.) *Xingwen: China Caves Project 1989-1992*. Brit. Cave. Res. Assoc. pp48, 1993.

Waltham, A.C. (1981). The kartstic evolution of the Matienzo depression, Spain. *Zeit. Geomorph.*, **25**, 300-312.

Wei, Q. Y., Li, T. C., Chao, G. Y., Chang, W. S., Wang, S. P., Wei, S. F. (1983). Results from China, In *Geomagnetism of baked clays and recent sediments,* (Eds.) K. M. Creer, P. Tucholka, C. E. Barton, 324 pp., Elsevier.

Wendt, I. and Carl, C. (1991). The statistical distribution of the mean squared weighted deviation. *Chem. Geol. (Isotope Geoscience Section),* **86**, 275-285.

Yang, S., Shaw, J. and Wei, Q.Y. (1993). Tracking a non-dipole geomagnetic anomaly using new archaeointensity results from north-east China. *Geophys. J. Int.*, **115**, 1189-1196.

York, D. (1969). Least squares fitting of a straight line with correlated errors. *Earth Planet. Sci. Letters.*, **5**, 320-324.

Yukutake, T and Tachinaka, H. (1969). Separation of the earth's magnetic field into the drifting and standing parts. *Bull.Earthq. Res. Inst., Univ. Tokyo.* **47**, 65-97.

Yukutake, T. and Tachinaka, H. (1968). The non-dipole part of the eath's magnetic field. *Bull. Earthq. Res. Inst., Univ. Tokyo.* **46**, 1027-1074.

Yukutake, T. (1962). The westward drift of the magnetic field of the earth. *Bull. Earthquake Res. Inst. Univ. Tokyo,* **40**, 1.

Yukutake, T. (1967). The westward drift of the earth's magnetic field in historic times. *J. Geomag. Geoelectr.*, **19, No.2**, 103-116.

Yukutake, T. (1968). Free decay of non-dipole components of the geomagnetic field. *Phys. Earth Planet. Int.*, **1**, 93-96.

Yukutake, T. (1970). Geomagnetic secular variation. Comments on Earth sciences. *Geophys.***1**, 55.

Yukutake, T. (1979). Geomagnetic secular variations on the historical time scale. *Phys. Earth Planet. Int.* **20**, 83-95.

Yukutake, T. (1993). The geomagnetic non-dipole field in the Pacific. *J. Geomag. Geoelectr.*, **45**, 1441-1453.

Zijderveld, J.D.A. (1967). AC demagnetisation of rocks: analysis of results. In: *Methods in Palaeomagnetism.* (Eds) D.W. Collinson, K.M. Creer and S.K. Runcorn, Elsevier.

Appendix A

AF cleaned directions from SC01.

Sub-sample	Dist. from top (mm)	Dec (°)	Inc (°)	α_{95} (°)	χ x 10^{-8} m^3kg^{-1}	NRM x10^{-8} Am^2kg^{-1}	NRM_{200mT} x10^{-8} Am^2kg^{-1}
SC01B	12.25	354.2	27.4	0.8	-2.0	68.0	22.5
2B	37	349.9	36.5	0.7	-0.1	88.6	77.4
3B	61	348.8	45.8	0.8	0.4	122.3	110.6
4B	84.5	351.9	42.0	1.2	-0.1	95.0	89.0
5B	107.5	1.3	38.1	1.3	0.0	80.7	73.6
6B	132	2.8	30.8	2.1	0.1	62.0	55.6
7B	156.5	350.8	31.6	2.7	-0.3	50.1	43.8
8B	180.5	342.9	45.0	2.0	-0.1	61.2	54.1
9B	204.5	348.7	44.0	0.7	-0.1	133.2	117.4
10B	229.5	349.2	46.3	0.6	0.7	178.7	156.6
11B	252.5	351.3	38.8	0.9	0.7	155.3	137.7
12B	277	351.7	36.9	1.1	0.4	133.4	117.7
13B	300.5	356.5	36.9	2.3	0.3	202.7	183.1
14B	324.5	358.8	33.2	0.7	0.8	298.8	288.7
15B	349.5	357.8	38.9	2.4	0.4	170.1	157.0
16B	373.5	349.6	38.4	2.5	0.5	179.1	162.0
17B	397.5	1.1	38.9	1.0	0.1	303.1	276.1
18B	421	356.2	40.7	1.5	0.4	177.7	161.3
19B	444.5	347.0	43.3	1.4	0.9	104.4	93.7
20B	468	354.4	43.5	2.4	1.0	172.4	153.7
21B	491.5	353.9	42.2	1.9	1.6	374.4	345.1
22B	516.5	351.8	41.4	2.3	1.5	465.1	489.8
23B	540	356.1	37.2	1.2	1.2	379.8	338.9
24B	564.5	0.8	36.8	0.8	0.6	378.4	331.6
25B	588.5	356.5	39.8	0.7	0.6	366.3	322.4
26B	612.5	0.5	46.3	0.7	1.2	635.8	476.8

Appendix B

AF cleaned directions from SC02.

Sub-sample	Dist. from top (mm)	Dec (°)	Inc (°)	MAD (°)	χ x 10^{-8} m^3kg^{-1}	NRM x10^{-8} Am^2kg^{-1}	NRM_{200mT} x10^{-8} Am^2kg^{-1}
SC021B	4.5	359.5	41.2	11.0	-0.4	12.2	10.2
2B	18	360.0	49.3	9.7	-0.4	8.2	7.1
3B	28	341.1	61.8	6.5	-0.4	7.8	6.6
4B	41	345.3	55.5	7.8	-0.4	11.6	10.5
5B	53	2.5	44.2	7.1	-0.4	8.8	8.6
6B	65	7.8	40.2	4.5	-0.4	9.1	8.0
7B	76	339.5	45.6	7.5	-0.3	7.8	7.2
8B	88	339.3	49.3	2.8	-0.3	20.6	18.4
9B	100	342.6	52.6	4.7	-0.4	14.3	12.8
10B	112	353.7	48.9	3.7	-0.3	27..5	24.5
11B	124	360.0	43.1	2.7	-0.2	30.0	26.8
12B	136	355.0	42.6	4.6	-0.2	31.2	27.5
13B	147	0.3	50.1	5.0	-0.3	26..8	23.9
14B	160	355.7	43.6	4.7	-0.3	19..0	17.1
15B	171	1.4	42.1	3.8	-0.2	34.1	30.1
16B	184	354.6	50.9	5.8	-0.3	20.2	18.1
17B	196	2.3	51.7	6.2	-0.4	12.5	10.8
18B	208	352.1	45.3	5.5	-0.3	9.1	7.5
19B	220	350.6	49.9	4.4	-0.3	17.2	15.7
20B	232	346.5	39.2	11.3	-0.3	9.6	8.7
21B	245	352.9	50.9	7.4	-0.4	7.6	6.5
22B	256	1.2	48.6	2.2	1.4	151.7	133.4
23B	267	2.7	55.0	2.4	0.4	817.7	730.8

Appendix C

AF cleaned directions from PT02.

Sub-sample	Dist. from top (mm)	Dec (°)	Inc (°)	MAD (°)	χ x 10^{-8} m^3kg^{-1}	NRM x10^{-8} Am^2kg^{-1}	NRM_{200mT} x10^{-8} Am^2kg^{-1}
PT021B	6	349.7	33.0	8.9	0.0	36.9	28.8
2B	20	337.1	26.1	5.5	0.0	27.6	22.5
3B	33	333.4	36.4	8.1	0.0	22.0	16.2
4B	45	341.9	26.8	7.3	0.3	63.1	46.4
5B	55.5	331.9	28.8	6.8	0.5	36.3	31.5
7B	80	346.6	33.4	6.2	0.1	41.2	34.1
8B	92	0.8	64.2	1.7	-0.1	17.2	12.3
9B	103	342.8	41.2	4.5	-0.3	23.3	17.8
10B	115	341.0	45	4.6	-0.1	13.1	9.6
14B	163	359.0	59.3	13.8	-0.1	15.1	10.9
15B	177	351.9	41.7	5.1	-0.3	13.6	11.2
16B	186.5	29.0	22.8	6.8	0.3	7.2	63.3
17B	199	355.6	42.7	6.4	-0.1	4.3	35.5
18B	211	17.2	62.7	9.6	-0.1	1.2	9.8
19B	222	352.7	51.8	14.2	-0.2	5.3	44.3
20B	235	345.6	53.0	5.3	-0.2	2.5	18.2
21B	247.4	31.9	42.0	1.5	0.0	8.6	79.8
23B	270	356.4	57.1	8.5	-0.2	29.6	79.8
24B	283	353.5	46.1	5.5	-0.1	20.5	21.2
25B	295.5	343.4	47.8	6.0	-0.1	25.6	19.1
26B	307	348.9	45.6	3.7	-0.2	21.5	15.1
27B	319.5	358.7	49.0	6.1	0.0	13.2	20.0
28B	333.5	343.2	45.7	4.3	0.0	67.7	55.9
29B	360	330.2	48.6	7.5	0.0	52.1	39.4
30B	373	353.6	43.4	8.3	0.0	50.4	40.9
31B	385	336.8	43.8	5.8	0.1	77.7	56.8
32B	398	343.9	45.3	6.4	0.2	75.0	64.7

Sub-sample	Dist.from top (mm)	Dec (°)	Inc (°)	MAD (°)	χ x 10^{-8} m^3kg^{-1}	NRM x10^{-8} Am^2kg^{-1}	NRM_{200mT} x10^{-8} Am^2kg^{-1}
PT0233B	408.5	342.3	41.1	6.6	0.0	67.4	58.0
34B	421	346.2	48.6	4.7	1.1	149.3	127.3
36B	445	353.7	41.0	4.3	1.9	272.1	238.3
37B	457	349.8	43.4	2.5	0.9	236.6	213.9
38B	468	352.3	41.4	3.5	1.4	300.6	274.1
39B	480	356.5	38.7	2.6	1.4	271	246.5
40B	492.5	352.4	37.5	2.6	0.6	221.6	138.3
41B	506	358.7	38.3	5.3	0.5	159.6	119.6

Appendix D

AF cleaned directions from PT03.

Sub-sample	Dist. from top (mm)	Dec (°)	Inc (°)	MAD (°)	χ x 10^{-8} m^3kg^{-1}	NRM x10^{-8} Am^2kg^{-1}	NRM_{200mT} x10^{-8} Am^2kg^{-1}
PT031B	11.5	351.6	34.9	10.2	-0.2	18.4	15.6
2B	36.5	359.9	58.3	11.1	0.2	24.2	23.5
3B	61.5	6.3	44.3	7.8	-0.1	50.3	45.7
4B	86.5	353.1	33.6	3.3	-0.1	51.1	46.3
5B	111.5	349.8	49.0	4.3	-0.1	80.1	75.0
6B	136.5	355.8	51.0	3.8	-0.0	66.1	58.0
7B	161.5	358.2	44.8	1.8	-0.1	87.0	78.2
8B	186.5	5.9	41.6	2.7	-0.1	78.5	73.9
9B	211.5	9.2	40.4	2.3	-0.2	81.3	72.4
10B	236.5	2.7	43.6	2.2	-0.1	101.9	90.3
11B	261.5	6.4	35.4	2.9	-0.1	43.5	39.8
12B	286.5	8.3	41.1	2.6	-0.2	64.9	57.4
13B	311.5	3.0	49.7	2.8	-0.2	52.4	46.2
14B	336.5	6.3	47.7	3.5	-0.1	69.7	61.7
15B	361.5	7.6	33.5	3.9	3.2	100.8	66.6

Appendix E

AF cleaned directions from PT04.

Sub-sample	Dist. from top (mm)	Dec (°)	Inc (°)	MAD (°)	χ x 10^{-8} m^3kg^{-1}	NRM x10^{-8} Am^2kg^{-1}	NRM_{200mT} x10^{-8} Am^2kg^{-1}
PT041B	14	350.6	50.9	11.2	-0.3	8.5	7.0
4B	81	3.4	44.2	6.2	-0.1	39.9	32.4
5B	104	4.1	38.1	6.0	0.8	89.8	73.2
6B	127	358.5	41.1	9.1	-0.1	34.2	29.0
7B	153	353.7	56.9	9.9	-0.3	7.1	6.2
8B	180	352.8	46.9	6.9	-0.2	15.7	13.4
10B	229	335.8	9.0	5.1	0.1	32.6	24.3
11B	255	345.1	31.0	5.7	0.1	48.9	40.9
12B	281.5	351.8	39.8	4.1	-0.2	19.5	16.4
13B	307	339.8	45.7	8.0	-0.2	21.2	14.6
14B	332.5	349.7	22.0	7.8	0.0	17.7	13.2
15B	365.5	2.8	40.8	3.6	-0.2	17.0	14.5
16B	393.5	0.9	44.3	7.2	-0.3	20.5	16.9
17B	419	357.3	49.7	2.4	-0.5	42.2	36.3
18B	445	349.9	48.6	3.5	-0.3	14.2	12.7
19B	471	343.2	45.1	7.7	-0.4	35.3	32..0
20B	496.5	358.9	37.8	4.8	-0.2	38.0	34.0
21B	521	354.5	41.1	3.7	-0.1	81.7	74.6
22B	547	1.6	35.9	2.9	0.0	36.2	32.4
23B	575	9.1	34.0	2.6	-0.2	44.5	40.5
24B	601	16.2	32.1	8.2	-0.3	30.4	27.8
25B	626.5	6.9	33.7	4.1	0.0	123.2	114.4

Appendix F

AF cleaned directions from AG02.

Sub-sample	Dist. from top (mm)	Dec (°)	Inc (°)	MAD (°)	χ x 10^{-8} m^3kg^{-1}	NRM x10^{-8} Am^2kg^{-1}	NRM_{200mT} x10^{-8} Am^2kg^{-1}
AG021B	11.5	352.1	60.1	4.1	0.1	42.4	24.4
3B	35.5	6.6	58.0	3.7	0.0	27.2	19.3
4B	47.5	6.8	46.5	5.8	-0.2	22.0	14.8
5B	59.5	4.1	43.5	4.2	-0.3	30.6	22.4
7B	84.5	9.3	50.7	7.6	-0.2	10.0	7.3
8B	96.5	6.1	46.2	7.0	-0.1	23.8	16.9
9B	108.5	12.2	56.3	10.2	1.6	44.5	27.5
14B	169.5	5.8	61.1	6.0	0.7	34.5	23.5
15B	181.5	356.2	67.5	8.8	0.0	10.6	7.1
16B	192.5	351.3	50.3	5.1	-0.8	29.3	18.4
17B	204.5	353.4	52.1	4.2	-0.2	17.0	9.8
18B	216.5	3.5	53.0	7.5	0.4	16.5	11.3
19B	228.5	0.5	58.8	3.1	0.4	91.5	48.5
21B	253.5	4.4	63.0	2.8	-0.1	31.8	17.9
22B	264.5	4.1	62.9	6.0	-0.1	14.4	8.6
23B	276.5	6.2	62.1	1.9	0.1	63.9	36.6
24B	288.5	3.6	56.2	1.5	0.2	93.6	58.2
25B	300.5	353.0	57.0	3.2	0.3	68.4	39.4
26B	312.5	353.6	52.0	4.4	0.0	37.9	24.3
27B	324.5	344.1	49.0	4.0	0.5	50.8	27.6
29B	348.5	353.6	57.2	1.8	0.3	72.5	43.0
30B	359.5	352.6	60.2	2.2	0.7	112.1	60.8
31B	372.5	340.0	54.6	5.0	0.7	57.1	32.1

Appendix G

Thermally cleaned directions from AG03.

Sub-sample	Dist. from top (mm)	Dec (°)	Inc (°)	MAD (°)	χ x 10^{-8} m^3kg^{-1}	NRM x10^{-8} Am^2kg^{-1}	$NRM_{300°C}$ x10^{-8} Am^2kg^{-1}
AG033B	50.0	359.2	55.3	9.4	-0.2	19.0	10.3
4B	79.0	5.5	60.3	5.5	-0.1	72.3	55.6
6B	126.0	358.2	53.5	9.7	0.1	20.2	15.3
7B	151.0	12.3	64.2	7.9	0.2	31.5	23.2
11B	346.0	357.1	52.1	1.8	-0.4	33.5	26.3
12B	370.0	7.8	50.2	9.0	-0.3	27.8	15.8
17B	499.0	11.8	60.6	5.4	0.0	6.6	3.8
20B	571.0	15.2	25.4	6.7	0.1	63.7	42.9
21B	595.0	354.4	44.9	8.2	-0.2	42.7	31.9
23B	619.0	346.6	45.5	3.6	0.5	58.7	35.7

Appendix H

Susceptibility of TR01 sub-samples.

Sub-sample	Dist.from top (mm)	χ x 10^{-8} m^3kg^{-1}	Sub-sample	Distance from top (mm)	χ x 10^{-8} m^3kg^{-1}
TR011B	9.5	0.0	7B	77.5	-0.2
2B	20.5	-0.1	8B	91.5	-0.2
3B	31.5	-0.3	9B	103.5	-0.1
4B	44.5	-0.2	10B	115.5	0.1
5B	55.5	-0.3	11B	127.5	-0.1
6B	67.5	0.0	12B	139.5	-5.0

Sub-sample	Distance from top (mm)	χ x 10^{-8} m^3kg^{-1}	Sub-sample	Distance from top (mm)	χ x 10^{-8} m^3kg^{-1}
13B	151.3	-0.2	27B	340.5	-0.2
14B	164.5	-0.2	28B	352.5	-0.2
15B	177.5	-0.2	29B	364.5	-0.2
16B	188.5	0.0	30B	374.5	-0.1
17B	200.5	-0.2	31B	387.5	-0.2
18B	231.5	-1.9	32B	406.5	-0.1
19B	243.5	-0.2	33B	417.5	-0.2
20B	256.5	-0.1	34B	430.5	-0.2
21B	267.5	-0.2	35B	443.5	-0.1
22B	280.5	0.0	36B	455.5	-0.4
23B	292.5	-0.2	37B	466.5	-0.2
24B	304.5	-0.2	38B	478.5	-0.2
25B	315.5	-0.2	39B	491.5	-0.1
26B	327.5	0.0	40B	504.5	0.1

Appendix I

Susceptibility of TR02 sub-samples.

Sub-sample	Distance from top (mm)	χ x 10^{-8} m^3kg^{-1}	Sub-sample	Distance from top (mm)	χ x 10^{-8} m^3kg^{-1}
1B	7.0	-0.2	8B	170.0	-0.1
2B	25.5	-0.3	9B	194.0	-0.2
3B	48.5	0.1	10B	242.0	-0.4
4B	73.5	-0.5	11B	262.5	-0.6
5B	98.0	-0.3	12B	287.5	-0.1
6B	122.5	-0.1	13B	312.5	0.0
7B	146.5	-0.2	13C	312.5	0.0

Sub-sample	Distance from top (mm)	χ x 10^{-8} m^3kg^{-1}	Sub-sample	Distance from top (mm)	χ x 10^{-8} m^3kg^{-1}
14B	336.0	-0.1	19B	462.5	-0.2
14C	336.0	0.1	19C	462.5	-0.3
15B	359.0	0.2	20B	487.5	0.1
15C	359.0	0.5	21B	511.0	0.1
16B	383.0	0.1	21C	511.0	0.2
16C	383.0	-0.4	22B	534.5	0.5
17B	407.0	-0.2	22C	534.5	0.2
17C	407.0	0.1	23B	559.0	-0.1
18B	443.0	-0.2	23C	559.0	0.2
18C	443.0	-0.3	24B	583.0	0.8

Appendix J. Uranium Series Dating Procedure

Note that this memo applies to the dissolution and isotope separation of calcite speleothems. Other materials may require subtle changes in procedure.

A) Sample Preparation

1. Weigh sample and note down sample number and details on dating sheet.
2. Place sample in labelled 250 ml beaker and add just enough 7M HNO_3 to cover sample. More acid can be added if the solution saturates before complete dissolution.
3. Filter solution using Whatman 54 acid hardened filter paper. Rinse filter paper with acid once drained through.
4. Carefully add 0.5ml $^{232}U/^{228}Th$ spike solution and up to 1ml $FeCl_3$ (depending on Fe content of dissolved sample).
5. Boil sample down to approximately 100ml, and add 1-2ml $HCLO_4$. Reduce heat, cover and reflux for 30 minutes.
6. Add a few mls of 7M HNO_3 and increase volume to just under 200 mls with distilled water.
7. Heat whilst stirring and boil for 10 minutes (to drive off CO_2).
8. Turn off heat; cool until sign of boiling cease. Increase stirring speed and add just enough NH_3 to produce a dark brown precipitate which remains.
9. Cover and leave for several hours allowing precipitate to flocculate and sink to base of beaker.
10. Transfer to centrifuge tubes flushing all precipitate from the beaker with distilled water. From a squeezy bottle rinse sides of beaker with 9N HCl and add 0.5 ml $FeCl_3$ to the acid rinse which is left in the beaker. Once centrifuged pour clear supernate from the centrifuge tubes back into this beaker. Leave first precipitate in centrifuge tube to dry.
11. Repeat steps 7 - 10 for the second scavenge of U and Th. This time the supernate and washings are discarded.
12. Transfer precipitate to one centrifuge tube and leave to dry for several days until surface of precipitate begins to crack.

The above procedure takes approximately 2 days plus precipitate drying time. Thus, it is useful to keep a set of samples prepared in advance for the following stage which can be achieved the day before the previous samples come off the alpha-spectrometer.

B) Removal of Iron and Further Destruction of Organics

13. Dissolve dried precipitate in centrifuge tube with 5ml conc. HCl.
14. Pour into separating funnel and rinse centrifuge tube with 9N HCl.
15. Add an approximately equal measure of Iso-Propyl Ether (IPE) and shake funnel vigorously several times. Hold funnel upside down and open valve to allow degassing between shakes.
16. Remove bung and leave for 5 mins, or until the liquid interface is clearly defined.
17. Drain lower layer into a new beaker (pre-rinsed with 9N HCl).
18. Repeat steps 14 - 17 if yellow coloration remains (until aqueous layer becomes clear).
19. Heat beaker very gently on hot plate. Solution becomes cloudy and ether fumes are seen to rise up the beaker sides.
20. When solution becomes clear and ether fumes have disappeared, remove from heat and add a few drops of conc. HCl.
21. If after repeating steps 14 - 20 the yellow colour remains there is another organic chelating the Fe (+ U and Th). In order to break down the organic the solution must be boiled down and refluxed with more $HCLO_4$.

This procedure can be performed the day before you intend to count the sample on the alpha spectrometer. However, if further destruction of organics is required extra delays will be incurred. **NOTE: From experience a slight yellow coloration after IPE treatment appears to have little effect on yield or the cleanliness of the spectra.**

C) Separation of U from Th

22. Set up first ion exchange column with approx. 5 cm depth of anion exchange resin and rinse several times with 0.1M HCl to remove any organics from the resin.
23. Precondition the resin with 2 x 20ml washes of 9N HCl.
24. Add sample (which should have cooled from step 20)
25. Start collecting for Th in 250ml beaker pre-rinsed with 9N HCl!!!
26. Set drip rate at 1 drip every 2 seconds.
27. When solution drained through add 20ml 9N HCl. Remaining Th should be eluted.
28. Change beakers and add 50ml 0.1M HCl to elute U.

While waiting for Th to drip through (can be 2 Hours) now is a good time to set up the next columns (U and Th). Once past this stage both the U and Th should be put through the subsequent columns simultaneously. This saves a great deal of time although a careful record should be kept in a note book as to what stage each column is at. The next sections are in the correct chronological sequence. So far the first column will have taken about 2 - 3 hours.

D) Thorium Preparation

29. Set up third ion exchange column with approx. 5cm depth of cation exchange resin. This should be rinsed thoroughly with 0.1M HCl.
30. Precondition with 2 x 20ml 2M HCl.
31. Dilute the Th elute from step 27 with 2 volumes of distilled water. This alters the molarity from 9M to 3M. Do not dilute more than necessary; Th sticks to glassware <pH 3.
32. Add sample to column. Set drip rate to 1 drip every 2 seconds
33. When solution drained through wash with 20ml 2M HCl.
34. Elute Th using 50ml 6M H_2SO_4 into a *50ml* Pyrex beaker.

E) Uranium Preparation

35. Gently evaporate the U elute from step 28 to almost dryness.
36. Dissolve the residue in 5ml conc. HNO_3 and 5ml 7M HNO_3.
37. Set up second ion exchange column with approx. 5 cm depth of anion exchange resin. This should be thoroughly rinsed with 0.1M HCl.
38. Add sample to column setting drip rate as before.
39. When solution drained through wash with 20ml 7M HNO_3 (removes remaining Fe).
40. When solution drained through wash with 10ml 9M HCl (removes remaining Th).
41. Discard elutant.
42. Elute U with 50ml 0.1 HCl into a *50ml* Pyrex beaker.

Procedures D and E will take approximately 3 hours to complete. Ideally Th should be plated and counted first since it has a habit of sticking to glassware and vanishing into thin air for no apparent reason!! Thus it is suggested that the following electroplating section is performed with Th elute first.

F) Electroplating

There are a number of electroplating methods in common use today and some knowledge of them is desirable. It has been found that the difference in yields between the various methods can be large. A great deal of experimentation is needed to find a method that is satisfactory in terms of yield, plating time, and ease of preparing the elute for electroplating.

Initial electroplating was performed using the following technique.

1. Slowly evaporate the U elute to approximately 5 ml ensuring that the beaker does not dry out. Make up volume with H_2O.
2. Add a drop of HNO3 to Th elute to oxidise any remaining organics.
3. Add a few drops of thymol blue indicator solution to both U and Th solutions.
4. Add NaOH slowly and adjust pH to 3.0 (straw colour).
5. Transfer solutions to the large electroplating cells and make up the volume with electroplating solution.
6. Electroplate at 0.4A for 4 hours topping up electrolyte as required.
7. Turn off current, empty solution into original beakers, wash and label planchets.
8. Count on alpha-spectrometers.

This technique does not provide good chemical yields for calcite speleothems.

After experimentation we found that the electroplating method proposed by Laars Hallstadius to give 40-50% greater yields although variable. Reference is Hallstadius, L. (1984). A method for the electrodeposition of actinides. *Nucl. Instr. Meth.*, **223**, 266-267.

1. Evaporate the sample to a few mls in a 100ml beaker (Thorium is in sulphuric acid so heating should be ***very*** gentle).
2. Remove from heat and cool on gauze.
3. Add 1ml 0.3M Na_2SO_4 (acts as a carrier).
4. Evaporate to total dryness (Takes up to 2 hours for Th).
5. Cool and add exactly 0.3ml conc. H_2SO_4.
6. Warm and swirl to dissolve residue. Avoid evaporating H_2SO_4 more than necessary.
7. Add 4ml distilled water and 2 drops 0.2% thymol blue.
8. Dropwise add NH_3 to a yellow - yellow orange colour.

9. Pour solution into electrodeposition cell and rinse 50ml beaker with 5ml 0.1% H_2SO_4.
10. Pour into cell and adjust pH. to 2.1 - 2.4 with NH_3, or, if the end-point is overstepped, 20% H_2SO_4.
11. Electrolyse for 0.6A for 2 Hours (the original technique suggests 1.2A for 1 hour but our equipment will not tolerate this current for so long).
12. Add 1ml NH_3 1min before switching off current.
13. **This step should be accomplished in one smooth and quick operation! Have the required equipment and chemicals ready!!** Turn off current, empty cell into original 50ml beaker, rinse planchet (still in cell) with distilled water. Panic over. Now dismantle cell, rinse again with water **and acetone**, dry and label.
14. Count.

Sub-samples	Acid Molarity	U Yield (%)	Th Yield (%)	$^{234}U/^{238}U$	$^{230}Th/^{234}U$	$^{230}Th/^{232}Th$	Uncorrected age (ka)	Corrected age (ka)
SC01 15+16B (1)	HNO_3 2M	20	35	1.27±0.06	0.049±0.007	1.31±0.27	5.5±0.8	-0.8±1.8
SC01 15+16B (2)	HNO_3 4M	18	45	1.29±0.06	0.047±0.006	1.16±0.22	5.2±0.7	-1.6±1.7
SC01 15+16B (3)	HNO_3 7M	14	35	1.34±0.07	0.061±0.007	1.13±0.18	6.8±0.8	-2.3±2.0
PT02 21-23B (1)	HNO_3 2M	58	68	1.30±0.02	0.029±0.002	4.81±1.51	3.2±0.3	2.2±0.6
PT02 21-23B (2)	HNO_3 4M	57	61	1.26±0.02	0.047±0.003	3.05±0.44	5.2±0.3	2.7±0.7
PT02 21-23B (3)	HNO_3 7M	44	76	1.27±0.02	0.032±0.002	3.14±0.65	3.5±0.3	1.8±0.6
PT03 11+12B (1)	HNO_3 2M	78	63	1.78±0.05	0.028±0.006	2.23±0.99	3.1±0.6	1.1±1.5
PT03 11+12B (2)	HNO_3 4M	74	58	1.75±0.05	0.036±0.006	2.84±1.34	4.0±0.7	1.9±1.6
PT03 11+12B (3)	HNO_3 7M	70	58	1.72±0.05	0.059±0.007	2.54±0.67	6.5±0.7	2.7±1.7
PT04 17+18B (1)	HNO_3 2M	48	52	1.36±0.04	0.048±0.006	2.7±0.75	5.4±0.6	2.4±1.4
PT04 17+18B (2)	HNO_3 4M	9	35	1.47±0.09	0.064±0.007	2.21±0.46	7.1±0.8	2.3±1.7
PT04 17+18B (3)	HNO_3 7M	15	29	1.49±0.07	0.109±0.010	1.85±0.26	12.4±1.1	2.5±2.4

Appendix K (1). U-series data from leachate-leachate analysis of sub-samples from SC01, PT02, PT03 and PT04. For these experiments all dates were corrected using an initial thorium ratio of 1.5 . Errors are to one sigma and are based on counting statistics.

Sub-Samples	$^{238}U/^{232}Th$	1sigma %error	$^{234}U/^{232}Th$	1sigma %error	$^{230}Th/^{232}Th$	1sigma %error	$\rho^{238/232-234/232}$	$\rho^{238/232-230/232}$	$\rho^{234/232-230/232}$
SC01 15+16B (1)	11.857	15.6	15.15	15.5	1.317	20.1	0.956	0.728	0.724
SC01 15+16B (2)	7.96	14.5	10.273	14.4	1.156	18.8	0.95	0.721	0.716
SC01 15+16B (3)	5.688	12.6	7.634	12.5	1.134	15.8	0.925	0.712	0.704
PT02 21-23B (1)	105.48	30.4	137.08	30.3	4.8	31.3	0.999	0.966	0.965
PT02 21-23B (2)	47.69	13.3	60.17	13.3	3.05	14.4	0.993	0.909	0.908
PT02 21-23B (3)	44.9	19.3	57.42	19.3	3.14	20.6	0.996	0.929	0.929
PT03 11+12B (1)	54.82	39.8	97.82	39.7	2.235	44.3	0.998	0.894	0.894
PT03 11+12B (2)	57.94	44.1	101.38	44.1	2.84	47.3	0.998	0.93	0.929
PT03 11+12B (3)	30.48	23.6	52.5	23.5	2.54	25.9	0.993	0.902	0.900
PT04 17+18B (1)	38.36	25.9	52.29	25.9	2.7	28.2	0.995	0.91	0.909
PT04 17+18B (2)	5.76	18.8	8.48	18.6	2.2	20.4	0.943	0.846	0.836
PT04 17+18B (3)	5.66	12.6	8.49	12.4	1.85	14.1	0.922	0.796	0.783

Appendix K (2). Errors and error correlations for HNO leached sub-samples from SC01, PT02, PT03 and PT04 Errors and correlations have been calculated using the Ludwig and Titterington (1994) equations (section 4.9).